

# **Exploiting Cooperative Effects in s-Block Organometallics for New Applications in Synthesis and Catalysis**

**Laia Davin Cardona**

Department of Pure and Applied Chemistry

University of Strathclyde

A thesis submitted the Department of Pure and Applied Chemistry, University of  
Strathclyde, in part fulfilment of the requirements for the degree of

*Doctor of Philosophy*

2017

This thesis is the result of the author's original research. It has been composed by the author and has not been previously submitted for examination which has led to the award of a degree.

The Copyright of this thesis belongs to the author under the terms of the United Kingdom Copyrights Acts as qualified by the University of Strathclyde Regulation 3.49. Due acknowledgements must always be made to the use of any material contained in, or derived from, this thesis.

Laia Davin Cardona

April 2017

*“When we try to pick up anything by itself,  
we find it hitched to everything else in the universe.”*

*- John Muir*

*Als meus pares Josep M. i Rosa*

## **Acknowledgements**

Coming to Scotland to study the PhD has definitely been an intense and life-changing experience. There are a large number of people I would like to acknowledge for their support, motivation and friendship during these 3 and a half years.

Firstly, I would like to thank my supervisor Prof. Eva Hevia for giving me the opportunity to work in her research group. Thank you for your enormous support, encouragement and guidance during all the years of my PhD. I am extremely grateful for your enthusiasm, for always being available and happy to help even when you were on maternity leave. Thanks as well for giving me the opportunity to attend two international conferences in Germany and France, which we really enjoyed, and for allowing me to represent the Hevia group in the USIC organising committee.

I would also like to acknowledge the other supervisors of the group, Prof. Mulvey, Dr O'hara and Dr Robertson for all the chemistry discussions and suggestions to this project, as well as all the football days. I am also thankful to Dr Kennedy for all the help in elucidating the crystal structures of my compounds and Prof. Clegg for measuring and solving some of the structures at the synchrotron.

Enormous thanks to the postdocs in the Hevia group. Alberto, thank you for all your help during all these years especially at the start of my PhD and for patience

teaching me all the techniques. Ross, thanks a lot for your enormous help and advice with the Nacnac project and X-Ray but specially for becoming a great friend.

I would also like to thank all the people of the team, who made all this time really enjoyable, most of them becoming friends for life. Special mention goes to Silvia, thanks for your friendship since day 1, for all the great times in Glasgow, lunches, coffees and now Skypes. I am really thankful for all your support and really pleased to have met you. Thank you to Marco and Lewis, my sportive friends, for being so crazy and fun. Thanks to Marina for your friendship, for all the coffee, cake and shopping times together and the great weekend in London. Thanks to Sam and Andy, who started the PhD at the same time as me. Special thanks to Sam, who has been my “sister of PhD”, for becoming a great friend and we have supported each other through the good and bad times of the PhD. Also thanks to Vicky, for all the yoga days; Michael and Etienne as well as the new members of the team, Leonie and Richard. Thanks as well to the former members of the group: Jenny, Sarah, Tobi, Markus, Tracy, Donna, Ana, Màrius, Javi, Antonio and María. I would also like to thank Janie-Anne, Isabel and Craig, for always being extremely helpful. Thanks to Chris for giving me the opportunity to mentor in the teaching labs and also the undergraduate students that contributed to some results of this thesis.

I would also like to thank Lola, Marta, Maria, Carla, Carol, Neus, Alex, Albert and Andrea who became my family in Glasgow, as well as all the Scottish climbing friends. Specially, thanks to my favourite climbers: Jess, James and Megan for all the fun times training (and not training), we really need to plan a climbing trip soon!

També m'agradaria agrair a tots aquells que han vingut a visitar-me a Glasgow i tots els que heu estat a prop malgrat la distància. Moltíssimes gràcies als escaladors més forts i divertits del món, per venir múltiples vegades i per ser un gran exemple de motivació en tot moment: Roger, Edu, Joan, Albert, Àger, Núria, Júlia i Estela,

moltes gràcies. Gràcies també a totes les meves amigues de sempre, per seguir-hi sent: Mariona, Èlia, Laia R., Gemma, Laia B., Anna, Clara, Mar, Joana, Àngels, i Núria. I també a tots els amics químics: Miki, gràcies per tots els consells i suport en tot moment; Raul, Víctor, Joan, Sonia, Mireia, Maria i Adrià (que no és químic, però quasi!). Inma, Miquel i Arnald moltes gràcies per introduir-me en el món de la recerca. Muchísimas gracias también a la familia Martín Román, por ser mi segunda familia y apoyarme siempre.

Finalment, m'agradaria agrair a tota la meva família per ser un suport incondicional, en especial a les meves dues àvies, per ser un gran exemple de lluitadores. Roger, moltíssimes gràcies per ser el millor germà gran que es pot tenir i alhora amic. Gràcies pels teus consells, ajuda i suport en tot moment. Pares, no tinc paraules per agrair-vos tot el que m'heu donat. Gràcies per sempre estar al meu costat, per creure en mi i per ser un referent vital. Aquesta tesi és fruit de tot el que m'heu proporcionat. Gràcies, de tot cor.

## Abstract

Focussing on group 1 and group 2 metals, this thesis advances the use of polar organometallics in catalysis, in particular intermolecular hydroamination processes; as well as other key stoichiometric transformations, namely deprotonative metallation and C-F bond activation.

Group 1 alkyl compounds  $MCH_2SiMe_3$  ( $M = Li, Na$  or  $K$ ) have proved to be efficient catalysts for intermolecular hydroamination of a wide range of substituted vinylarenes and alkynes at room temperature and with short timescales. Similarly, advancing in the concept of s-block cooperative bimetallic catalysis, alkali-metal magnesiate complexes  $[MMg(CH_2SiMe_3)_3]$  and  $[(donor)_2M_2Mg(CH_2SiMe_3)_4]$  ( $M = Li, Na$  or  $K$ ) have shown that they can also act as catalysts for these hydroamination processes, although longer times and high temperature conditions are required in some cases. Reactivity studies show an alkali-metal effect with potassium being significantly more reactive than lithium. New insights into the constitution of the potential organometallic intermediates involved in these processes have also been gained by combining X-Ray crystallographic and NMR studies (including DOSY NMR).

The second part of this thesis assesses cooperative effects of single-metal organomagnesium complexes in deprotonation and C-F bond activation processes. Using a specially designed metallating base, which combines within the same molecule a sterically demanding  $\beta$ -diketiminate ligand with a kinetically activated TMP base [ $^{Dipp}NacnacMg(TMP)$ ], regioselective magnesiation of heterocyclic and



aromatic molecules, including pyrazine or 1,2,4,5-tetrafluorobenzene, can be achieved at room temperature. Structural studies of these metallated intermediates have revealed a crucial stabilising role of the  $\beta$ -diketiminato ligand, which facilitates the trapping of the sensitive anions formed. Additionally, they have provided important clues to rationalise the stability of these species in solution. Contrastingly [<sup>Dipp</sup>NacnacMg(THF)Bu] complex is a much more kinetically retarded base, which fails to metallate these substrates promoting in some cases, when confronted with fluoroarenes, C-F bond activation process via nucleophilic aromatic substitution.

## Publication in a Peer Reviewed Journal

[1] “Regioselective magnesiation of *N*-heterocyclic molecules: securing insecure cyclic anions by a  $\beta$ -diketiminato-magnesium clamp” - L. Davin, R. McLellan, A. Hernán-Gómez, W. Clegg, A. R. Kennedy, M. Mertens, I. A. Stepek, E. Hevia, *Chem. Commun.* **2017**, 53, 3653–3656.

Chapter 4 is adapted from the publication above.

## Conference Presentations

L. Davin, A. Hernán-Gómez, E. Hevia, Alkali-Metal-Catalysed Intermolecular Hydroamination Reactions of Vinylarenes and Alkynes, *Universities of Scotland Inorganic Conference (USIC-48)*, University of Glasgow, Glasgow, **2014**. (Poster Presentation)

L. Davin, E. Hevia, s-Block Metal Catalysts for Intermolecular Hydroamination Reactions, *University of Strathclyde Inorganic Section Meeting*, West Brewery, Glasgow, **2015**. (Oral Presentation)

L. Davin, E. Hevia, s-Block Metal Catalysts for Intermolecular Hydroamination Reactions, *Universities of Scotland Inorganic Conference (USIC-49)*, University of Heriot-Watt, Edinburgh, **2015**. (Oral Presentation)

L. Davin, A. Hernán-Gómez, E. Hevia, Regioselective Deprotonation of N-Heterocyclic Molecules Using  $\beta$ -diketiminato Stabilized Magnesium Bases, (*IRIS-14*), Regensburg, Germany, **2015**. (Poster Presentation)

L. Davin, A. Hernán-Gómez, E. Hevia, Alkali-Metal Catalysts for Intermolecular Hydroamination Reactions, (*ISCC-11*), Rouen, France, **2016**. (Poster Presentation)

L. Davin, E. Hevia, Regioselective Magnesiation of Heterocyclic and Fluorinated Aromatic Molecules, *Universities of Scotland Inorganic Conference (USIC-50)*, University of Strathclyde, Glasgow, **2016**. (Poster Presentation)

## Abbreviations

Ac	Acetate
Ar*	2,6- <sup>i</sup> Pr <sub>2</sub> -C <sub>6</sub> H <sub>3</sub>
bpy	4,4'-Bipyridine
Bu	butyl
Bz	benzyl
CCDC	Cambridge Structural Database
CDCl <sub>3</sub>	Deuterated chloroform
Cy	Cyclohexyl
C <sub>6</sub> D <sub>6</sub>	Deuterated benzene
D	Diffusion coefficient
DA	Diisopropylamide
DFT	Density Functional Theory
DOSY	Diffusion-ordered NMR spectroscopy
<sup>Dipp</sup> Nacnac	Ar*NC(Me)CHC(Me)NAr*

---

<sup>Dipp</sup> BIAN	Bis[(2,6-diisopropylphenyl)imino]acenaphthene
DMAP	4-Dimethylaminopyridine
DME	Dimethoxyethane
DMF	Dimethylformamide
DMG	Direct Metallating Group
DMSO	Dimethyl Sulfoxide
DoM	Direct <i>ortho</i> -Metallation
<i>d</i> <sub>8</sub> -THF	Deuterated tetrahydrofuran
<sup>Dtb</sup> BIAN	1,2-Bis[(2,5-di-tert-butylphenyl)imino]acenaphthene
ECC	External Calibration Curves
Et <sub>2</sub> O	Diethyl Ether
FeCp <sub>2</sub>	Ferrocene
g	Grams
GC	Gas Chromatography
η	Viscosity
h	Hours
HBpin	Pinacolborane
HMDS	Bis(trimethylsilyl)amide
HMPA	Hexamethylphosphoramide

---

ICC	Internal Calibration Curves
IR	Infrared
<i>i</i> Pr	Isopropyl
$k_B$	Boltzmann constant
L	Neutral Lewis donor
LDA	Lithium diisopropylamide
M	Molar
MCH	Methylcyclohexane
Me	Methyl
Me-THF	2-Methyltetrahydrofuran
Me <sub>6</sub> TREN	Tris[2-(dimethylamino)ethyl]amine
MHz	Megahertz
ml	Millilitres
mmol	Millimols
MW	Molecular Weight
NMR	Nuclear Magnetic Resonance
	s - singlet
	d - doublet
	t - triplet

---

	q - quartet
	sept - septet
	m - multiplet
	br - broad
<i>n</i> Bu	(CH <sub>2</sub> ) <sub>3</sub> CH <sub>3</sub>
Ph	Phenyl
PhN	Phenyl naphthalene
PMDETA	<i>N,N,N',N'',N''</i> -Pentamethyldiethylenetriamine
ppm	Parts per million
r	Radius
RT	Room temperature
T	Temperature
<i>t</i> Bu	C(CH <sub>3</sub> ) <sub>3</sub>
TEMPO	2,2,6,6-Tetramethyl-1-piperidinyloxy
THF	Tetrahydrofuran
TMEDA	<i>N,N,N',N'</i> -Tetramethylethylenediamine
TMS	Tetramethylsilane
TMP(H)	2,2,6,6-tetramethylpiperidine
Tol	Toluene

TPhN	1,2,3,4-tetraphenylnaphthalene
9-BBN	9-Borabicyclononane
15-crown-5	1,4,7,10,13-Pentaoxacyclopentadecane
18-crown-6	1,4,7,10,13,16-hexaoxacyclooctadecane



## Table of Numbered Compounds

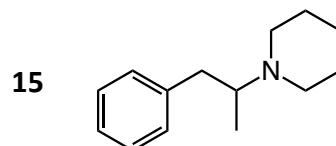
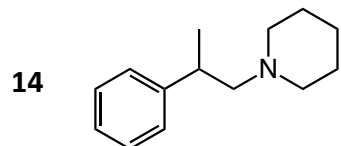
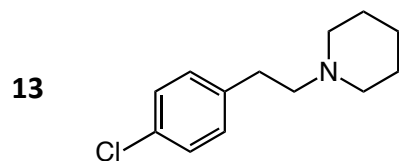
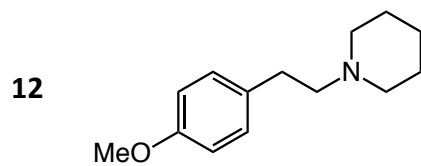
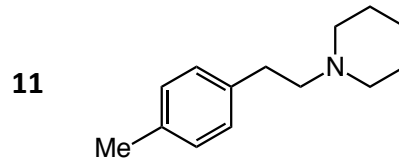
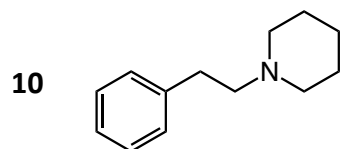
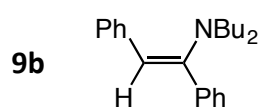
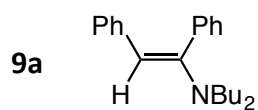
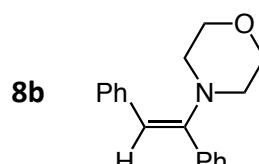
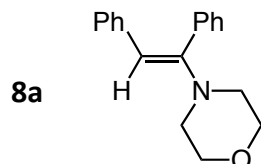
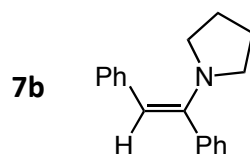
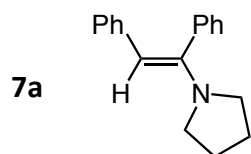
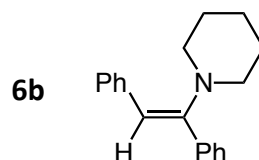
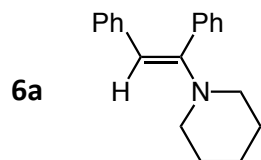
No	Compound	No	Compound
1a	<chem>c1ccccc1C#Cc2ccccc2</chem>	1b	<chem>C=CC1=CC=CC=C1</chem>
1c	<chem>CC1=CC=C(C=C1)C=C</chem>	1d	<chem>COC1=CC=C(C=C1)C=C</chem>
1e	<chem>ClC1=CC=C(C=C1)C=C</chem>	1f	<chem>Fc1ccc(C=C)cc1</chem>
1g	<chem>Brc1ccc(C=C)cc1</chem>	1h	<chem>CC(=C)c1ccccc1</chem>
1i	<chem>CC=CC1=CC=CC=C1</chem>	1j	<chem>CC(=C)C=C</chem>
2a	<chem>C1CCNCC1</chem>	2b	<chem>C1CCNC1</chem>
2c	<chem>C1CCNCCO1</chem>	2d	<chem>CCCCN</chem>
2e	<chem>CN(C)c1ccccc1</chem>	2f	<chem>CN(C)c1ccccc1</chem>
2g	<chem>CN(C)c1ccccc1</chem>	2h	<chem>Nc1ccccc1</chem>

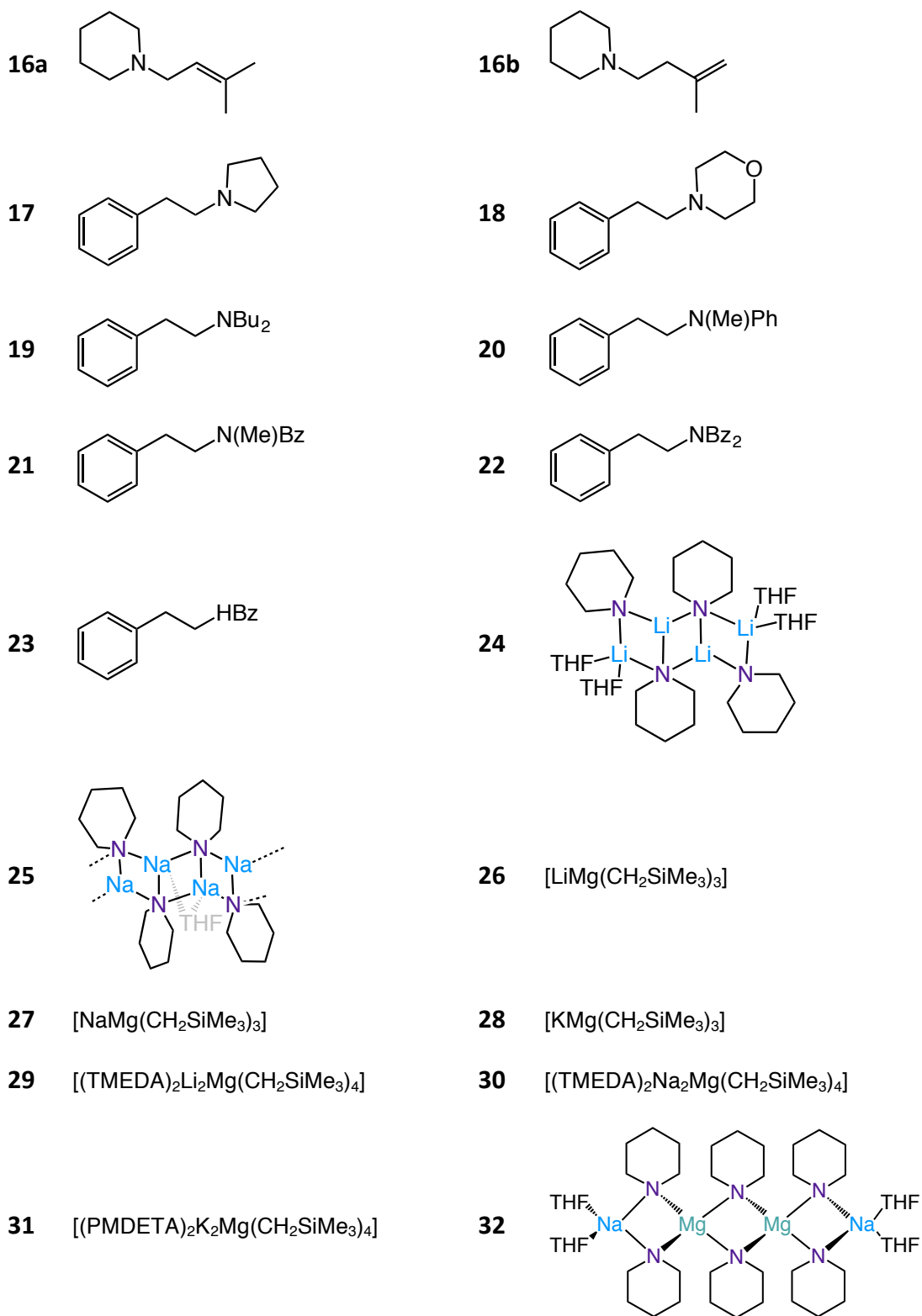
**2i** BzNH<sub>2</sub>

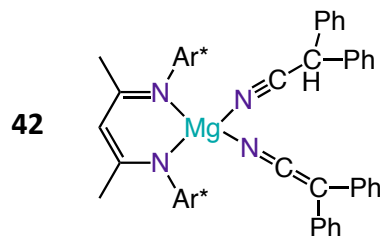
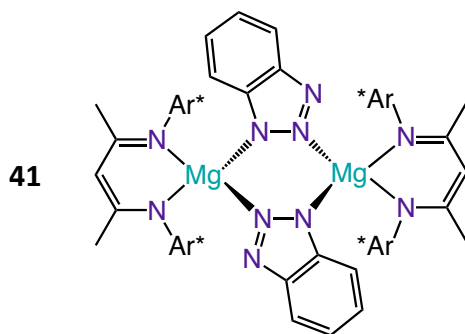
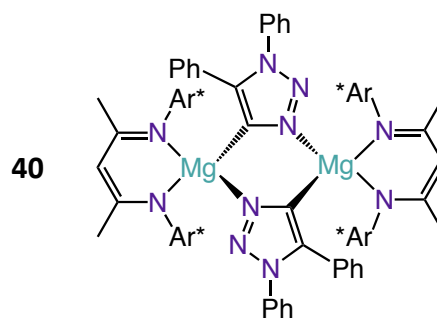
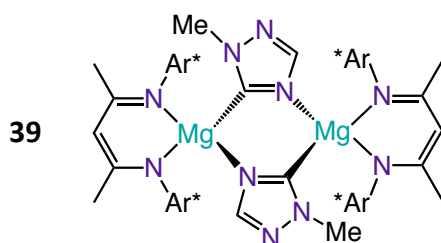
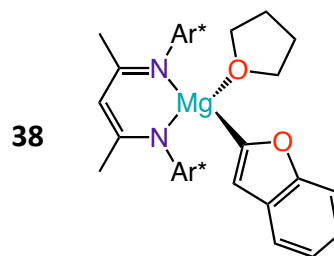
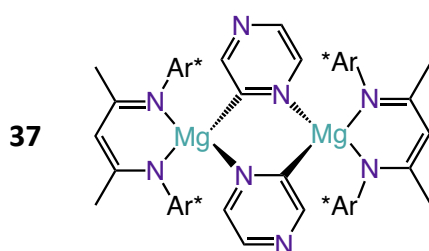
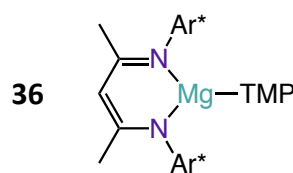
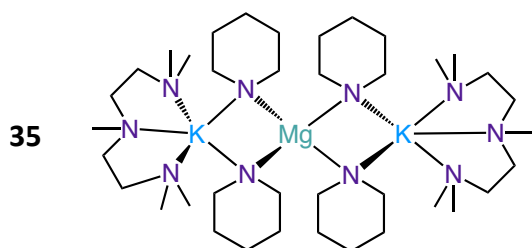
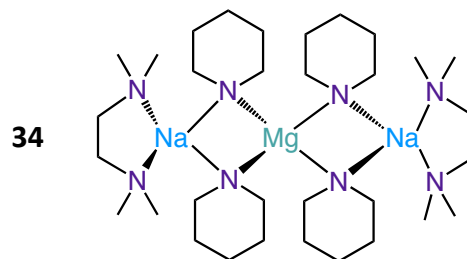
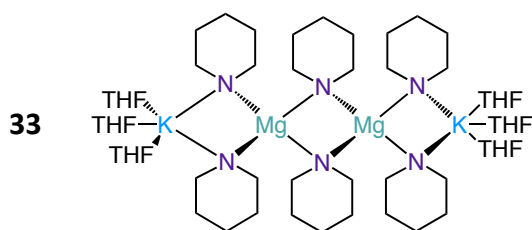
**3** LiCH<sub>2</sub>SiMe<sub>3</sub>

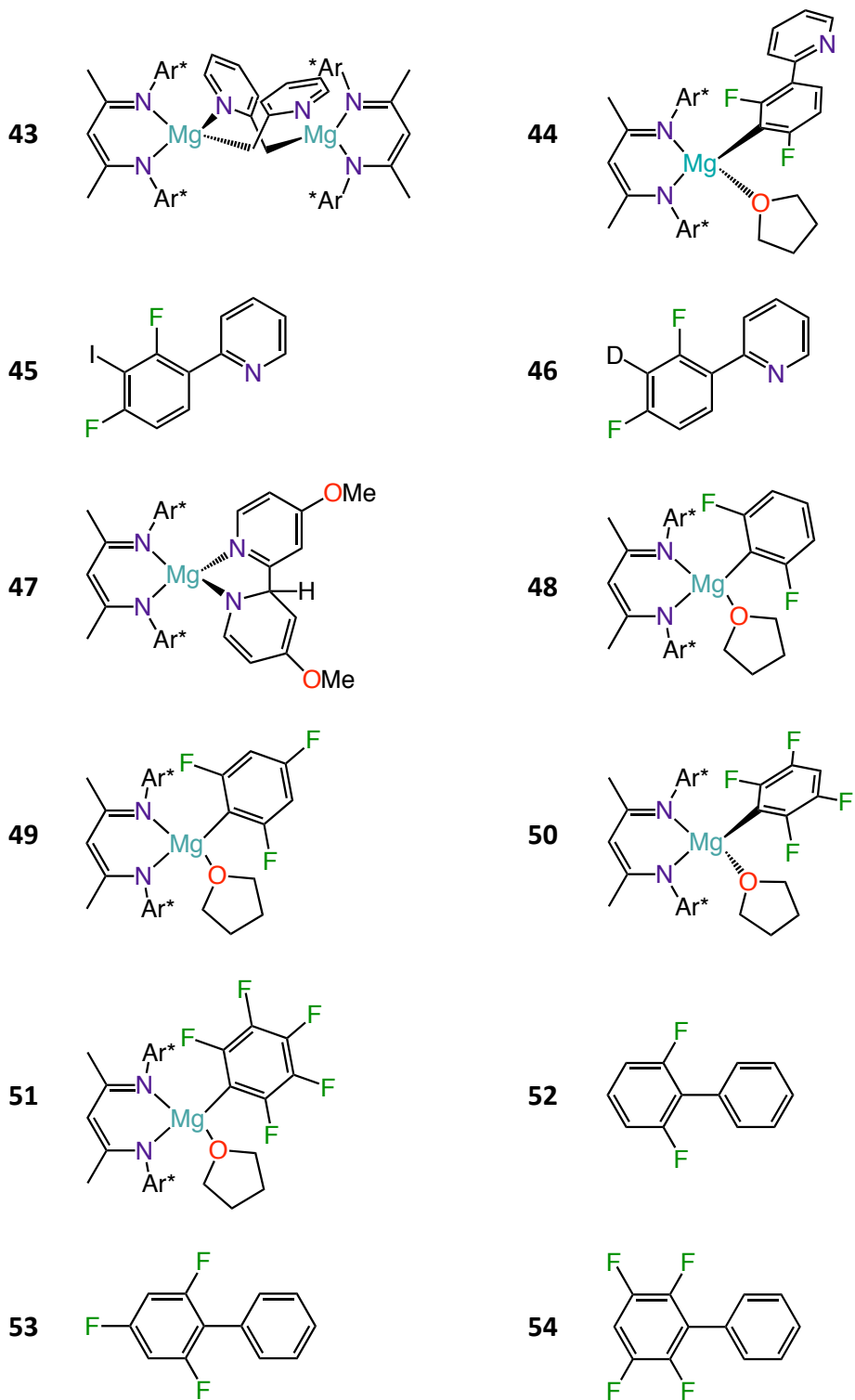
**4** NaCH<sub>2</sub>SiMe<sub>3</sub>

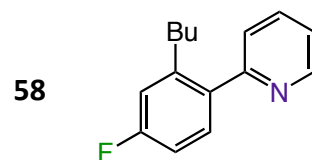
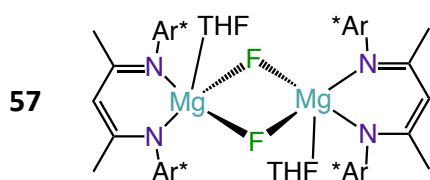
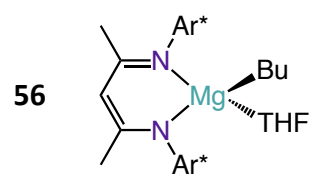
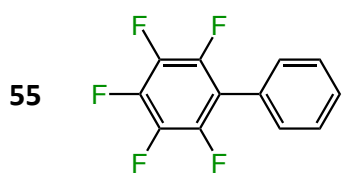
**5** KCH<sub>2</sub>SiMe<sub>3</sub>











## Contents

Acknowledgements .....	V
Abstract.....	VIII
Publication in a Peer Reviewed Journal .....	X
Conference Presentations .....	XI
Abbreviations.....	XII
Table of Numbered Compounds.....	XVII
Contents.....	XXIII
Chapter 1 Introduction to s-Block Organometallics .....	1
1.1 Group 1: Alkali-Metal Organometallics.....	1
1.1.1 General Aspects .....	1
1.1.2 Alkali-Metal Amides: Structural Insights.....	4
1.1.3 Synthetic Applications of Organoalkali-Metal Compounds .....	10
1.2 Group 2: Organomagnesium Chemistry .....	16
1.2.1 Grignard and Turbo-Grignard Reagents.....	16
1.2.2 Magnesium Amides .....	19
1.2.3 Sterically Demanding Ligands In Group 2: $\beta$ -diketiminato Ligands.....	22
1.3 Ate Compounds .....	30
1.3.1 Alkali-Metal Magnesiates .....	30
1.4 Aims and Structure of this Thesis.....	35
Chapter 2 Group 1 Metal-Catalysed Intermolecular Hydroamination Reactions.....	36
2.1 Introduction .....	36
2.1.1 Intermolecular Hydroamination Reactions.....	36
2.2 Results and Discussion .....	44

---

2.2.1	Optimisation of the Reaction Conditions.....	44
2.2.2	Substrate Scope .....	50
2.2.3	Mechanistic Investigations .....	61
2.3	Conclusions .....	80
2.4	Experimental.....	81
2.4.1	Synthesis of Active Species .....	81
2.4.2	General Experimental Procedure for Catalytic Hydroamination Reactions at NMR Tube Scale .....	82
2.4.3	General Procedure for Catalytic Hydroamination Reactions of Styrene Derivatives .....	84
Chapter 3	Hydroamination Reactions Using Alkali-Metal Magnesiate Precatalysts.....	93
3.1	Introduction .....	93
3.1.1	Hetero-Bimetallic Main Compounds in Catalysis.....	93
3.2	Results and Discussion .....	100
3.2.1	Optimisation of the Reaction Conditions.....	100
3.2.2	Substrate Scope .....	107
3.2.3	Study of the Catalytic Cycle .....	111
3.3	Conclusions .....	130
3.4	Experimental.....	132
3.4.1	Synthesis of Active Species .....	132
3.4.2	General Experimental Procedure for Catalytic Hydroamination Reactions at NMR Tube Scale .....	135
Chapter 4	Regioselective Magnesiation of Heterocyclic Molecules .....	136
4.1	Introduction .....	136
4.2	Results and Discussion .....	144
4.2.1	Magnesiation of N/O-Heterocycles: Pyrazine and Benzofuran .....	144
4.2.2	Magnesiation of Triazoles.....	158
4.2.3	Magnesiation of Related Organic Substrates: Benzotriazole and Diphenylacetonitrile .....	165
4.2.4	Magnesiation of Pyridine Derivatives .....	177
4.3	Conclusions .....	198
4.4	Experimental.....	199



---

4.4.1	Synthesis of Active Species .....	199
4.4.2	DOSY NMR Studies .....	210
4.4.3	Preliminary Electrophilic Quenching Studies .....	210
Chapter 5	Deprotonation and C-F Activation of Fluorinated Aromatic Molecules .....	212
5.1	Introduction .....	212
5.1.1	C-H metallation of fluoroaromatics .....	213
	Fluoroaromatics in C-F Activation .....	216
5.2	Results and Discussion .....	225
5.2.1	Magnesium of Fluorinated Aromatic Substrates .....	225
5.2.2	C-F Activation of Fluoroarenes Using [ <sup>Dipp</sup> NacnacMg(THF)Bu] Base ...	237
5.3	Conclusions .....	245
5.4	Experimental .....	246
5.4.1	Synthesis of Active Species .....	246
5.4.2	General Experimental Procedure for Negishi Cross-Coupling Reactions 250	
5.4.3	C-F Activation 2-(2,4-difluorophenyl)pyridine .....	252
5.4.4	General Experimental Procedure for Metallation Reactions at NMR Tube Scale .....	253
5.4.5	DOSY NMR Studies .....	254
Chapter 6	Conclusions and Outlook .....	255
Chapter 7	Experimental .....	259
7.1	General Experimental Techniques .....	259
7.1.1	Schlenk Techniques .....	259
7.1.2	Glovebox .....	260
7.1.3	Solvent Purification .....	261
7.1.4	Analytical Procedures .....	262
7.2	Synthesis of Starting Materials .....	263
7.3	Crystallographic Data .....	268
References	.....	275

# Chapter 1 Introduction to s-Block Organometallics

## 1.1 Group 1: Alkali-Metal Organometallics

### 1.1.1 General Aspects

Alkali-metal organometallic compounds, in particular organolithium and Grignard reagents, are amongst the most widely used organometallic reagents in synthesis playing a pivotal role in a myriad relevant organic transformations.<sup>[1,2]</sup> Over the years, structural studies on the constitution of these reagents have advanced the understanding of their unique reactivities by providing valuable structural/reactivity correlations.<sup>[3]</sup> However, in many cases structures in the solid state differ from solution, and their level of aggregation can also vary in different solvents significantly.<sup>[4]</sup> Employing methods such as NMR spectroscopy, including DOSY NMR,<sup>[5]</sup> new light has been shed on the constitution of these species which has contributed to determine their reactivity and reaction mechanisms, as well as to provide a tool to improve yields and/or selectivities.<sup>[6,7]</sup>

The typical formula for organometallic alkali-metal complexes is displayed in Figure 1.1.

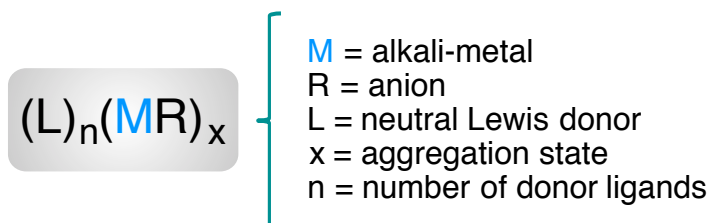


Figure 1.1: General formula for alkali-metal organometallics.

The aggregation state (determined by  $x$  in Figure 1.1) can range from  $x = 1$ , forming a monomer, to  $x = \infty$  that corresponds to a polymer. The aggregation is determined by the identity of the cation and anion, the presence of donors (L) and their degree of ligation ( $n$ ) as well as the size and denticity of the anion (R) and the donor ligand (L).<sup>[8]</sup>

There exists an important correlation structure vs reactivity, where the aggregation state of the compound is inversely proportional to its reactivity.<sup>[9-11]</sup> For instance, linear  $n\text{BuLi}$  is less reactive than the branched  $t\text{BuLi}$  reagent in hydrocarbon solvents due to the different aggregation state and  $\text{pK}_a$  values (50 and 53 for  $n\text{BuLi}$  and  $t\text{BuLi}$  respectively<sup>[12]</sup>), where in donor free medium the former is a hexamer and the latter a tetramer (Figure 1.2).<sup>[9]</sup>

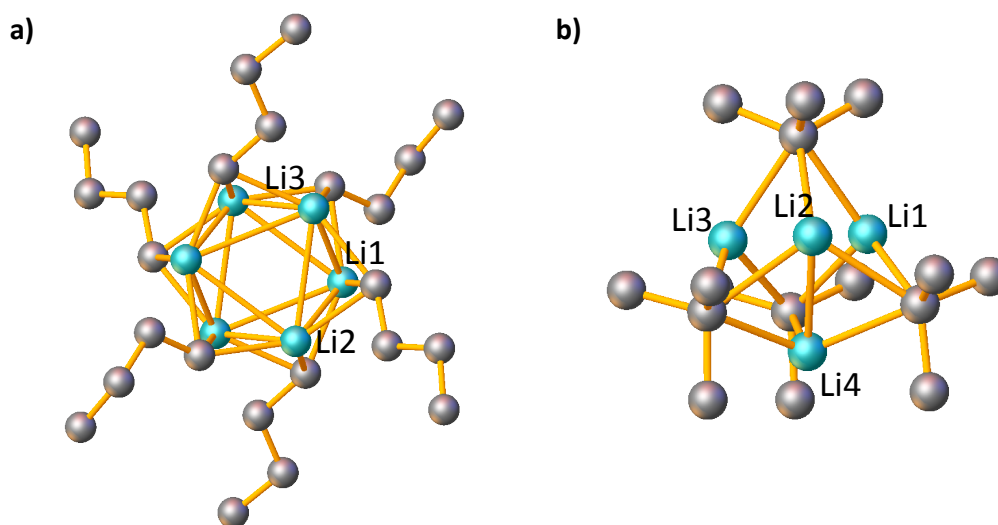


Figure 1.2: Molecular structures of a) hexameric *n*BuLi and b) tetrameric *t*BuLi. All hydrogen atoms have been omitted for clarity.<sup>[13]</sup>

Additionally, the strong polarity of the  $M^{\delta(+)}-C^{\delta(-)}$  bond imposes a high reactivity of the organoalkali-metal complexes, due to the high electropositivity of the alkali-metal, which increases while descending in the group.<sup>[14]</sup> The enhanced reactivity of the heavier alkali-metals may also lead to decomposition and a more difficult manipulation compared to organolithium compounds.<sup>[8,15,16]</sup> Generally, organolithium complexes display smaller aggregation states, and therefore better solubility than the heavier alkali-metals sodium and potassium. The addition of donor ligands or the identity of the anion can prevent the formation of lithium polymeric compounds, however, for sodium or potassium this is more challenging to achieve.<sup>[10]</sup>

The smaller aggregates produced by the addition of donors also enhances the reactivity of the organolithium. For example, when combining *n*BuLi with TMEDA the hexameric arrangement deaggregates to a dimer  $[n\text{BuLi-TMEDA}]_2$ ,<sup>[17]</sup> which

displays an enhanced reactivity compared to *n*BuLi for example in deprotonation reactions.<sup>[18]</sup>

### 1.1.2 Alkali-Metal Amides: Structural Insights

Among the diverse organoalkali-metal compounds, alkali-metal amides constitute one of the most important and commonly used polar organometallic reagents in synthesis.<sup>[19]</sup> The combination of their dual properties, high Brønsted basicity and poor nucleophilicity (especially for sterically hindered amides), enables them to be used for selective deprotonation reactions, making them good rivals to alkyl lithium reagents.<sup>[20]</sup> Additionally, they generally have good solubility in hydrocarbon solvents and are safer to handle compared to alkali-metal alkyl or hydride reagents.<sup>[21]</sup> Interestingly, the most important amides are the sterically demanding LiHMDS (bis(trimethylsilyl)amide), LiTMP (2,2,6,6-tetramethylpiperidine) and LDA (diisopropylamide), which are most popularly used by synthetic chemists for their safe handling, good solubility and relatively low cost (for LiHMDS and LDA).<sup>[20]</sup> Parallel to these synthetic considerations, research on the structure and the constitution of this family of organometallic reagents has also been carried out.<sup>[20]</sup> Some of these studies have shown that the chemistry in solution of these compounds can be extremely complicated, with the formation of several aggregates coexisting in equilibrium.<sup>[22–24]</sup>

The simplest lithium amides are mononuclear but it is possible to find them in a rich assortment of aggregation motifs due to the large polarity of the  $\text{Li}^{\delta+}\text{-N}^{\delta-}$  bonds (Figure 1.3). The most common form are dimers, which in solution can exhibit equilibrium with other structures.

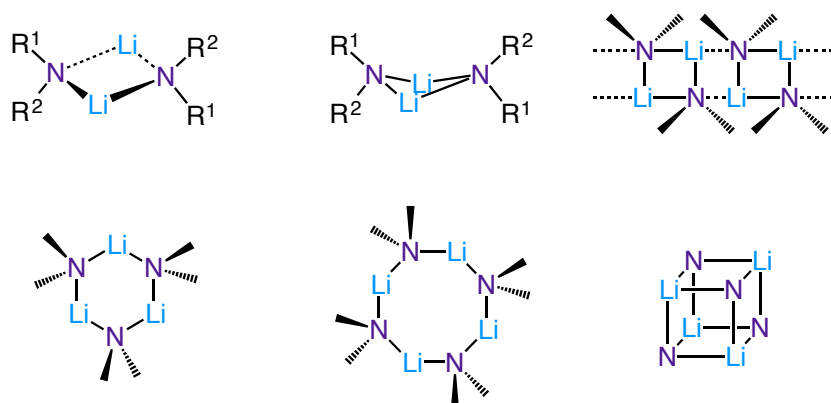


Figure 1.3: Different aggregations for lithium amides.

Lithium amides can be represented by  $(L)_n[Li(NR^1R^2)]_x$ . The lithium atom has a strong tendency to achieve the maximum coordination number compatible with steric constraints, and because of this cyclic structures are common for lithium compounds. As the N centres exhibit  $sp^3$  hybridisation, the substituents ( $R^1$  and  $R^2$ ) are projected above and below the  $(NLi)_n$  ring plane, inhibiting a close approach vertically when they try to associate. Although lithium amides cannot adopt *ring-stacking* association, they can approach edge to edge by lateral association, also called *ring-laddering*.<sup>[25,26]</sup> This tendency was first explained with the structure  $[(PMDETA)_2\{Li(N(C_4H_8))\}_3]$  by Snaith and co-workers.<sup>[25]</sup> Additionally, this ladder phenomenon can also be adopted in mixed alkali-metal complexes,<sup>[27]</sup> however, it is not observed for alkyl lithium compounds, which usually prefer to form three-dimensional or one-dimensional polymeric aggregates (Figure 1.4).<sup>[4]</sup>

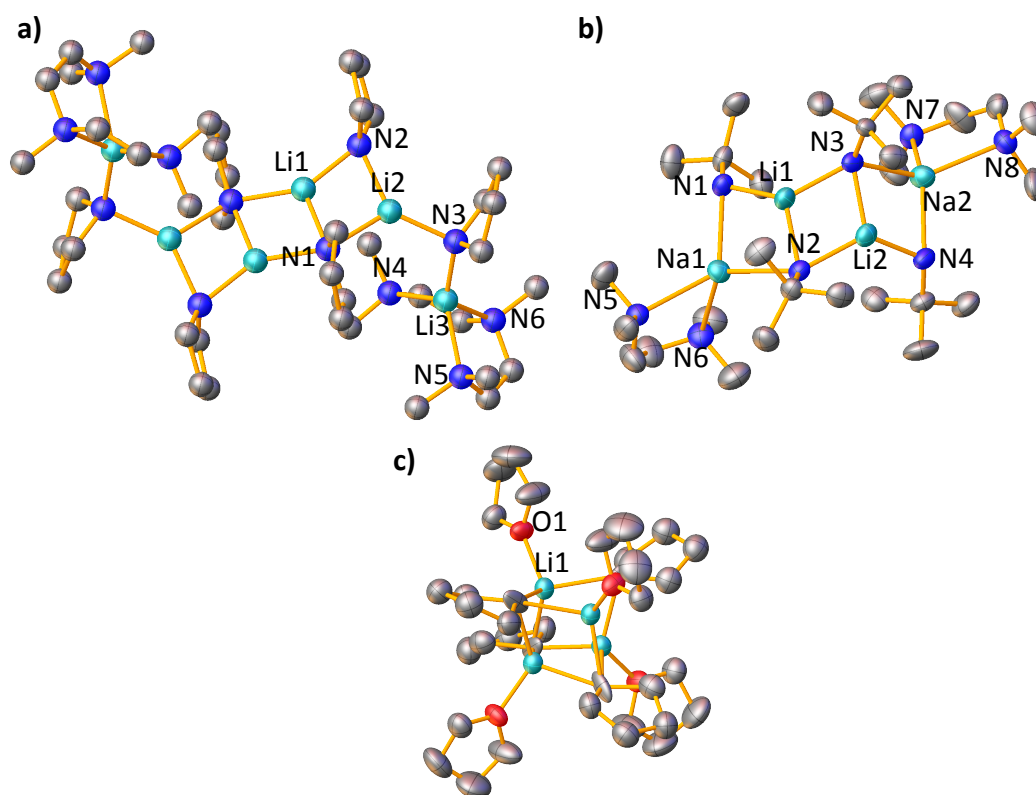


Figure 1.4: Molecular structures with 50% probability displacement ellipsoids. All hydrogen atoms have been omitted for clarity. a) Structure of  $[\{\text{PMDETA}\}_2\{\text{Li}(\text{N}(\text{C}_4\text{H}_9)_3)\}_3]$ , an example of a ladder association.<sup>[25]</sup> b) Structure of  $[\{\text{tBuN}(\text{H})_2\text{LiNa}\}\{\text{TMEDA}\}_2]$ , an example of a heterobimetallic ladder association.<sup>[27]</sup> c) Structure of  $[\{\text{Li}(\text{C}_5\text{H}_9)\}_4\{\text{THF}\}_4]$ , an example of a three-dimensional alkyl lithium compound.<sup>[28]</sup>

Figure 1.4 highlights the different association trends between lithium amides and alkyl lithium complexes. In Figure 1.4a the first example of an organonitrogen-lithium ladder structure is shown, formed by four Li-N rungs with two terminal NLi units complexed by PMDETA to prevent further association. Figure 1.4b shows another example of ladder association in a heterobimetallic compound, displaying a mixed lithium-sodium tetrameric ladder formed by two attached [NLiNa] rings complexed by two terminal TMEDA donors. In contrast, Figure 1.4c represents the first crystal structure of a secondary alkyl lithium solvated by THF,

$[\{\text{Li}(\text{C}_5\text{H}_9)\}_4\{\text{THF}\}_4]$ . This complex shows a tetrameric aggregation, with each lithium atom coordinated to THF forming the tetrasolvated, tetrameric aggregate.

Using more sterically demanding amides such as TMP or HMDS, cyclic motifs are obtained as shown in Figure 1.5.<sup>[20]</sup> LiTMP can form a trimer (Figure 1.5a) or a tetramer (Figure 1.5b) depending on the crystallisation temperatures employed,<sup>[29]</sup> with lower temperatures (below  $-35\text{ }^\circ\text{C}$ ) favouring the formation of the trimeric polymorph. Both lithium cyclotrimer and tetramer were also studied in a variety of solvents by NMR spectroscopy showing that  $(\text{LiTMP})_3$  and  $(\text{LiTMP})_4$  exist in equilibrium. Interestingly, related LDA forms an infinite helical structure in the solid state<sup>[30]</sup> (Figure 1.5c). Stalke has recently reported new insights regarding the solution constitution of LDA by DOSY NMR experiments, observing that when LDA is dissolved in toluene, equilibrium between trimeric and tetrameric aggregates (2:1 ratio) is present at room temperature. However, when cooling down the mixture higher oligomers are formed, illustrating that the lower the temperature, the more similar the solution structure is the solid-state polymer.<sup>[31]</sup>



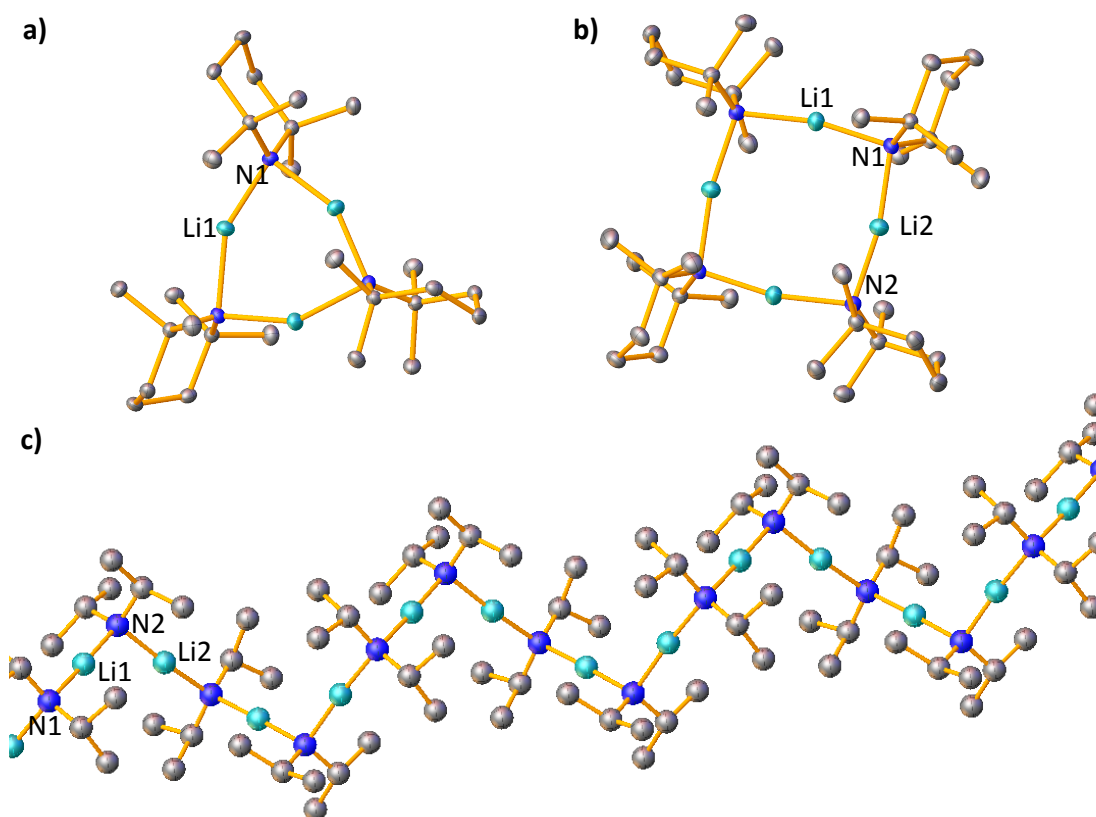


Figure 1.5: Molecular structures with 50% probability displacement ellipsoids. All hydrogen atoms have been omitted for clarity. a) Molecular structure of  $(\text{LiTMP})_3$  and b)  $(\text{LiTMP})_4$ .<sup>[29]</sup> c) Polymeric helical structure of LDA.<sup>[30]</sup>

Structural studies of alkali-metal amides of the heavier congeners sodium and potassium are much more scarce. This fact can be attributed to their higher reactivity (as they can react with common organic solvents such as THF or benzene) as well as their increasing ability to form higher oligomers, which makes the crystallization of these compounds for X-Ray crystallography more challenging.<sup>[19]</sup> Some of the heavier analogous alkali-metal amides have also been reported displaying cyclic motifs, in some cases, as shown in Figure 1.6 for NaHMDS<sup>[32,33]</sup> (although it has also been reported as a polymeric chain)<sup>[34]</sup> and KHMDS.<sup>[35]</sup>

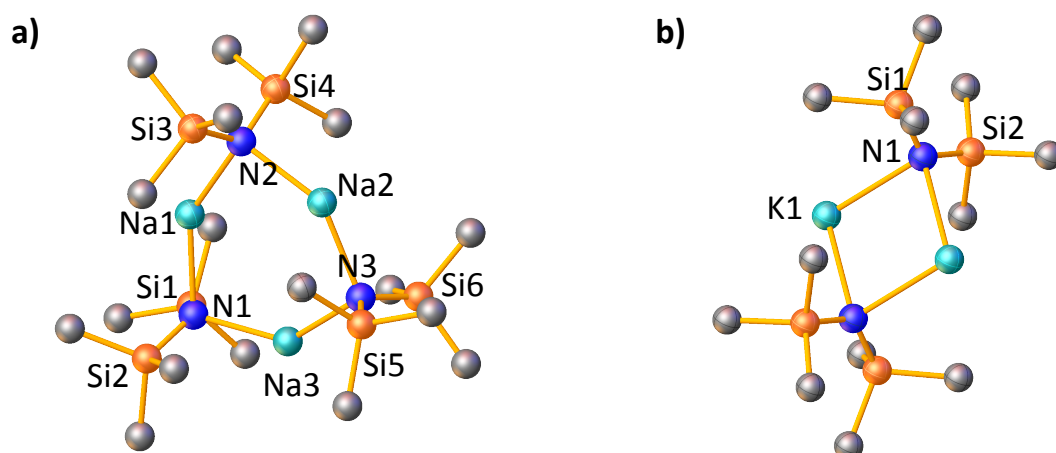


Figure 1.6: Molecular structures of a)  $(\text{NaN}(\text{SiMe}_3)_2)_3$ <sup>[33]</sup> and b)  $(\text{KN}(\text{SiMe}_3)_2)_2$ <sup>[35]</sup>. All hydrogen atoms have been omitted for clarity.

X-Ray diffraction revealed that NaHMDS can also adopt a trimeric aggregation in addition to the polymeric chain reported previously in 1977 by Atwood and Grüning.<sup>[34]</sup> Figure 1.6a shows that it can also exist as a cyclic trimer similar to the lithium homologue forming a six-membered ring. In contrast, the heavier KHMDS analogue adopts a dimeric motif forming a four-membered ring (Figure 1.6b).<sup>[35]</sup>

Other metal salts of bulky amides such as diphenylamide can crystallize with TMEDA donor.<sup>[36]</sup> As shown in Figure 1.7a, the potassium amide adopts a linear polymeric arrangement forming a four-membered  $(\text{KN})_2$  ring and stabilized by the TMEDA donor in order to complete the coordination sphere of the potassium ion.

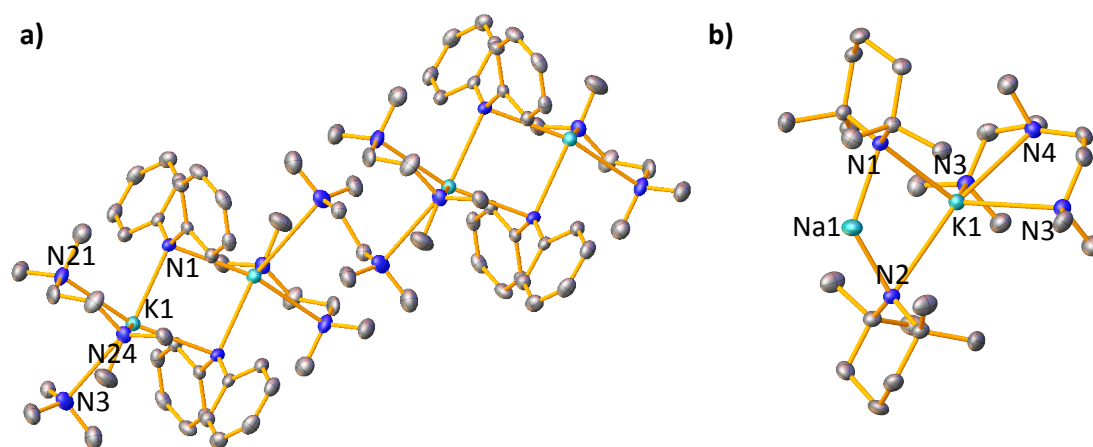


Figure 1.7: a) Structure of  $[\{(TMEDA)_{3/2}K(NPh_2)\}_\infty]^{[36]}$  and b)  $[(PMDETA)K(TMP)_2Na]^{[37]}$

Additionally, alkali-metal heterobimetallic amide bases can also be obtained.<sup>[37]</sup> An example of a mixed-metal amide is  $[(PMDETA)K(TMP)_2Na]$  using the bulky TMP amide and solvated by PMDETA donor. As Figure 1.7b shows, the bimetallic Na-K amide displays a monomeric arrangement with a four-membered  $[NaNKN]$  ring and one molecule of tridentate N-donor ligand PMDETA.

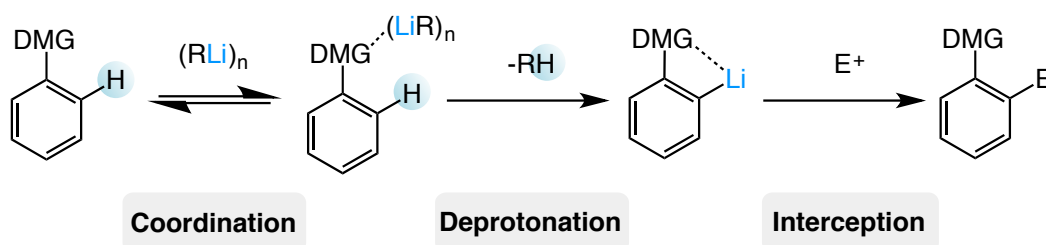
### 1.1.3 Synthetic Applications of Organoalkali-Metal Compounds

As mentioned above, alkali-metal organometallic compounds are highly reactive due to the strong polarity of the M-C bond. Amongst the wide range of polar organometallic reagents, lithium derivatives are the reagents of choice due to their greater solubility and ease of handling compared to their heavier sodium or potassium analogues.<sup>[19,21,38]</sup> Between the many applications of alkyl lithium and alkali-metal amide reagents in synthesis,<sup>[1,2]</sup> one of the most important is their use as powerful Brønsted bases to promote deprotonation reactions.

### 1.1.3.1 Deprotonative Metallation

Deprotonative metallation is one of the most recurrent synthetic methodologies for the functionalization of organic molecules.<sup>[2,39]</sup> This chemical process consists of transforming an inert C-H bond to generate more reactive C-M bond. Amongst the different reagents available, organolithiums are usually the reagents of choice.

One of the first reported precedents of the deprotonation reaction was in 1908 by Schorigin, obtaining phenylsodium when reacting diethylmercury with sodium metal in benzene.<sup>[40]</sup> In 1939 – 1940, pioneering and independent work by Wittig<sup>[41]</sup> and Gilman<sup>[42]</sup> developed the concept of Direct *ortho*-Metallation (DoM), when *ortho*-deprotonating anisole by *n*BuLi. The use of directing metallating groups (DMG) in aromatic compounds and heterocycles was exploited in the synthetic community, becoming one of the most powerful methods for regioselective deprotonation (Scheme 1.1).<sup>[43]</sup>



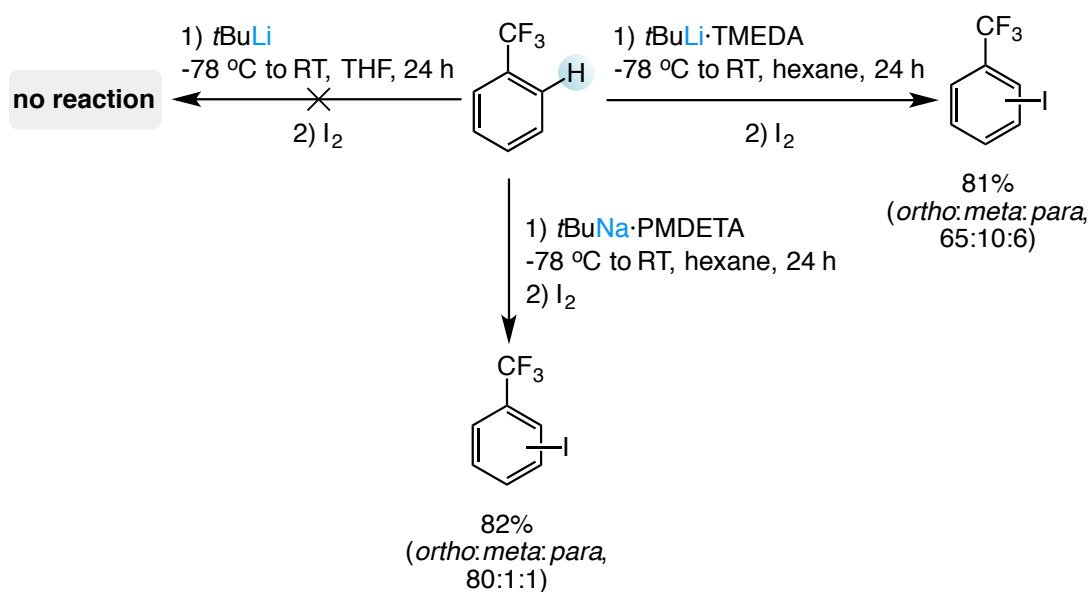
Scheme 1.1: General sequence of Directed *ortho*-Metallation (DoM) reaction.

The nature of the DMG should be unreactive towards the attack of the strong nucleophilic organometallic base, having no strongly electrophilic sites. The DMG should also have a Lewis basic coordinating site (through a necessary heteroatom) in order to establish a complex-induced proximity effect (CIPE),<sup>[44]</sup> approximating the organometallic reagent to the proton in the *ortho* position.<sup>[43]</sup> However, this

mechanism remains controversial and other effects apart from the metal coordination, such as inductive electron withdrawal and steric effects also play a key role in the formation of the product.<sup>[45–47]</sup>

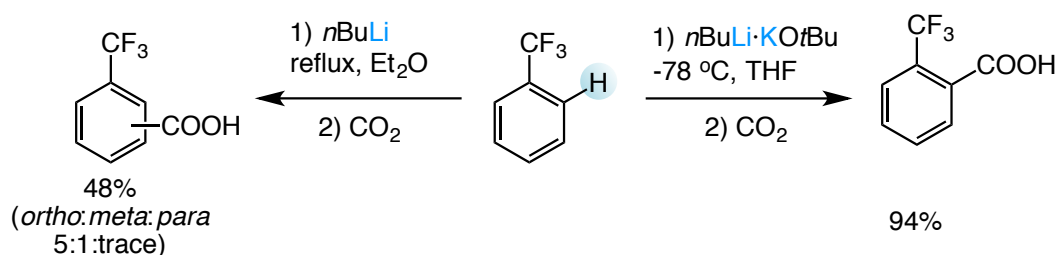
Along with their high reactivity, alkyl lithium reagents are most convenient to work because they are soluble in ether and frequently in alkanes, and many of them are commercially available.<sup>[48]</sup> Similarly, the heavier alkyl sodium and potassium analogs can also perform deprotonation reactions<sup>[49]</sup> and have a greater reactivity than alkyl lithiums. Both alkyl sodium and potassium can deprotonate benzene, although organolithiums can only deprotonate benzene in the presence of a Lewis donor, such as TMEDA (*N,N,N',N'*-Tetramethylethylenediamine) or PMDETA (*N,N,N',N'',N''*-Pentamethyldiethylenetriamine).<sup>[50]</sup> Additives such as TMEDA or potassium *tert*-butoxide can also enhance the reactivity of group 1 alkyl bases.<sup>[47,51]</sup> This sometimes translates into unique regioselectivities. As previously mentioned, Lewis donors can break the aggregates forming monomers and dimers in solution and increasing their kinetic reactivity. Similarly, mixing alkyl lithium reagents with potassium alkoxide leads to the formation of Lochmann-Schlosser superbases (LiC-KOR),<sup>[52–54]</sup> where the potassium alkoxide also decreases the aggregation state of the alkyl lithium reagent forming extremely reactive [LiKR(OR')]<sub>n</sub> species.<sup>[55]</sup>

Scheme 1.2 and Scheme 1.3 illustrate the different reactivity of different alkali-metal reagents towards the metallation of trifluoromethylbenzene. For instance, the addition of Lewis donors such as TMEDA or PMDETA with *t*BuLi or *t*BuNa (in hexane, -78 °C to room temperature for 24 hours) led to the deprotonation of trifluoromethylbenzene.<sup>[18]</sup> In contrast, *t*BuLi by itself does not undergo metallation (Scheme 1.2).



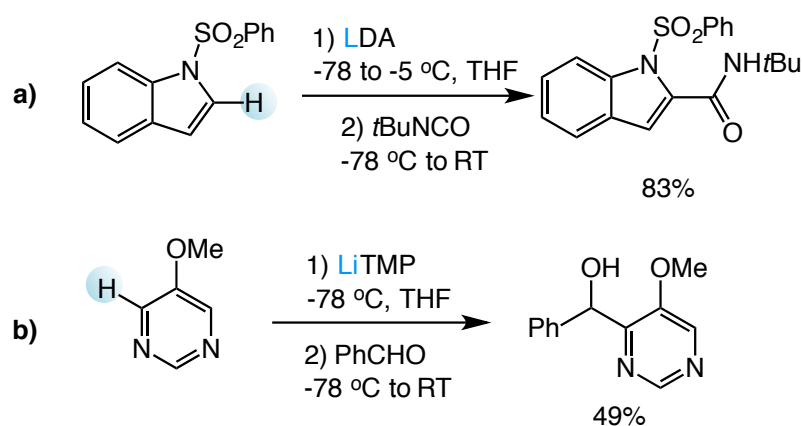
Scheme 1.2: Effect of Lewis donor additives for deprotonation of trifluoromethylbenzene using Group 1 reagents.<sup>[18]</sup>

Similarly, when  $n\text{BuLi}$  was treated with trifluoromethylbenzene, a mixture (48% yield) of the *ortho*, *meta* and *para* products (5:1:trace) were observed (using ether as a solvent and reflux conditions).<sup>[56]</sup> However, Schlosser has been able to improve the yield and regioselectivity of the same deprotonation reaction to 94% of the *ortho*-metallated product, by using the  $n\text{BuLi}\cdot\text{KO}t\text{Bu}$  superbases (THF at -78 °C).<sup>[57]</sup>



Scheme 1.3: Improvement of yield and regioselectivity with the LiC-KOR superbase.<sup>[57]</sup>

Competing with alkyl reagents, alkali-metal amides can also promote deprotonation reactions minimising competing side reactions such as nucleophilic additions,<sup>[58]</sup> due to their Brønsted basicity and poor nucleophilicity (Scheme 1.4).<sup>[20]</sup> Additionally they have a greater solubility in hydrocarbon solvents and are safer to handle than alkyl reagents. The sterically demanding alkali-metal “utility amides” 1,1,1,3,3,3-hexamethyldisilazide (HMDS), diisopropylamide (DA) and 2,2,6,6-tetramethylpiperidide (TMP) are the most commonly used by synthetic chemists.<sup>[20]</sup> Similar to alkyl reagents, mixed alkali-metal amides can also improve the selectivity of the deprotonation.<sup>[59]</sup>



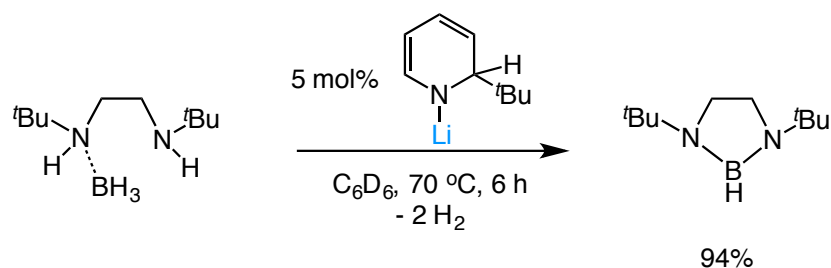
Scheme 1.4: a) and b) Examples of different reactions with alkali-metal “utility amides”.<sup>[60,61]</sup>

Although being one of the most popular reagents for deprotonation reactions in synthesis,<sup>[1,2]</sup> group 1 alkyl and amide reagents can suffer from limited selectivity and reduced functional group tolerance. This imposes in many cases the use of extremely low temperatures (-78 to -90 °C) in order to avoid competing side reactions.<sup>[39,62]</sup>

### 1.1.3.2 Alkali-Metals in Catalysis

While alkali-metal reagents are widely employed as stoichiometric reagents, their applications in catalysis remain less explored.<sup>[63]</sup> The high basic properties of s-block metals have been less exploited in catalytic processes, which started to emerge in the recent years. For instance, alkali-metal compounds such as lithium amides or sodium metal have been used in hydroamination reactions where harsh reaction conditions (more than 120 °C) are generally required.<sup>[64,65]</sup>

Breaking new ground in the field, recent studies by Hill have reported the dehydrocoupling of  $\text{Me}_2\text{NH}\cdot\text{BH}_3$  by MHMDS (M = Li, Na and K) precatalysts.<sup>[66]</sup> Furthermore, Mulvey and Robertson have introduced the use of a lithium dihydropyridine (1-lithio-2-alkyl-1,2-dihydropyridine) complex as an effective catalysts for the transformation of diamine boranes into cyclic 1,3,2-diazaborolidines (Scheme 1.5).<sup>[67]</sup>



Scheme 1.5: Dehydrogenation reaction using group 1 catalysts.<sup>[67]</sup>



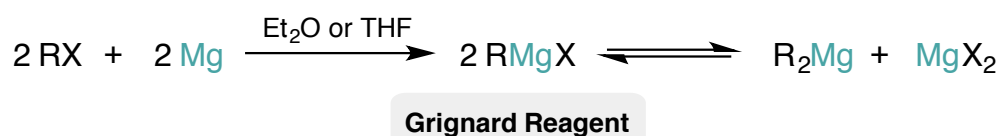
## 1.2 Group 2: Organomagnesium Chemistry

Magnesium is the 6<sup>th</sup> most abundant metal element on Earth. It is essential to life and takes an important role in photosynthesis as ATP energy source.<sup>[68]</sup> For example, a protein scaffold involving bimetallic magnesium plays a crucial role in the transfer of phosphate groups, which is an essential function of many intracellular biological enzymes.<sup>[69]</sup>

Organomagnesium reagents possess less polar metal-carbon bonds when compared with organolithium reagents, making them less reactive but offering in many cases greater levels of selectivity and a better functional group tolerance, and allowing the use of milder reaction conditions.<sup>[70]</sup>

### 1.2.1 Grignard and Turbo-Grignard Reagents

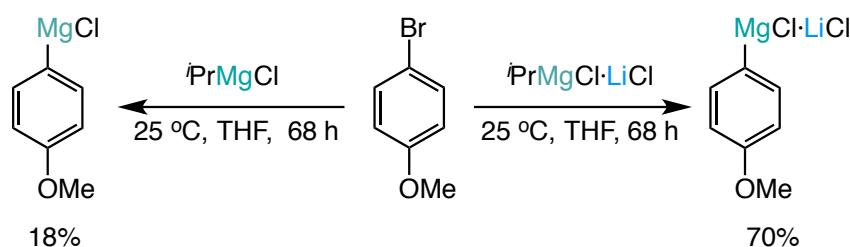
Alongside organolithium compounds, Grignard reagents are the most important and widely employed polar organometallic reagents in organic synthesis.<sup>[71]</sup> They are relatively easy to prepare by reacting magnesium metal with an organic halide compound in ether or THF solution, which facilitated their use in synthesis (Scheme 1.6). Grignard reagents, of general formula "RMgX" (R = organic group, X = halogen), were discovered by Victor Grignard in 1900. The importance of his contribution in the synthetic community was recognised very promptly and in 1912, he was awarded the Nobel Prize for Chemistry.<sup>[72,73]</sup>



Scheme 1.6: Direct synthesis of Grignard reagents via insertion into a carbon-halogen bond.



The addition of LiCl results in a dramatic improvement compared to the conventional Grignard reagents. Thus, the addition of LiCl decreases the aggregation state and therefore enhanced reactivities are achieved. For instance, Scheme 1.8 illustrates the considerable improvement of reactivity when employing Turbo-Grignard reagents. Additionally, these reagents display better solubility, regioselectivity and functional group tolerance compared to traditional Grignard reagents. Turbo-Grignard reagents were first reported in 2004<sup>[78]</sup> and are now commercially available from Sigma-Aldrich.

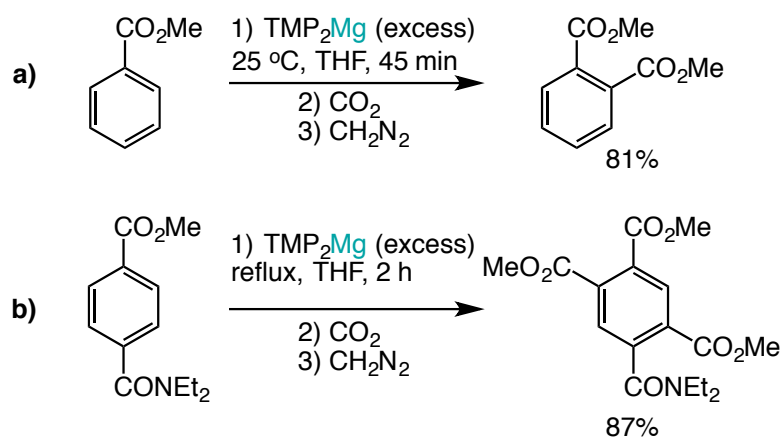


Scheme 1.8: Example of the better reactivity of a Turbo-Grignard reagent compared to a Grignard reagent.

Recently, Koszinowski and co-workers also contributed to the understanding of the effect of LiCl in Turbo-Grignards at the molecular level by analysing solutions of Grignard and Turbo-Grignard reagents in ethereal solvents.<sup>[79]</sup> By a combination of different experimental, spectrometric, and spectroscopic methods as well as quantum-chemical calculations, they have detected that both Grignard and Turbo-Grignard reagents are related via Schlenk equilibria. Additionally, anionic ate complexes can be more abundant when LiCl is added. The presence of a larger fraction of more nucleophilic and electron-rich ate complexes in the case of Turbo-Grignards explains their enhanced reactivity compared to Grignard reagents.

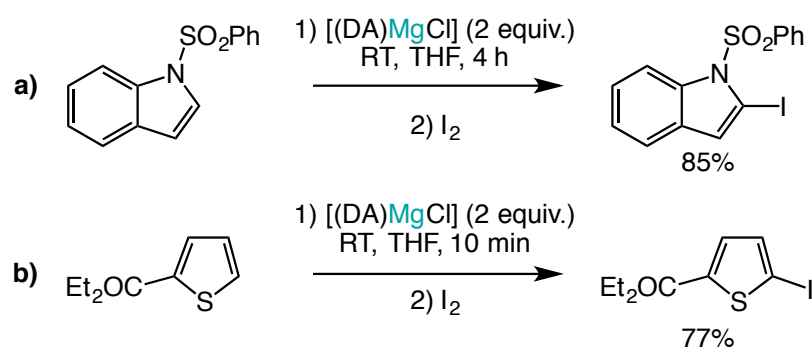
## 1.2.2 Magnesium Amides

Organomagnesium amides were first introduced in 1903 by Meunier.<sup>[80]</sup> 45 years after, Hauser and co-workers developed the use of these amido Grignard reagents (Hauser bases), with formula  $[(R_2N)MgX]$  and  $[(R_2N)_2Mg]$ , as Brønsted bases.<sup>[81]</sup> Furthermore, Eaton introduced sterically demanding amido ligands such as TMP in the Hauser bases and reported their success in *ortho*-deprotonation of aromatic compounds by using  $[(TMP)MgBr]$  or  $[(TMP)_2Mg]$  (Scheme 1.9).<sup>[82–84]</sup>



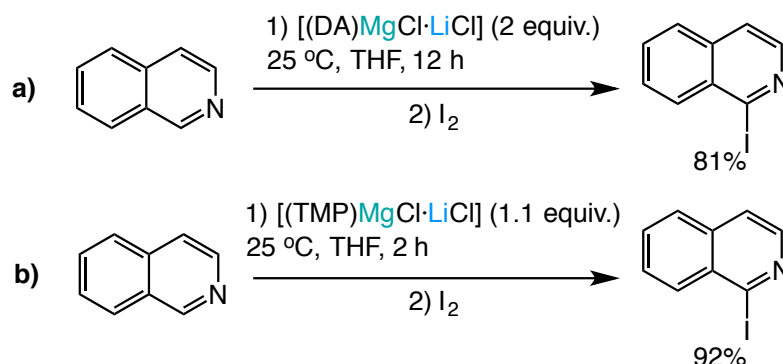
Scheme 1.9: Examples of magnesiation reactions.

Muzler expanded the scope of these regioselective magnesiations to pyridine carboxamides and carbamates by using  $[(TMP)MgCl]$  and Kondo and co-workers extended it to other heterocycles (Scheme 1.10).<sup>[85,86]</sup>



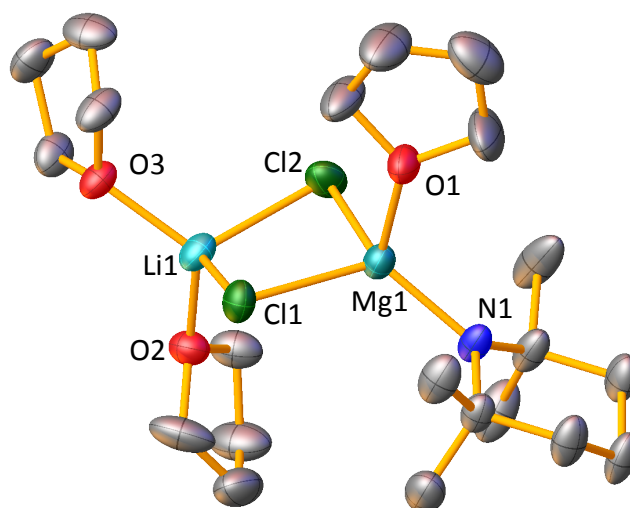
Scheme 1.10: Examples of deprotonation using the Hauser base [(DA)MgCl].

However, Hauser bases have also some limitations. They have low solubility in most organic solvents and large excess (2-12 equivalents) of the amide base and the electrophile (8-10 equivalents) are normally required in order to obtain high conversions and high reaction rates.<sup>[70]</sup> They also exhibit a weaker metallating ability compared to lithium reagents and some magnesium diamides such as [(DA)<sub>2</sub>Mg] can also react with substituents acting as reducing agents.<sup>[70]</sup> In order to overcome these limitations, LiCl-powered Hauser bases have also been developed by Knochel.<sup>[87]</sup> These Mg/Li bases, such as [(DA)MgCl·LiCl] or [(TMP)MgCl·LiCl], have excellent solubility in THF and display enhanced kinetic basicity and regioselectivity for magnesiation reactions (Scheme 1.11).



Scheme 1.11: Metallation ability of Turbo-Hauser bases.

The bimetallic constitution of [(TMP)MgCl·LiCl] (Figure 1.4) was established by Mulvey.<sup>[88]</sup> This complex adopts a monomeric arrangement, where both metals are connected by Cl anions, whereas the TMP group is coordinated terminally to magnesium. This coordination mode is proposed to be responsible of the enhanced kinetic basicity of this system, since only one bond needs to be broken to release the active base.<sup>[88]</sup>

Figure 1.8: Molecular structure of [(TMP)MgCl·LiCl] with 50% probability displacement ellipsoids. All hydrogen atoms have been omitted for clarity.<sup>[88]</sup>

Hauser and Turbo-Hauser bases have also been studied in solution. Advanced NMR studies (including DOSY) and structural studies by Mulvey have shed some light on the contribution of these reagents, which have aided to rationalize their unique reactivity.<sup>[88,89]</sup> Further contribution to this field by applying a recently new DOSY method considering external calibration curves (ECC), has provided a more accurate approximation of the aggregation state of these species in solution.<sup>[77,90]</sup> These solution studies suggested that the TMP ligand in [(TMP)MgCl·LiCl] is bulky enough to prevent dimerisation and a monomeric aggregation related to that of the solid state is suggested in solution (Figure 1.9).

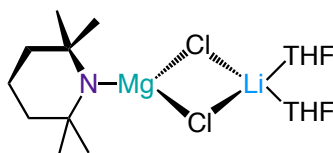


Figure 1.9: Suggested structure of [(TMP)MgCl·LiCl] in solution.<sup>[90]</sup>

As illustrated in Scheme 1.11, [(TMP)MgCl·LiCl] base has an enhanced reactivity over [(DA)MgCl·LiCl] base, which has a lower solubility in THF and requires longer times and higher amounts of base to complete the magnesiation reaction. Solid and solution studies of both species have reflected this different reactivity pattern. While [(TMP)MgCl·LiCl] is a monomer in THF solution<sup>[90]</sup> and solid state,<sup>[88]</sup> [(DA)MgCl·LiCl] is a dimer in the solid state<sup>[89]</sup> and forms different dimeric aggregates in solution.<sup>[77]</sup>

### 1.2.3 Sterically Demanding Ligands In Group 2: $\beta$ -diketiminate Ligands

In recent years, advances in the preparation of complexes containing sterically demanding ligands have been key for new advances in synthesis. Bulky ligands provide steric and sometimes electronic protection, where a wide variety has been

developed over the years and some of the most common are displayed in Figure 1.10.<sup>[91]</sup>

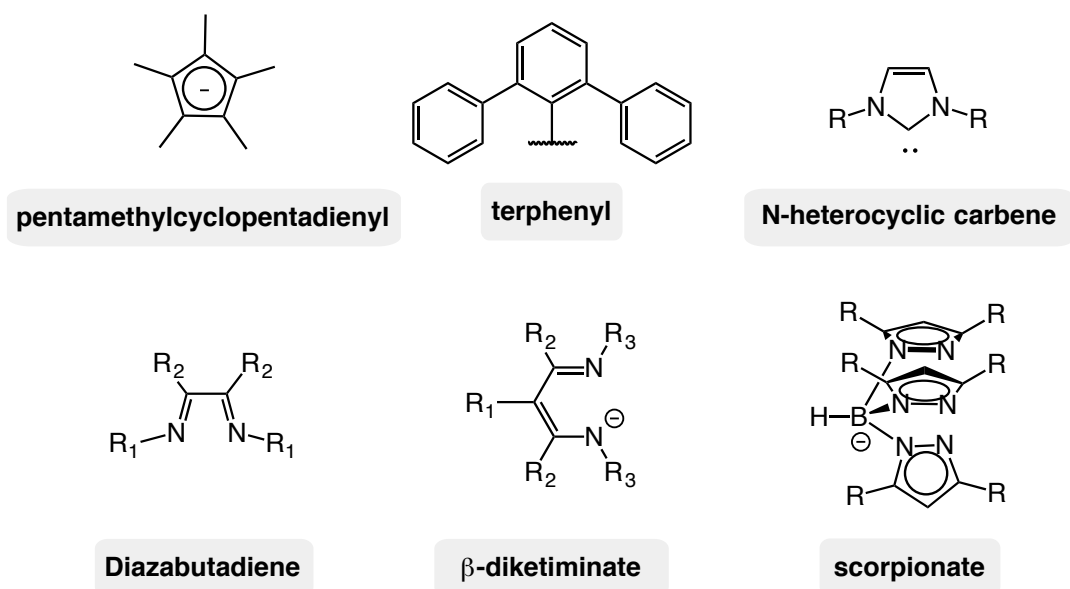


Figure 1.10: Examples of some sterically demanding ligands.

The versatile bidentate  $\beta$ -diketiminato ligands, commonly referred as “Nacnac”, are one of the most widespread systems in coordination chemistry. The  $\beta$ -diketiminato metal complexes can include metal centres of different oxidation states from across the different groups of the periodic table.<sup>[92,93]</sup> The bulky scaffold offers steric protection to the metal and in most situations acts as an spectator ligand, although in some cases it can also participate in some reactivity.<sup>[94]</sup>  $\beta$ -diketiminato ligands offer several opportunities for functionalization, possessing up to three different tuneable sites (Figure 1.11). By varying the different substituents, new steric and electronic properties can be offered,<sup>[95–97]</sup> where the  $\beta$ -C and N-aryl *ortho* substituents play an important role for steric effects and the  $\alpha$ -C and  $\beta$ -C positions are more influential for electronics.<sup>[95]</sup>



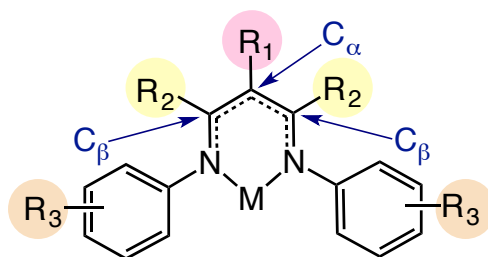


Figure 1.11: Substituent patterns in  $\beta$ -diketiminato scaffold.

Alkaline-earth metals supported by a  $\beta$ -diketiminato ligand have been widely employed in the recent years with many applications in synthesis of new compounds and in catalytic processes.<sup>[92,98–100]</sup> One of the most remarkable recent discoveries is the stabilisation of a dimeric Mg(I) complex, containing a covalent Mg(I)-Mg(I) bond and supported by a sterically demanding  $\{\text{D}^{\text{iPP}}\text{Nacnac}\}$  ligand ( $\text{D}^{\text{iPP}}\text{Nacnac} = \text{Ar}^*\text{NC}(\text{Me})\text{CHC}(\text{Me})\text{NAr}^*$ ;  $\text{Ar}^* = 2,6\text{-}i\text{-Pr}_2\text{-C}_6\text{H}_3$ ) (Figure 1.12).<sup>[101]</sup>

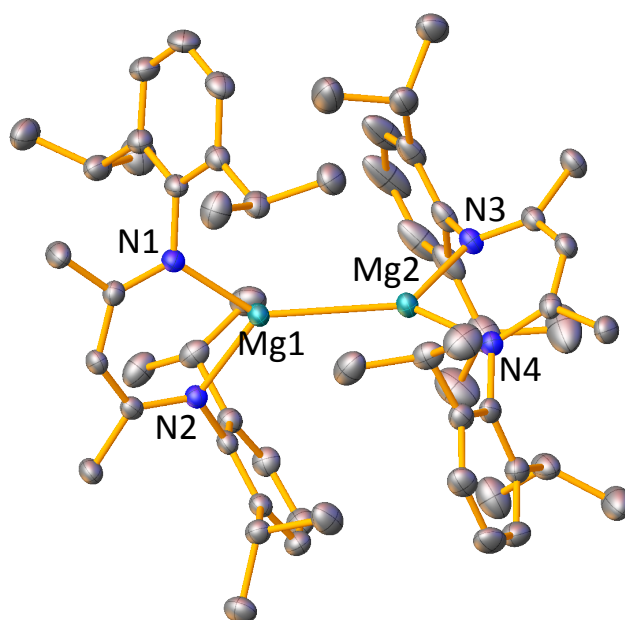
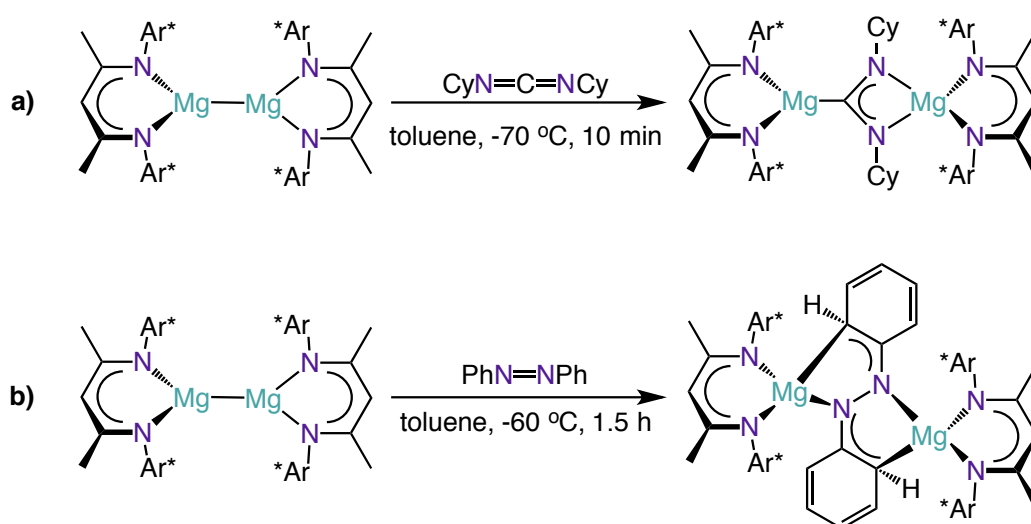


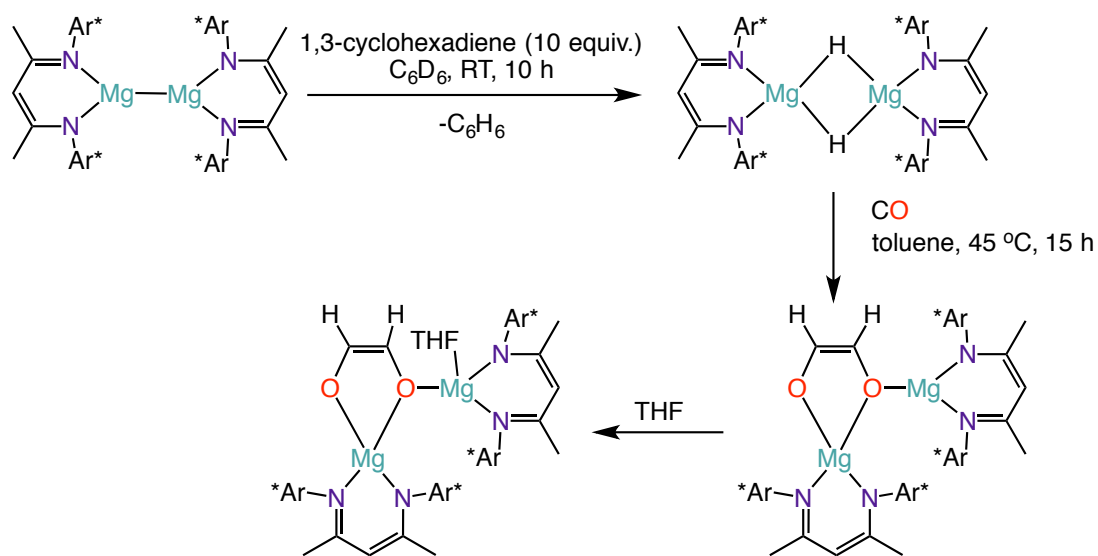
Figure 1.12: Molecular structure of  $[\text{D}^{\text{iPP}}\text{NacnacMg}]_2$  with 50% probability displacement ellipsoids. All hydrogen atoms have been omitted for clarity.<sup>[101]</sup>

From the isolation of this Mg(I) complex, the stabilisation of other Mg(I) dimers have emerged bearing a variety of  $\beta$ -diketiminato ligands with different steric bulk and denticity.<sup>[97]</sup> Additionally, the stabilisation of this new family of Mg(I) complexes has been key to recent breakthroughs in synthesis. For instance,  $[\text{DippNacnacMg}]_2$  can form stable dimeric adducts with different Lewis bases such as THF, dioxane or DMAP (DMAP = 4-Dimethylaminopyridine).<sup>[102]</sup> Furthermore, these magnesium (I) compounds have proved to be very effective as reducing agents for example of N-/O-functionalised unsaturated organic substrates such as carbodiimide,  $\text{CyN}=\text{C}=\text{NCy}$  (Cy = cyclohexyl), or azobenzene (Scheme 1.12).<sup>[101,103]</sup>



Scheme 1.12: Example of  $[\text{DippNacnacMg}]_2$  complex acting as reductant of unsaturated organic substrates.<sup>[101–103]</sup>

Notably, activation of CO has also been explored.<sup>[104]</sup> Hydrogenation of  $[\text{DippNacnacMg}]_2$  dimer by an excess of the transfer hydrogenation reagent 1,3-cyclohexadiene leads to the formation of the magnesium (II) hydride  $[\text{DippNacnacMg}(\mu\text{-H})]_2$  quantitatively at room temperature. Further exposure to CO at  $40\text{--}50^\circ\text{C}$  forms the C-C coupled product as shown in Scheme 1.13.

Scheme 1.13: CO activation reaction.<sup>[104]</sup>

Different applications illustrating the stabilizing power of the  $\beta$ -diketiminate ligand have also emerged. For example, Harder reported a multinuclear magnesium hydride cluster  $[Mg_8H_{10}]^{6+}$  stabilised by 3 bridging bis-( $\beta$ -diketiminate) ligands that shows complete hydrogen/desorption at 200 °C (see figure Figure 1.13),<sup>[105]</sup> and the recent development of  $\beta$ -diketiminate stabilised kinetically activated magnesium bases can also promote direct Mg–H exchange towards 1,3-benzoxazoles.<sup>[106]</sup>

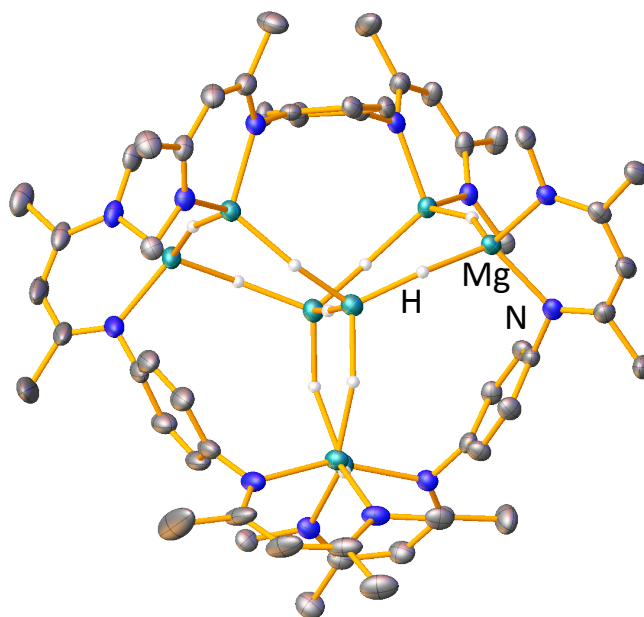
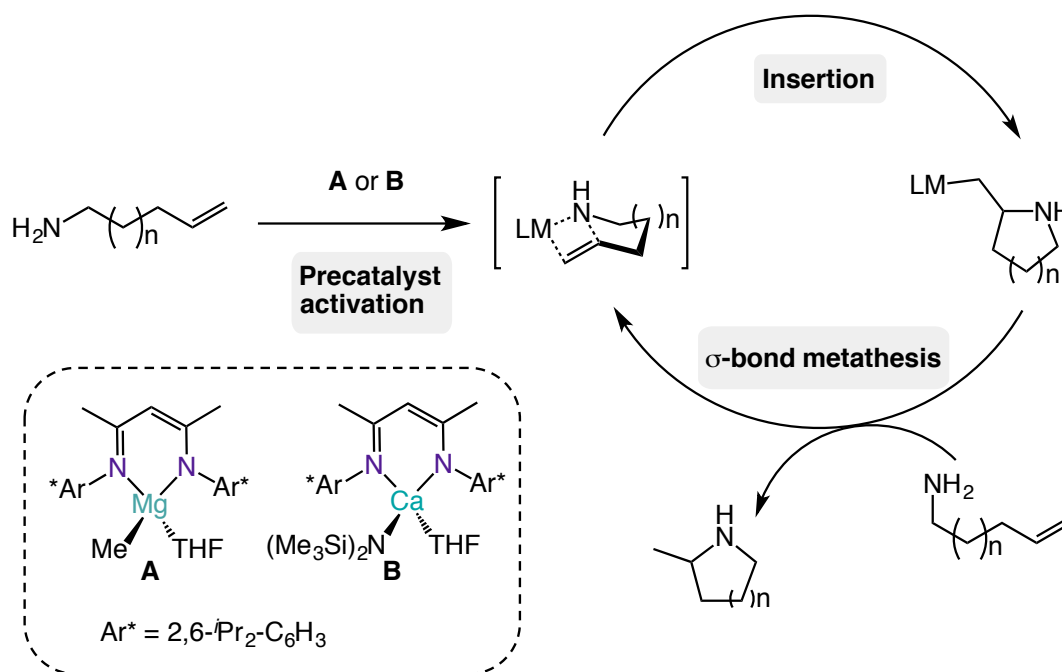


Figure 1.13: Molecular structure of Magnesium hydride cluster  $[\text{Mg}_8\text{H}_{10}]^{6+}$  stabilised by 3 bridged bis-( $\beta$ -diketiminate) ligands with 50% probability displacement ellipsoids. Some hydrogen atoms and the aryl substituents have been omitted for clarity.<sup>[105]</sup>

Furthermore, the extension of  $\beta$ -diketiminate compounds to magnesium's heavier congeners calcium, strontium and barium has also been explored.<sup>[63,92,98,107]</sup> Interestingly, the design of calcium hydride complexes stabilized by  $\beta$ -diketiminate ligands has been achieved.<sup>[108]</sup>

$\beta$ -diketiminate complexes can also act as successful catalysts in a myriad of reactions. The steric bulk of the  $\beta$ -diketiminate anionic ligand restricts the coordination to the metal, facilitating only one site towards reactivity while avoiding at the same time the formation of high aggregates. Additionally, it stabilises the intermediates facilitating their isolation in order to provide mechanistic information.<sup>[109]</sup> Magnesium  $\beta$ -diketiminate complexes have proved to be active initiators towards the polymerisation of *rac*-lactide<sup>[110–112]</sup> and Hill and co-workers

have shown a wide scope of catalytic reactions where magnesium  $\beta$ -diketiminato complexes act as efficient precatalysts for different processes such as hydroboration<sup>[113–115]</sup> or hydroamination reactions (Scheme 1.14).<sup>[116,117]</sup>



Scheme 1.14: Generalized postulated catalytic cycle for magnesium or calcium-mediated intramolecular hydroamination reaction.<sup>[117]</sup>

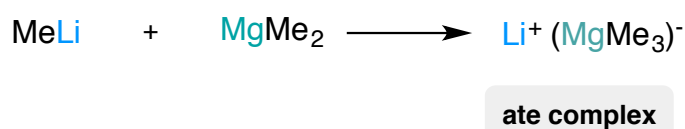
Scheme 1.14 illustrates the suggested catalytic cycle for intramolecular hydroamination processes catalysed by  $\beta$ -diketiminato magnesium or calcium complexes. Furthermore, the heavier calcium  $\beta$ -diketiminato complexes can also act as active catalysts for intramolecular hydroamination reactions<sup>[117,118]</sup> between other catalytic processes.<sup>[63,107,119]</sup>

Despite all the diverse applications of  $\beta$ -diketiminato magnesium complexes, their potential as metallating reagents has hardly been explored. Our group has recently introduced this new synthetic application by developing a magnesium complex that

combines a basic TMP group and a sterically demanding ligand  $\beta$ -diketiminato, [<sup>Dipp</sup>NacnacMg(TMP)], which can promote deprotonation reactions of 1,3-benzoazoles.<sup>[106]</sup>

## 1.3 Ate Compounds

An “ate” complex is a heterobimetallic entity composed of a cationic and anionic moiety contacted or separated depending on the system.<sup>[120]</sup> In general terms, these complexes are formed by pairing an organoalkali-metal reagent (generally lithium, sodium or potassium) with another organometallic reagent with a less polar M-C bond (such as magnesium or zinc) (Scheme 1.15).<sup>[12,72]</sup>



Scheme 1.15: Formation of a lithium magnesiate.

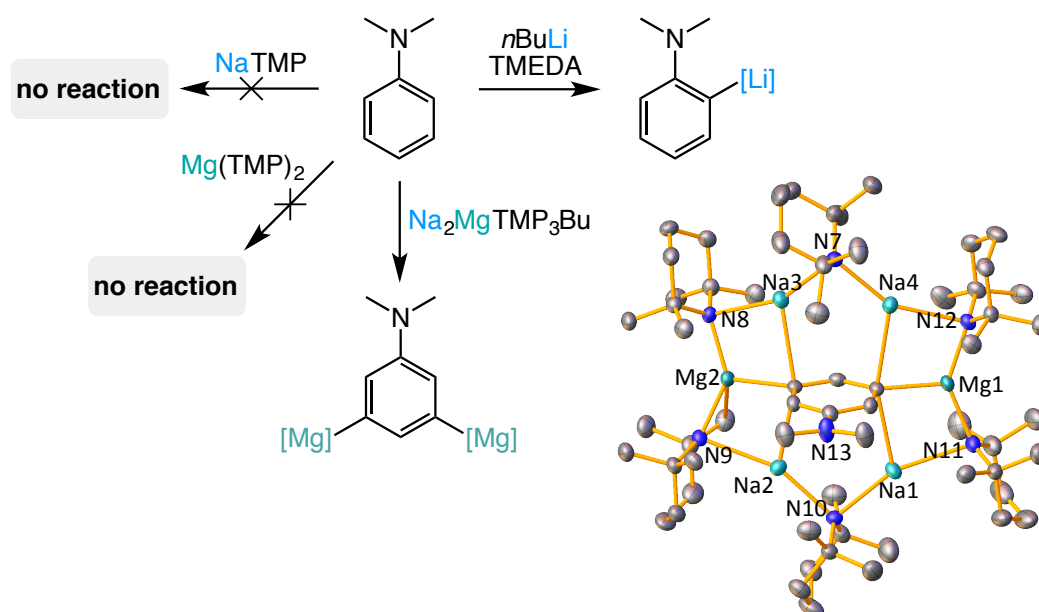
These compounds present a unique structure and chemistry, especially in metallation reaction where ates enable lots of improvements. Although the understanding of this chemistry is relatively new, the first zincate  $\text{NaZnEt}_3$  was synthesized in 1858 by Wanklyn.<sup>[121]</sup> Alkali metal magnesiates, zincates and aluminates in particular have been used with a great success in deprotonative metallation of for example challenging aromatic substrates.<sup>[48]</sup>

### 1.3.1 Alkali-Metal Magnesiates

Firstly prepared by Wittig,<sup>[122]</sup> alkali-metal magnesiates have emerged as a powerful family of organometallic reagents, which can participate in several cornerstone organic transformations.<sup>[120,123]</sup>

By switching on cooperative effects, these heterobimetallic reagents can exhibit enhanced reactivities and unique selectivities, which cannot be replicated by their

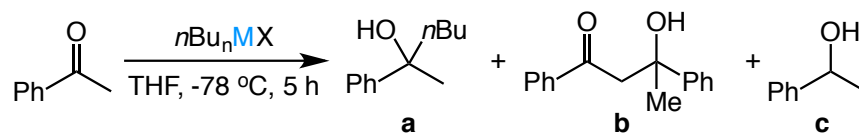
homometallic components. For instance, O'Hara and Mulvey have shown that dimethylaniline can be selectively *meta-meta* deprotonated by mixed-metal  $\text{Na}_2\text{Mg}(\text{TMP})_3\text{Bu}$  base, whereas both  $\text{NaTMP}$  or  $\text{Mg}(\text{TMP})_2$  fail to deprotonate this substrate. This is an unprecedented regioselectivity, which overcomes the long standing concept of directed *ortho*-metallation previously explained.<sup>[124]</sup>



Scheme 1.16: Summary of the metallating power of magnesiates. X-Ray structure of the *meta-meta* metallation of anisole by mixed-metal magnesiate base.<sup>[124]</sup>

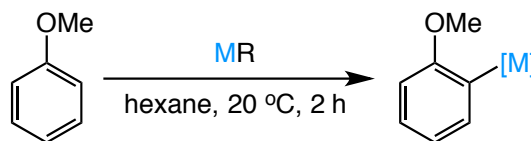
Alkali-metal magnesiates have found widespread applications, not only in deprotonative metallation chemistry,<sup>[48]</sup> but also in other fundamental organic processes such as metal-halogen exchange<sup>[78]</sup> and nucleophilic alkylation of ketones.<sup>[125]</sup> For instance, homoalkyl lithium magnesiates  $\text{LiMgR}_3$  have been used by Ishihara to promote alkylation of ketones, showing enhanced reactivities and chemoselectivities than single metal components of the magnesiate, as shown in Table 1.1 for the reaction of  $\text{LiMgBu}_3$  and acetophenone.<sup>[125]</sup>



Table 1.1: Addition to acetophenone with Li- or Mg- alkyl reagents.<sup>[125]</sup>

Entry	$n\text{-Bu}_n\text{MX}$	a	b	c
1	$n\text{BuLi}$	62	7	0
2	$n\text{BuMgCl}$	50	9	8
3	$n\text{Bu}_2\text{Mg}$	48	27	20
4	$n\text{Bu}_3\text{MgLi}$	82	0	0

Furthermore, recent studies by our group have established the excellent metallating ability of potassium homo-alkyl reagents.<sup>[126]</sup> By introducing the monosilyl  $\text{CH}_2\text{SiMe}_3$  group these compounds display enhanced solubility in hydrocarbon solvents and they are more stable than other C-base alkyl groups such as  $n\text{Bu}$  or  $t\text{Bu}$ .<sup>[127]</sup>

Table 1.2: Metallation of anisole using different alkyl Li, Na and K Mg reagents.<sup>[126]</sup>

Entry	MCH <sub>2</sub> SiMe <sub>3</sub>	Yield (%)
1	Mg(CH <sub>2</sub> SiMe <sub>3</sub> ) <sub>2</sub>	0
2	KCH <sub>2</sub> SiMe <sub>3</sub>	20
3	KMg(CH <sub>2</sub> SiMe <sub>3</sub> ) <sub>3</sub>	15
4	(PMDETA) <sub>2</sub> K <sub>2</sub> Mg(CH <sub>2</sub> SiMe <sub>3</sub> ) <sub>4</sub>	99
5	(TMEDA) <sub>2</sub> Li <sub>2</sub> Mg(CH <sub>2</sub> SiMe <sub>3</sub> ) <sub>4</sub>	5
6	(TMEDA) <sub>2</sub> Na <sub>2</sub> Mg(CH <sub>2</sub> SiMe <sub>3</sub> ) <sub>4</sub>	10
7	(PMDETA) <sub>2</sub> K <sub>2</sub> Mg(CH <sub>2</sub> SiMe <sub>3</sub> ) <sub>4</sub> +18-crown-6	0

As shown in Table 1.2 the higher-order magnesiate (Table 1.2, entry 4) proved to be an excellent magnesiating reagent in comparison to the lower-order congener or the KCH<sub>2</sub>SiMe<sub>3</sub> (Table 1.2, entries 2 and 3). Additionally, a dramatic alkali-metal effect is disclosed obtaining very low yields when the reaction is performed using the Li and Na higher-order magnesiate analogues. These studies have shown that higher order (or tetraorgano) potassium magnesiates [(PMDETA)<sub>2</sub>K<sub>2</sub>Mg(CH<sub>2</sub>SiMe<sub>3</sub>)<sub>4</sub>] can promote direct magnesiation of a wide range of cyclic molecules in excellent yields.

Related to this family of mixed-metal reagents triorgano (lower-order) sodium magnesiate [NaMg(CH<sub>2</sub>SiMe<sub>3</sub>)<sub>3</sub>]<sup>[128]</sup> has demonstrated excellent catalytic capabilities to promote hydroamination/cyclotrimerization processes of isocyanates and guanylation of amines.<sup>[129,130]</sup> Other reports using potassium calcates such as

[K<sub>2</sub>Ca(NPh<sub>2</sub>)<sub>4</sub>] or [K<sub>2</sub>Ca{(N(H)Dipp)}<sub>4</sub>], have also demonstrated catalytic ability towards hydroamination reactions of diphenylbutadiyne with a variety of anilines in contrast of their single-metal counterparts Ca(NPh<sub>2</sub>)<sub>2</sub> and KNPh<sub>2</sub>.<sup>[131–134]</sup> Further discussion of the catalytic activity of these reagents will be disclosed in Chapter 3.

## 1.4 Aims and Structure of this Thesis

Building on recent advances in s-block chemistry, the main aim of the thesis is to exploit cooperative effects for Group 1 and Group 2 organometallic systems to develop new applications in synthesis and catalysis. While some of these systems are mixed-metal complexes, which enables metal-metal cooperativity (Chapter 3), a main focus of the thesis is to explore metal-ligand and ligand-ligand cooperative effects in single metal systems. This include the use of group 1 alkyl compounds combined with several donors as precatalyst in intramolecular hydroamination complexes (Chapter 2) as well as designing new Mg platforms to promote deprotonative metalation (Chapter 4) and C-F bond activation processes (Chapter 5). The latter complexes combine a highly sterically demanding  $\beta$ -diketiminato ligand ( $^{\text{Dipp}}\text{Nacnac}$ ) with a highly reactive anionic group (amide TMP or Bu group). In these systems the  $\beta$ -diketiminato ligand can act as steric stabilizer providing shelter for the highly reactive anions generated in the metallation processes.

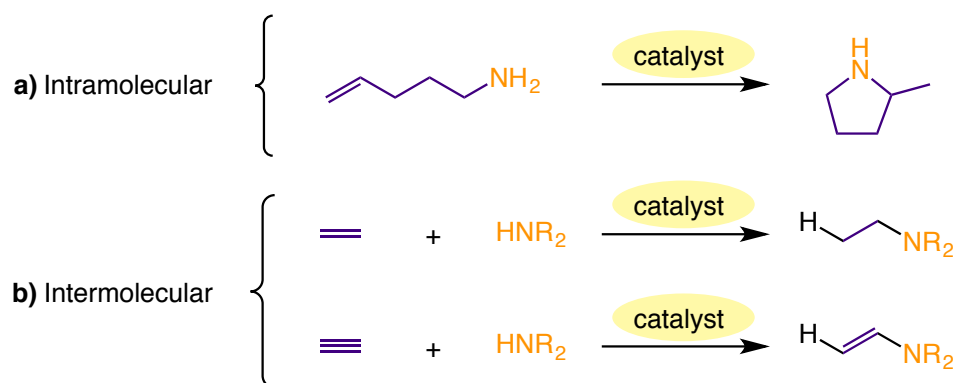
s-Block organometallics are starting to gather momentum in catalysis, with the vast majority of studies focussing on heavier alkaline-earth metals (i.e. Ca, Ba, Sr). This thesis opens new ground in this evolving field by assessing the catalytic applications of group 1 complexes as well as those of alkali-metal magnesiate complexes for challenging intermolecular hydroamination processes of alkenes and alkynes. Using mixed-metal systems, new insights into s-block cooperative catalysis have been gained, including a greater understanding on the role of each metal during the hydroamination process.

# Chapter 2    Group    1    Metal-Catalysed Intermolecular Hydroamination Reactions

## 2.1 Introduction

### 2.1.1 Intermolecular Hydroamination Reactions

Hydroamination reactions can be described as the addition of a N-H fragment across an unsaturated C-C bond. They constitute one of the most powerful atom-efficient and waste-minimized methodologies to access amines in organic synthesis.<sup>[64,135–139]</sup> These nitrogen-containing species have a great importance as lead structures among numerous pharmaceuticals, biological systems, natural products and industrially basic and fine chemicals.<sup>[140–143]</sup> However, the high kinetic hurdle of these processes imposes in most cases the use of metal catalysts (Scheme 2.1).<sup>[144,145]</sup>



Scheme 2.1: Hydroamination reactions via a) intramolecular or b) intermolecular.

Despite their high synthetic value, hydroamination reactions have found significant interest only over the last two decades, where the use of transition-metal catalytic systems such as rhodium, ruthenium, titanium or palladium have seen significant progress due to their good tolerance of polar functional groups.<sup>[146,147]</sup> Pioneering work by the groups of Hill and Harder have revealed that alkaline-earth metal complexes can also act as catalysts, being a cheaper and more sustainable synthetic alternative.<sup>[116,148,149]</sup> Particularly, those of the heavier elements (calcium and strontium) can show excellent catalytic capabilities,<sup>[148]</sup> not only in intramolecular processes but also in the more experimentally challenging intermolecular hydroamination reactions.<sup>[63,116]</sup> Alkaline-earth metal complexes can facilitate these reactions under relatively mild conditions.<sup>[116,118,149]</sup> For example, heavier alkaline-earth amides such as  $[\text{Sr}\{\text{N}(\text{SiMe}_3)_2\}_2]_2$  can catalyse the hydroamination reaction of styrene and piperidine at 60 °C in 5 hours obtaining a 79% yield. Work by Hill or Carpentier and Sarazin have also disclosed that the catalyst activity increases when the ionic radius of the metal is bigger,<sup>[116,150]</sup> the same effect that has been observed in organolanthanide(III) hydroamination catalysis, which has been extensively studied by Marks.<sup>[135,151,152]</sup> Interestingly, the use of alkali-metal based catalysts has hardly been explored, although some work using alkali-metal catalysts

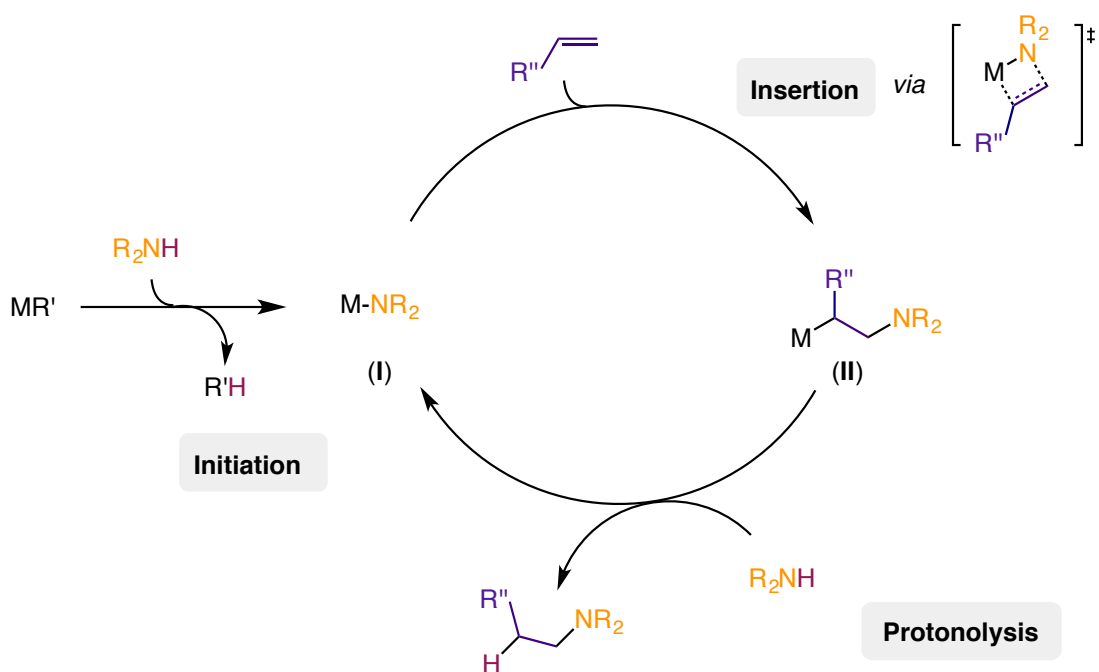
such as *sec*-BuLi or Na metal has been known since the 1950's.<sup>[64,145,153–157]</sup> Alkali-metal catalysed hydroamination reactions impose harsh reaction conditions such as high temperatures (reaction of piperidine and styrene requires 130 °C using sodium metal as catalyst, for example) and poor mechanistic understanding is provided.<sup>[64,155–157]</sup> Recent reports using LiN(SiMe<sub>3</sub>)<sub>2</sub> or KOtBu precatalysts have improved the yields of these reactions using alkali-metal catalysts, although high temperatures (100 - 120 °C) are still required.<sup>[65,140]</sup> Moreover, the gap in studies using the heavier alkali-metal derivatives (sodium and potassium) as catalysts, is particularly surprising considering the greater nucleophilicity compared to the analogous lithium complexes. Previous report by Galle in 1980's has shown the greater activity of sodium and potassium diethylamides compared to the lithium analogue for hydroamination of ethylene.<sup>[156]</sup> In these studies, higher reaction rates are obtained for the heavier metal sodium and potassium complexes under similar conditions (1 mol% at 45 °C), however, these heavier alkali-metal dialkylamide catalysed reactions decrease in rate after 25% conversion due to decomposition of the catalyst.

Multiple efficient catalysts have been reported for intra- and intermolecular hydroamination, while the intermolecular process has been studied just for alkynes. From a thermodynamic perspective, intermolecular hydroamination reactions are more entropically demanding than the cyclisation of aminoalkene and aminoalkyne processes.<sup>[136,152]</sup> The reactivity of the unsaturated fragment decreases from alkyne > allene ≈ diene > vinylarene >> unactivated alkene, making the intermolecular hydroamination of simple alkenes the most challenging type of reaction.<sup>[135,139]</sup>

These intermolecular processes using s-block catalysts seem to operate via activation of the amine rather than activation of the alkene or alkyne, similarly to lanthanide catalysts.<sup>[64,65]</sup> The metal-carbon amido  $\sigma$ -bonds formed, are typically

very reactive, contrary to late transition-metals.<sup>[135]</sup> Furthermore, their high basicity can provide side reactions, such as alkene isomerization,<sup>[158]</sup> and many of these compounds are extremely air and moisture sensitive, which can complicate their manipulation.<sup>[63]</sup>

In contrast to transition-metals, alkali and alkaline-earth metal catalysts can not operate via oxidative addition or reductive elimination. DFT (density functional theory) studies performed by Hill<sup>[149]</sup> and Hultzsch,<sup>[65]</sup> suggested the formation of the hydroamination products via metal-amide intermediate species (Scheme 2.2).



Scheme 2.2: Base-catalyzed amination via metal amide species.

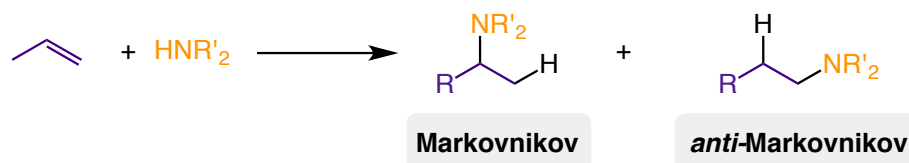
The mechanism proposed in Scheme 2.2 is widely accepted for group 1<sup>[65]</sup> and 2 metals.<sup>[144,149,159]</sup> The initiation or the catalyst activation step consists of the deprotonation of the amine and the formation of a nucleophilic metal-amide intermediate. (Scheme 2.2) The chosen precatalyst is important not only for its own



stability, but also in terms of favouring this deprotonative step towards the formation of the amide compound. In these studies using s-block catalysts, this first step has generally been found to be fast and exothermic, having a minimal effect on the reaction rate of the hydroamination process, while contrastingly, the insertion of the unsaturated organic molecule in the M-N bond tends to be the rate-determining step. The amide intermediate (I) formed needs to be strongly nucleophilic to favour the addition of the unsaturated bond in the insertion process. This nucleophilic addition proceeds via a transition state formed via a highly polarized four membered ring,<sup>[116]</sup> forming an intermediate (II), which now presents a M-C bond. The activation energy for the insertion step is large and the intermediate formed is highly reactive and forms the product immediately upon protonation by the starting amine. In the final step of the catalytic cycle the final product is formed and regeneration of the active nucleophilic species takes place.

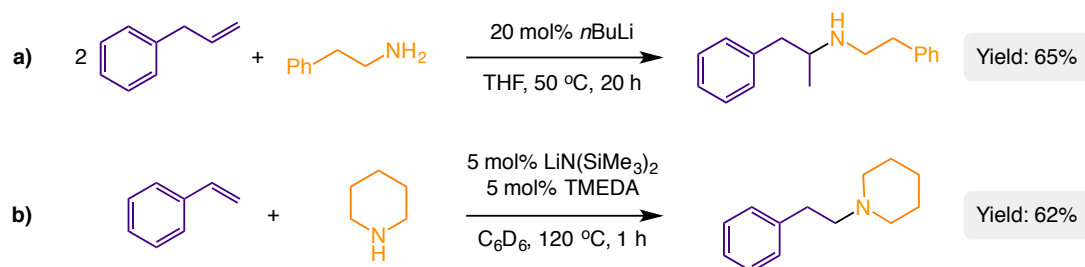
In intermolecular hydroamination reactions, the design of the catalyst plays an important part facilitating the amine deprotonation to give the amide intermediate (I), which should be nucleophilic enough to insert into the unsaturated bond. As previously mentioned, computational and experimental studies using alkaline-earth catalysts, have shown that the hydroamination reaction tends to proceed at lower rates with decreasing metal ionic radius. These studies, provided lower activation barrier values ( $\Delta G = 16.7$  and  $8.6$  kcal/mol in the insertion and protonolysis step respectively) in the Ca-based cycle compared to Mg ( $\Delta G = 21.0$  and  $19.8$  kcal/mol in the insertion and protonolysis step respectively).<sup>[116]</sup> Assessing the important role of the metal in intramolecular hydroamination reactions, recent studies by Harder have proved the important role of a Lewis acidic metal in order to activate the unactivated C=C bonds. In contrast, hydroamination reactions of more activated bonds such as C=O or C=N, can form the new amine product by using the metal-free catalysts:  $[\text{Ph}_2\text{N}^-][\text{Me}_4\text{N}^+]$  and  $[\text{Ph}_3\text{C}^-][\text{Me}_4\text{N}^+]$ .<sup>[144]</sup>

In general, the addition of amines to olefins can provide two products: the Markovnikov and the *anti*-Markovnikov products, a process controlled by reaction kinetics and thermodynamics, and factors such as the structure of the intermediate catalyst can determine the regioselectivity of the reaction (Scheme 2.3).<sup>[145]</sup>



Scheme 2.3: Intermolecular hydroamination reaction.

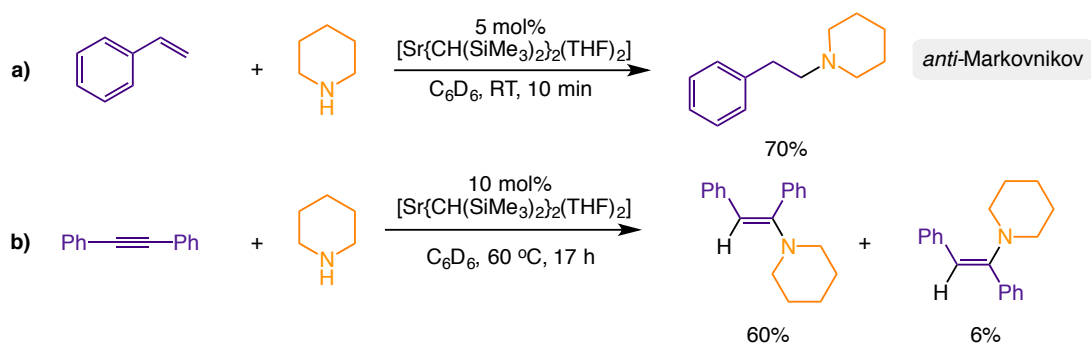
While in most cases Markovnikov selectivity is observed, a significant amount of research efforts have focussed on the design of systems that can promote the formation of the *anti*-Markovnikov products, which is recognised as one of the main challenges in the field.<sup>[64]</sup> In alkali-metal catalysts, Markovnikov products are normally formed when short-chain aliphatic olefins are reacted due to the higher stability of the carbocation intermediate. Contrastingly, *anti*-Markovnikov product appears to be favoured with aryl olefins due to the better stability of the benzylic anion intermediate formed compared to the Markovnikov analogue. (Scheme 2.4).<sup>[64,65,145]</sup>



Scheme 2.4: Example of the formation of Markovnikov<sup>[60]</sup> and *anti*-Markovnikov<sup>[65]</sup> hydroamination products.

This *anti*-Markovnikov regioselectivity is determined by the insertion step, through the formation of a more stable transition states, due to the interaction between the metal and the aromatic ring of the vinylarene or aromatic alkynes, and also the resonance stabilization of the generated benzyl carbanion.<sup>[65]</sup>

The intermolecular hydroamination of alkynes is generally viewed as being easier than that of alkenes because of the higher reactivity and electron density of the triple carbon bonds. However, there is also a steric effect to consider that could also be an impediment to the addition.<sup>[149]</sup> Reactions of unsymmetric internal alkynes are more challenging because of the formation of two products and terminal alkynes are in general more reactive than their internal analogues.<sup>[135]</sup>



Scheme 2.5: Examples of intermolecular hydroamination reactions.

Examples on the hydroamination reaction of styrene and diphenylacetylene with piperidine are shown in Scheme 2.5 using a Sr alkyl as a catalyst. In this case the reaction with diphenylacetylene is significantly slower, which is rationalised in terms of the greater steric congestion in the alkyne.

Identifying a gap in the ability of alkali-metal catalysts towards hydroamination of olefins and the harsh reaction conditions usually required (over 100 °C and long reaction times<sup>[65,140,153]</sup>), the aim of this chapter is to expand the knowledge of

intermolecular hydroamination processes catalysed by alkali-metal alkyl compounds  $MCH_2SiMe_3$  ( $M = Li, Na, K$ ) as well as the scope and limitations of these transformations. Furthermore, the potential organometallic intermediates involved in these transformations have been studied in order to obtain new insights into their constitution by combining X-Ray crystallography and DOSY NMR studies.

## 2.2 Results and Discussion

### 2.2.1 Optimisation of the Reaction Conditions

In order to perform the catalytic hydroamination reactions, a systematic procedure has been adopted. All the reactions were carried out in a J. Young's NMR tube under argon atmosphere and at NMR scale. Identical reaction conditions were considered in all the reactions performed: 10 mol% of ferrocene has been used as internal standard as well as 0.81 M solutions on substrate. An initial  $^1\text{H}$  NMR spectrum of the reaction mixture was recorded prior to the addition of the precatalyst. In that way, it has been possible to assess if the background reaction takes place without the precatalyst at room temperature and also to calculate the exact amount of the starting materials employed by integration against the resonance of the internal standard ferrocene. After the introduction of the organometallic precatalyst, the conversions were measured by integration of the resonances in the  $^1\text{H}$  NMR spectra recorded from the addition of the catalyst (time zero) to different intervals of time until full conversion.

Initially, the reaction of diphenylacetylene (**1a**) and piperidine (**2a**) was studied. Illustrating the high kinetic barrier of the process, no reaction took place in the absence of the catalyst even under forcing conditions (heating the J. Young's NMR tube at 80 °C over 48 hours in  $\text{C}_6\text{D}_6$  or  $d_8$ -THF). (Figure 2.1)  $^1\text{H}$  NMR studies of the reaction have shown the non-variation of the corresponding signals of the starting materials **1a** (multiplets ranging from 7.41 to 7.59 and 7.24 to 7.38 ppm in  $d_8$ -THF) and **2a** (multiplets ranging from 2.61 to 2.80 and 1.34 to 1.56 ppm in  $d_8$ -THF) even heating the reaction at 80 °C for 2 days (Figure 2.1).

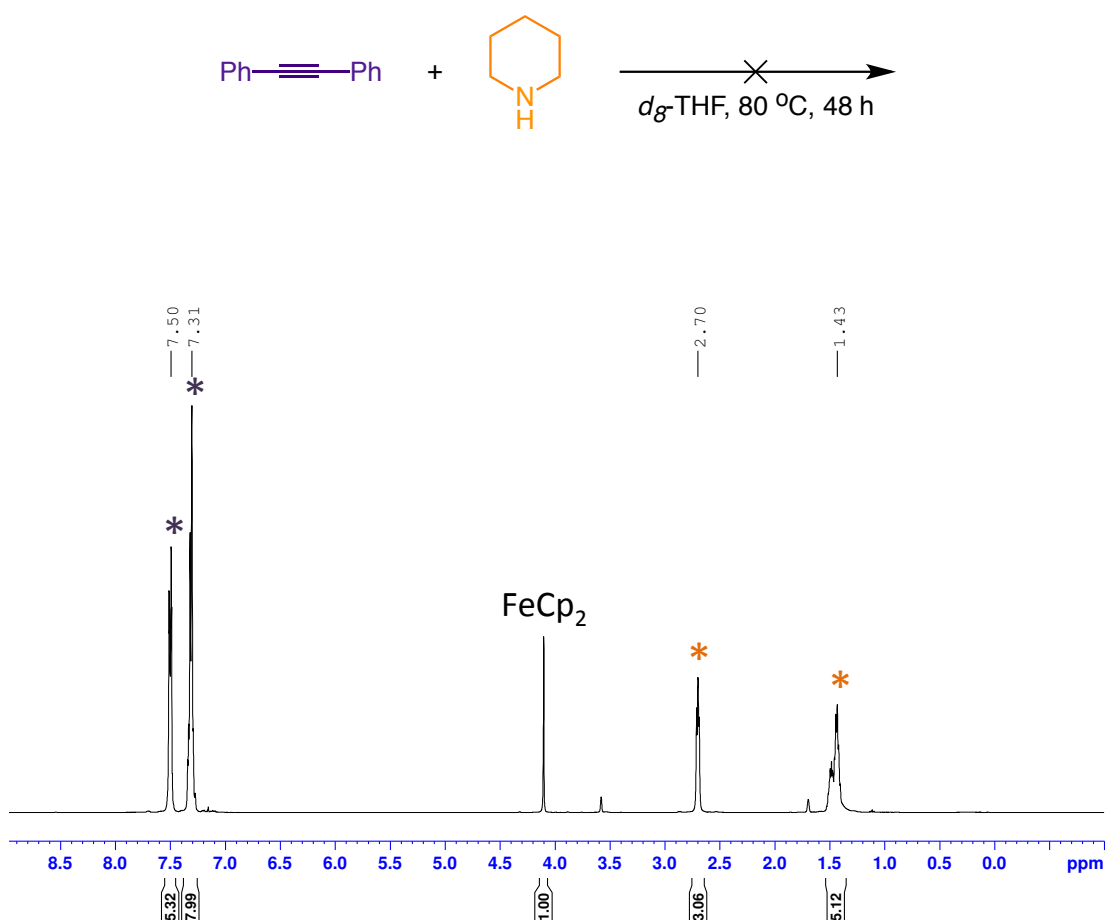


Figure 2.1:  $^1\text{H}$  NMR spectrum of a mixture of diphenylacetylene (**1a**) and piperidine (**2a**) in absence of precatalyst in  $d_8$ -THF.

Therefore, alkali-metal alkyls  $\text{MCH}_2\text{SiMe}_3$  [ $\text{M} = \text{Li}$  (**3**),  $\text{Na}$  (**4**) and  $\text{K}$  (**5**)] were used as precatalysts since it is known that the choice of the precatalyst plays a key role upon the catalyst initiation.<sup>[149]</sup> While **3** is commercially available as a 1M solution in pentane, **4** and **5** were prepared by metathesis of [(trimethylsilyl)methyl]lithium with sodium (**4**) or potassium *tert*-butoxide (**5**) in *n*-hexane.<sup>[127]</sup> Additionally, compounds **3**, **4** and **5** can be stored in the glovebox as solids without decomposition and present enough solubility in THF and benzene in the catalytic

amounts used. The reaction of diphenylacetylene (**1a**) and piperidine (**2a**) was studied in  $C_6D_6$  and  $d_8$ -THF and a 5 mol% loading of the three different alkali-metal alkyl species (**3**, **4** and **5**) (Table 2.1).

Table 2.1: Comparison of alkali-metal precatalysts for the reaction of **1a** and **2a**.

Reaction scheme: Diphenylacetylene (**1a**) + Piperidine (**2a**)  $\xrightarrow[\text{solvent, RT, time}]{5 \text{ mol\% } MCH_2SiMe_3 \text{ (3, 4 or 5)}}$  (6a) - E + (6b) - Z

Entry	Precatalyst $MCH_2SiMe_3$	Solvent	t (h)	Yield (%) <sup>[a]</sup>	E:Z <sup>[b]</sup>
1	Li ( <b>3</b> )	$C_6D_6$	24	5	100:0
2	Li ( <b>3</b> )	$d_8$ -THF	24	35 <sup>[c]</sup>	83:17
3	Na ( <b>4</b> )	$C_6D_6$	24	42	90:10
4	Na ( <b>4</b> )	$d_8$ -THF	1	100	40:60 <sup>[d]</sup>
5	K ( <b>5</b> )	$C_6D_6$	12	100	86:14
6	K ( <b>5</b> )	$d_8$ -THF	0.25	100	92:8

<sup>[a]</sup> Yields determined by  $^1H$  NMR using ferrocene as an internal standard. <sup>[b]</sup> Determined by  $^1H$  NMR spectroscopy. <sup>[c]</sup> 100 % conversion and 87:13 ratio heating during 9 hours at 80 °C. <sup>[d]</sup> 90:10 ratio was obtained after heating at 80 °C for 1 hour.

Figure 2.2 shows an example of a  $^1H$  NMR spectrum of the hydroamination product of the reaction of diphenylacetylene (**1a**) and piperidine (**2a**) with 5 mol% of **4**. The signals corresponding to the characteristic protons of the products appear at 5.62 and 5.66 ppm for the isomers **6a** (E) and **6b** (Z) respectively, resulting from the formal addition of piperidine (**2a**) into diphenylacetylene (**1a**).

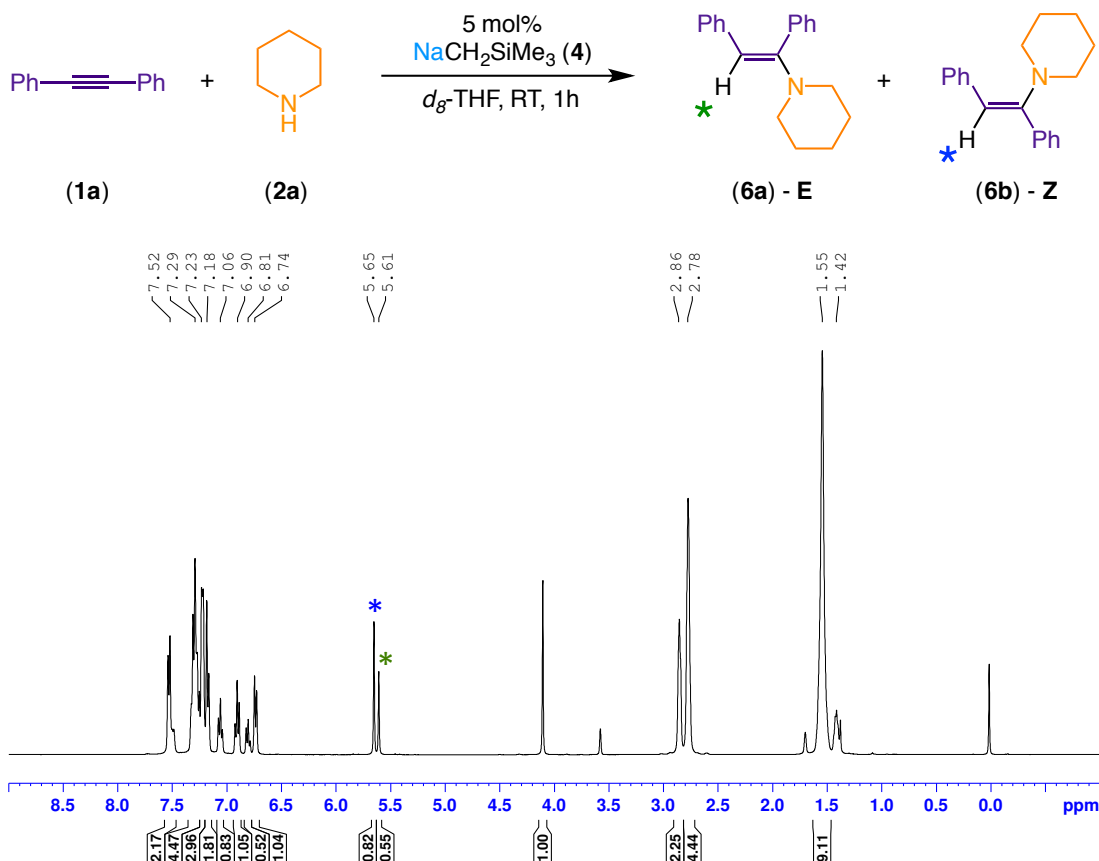


Figure 2.2: <sup>1</sup>H NMR spectrum of the formation of the E and Z hydroamination product after 1 hour of reaction at RT in d<sub>8</sub>-THF, using precatalyst 4.

Remarkably, these group 1 alkyls are able to catalyse the hydroamination reaction at room temperature, in some cases with short periods of time (15 minutes, Table 2.1 entry 6). As shown in Table 2.1, the reactions take place significantly faster in polar THF rather than in non-coordinating solvent benzene (Table 2.1, entry 3 vs 4). Additionally, a dramatic alkali-metal effect is observed with LiCH<sub>2</sub>SiMe<sub>3</sub> (3) being the slowest precatalyst, requiring 24 hours at room temperature to achieve 35% yield (Table 2.1, entry 2). However, forcing the conditions to 80 °C, 100% of yield is obtained after 9 hours, again with a good selectivity (E:Z; 87:13). Contrastingly,



when the sodium precatalyst  $\text{NaCH}_2\text{SiMe}_3$  (**4**) is used, the hydroamination process is drastically faster, affording **6a** and **6b** in a 40 and 60% respectively, with 100% conversion of alkyne **1a**. This reactivity trend is similar to that described for Hill *et al.* in group 2 complexes  $[\text{Dipp}^{\text{Nacnac}}\text{M}(\text{HMDS})(\text{THF})]$  and  $[\text{Dipp}^{\text{Nacnac}}\text{MMe}(\text{THF})]$  ( $\text{Dipp}^{\text{Nacnac}} = \text{Ar}^*\text{NC}(\text{Me})\text{CHC}(\text{Me})\text{NAr}^*$ ;  $\text{Ar}^* = 2,6\text{-}i\text{Pr}_2\text{-C}_6\text{H}_3$ ) where lower reaction rates were observed when decreasing metal ionic radius of the precatalyst.<sup>[116]</sup> This alkali-metal effect could also be related to the different aggregation state of the active species in solution and the polarity of the M-N bonds of the amido-intermediates that could be involved in these reactions. The amide intermediate formed needs to be strongly nucleophilic to be added to the unsaturated bond of the diphenylacetylene in the second step of the reaction.<sup>[144]</sup> An explanation for this rate variation using the different alkali-metal catalysts could be provided by the increase in the nucleophilicity of the amide formed when descending group 1.

The hydroamination reaction of **1a** with **2a** has also been reported by Hill *et al.*,<sup>[149]</sup> using  $[\text{Sr}\{\text{CH}(\text{SiMe}_3)_2\}_2(\text{THF})_2]$  precatalyst, affording a mixture of **6a** and **6b** (91:9). To perform this reaction it is required to use of 5 mol% of the strontium precatalyst and to heat at 60 °C during 2 hours in  $d_8$ -THF. These excellent studies highlight the need of harsher conditions in order to promote the hydroamination reactions, which contrast to our findings using **3** and **4**. Interestingly, despite the fact that complexes **3**, **4**, and **5** decompose rapidly in THF, here under the conditions of study they work efficiently as precatalysts.<sup>[161]</sup> The use of the monosilyl  $\text{CH}_2\text{SiMe}_3$  fragment improves the stability of the organometallic compounds used as precatalysts due to the bulkiness of the anionic ligand and the lack of  $\beta$ -hydrogens that makes the organometallic species resistant to  $\beta$ -hydride elimination.<sup>[128,162–165]</sup> As well, these compounds can be stored in the glovebox as solids, which facilitates their manipulation. The first step in order to initiate the catalytic reaction is the deprotonation of the amine to form the active catalyst. When precatalysts **3**, **4** and

**5** are reacted with the amine, TMS is liberated making the acid-base equilibrium non-reversible towards the formation of the amide species. Agreeing with this, Hill has reported some examples where this equilibrium lies towards the starting materials using HMDS or  $\beta$ -diketiminato ligands<sup>[149,166]</sup> and could also explain the harsh reaction conditions needed (120 °C) when using LiHMDS or KOtBu precatalysts.<sup>[65,140]</sup>

Also, it is possible to improve the selectivity of the E:Z products (**6a** and **6b** respectively) to 90:10, either after 7 hours at room temperature or heating at 80 °C for one more hour. The heavier alkali-metal  $\text{KCH}_2\text{SiMe}_3$  (**5**) proved to be the most effective catalyst in terms of reaction rate and selectivity, as compounds **6a** and **6b** are formed in just 15 minutes at room temperature. 100% yield was obtained with an excellent selectivity (E:Z; 92:8).

Furthermore, in order to assess the role of these transformations, we carried out the hydroamination reaction between **1a** and **2a** in  $\text{C}_6\text{D}_6$  adding a 5 mol% of the TMEDA donor (Table 2.2). Following a similar trend to that reported by Hill *et al.* using  $[\text{Sr}\{\text{CH}(\text{SiMe}_3)_2\}_2(\text{THF})_2]$  as precatalyst,<sup>[149]</sup> here we observe the dependence of different solvents with this system, proving that the reaction rate accelerates with increased polarity.

Table 2.2: Comparison of the reactivity in different polarities.

Reaction scheme:  $\text{Ph-C}\equiv\text{C-Ph}$  (1a) + piperidine (2a)  $\xrightarrow[\text{solvent, RT, 1h}]{5 \text{ mol\% } \text{NaCH}_2\text{SiMe}_3 \text{ (4)}}$  (6a) - E + (6b) - Z

Entry	Solvent	Additive	Yield (%) <sup>[a]</sup>	E:Z <sup>[b]</sup>
1	$\text{C}_6\text{D}_6$	-	5	16:84
2	$\text{C}_6\text{D}_6$	5 mol% TMEDA	21	77:23

---

<b>3</b>	<i>d</i> <sub>8</sub> -THF	-	100	40:60
----------	----------------------------	---	-----	-------

<sup>[a]</sup> Yields determined by <sup>1</sup>H NMR using ferrocene as an internal standard. <sup>[b]</sup> Determined by <sup>1</sup>H NMR spectroscopy.

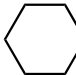
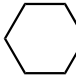
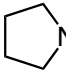
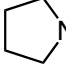
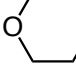
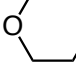
---

Also, the bidentate TMEDA donor accelerates the process when it takes place in the hydrocarbon solvent C<sub>6</sub>D<sub>6</sub> from 5 to 21% yield after 1 hour of reaction (Table 2.2, entry 1 vs 2). Additionally, the fact that the TMEDA is a chelating ligand makes the coordination sphere of the sodium more saturated compared to the more labile THF molecule, which is superior in terms of reactivity (100% yield after 1 hour of reaction) (Table 2.2, entry 2 vs 3).

### 2.2.2 Substrate Scope

To test the substrate scope of this approach a range of aliphatic and aromatic amines have been studied. Interestingly, it was found that when using sodium or potassium complexes **4** and **5** as precatalysts (5 mol% of precatalyst in *d*<sub>8</sub>-THF at room temperature), excellent conversions to the relevant aminoalkenes were observed (Table 2.3).

Table 2.3: Intermolecular hydroamination of diphenylacetylene (**1a**) and a range of secondary amines (**2a-2h**) catalyzed by sodium and potassium precatalysts in *d*<sub>8</sub>-THF at room temperature.

Entry	Amine	Precatalyst <b>MCH<sub>2</sub>SiMe<sub>3</sub></b>	t (h)	Product	Yield (%) <sup>[a]</sup>	E:Z <sup>[b]</sup>
$\text{Ph-C}\equiv\text{C-Ph} + \text{R}_2\text{NH} \xrightarrow[\text{d}_8\text{-THF, RT, time}]{5 \text{ mol\% } \text{MCH}_2\text{SiMe}_3 \text{ (4 and 5)}} \text{Ph-CH=CH-Ph-NHR}_2 + \text{Ph-CH=CH-Ph-NR}_2$ <p style="text-align: center;">(1a)                      (2a-2h)                      (6a-9a) - E                      (6b-9b) - Z</p>						
1	 NH ( <b>2a</b> )	Na ( <b>4</b> )	1	<b>6</b>	100	40:60 <sup>[c]</sup>
2	 NH ( <b>2a</b> )	K ( <b>5</b> )	0.25	<b>6</b>	100	92:8
3	 NH ( <b>2b</b> )	Na ( <b>4</b> )	3	<b>7</b>	100	73:27 <sup>[d]</sup>
4	 NH ( <b>2b</b> )	K ( <b>5</b> )	1	<b>7</b>	100	100:0
5	 NH ( <b>2c</b> )	Na ( <b>4</b> )	4	<b>8</b>	100	55:45 <sup>[e]</sup>
6	 NH ( <b>2c</b> )	K ( <b>5</b> )	0.25	<b>8</b>	86	95:5
7	<i>n</i> Bu <sub>2</sub> NH ( <b>2d</b> )	Na ( <b>4</b> )	1	<b>9</b>	100	65:35
8	<i>n</i> Bu <sub>2</sub> NH ( <b>2d</b> )	K ( <b>5</b> )	0.25	<b>9</b>	100	88:12
9	Ph(Me)NH ( <b>2e</b> )	Na ( <b>4</b> )	24	-	0 <sup>f</sup>	-
10	Ph(Me)NH ( <b>2e</b> )	K ( <b>5</b> )	24	-	0	-
11	Bz(Me)NH ( <b>2f</b> )	Na ( <b>4</b> )	24	-	0	-
12	Bz(Me)NH ( <b>2f</b> )	K ( <b>5</b> )	24	-	0	-

<b>13</b>	Bz <sub>2</sub> NH ( <b>2g</b> )	Na ( <b>4</b> )	24	-	0	-
<b>14</b>	Bz <sub>2</sub> NH ( <b>2g</b> )	K ( <b>5</b> )	24	-	0	-
<b>15</b>	Ph <sub>2</sub> NH ( <b>2h</b> )	K ( <b>5</b> )	24	-	0 <sup>[f]</sup>	-

<sup>[a]</sup> Yields determined by <sup>1</sup>H NMR using ferrocene as an internal standard. <sup>[b]</sup> Determined by <sup>1</sup>H NMR integration of spectra. <sup>[c]</sup> 90 - 10 ratio was obtained after heating at 80 °C for 1 hour. <sup>[d]</sup> 100 - 0 ratio after 7 hours at RT. <sup>[e]</sup> 60 - 40 ratio after 6 hours at RT. <sup>[f]</sup> 0% yield after heating at 80 °C for one hour.

Table 2.3 shows the different conversions obtained when diphenylacetylene (**1a**) is reacted with a large variety of amines including cyclic and acyclic amines. Under similar reaction conditions, half of the amines that have been used afford full conversions in relatively low periods of time (Table 2.3, entries 1 to 8), whereas other amines (Table 2.3, entries 9 to 15) do not show any reaction at all. As seen in the previous reactions, the potassium precatalyst remains superior regarding the selectivity of the E product.

Six and five membered ring cyclic amines (**2a-2c**), as well as dibutylamine (**2d**), provide the desired hydroamination products (from **6** to **9**) in very short periods of time (one hour or less when using the potassium precatalyst) at room temperature (Table 2.3, entries 1-8). However, when using bulkier secondary amines such as N-methylaniline, N-benzylmethylamine, dibenzylamine or diphenylamine with aryl groups the hydroamination reaction does not take place, probably because the less nucleophilic amides formed prevent the formation of the relevant aminoalkene products, even forcing the reaction conditions at 80 °C during 24 hours and using the potassium precatalyst (Table 2.3, entries 10 to 15). It should be noted that hydroamination of alkynes to give products such as **7b** or **8a** requires very harsh reaction conditions and generally employs transition metal catalysts, apart from the previously mentioned strontium catalyst by Hill that can achieve the formation of

**6a** and **6b** (91:9) at 60 °C after 2 hours in  $d_8$ -THF.<sup>[149]</sup> Gold or nickel catalysts can also catalyse these reactions requiring 140 °C during 72 hours to afford product **7b** in a 29% yield using 5 mol% of  $[(\text{PhO})_3\text{P}]_2\text{NiCl}_2$  catalyst or 110 °C during an hour in order to obtain **8a** in yields ranging from 68 to 76% using 5 mol% of  $[\text{Au}(\text{SMe}_2)\text{Cl}]$  in the presence of different P,N-substituted phenylene ligands.<sup>[167,168]</sup>

In order to investigate more challenging reactions we then moved to the study of hydroamination of alkenes. These reactions are known to be more challenging than alkynes in terms of the weakness of the  $\pi$ -bond in the C=C triple bond.<sup>[149]</sup> To assess the functional group tolerance of this approach, the reaction of piperidine **2a** with a range of substituted vinylarenes was investigated, in  $d_8$ -THF and using 5 mol% of the  $\text{MCH}_2\text{SiMe}_3$  [M = Na (**4**), K (**5**)] precatalyst (Table 2.4).

Table 2.4: Hydroamination reaction of *para*-substituted vinylarenes with **2**.

$\text{X-C}_6\text{H}_4\text{-CH=CH}_2$  (1b-1f) + Piperidine (2a)  $\xrightarrow[\text{d}_8\text{-THF, RT, time}]{5 \text{ mol\% } \text{MCH}_2\text{SiMe}_3 \text{ (4 and 5)}}$   $\text{X-C}_6\text{H}_4\text{-CH}_2\text{-CH}_2\text{-N(CH}_2\text{)}_5$  (10-13)

Entry	Alkene (X-)	Precatalyst $\text{MCH}_2\text{SiMe}_3$	t (h)	Product	Yield (%) <sup>[a,b]</sup>
1	H- ( <b>1b</b> )	Li ( <b>3</b> )	0.25	<b>10</b>	100
1	H- ( <b>1b</b> )	Na ( <b>4</b> )	0.25	<b>10</b>	100 (88)
2	H- ( <b>1b</b> )	K ( <b>5</b> )	0.25	<b>10</b>	100
3	Me- ( <b>1c</b> )	Na ( <b>4</b> )	0.25	<b>11</b>	100 (70)
4	MeO- ( <b>1d</b> )	Na ( <b>4</b> )	0.25	<b>12</b>	100 (84)
5	Cl- ( <b>1e</b> )	Li ( <b>3</b> )	0.25	<b>13</b>	100 (85)

---

<b>6</b>	Cl- ( <b>1e</b> )	Na ( <b>4</b> )	24	-	0
<b>7</b>	Cl- ( <b>1e</b> )	K ( <b>5</b> )	24	-	0
<b>8</b>	F- ( <b>1f</b> )	Li ( <b>4</b> )	24	-	0
<b>9</b>	F- ( <b>1f</b> )	Na ( <b>4</b> )	24	-	0
<b>10</b>	F- ( <b>1f</b> )	K ( <b>5</b> )	24	-	0
<b>11</b>	Br- ( <b>1g</b> )	Li ( <b>5</b> )	24	-	0

---

<sup>[a]</sup> Yields determined by <sup>1</sup>H NMR using ferrocene as an internal standard. <sup>[b]</sup> Isolated yields in parenthesis.

---

The reaction of vinylarenes and piperidine (**2a**) provides the *anti*-Markovnikov product, with no byproducts detected. This regioselectivity is determined in the alkene insertion step of the hydroamination reaction, which is believed to occur via a more stable four-membered transition state.<sup>[65]</sup>

Different *para*-substituted vinylarenes (alkenes **1c-1g**) were studied in order to show an electronic trend in the reactivity with different electron density groups. It is known that electron-withdrawing substituents in *para*-positions stabilises the negative charge formed during the transition state of the carbon-nitrogen bond formation.<sup>[149]</sup>

In our studies, the presence of electron-donating substituents, such as methyl and methoxy in the *para*-position (Table 2.4, entries 3 and 4), provide the addition products **11** and **12** in very short periods of time (15 minutes) and at room temperature. The same reactions were found in the literature with the use of other catalysts. Hill *et al.* were also able to obtain the hydroamination products in excellent yields (95 and 90% NMR yields) at room temperature catalysing the

reactions with 5 mol% of the strontium precatalyst  $[\text{Sr}\{\text{CH}(\text{SiMe}_3)_2\}_2(\text{THF})_2]$ .<sup>[149]</sup> Also, Hultsch *et al.* were able to afford product **10** in a 62% yield, using 5 mol% of  $\text{LiN}(\text{SiMe}_3)_2$ , 5mol% of TMEDA in  $\text{C}_6\text{D}_6$  and heating at 120 °C during 1 hour.<sup>[65]</sup> In our case, compound **10** can be prepared at room temperature in 15 minutes using any of the three precatalysts including the lithium alkyl **3**. This can be rationalised in terms of the importance of the precatalyst ligand used. When using precatalyst **3**, the formation of TMS drives the initiation reaction towards the products making it non-reversible. However, when using  $\text{LiN}(\text{SiMe}_3)_2$ , harsher reaction conditions (120 °C) are needed in order to form the catalyst amide. Some of the reported reactions of *para*-substituted vinylarenes are catalysed by transition metal catalysts such as ruthenium, where they require harsher reaction conditions (100 °C during 72 hours of reaction to afford 67% yield of product **11**, for example).<sup>[169]</sup>

When halide-substituted vinylarenes **1e** and **1g** were reacted with piperidine **2a** using precatalyst **4** and **5**, no reaction was observed suggesting a faster deactivation of the catalyst, perhaps by the formation of the corresponding sodium or potassium halide, as a white precipitate was obtained at the bottom of the J. Young's NMR tube. Deactivation of the catalyst has also been reported when  $[\text{Sr}\{\text{N}(\text{SiMe}_3)_2\}_2]$  precatalyst is used for the *para*-fluorostyrene (**1f**) and piperidine (**2a**), where it is proposed that deactivation of the catalyst occurs by a competing C-F activation process.<sup>[149,170]</sup> Interestingly, when the lithium precatalyst (**3**) was used for the reaction between **1e** and **2a**, the hydroamination product **13** was obtained in quantitative yields after 15 min at RT and no decomposition of the catalyst occurred (Table 2.4, entry 5). However, **3** also failed to promote the hydroamination reaction when the fluoro- and bromoderivative **1f** and **1g** were employed, suggesting a decomposition of the catalyst (Table 2.4, entry 8 and 11).

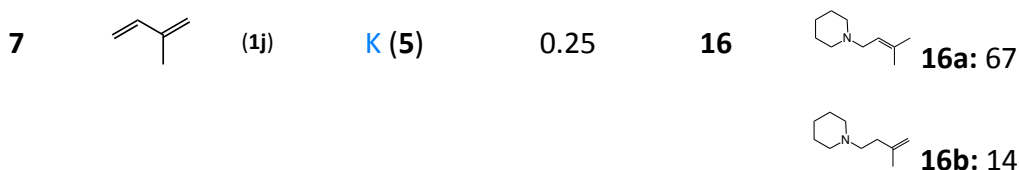


Furthermore, a range of substituted olefins in the  $\alpha$ - and  $\beta$ -carbon centres of the C=C group, which were also treated with piperidine (**2a**) were studied. In general, good conversions were observed in very short periods of time at room temperature (Table 2.5).

Table 2.5: Hydroamination reaction with piperidine (**2a**) and different olefins (**1g-1i**) in  $d_8$ -THF at room temperature.

Reaction scheme: Olefin (**1g-1j**) + Piperidine (**2a**)  $\xrightarrow[5 \text{ mol\% } MCH_2SiMe_3 \text{ (4 and 5)}]{d_8\text{-THF, RT, time}}$  Product (**14-16**)

Entry	Alkene	Precatalyst $MCH_2SiMe_3$	t (h)	Product	Yield (%) <sup>[a,b]</sup>
1	(1b)	Na ( <b>4</b> )	0.25	<b>10</b>	100 (88)
2	(1b)	K ( <b>5</b> )	0.25	<b>10</b>	100
3	(1h)	Na ( <b>4</b> )	0.25	<b>14</b>	100 (88)
4	(1i)	Na ( <b>4</b> )	5	<b>15</b>	38(38)*
5	(1i)	K ( <b>5</b> )	24	<b>15</b>	0
6	(1j)	Na ( <b>4</b> )	24	<b>16</b>	0 <sup>[c]</sup>
6	(1j)	Na ( <b>4</b> )	24	<b>16</b>	0 <sup>[c]</sup>




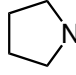
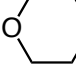
<sup>[a]</sup> Yields determined by <sup>1</sup>H NMR using ferrocene as an internal standard. <sup>[b]</sup> Isolated yields in parenthesis. <sup>[c]</sup> 5% conversion after 24h heating at 80 °C. \* Presence of byproducts, see experimental part.

By introducing a methyl group in the alkene using  $\alpha$ -methylstyrene, we wondered if an electronic and steric effect would be found to destabilise the negative charge in the transition state during the formation of the newly N-C bond. Full conversion to the product **14** was achieved when reacting  $\alpha$ -methylstyrene (**1h**) with piperidine (**2a**) after 15 minutes using the sodium precatalyst **4** (Table 2.5, entry 3). Contrastingly, some alkene polymerisation appeared to compete with hydroamination reaction when the *trans*- $\beta$ -methylstyrene (**1i**) and the piperidine (**2a**) were employed, affording product **15** in a low 38% yield, when precatalyst **4** was employed. Additionally, this reaction does not take place when  $\text{KCH}_2\text{SiMe}_3$  (**5**) is used as a precatalyst, even forcing the reaction conditions at 80 °C for 24 hours. Showing an interesting alkali-metal effect, for isoprene (**1j**) relative good conversions at room temperature were observed using the potassium precatalyst **5** (67% of **16a** and 14% of **16b**; Table 2.5, entry 7) whereas the sodium compound **4** fails to catalyse this reaction even under forcing reaction conditions (80 °C during 24 hours) (Table 2.5, entry 6). The reaction of  $\alpha$ -methylstyrene (**1h**) and piperidine (**2a**) is reported in the literature using a  $\text{LiN}(\text{SiMe}_3)_2$  precatalyst as well as the already mentioned  $[\text{Sr}\{\text{N}(\text{SiMe}_3)_2\}_2]_2$  and ruthenium complex precatalysts, require again long periods of time and high temperatures.<sup>[65,149,171]</sup> The relatively low yields obtained in some of these reactions, suggest that some of these products could be

polymerised as it is known that group 1 organometallic compounds have a history as initiators of anionic polymerisation of alkenes such as styrene, butadiene or isoprene.<sup>[63,158,172–174]</sup> It has been reported that lithium amides can initiate anionic polymerization of dienes.<sup>[174]</sup> For example, N-lithiopyrrolidinide·2THF can initiate the copolymerisation of butadiene and styrene. Other reports show the anionic telomerisations of isoprene with secondary amines, such as pyrrolidine, piperidine and morpholine, using sodium metal.<sup>[172]</sup>

The intermolecular hydroamination reaction has also been explored by using a wide range of amines reacted with styrene (**1b**). Again, all the reactions afford the *anti*-Markovnikov addition product, consistent with the presence of the nucleophilic addition step in the catalytic cycle.

Table 2.6: Intermolecular hydroamination of styrene (**1b**) with different amines in *d*<sub>8</sub>-THF at room temperature.

Entry	Amine	Precatalyst MCH <sub>2</sub> SiMe <sub>3</sub>	t (h)	Product	Yield (%) <sup>[a,b]</sup>
1	 NH ( <b>2a</b> )	Na ( <b>4</b> )	0.25	<b>10</b>	100 (88)
2	 NH ( <b>2b</b> )	Na ( <b>4</b> )	0.25	<b>17</b>	100 (88)
3	 NH ( <b>2c</b> )	Na ( <b>4</b> )	0.25	<b>18</b>	100 (80)

<b>4</b>	<sup>n</sup> Bu <sub>2</sub> NH ( <b>2d</b> )	Na ( <b>4</b> )	0.25	<b>19</b>	95 (74)
<b>5</b>	Ph(Me)NH ( <b>2e</b> )	Na ( <b>4</b> )	24	-	0
<b>6</b>	Ph(Me)NH ( <b>2e</b> )	K ( <b>5</b> )	8 <sup>c</sup>	<b>20</b>	73 (69)
<b>7</b>	Bz(Me)NH ( <b>2f</b> )	Na ( <b>4</b> )	0.25	<b>21</b>	91 (84)
<b>8</b>	Bz <sub>2</sub> NH ( <b>2g</b> )	Na ( <b>4</b> )	0.25	<b>22</b>	81 (72)
<b>9</b>	Ph <sub>2</sub> NH ( <b>2h</b> )	Na ( <b>4</b> )	24 <sup>c</sup>	-	0
<b>10</b>	Ph <sub>2</sub> NH ( <b>2h</b> )	K ( <b>5</b> )	24 <sup>c</sup>	-	0
<b>11</b>	BzNH <sub>2</sub> ( <b>2i</b> )	Li ( <b>3</b> )	8	<b>23</b>	81
<b>12</b>	BzNH <sub>2</sub> ( <b>2i</b> )	Na ( <b>4</b> )	0.25	<b>23</b>	51
<b>13</b>	BzNH <sub>2</sub> ( <b>2i</b> )	K ( <b>5</b> )	0.25	<b>23</b>	11
<b>14</b>	BzNH <sub>2</sub> ( <b>2i</b> )	Li ( <b>3</b> )	0.25 <sup>[c]</sup>	<b>23</b>	84 (65)

<sup>[a]</sup> Yields determined by <sup>1</sup>H NMR using ferrocene as an internal standard. <sup>[b]</sup> Isolated yields in parenthesis. <sup>[c]</sup> Reaction at 80 °C.

Reacting cyclic (**2a-2c**) and aliphatic (**2d**) amines, with styrene (**1b**) it was possible to observe full conversion towards the formation of the hydroamination product

instantly (less than 15 minutes) using  $\text{NaCH}_2\text{SiMe}_3$  (**4**) precatalyst at room temperature (Table 2.6, entries 1 to 4). When using bulkier amines with aromatic groups the hydroamination product is not always formed (Table 2.6, entries 5 to 14). In the case of the N-methylaniline (**2e**) the potassium compound **6** is the only precatalyst that can afford the formation of the final product. After 8 hours of reaction at 80 °C, a 73% yield of the amine **20** obtained, although the same yield can be accomplished at room temperature after 24 hours (Table 2.6, entry 6). Contrastingly, product **21**, resulting from the reaction of N-benzylamine (**2f**) and styrene (**1b**), is formed in 91% yield in 15 minutes (Table 2.6, entry 7) suggesting the formation of a more nucleophilic amide, which allows a faster addition reaction compared to when N-methylaniline (**2e**) is employed. Dibenzylamine (**2g**) reaction with styrene (**1b**) led to a 81% of product **22** in just 15 minutes at room temperature, in contrast of the diphenylamine (**2h**) that prevents the formation of the final product, even using the precatalyst **6** and forcing the reaction conditions.

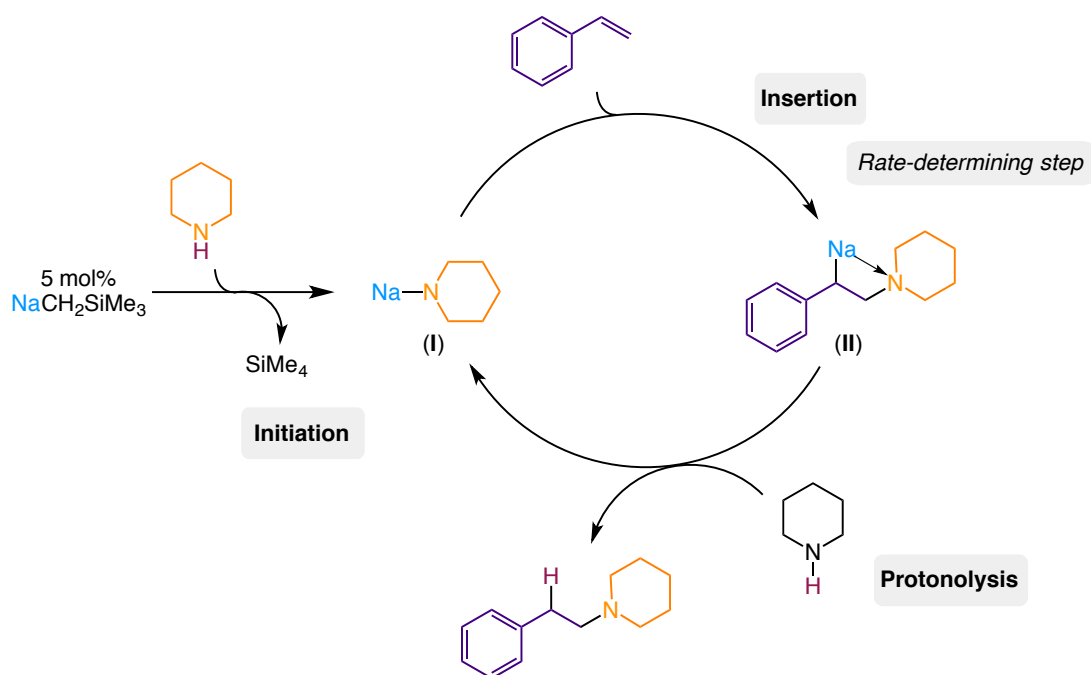
Moving to the reaction of styrene (**1b**) with the primary amine benzylamine (**2i**) a different behaviour of the alkali-metal precatalyst trend has been observed. In this case, the lithium precatalyst (**3**) appears to be the most selective to the hydroamination product **23** (81% after 8h at room temperature; Table 2.6, entry 11). The reaction of styrene (**1b**) and benzylamine (**2i**) also takes place at room temperature to full conversion in 15 minutes when the sodium and potassium precatalysts are used (Table 2.6, entries 12 and 13). However, the hydroamination products are formed in much lower yields (51 and 11%) than when the lithium precatalyst (**3**) is used (Table 2.6, entries 11, 12 and 13). Additionally, an 84% yield of product **23** can be afforded after 15 minutes using the lithium precatalyst (**3**) and heating the reaction at 80 °C (Table 2.6, entry 14).

As evidenced in the results presented in Table 2.6, amines with aromatic substituents such as N-methylaniline or N-benzylamine tend to display a lower reactivity compared to those with alkyl substituents, which can be rationalised considering the formation of a less nucleophilic metal amide due to the electron-withdrawing character of the aromatic substituents.

### 2.2.3 Mechanistic Investigations

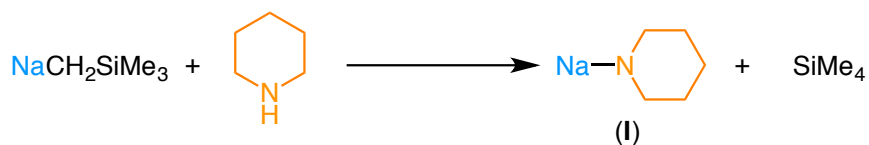
In order to get some insights on the mechanism of these reactions and the possible constitution of the organometallic intermediates involved, we performed a series of stoichiometric studies.

As mentioned in the introduction, alkaline and alkaline-earth metal catalysts are thought to operate via activation of the amine to the formation of a catalytic active amide.<sup>[64]</sup> This amide needs to be nucleophilic enough to get inserted into the unsaturated fragment and finally form the final hydroamination product through protonolysis of the amine used. The active metal-amido catalyst is recycled closing the catalytic cycle (Scheme 2.6). DFT calculations with alkali-metal<sup>[65]</sup> or alkaline earth metal<sup>[116,159]</sup> catalysts for intermolecular hydroamination reactions have been reported suggesting the same catalytic cycle that we propose for our system.



Scheme 2.6: Proposed catalytic cycle for hydroamination reactions with monometallic precatalysts.

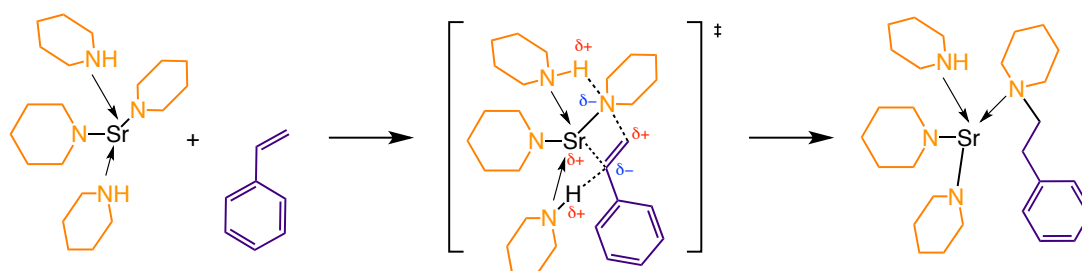
As previously mentioned, another important aspect to consider is the ability of the precatalyst to metallate the relevant amine in order to initiate the catalytic cycle. The initiation step is dependent of the identity of the precatalyst and the acidity of the resultant acid/basic pair, making the equilibrium irreversible towards the formation of the metal amide, the active catalyst of the reaction (Scheme 2.7).



Scheme 2.7: Initiation step for the formation of active species (I).

Additionally, the metal amide intermediate (I) needs to be strongly nucleophilic to insert into the unsaturated moiety. Furthermore, some theoretical calculations

have shown that this step requires large activation energy due to the unfavourable interaction between the N lone pair and the  $\pi$ -system of the unsaturated compound.<sup>[65]</sup> This nucleophilic addition is going to determine the regioselectivity of the reaction depending if this nucleophilic attack is Markovnikov or *anti*-Markovnikov, which depends on the intermediate carbanion formed. In our studies using aryl olefines, only *anti*-Markovnikov products are obtained, similarly to the reported hydroamination products catalysed by  $\text{LiN}(\text{SiMe}_3)_2/\text{TMEDA}$  catalyst, where the Gibbs energies obtained for the *anti*-Markovnikov structures are more stable compared to the Markovnikov ones due to the better stability of the benzylic anion intermediate formed.<sup>[65,145]</sup> As a consequence of the nucleophilic addition, a highly polarised four-membered ring intermediate (**II**) is formed. Hill and co-workers have proposed a transition state for the insertion of styrene based on the results obtained in their kinetic studies, when using strontium catalyst (Scheme 2.8).<sup>[149]</sup> In the transition state proposed, the negatively polarized benzylic carbon is stabilised by additional piperidine molecules and the metal may be coordinated by a second or third amine (Scheme 2.8).<sup>[149]</sup> This suggestion can be related with the intermediate described by Sadow in intramolecular hydroaminations with a magnesium amidoalkene complex that only forms the product when a further equivalent of substrate is added.<sup>[175]</sup>

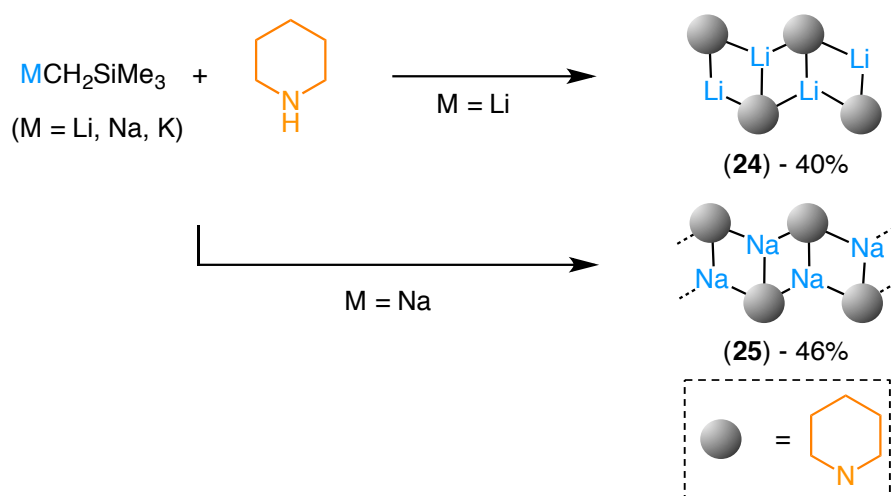


Scheme 2.8: Proposed insertion transition state by Hill.<sup>[149]</sup>



Intermediate **II**, which could be expected to be highly reactive and should form the hydroamination product rapidly through protonation by the starting amine and regenerating the active amide **I**. Computational studies, done by Hill or Tobisch using group 2 metal catalysts also agree with the proposed catalytic mechanism, which is viewed as “lanthanide-mimetic” due to the similarities between early main group metals (group 1 and 2) and lanthanides.<sup>[116,159]</sup> The lack of d electrons makes them operate via activation of the amine mechanism, rather than the activation of the alkene that is common for transition-metals since their  $\pi$ -bonding is more effective.<sup>[135]</sup>

In order to get some structural insights on the proposed amido species **I** which add as nucleophiles across the C=C or C $\equiv$ C of the unsaturated substrates, the reaction of the relevant alkyl precatalyst MCH<sub>2</sub>SiMe<sub>3</sub> with 1 equivalent of piperidine using a mixture of hexane/THF as solvent has been conducted (see Scheme 2.9). Compounds [(THF){LiNC<sub>5</sub>H<sub>10</sub>}]<sub>4</sub> (**24**) and [(THF){NaNC<sub>5</sub>H<sub>10</sub>}]<sub>2</sub>∞ (**25**) were isolated as colourless crystalline solids in 40 and 46% yields respectively. X-Ray crystallographic studies confirmed the formation of the metal amides, which have been also characterised by <sup>1</sup>H and <sup>13</sup>C NMR spectroscopy as well as elemental analysis experiments.



Scheme 2.9: Synthesis of lithium and sodium amide compounds.

Attempts to isolate potassium amides as crystalline solids using amines **2a-2i** resulted in the formation of highly insoluble solids, which could not be recrystallized precluding X-ray crystallographic studies. Different solvent combinations were probed as well as the addition of Lewis donors such as TMEDA and PMDETA. However, in all cases amorphous solids were obtained. In this regard, a search in the Cambridge Structural Database (CCDC) shows around 96 amides have been structurally characterised, including a potassium-nitrogen ladder  $[\{KN_3C_6H_4\}(HMPA)]_\infty$  which contains HMPA (hexamethylphosphoric triamide), strong donor which is also a very carcinogenic phosphoramidate stabilising the potassium cations (Figure 2.3).<sup>[176]</sup>

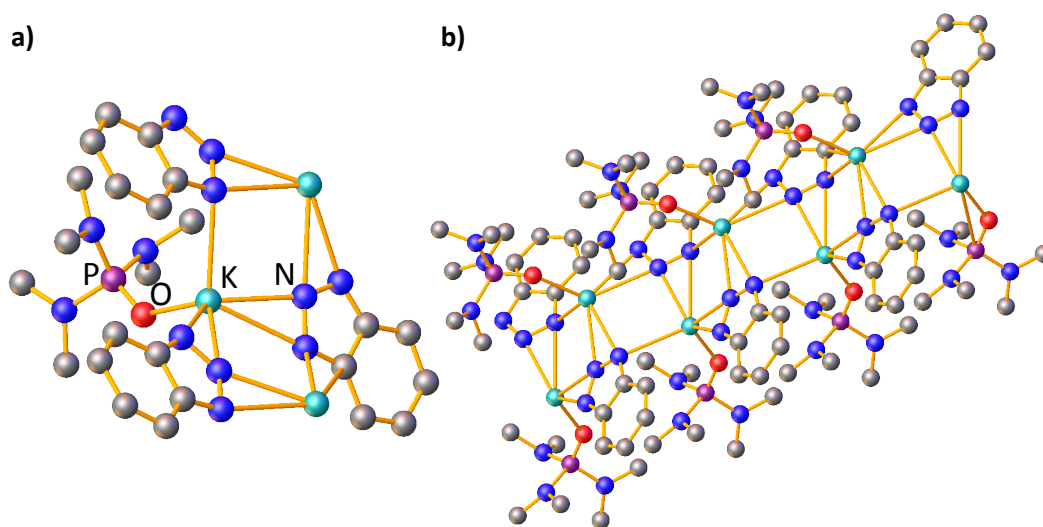


Figure 2.3: Molecular structure of  $[\{KN_3C_6H_4\}(HMPA)]_\infty$ . All hydrogen atoms have been omitted for clarity. a) View of a trinuclear section. b) View of the ladder in the extended structure.<sup>[176]</sup>

X-Ray crystallographic studies established the molecular structure of **24** and **25**, which exhibits a typical ladder arrangement<sup>[25,26]</sup> of two attached  $(NLi)_2$  rings solvated by four molecules of THF for **24** (Figure 2.4) and a polymeric ladder composed of infinite  $(NNa)_2$  rings laterally associated for **25** (Figure 2.5).

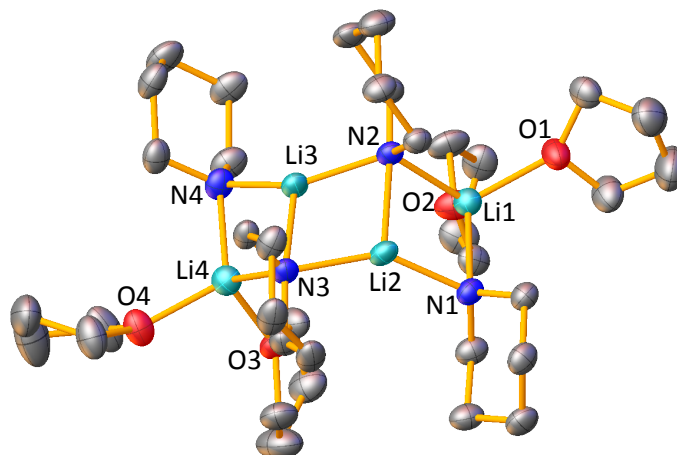


Figure 2.4: Molecular structure of the lithium amide tetramer (**24**) with 50% probability displacement ellipsoids. All hydrogen atoms have been omitted for clarity. Selected bond lengths (Å) and bond angles (°): Li1-N1 2.092(5), Li1-N2 2.045(5), Li2-N1 2.052(5), Li2-N2 1.958(5), Li2-N3 2.028(5), Li3-N1 2.028(5), Li3-N3 2.042(5), Li3-N4 1.960(5), Li4-N3 2.095(6), Li4-N4 2.028(6), N1-Li1-N2 101.0(3), Li1-N2-Li2 76.1(2), N2-Li2-N1 105.5(3), Li2-N1-Li1 73.1(2), N1-Li2-N3 105.6(3), Li2-N3-Li3 71.0(2), N3-Li3-N1 106.0(3), Li3-N1-Li2 70.8(2), N3-Li4-N4 101.7(3), Li3-N3-Li4 71.9(2), N4-Li3-N3 106.1(3), Li4-N4-Li3 75.0(2).

Molecular structure of the lithium amide **24** is formed by three four-membered rings that have a planar disposition, where the sum of the corresponding internal angles is  $\approx 360^\circ$  ( $[\text{Li1N2Li2N1}] = 355.7^\circ$ ;  $[\text{N1Li2N3Li3}] = 353.4^\circ$ ;  $[\text{Li3N3Li4N4}] = 354.7^\circ$ ). The angles within the planar rings average at  $104.3^\circ$  at Li and  $73.0^\circ$  at N, consistently with the reported angle values for similar Li-N containing complexes.<sup>[177]</sup> Bond dimensions of **24** are influenced by the solvation by the THF molecules giving different metal coordination numbers (4 for Li1 and Li4; 3 for Li2 and Li3). Both terminal lithium atoms Li1 and Li4 exhibit a tetrahedral coordination (angles around Li ranging from  $94.4(2)^\circ$  to  $118.9(2)^\circ$ ). The four Li-N rungs show similar distances (average  $2.04(1)$  Å), whereas, Li-N distances involving the terminal Li atoms present slightly elongated distances (average  $2.06(3)$  Å) because of the solvating molecules influence. The bond lengths of the outer edges of the ladder

that are unaffected by the solvation of the THF (Li2-N3 and Li3-N1), also present shorter Li-N distances (average 2.03(0) Å) similarly to other Li amide structures reported.<sup>[178]</sup>

Contrastingly, X-Ray crystallographic studies for amide (**25**) propose a polymeric ladder structure (Figure 2.6) made up of {(THF)[NaNC<sub>5</sub>H<sub>10</sub>]<sub>2</sub>} units (Figure 2.5).

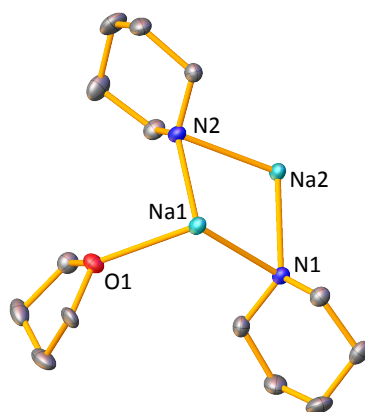


Figure 2.5: Asymmetric unit of compound **25** with 50% probability displacement ellipsoids. All hydrogen atoms have been omitted for clarity.

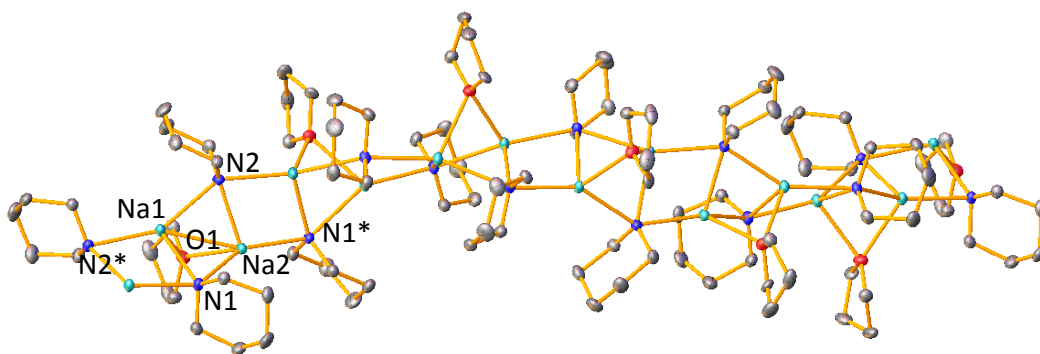


Figure 2.6: Polymeric structure of the polymeric sodium amide (**25**) with 50% probability displacement ellipsoids. All hydrogen atoms have been omitted for clarity. Selected bond lengths (Å) and bond angles ( $^{\circ}$ ). \*Values generated by symmetry: Na1-N1 2.470(3), Na1-N1\* 2.520(3), Na1-N2 2.412(2), Na2-N1 2.411(2), Na2-N2 2.471(3), Na2-N2\* 2.520(2), N1-Na1-N2 96.73(8), Na1-N2-Na2 68.33(7), N2-Na2-N1 96.77(8), Na2-N1-Na1 68.36(6), N1-Na1-N1 149.3(1), Na2-N2-Na2 142.8(1).

The centrosymmetric structure **25** displays a polymeric arrangement composed of infinite  $(\text{NNa})_2$  rings laterally associated adopting a double helical assembly (angles between adjacent  $(\text{NNa})_2$  rings is  $60.0^{\circ}$ ). This is evident when observed from an axial direction, existing as a hollow tubular assembly (Figure 2.7).

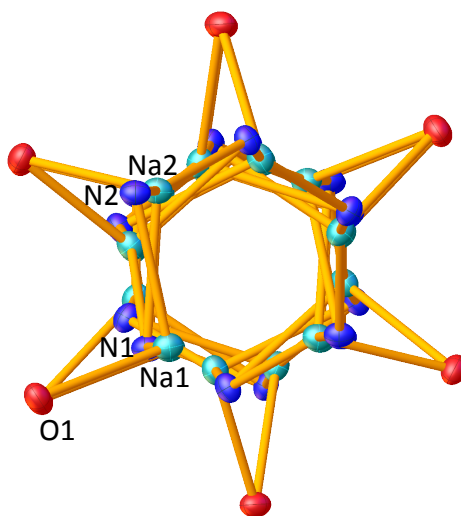


Figure 2.7: Axial view of the helix molecular structure of compound **25** with 50% probability displacement ellipsoids. All hydrogen atoms and cyclic groups have been omitted for clarity.

The amide compound presents a pseudolinear N-Na double chain ( $[N1Na1N1] = 149.3(1)^\circ$  and  $[Na2N2Na2] = 142.8(1)^\circ$ ) in which the THF ring groups are on the exterior of the helix (Figure 2.7). This THF solvating molecule acts as a bridge between the Na1 and Na2 atoms giving rise to four-coordinated sodium atoms exhibiting a tetrahedral coordination (angles around Na ranging from  $87.37(7)^\circ$  to  $149.33(8)^\circ$ ). The four-membered ring of the asymmetric unit does not show a totally planar disposition (sum of angles  $[Na1N2Na2N1] = 330.2^\circ$ ) due to the solvating effect of the solvent ligand which bridges two of the Na ring vertex in a diagonal manner. Bond dimensions within the ladder framework are longer in comparison with those found for the lithium amide structure (**24**) (average of  $[Na-N]$  2.47(5) vs  $[Li-N]$  2.03(5) Å). Furthermore, those Na-N rung bonds present a shorter distance compared to those forming the edge (average 2.41(0) vs 2.50(3) Å respectively). Additionally, there are alternating long and short N-Na rungs because of the bridging THF molecule in the former ones ( $[Na-N] = 2.47(0)$  vs  $[Na-N^*] = 2.52(0)$  Å) according to other Na-N containing polymeric ladders reported.<sup>[27]</sup>

In order to have a better understanding on the constitution of amide compounds **24** and **25**,  $^1\text{H}$  DOSY NMR studies were performed in  $d_8$ -THF solutions. Diffusion-ordered spectroscopy (DOSY) is the main technique to predict the arrangement of the species in solution. This 2D technique combines the regular chemical shift data obtained in one dimension and the separation of the species by particle size (by their diffusion properties), provided in the second dimension.<sup>[179]</sup> This method has been applied in different areas with the purpose of estimating molecular volumes, calculating the aggregation degree of compounds, studying host-guest interactions, recognizing hydrogen bonds and providing the presence and extent of ion pairing.<sup>[180]</sup>

In our case,  $^1\text{H}$  DOSY NMR is applied for the estimation of molecular weights of our amide compounds. Williard *et al.* pioneered a method to correlate the diffusion coefficient values (D values) with the molecular weights (MW) of the species in solution using internal calibration curves (ICC). Molecules possessing larger volumes, which afford reduced D values, diffuse more slowly than smaller species. Using this method, D is correlated with the molecular radii by the Stokes – Einstein equation.<sup>[181]</sup> ((eq 1:  $D = k_B T / (6\pi\eta r)$ ); where D is the diffusion coefficient,  $k_B$  is the Boltzmann constant, T is the temperature in K,  $\eta$  is the viscosity of the solution and r is the radius of the molecular sphere). Assuming spherical shapes of the species and postulating that the volume of an aggregate is proportional to its formula weight, there exist a linear correlation between the measured diffusion coefficients and the formula weights of aggregates in solution: (eq 2:  $\log D = a \log FW + b$ ). Using MW of known molecules to establish a calibration curve, empirical unknown MW can be interpolated providing a rapid determination of the values. However, this ICC-method has some important drawbacks and estimates the MW with a significant error of  $\pm 30\%$ . Recently, Stalke has reported a new methodology to determine the molecular weight of small molecules in DOSY NMR by using external



calibration curves (ECC) with normalized diffusion coefficients. This ECC-method reduces the error of the predicted MW to a maximum of  $\pm 9\%$  and only one internal reference is sufficient. Additionally, this method is independent of NMR-device properties and temperatures or viscosity obtaining a more accurate determination of MW in solution.<sup>[7,182,183]</sup>

For our study we applied the ECC-method, using 40 mM solution of amides **24** and **25** in  $d_8$ -THF and using tetramethylsilane (TMS) as internal standard. The 2D  $^1\text{H}$  DOSY NMR spectrum obtained for compound **24** is presented in Figure 2.8.

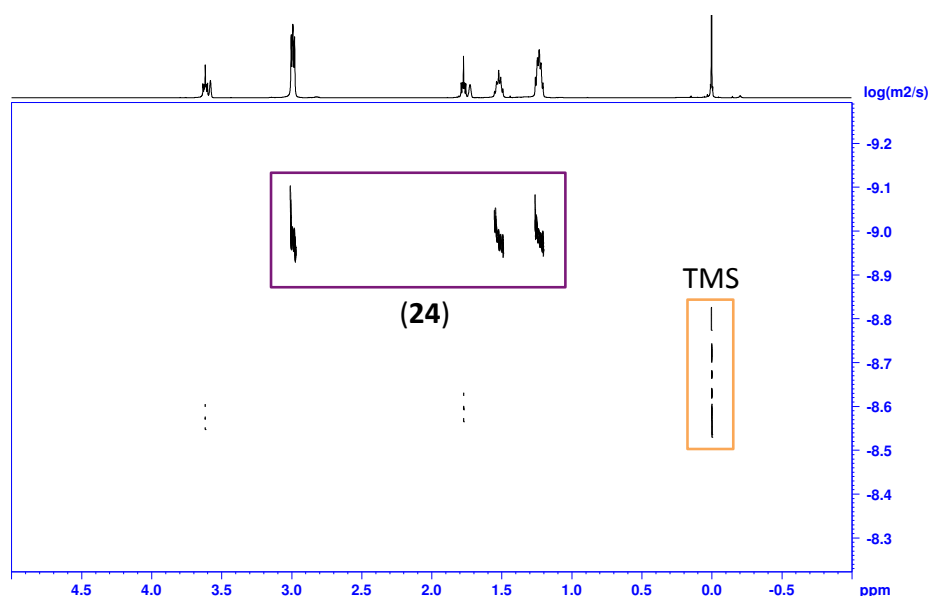


Figure 2.8:  $^1\text{H}$  DOSY experiment in  $d_8$ -THF of a mixture of compound **24** (40 mM) and the internal standard TMS.

This experiment revealed the diffusion coefficient obtained with a value of  $D = 1.043 \cdot 10^{-10} \text{ m}^2/\text{s}$  when the lithium amide compound is dissolved in  $d_8$ -THF. The errors of possible aggregation states of the lithium amide **24** are presented in Table 2.7 considering the estimated formula weight 355 g/mol obtained for **24**.

Table 2.7: Possible lithium amide (**24**) species in solution and the corresponding errors for  $MW_{est}=355$  g/mol.

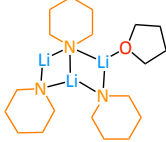
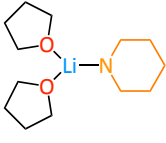
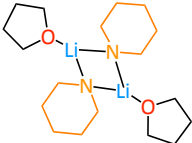
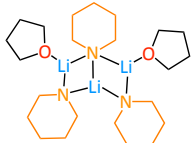
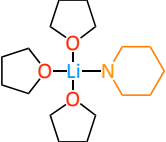
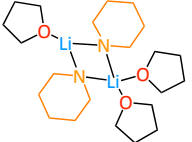
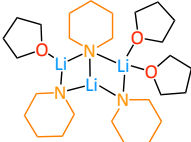
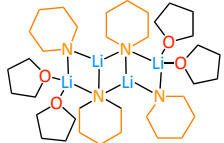
	monomer	dimer	trimer	tetramer
<b>1 THF</b>				
<b>MW (g/mol)</b>			345.35	
<b>Error (%)</b>			-3	
<b>2 THF</b>				
<b>MW (g/mol)</b>	235.30	326.38	417.46	
<b>Error (%)</b>	-51	-9	15	
<b>3 THF</b>				
<b>MW (g/mol)</b>	307.40	398.49	489.57	
<b>Error (%)</b>	-15	11	28	
<b>4 THF</b>				
<b>MW (g/mol)</b>				652.76
<b>Error (%)</b>				46

Table 2.7 suggests different lithium species including some of the corresponding dimeric equilibriums with exchange of THF molecules. Regarding the error obtained while comparing the estimated and the real molecular weight,  $^1\text{H}$  DOSY NMR suggests different possible aggregation states. The retention of the solid state molecular structure **24** in  $d_8$ -THF solution is very improbable since the error obtained from the  $^1\text{H}$  DOSY NMR studies is 46. Breaking the molecular structure into halves, DOSY studies suggests -9 and -11% of error when the dimer is solvated with two or three THF molecules, respectively, suggesting their possible existence in solution. A trimer with one molecule of THF appears to have a very low error of -3% and the smaller monomer aggregate with three molecules of THF corresponds to an error of -15%. Additionally, equilibriums between dimers have also been calculated, (Table 2.8) suggesting the possibility of equilibrium between dimers with two and three molecules of THF when the lithium amide is in THF solution.

Table 2.8: Possible equilibriums of dimeric lithium amide (**24**) species in solution and the corresponding errors for  $\text{MW}_{\text{est}}=355$  g/mol.

Equilibrium between dimers	MW (g/mol)	Error (%)
$[[\text{Li}\{\text{N}(\text{CH}_2)_5\}]_2(\text{THF}) + 2\text{THF} \rightleftharpoons [\text{Li}\{\text{N}(\text{CH}_2)_5\}]_2(\text{THF})_3$	326.38	-9
$[[\text{Li}\{\text{N}(\text{CH}_2)_5\}]_2(\text{THF})_2 + \text{THF} \rightleftharpoons [\text{Li}\{\text{N}(\text{CH}_2)_5\}]_2(\text{THF})_3$	362.435	2
$[[\text{Li}\{\text{N}(\text{CH}_2)_5\}]_2(\text{THF})_2 + 2\text{THF} \rightleftharpoons [\text{Li}\{\text{N}(\text{CH}_2)_5\}]_2(\text{THF})_4$	398.485	11
$[[\text{Li}\{\text{N}(\text{CH}_2)_5\}]_2(\text{THF})_3 + \text{THF} \rightleftharpoons [\text{Li}\{\text{N}(\text{CH}_2)_5\}]_2(\text{THF})_4$	434.54	18

Although the trisolvated lithium compound is not the typical for lithium amides in solution, a similar process has been observed by Collum *et al.*<sup>[184]</sup> In their kinetic studies of the lithiation of 1,4-bis(trifluoromethyl)benzene with lithium diisopropylamide in THF, an equilibrium of LDA disolvated and trisolvated dimers in THF solution is proposed.

Similarly, the DOSY NMR studies were carried out for the sodium amide **25**, in a 40 mM  $d_8$ -THF solution with TMS as internal standard. In the same manner to the results obtained with the lithium amide **24**, the  $^1\text{H}$  DOSY NMR technique suggested different possible aggregation states in  $d_8$ -THF solution (Figure 2.9).

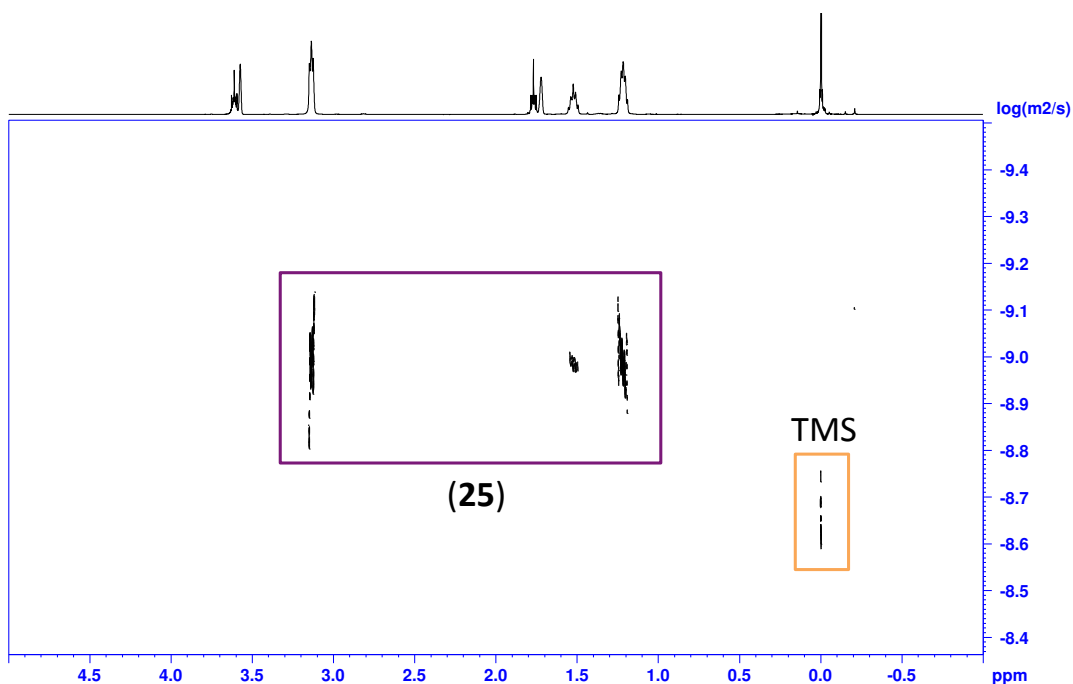
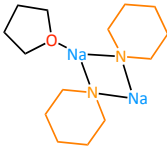
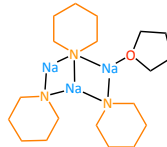
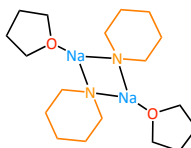
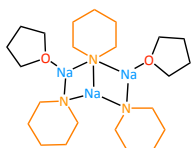
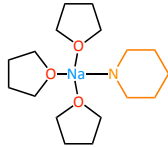
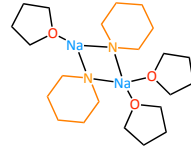
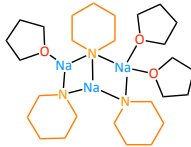
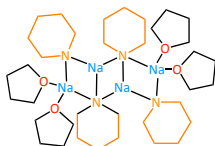


Figure 2.9:  $^1\text{H}$  DOSY experiment in  $d_8$ -THF of a mixture of compound **25** (40 mM) and the internal standard TMS.

The diffusion coefficient value obtained was  $D = 1.027 \cdot 10^{-9} \text{ m}^2/\text{s}$  and the estimated molecular weight 399 g/mol when the sodium amide compound is dissolved in  $d_8$ -THF. The errors of possible aggregation states of the sodium amide **25** are presented in Table 2.9 as well as possible dimeric equilibriums with THF exchange.

Table 2.9: Possible sodium amide (**25**) species in solution and the corresponding errors for  $MW_{est}=399$  g/mol.

	monomer	dimer	trimer	tetramer
<b>1 THF</b>				
<b>MW (g/mol)</b>		286.37	393.50	
<b>Error (%)</b>		-39	1	
<b>2 THF</b>				
<b>MW (g/mol)</b>		358.48	465.61	
<b>Error (%)</b>		-11	14	
<b>3 THF</b>				
<b>MW (g/mol)</b>	323.45	430.58	537.72	
<b>Error (%)</b>	-23	7	26	
<b>4 THF</b>				
<b>MW (g/mol)</b>				716.96
<b>Error (%)</b>				44

Similar possible arrangements of the active species of the lithium and sodium amides were obtained in the  $^1\text{H}$  DOSY NMR studies. As is presented in Table 2.9, the sodium polymer structure is broken up when dissolved in THF. Considering the error obtained in  $^1\text{H}$  DOSY NMR for tetramers (44% for  $[\text{Na}\{\text{N}(\text{CH}_2)_5\}]_4(\text{THF})_4$ ) and monomers (-23% for  $[\text{Na}\{\text{N}(\text{CH}_2)_5\}](\text{THF})_3$ ) and considering the dimeric asymmetric unit for **25** in the solid state, the presence of a tetramer or a monomer in solution seems to be dismissed. However, when a trimer with a molecule of THF is proposed, -1% of error is obtained, suggesting the possibility of  $[\text{Na}\{\text{N}(\text{CH}_2)_5\}]_3(\text{THF})$  species in solution. As well, the dimeric aggregates with two and three molecules of THF seem to be also possible, since the error obtained is -11 and 7% respectively. Similar to **24**, equilibriums between dimers have also been suggested, (Table 2.10) proposing the possibility of a similar equilibrium of the one previously obtained for the lithium amide, considering an equilibrium of dimers with two and three molecules of THF when the sodium amide is in THF solution.

Table 2.10: Possible equilibriums between sodium amide (**25**) species in solution and the corresponding errors for  $\text{MW}_{\text{est}}=399$  g/mol.

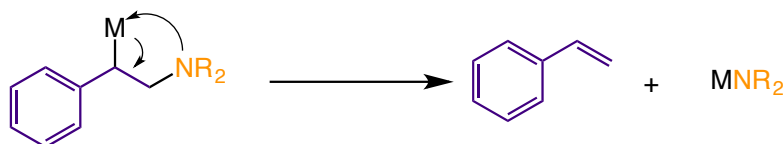
Equilibrium between dimers	MW (g/mol)	Error (%)
$[\text{Na}\{\text{N}(\text{CH}_2)_5\}]_2(\text{THF}) + \text{THF} \rightleftharpoons [\text{Na}\{\text{N}(\text{CH}_2)_5\}]_2(\text{THF})_2$	322.425	-22
$[\text{Na}\{\text{N}(\text{CH}_2)_5\}]_2(\text{THF}) + 2\text{THF} \rightleftharpoons [\text{Na}\{\text{N}(\text{CH}_2)_5\}]_2(\text{THF})_3$	358.475	-9
$[\text{Na}\{\text{N}(\text{CH}_2)_5\}]_2(\text{THF})_2 + \text{THF} \rightleftharpoons [\text{Na}\{\text{N}(\text{CH}_2)_5\}]_2(\text{THF})_3$	394.53	2
$[\text{Na}\{\text{N}(\text{CH}_2)_5\}]_2(\text{THF})_2 + 2\text{THF} \rightleftharpoons [\text{Na}\{\text{N}(\text{CH}_2)_5\}]_2(\text{THF})_4$	430.585	11
$[\text{Na}\{\text{N}(\text{CH}_2)_5\}]_2(\text{THF})_3 + \text{THF} \rightleftharpoons [\text{Na}\{\text{N}(\text{CH}_2)_5\}]_2(\text{THF})_4$	466.635	18

Although  $^1\text{H}$  DOSY NMR is not a conclusive technique, all these different aggregates are possible in solution and DFT calculations will be performed in order to obtain

more conclusive evidence of the energy values for these species to undergo to nucleophilic addition when reacted with styrene.

The lack of solubility in  $d_8$ -THF of all the potassium amides attempted (prepared by reaction of  $\text{KCH}_2\text{SiMe}_3$  with one molar equivalent of the amine) precluded a similar DOSY study for these derivatives.  $^1\text{H}$  NMR studies were not possible to perform in  $\text{C}_6\text{D}_6$  due to the low solubility of the amide compounds **24** and **25** suggesting a higher degree of aggregation compared to a more polar solvent as  $d_8$ -THF.

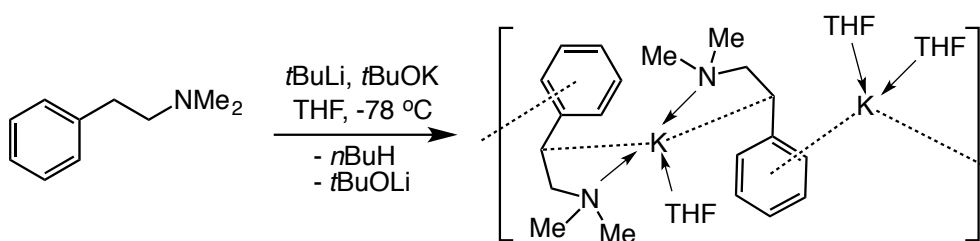
In order to get further mechanistic insights of the catalytic cycle, structural characterisation of intermediate **II** was also attempted. To do so, stoichiometric amounts of amides **24** or **25** with and diphenylacetylene (**1a**) or styrene (**1b**) were reacted. Unfortunately, no single crystals or solids were obtained. Monitoring these addition reactions by NMR in a J. Young's NMR tube in  $d_8$ -THF resulted in intractable mixtures. The reasons of these unsuccessful reactions could be attributed to three different pathways of decomposition. It is known that alkali-metal compounds can react with THF to give ring opening reaction of THF. Since in this case the reactions are in a much higher concentration than in the catalytic conditions, this could suggest a rapid decomposition of the species reacting with THF. Additionally, a competing  $\beta$ -elimination reaction can also take place, regenerating the starting materials (Scheme 2.10).



Scheme 2.10:  $\beta$ -elimination reaction and re-generation of the starting materials.

A third potential decomposition pathway could be attributed to the formation of polymers. As previously mentioned, anionic polymerisation reactions can also be

activated by lithium and sodium amides when treated with styrene, which could also be a potential product formed during the attempts to isolate intermediate **II**.<sup>[185]</sup> Highlighting the highly unstable nature of these intermediates, Strohmann has reported the metallation of a phenethylamine derivative, which appears to form the suggested intermediate **II** of the hydroamination reactions studied (Scheme 2.11).<sup>[186]</sup>



Scheme 2.11: Metallation of 2-phenylethyldimethylamine.<sup>[186]</sup>

As illustrated in the synthesis of this intermediate, cryogenic reaction conditions are needed (-78 °C) suggesting the difficulty to form intermediate **II** from the addition reaction.



## 2.3 Conclusions

In this chapter, we have assessed s-block metal catalysed intermolecular hydroamination processes of alkenes and alkynes using group 1 monosilyl complexes  $[MCH_2Si(Me)_3]$  [M = Li, **3**; Na, **4**; and K, **5**].

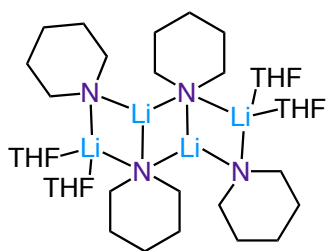
A systematic study using  $MCH_2SiMe_3$  reagents has been performed using a wide range of substituted vinylarenes and variety of amines such as piperidine or morpholine, finding that the reactions occur at room temperature with short timescales. Interestingly, comparative reactivity studies have uncovered a dramatic alkali-metal effect that is dependent on the reaction system, using 5 mol% of the alkali-metal precatalyst. The use of these alkali-metal alkyl compounds  $[MCH_2Si(Me)_3]$  (M = Li, Na, K) in THF solutions afforded excellent yields in mild conditions, which suggest that the nucleophilic addition of the reagent to the unsaturated organic molecule is favoured over the decomposition of the active-amide species (catalyst) in the ethereal THF solvent.

By combining X-ray crystallography with NMR studies (including  $^1H$  DOSY NMR experiments), new insights into the constitution of the possible organometallic intermediates involved in the catalytic process have been gained.

## 2.4 Experimental

### 2.4.1 Synthesis of Active Species

- Synthesis of  $[\text{Li}\{\text{N}(\text{C}_5\text{H}_{10})\}(\text{THF})]_4$  (**24**)



To a solution of  $[\text{Li}(\text{CH}_2\text{SiMe}_3)]$  (1 mL of a 1 M solution of  $[\text{Li}(\text{CH}_2\text{SiMe}_3)]$  in pentane) in hexane (10 mL), piperidine (0.1 mL, 1 mmol) was added and the white suspension was stirred during one hour at room temperature. THF was added (1 mL) and the yellowish solution was transferred to the freezer ( $-15\text{ }^\circ\text{C}$ ). Colourless crystals were obtained after 24 hours, which were isolated and placed into a glovebox (0.036 g, 40%). The THF molecules were removed when the crystals were isolated *in vacuo*.

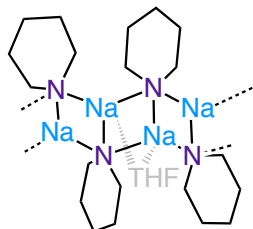
$^1\text{H}$  NMR (400.13 MHz,  $d_8$ -THF, 298 K)  $\delta$  2.99 (m, 4H,  $\text{N}(\text{CH}_2\text{CH}_2)_2\text{CH}_2$ ), 1.52 (m, 2H,  $\text{N}(\text{CH}_2\text{CH}_2)_2\text{CH}_2$ ), 1.23 (m, 4H,  $\text{N}(\text{CH}_2\text{CH}_2)_2\text{CH}_2$ ).

$^{13}\text{C}$  NMR (400.13 MHz,  $d_8$ -THF, 298 K)  $\delta$  56.9 ( $\text{N}(\text{CH}_2\text{CH}_2)_2\text{CH}_2$ ), 32.8 ( $\text{N}(\text{CH}_2\text{CH}_2)_2\text{CH}_2$ ), 28.9 ( $\text{N}(\text{CH}_2\text{CH}_2)_2\text{CH}_2$ ).

$^7\text{Li}$  NMR (155.5 MHz,  $d_8$ -THF, 298 K)  $\delta$  2.51.

**Elemental analysis:** ( $\text{C}_5\text{H}_{10}\text{NLi}$ ) *Calculated:* C: 65.94 % H: 11.07 % N: 15.38 %. *Found:* C: 64.46 % H: 11.07 % N: 15.38 %.

- **Synthesis of  $[\text{Na}_2\{\text{N}(\text{CH}_2)_4\text{CH}_2\}_2(\text{THF})]_\infty$  (25)**



To a solution of  $[\text{Na}(\text{CH}_2\text{SiMe}_3)]$  (0.22 g, 2 mmol) in hexane (10 mL), piperidine (0.2 mL, 2 mmol) was added. The white suspension was stirred during 1 hour at room temperature and THF (3 mL) was added. The yellowish solution was placed to the fridge and after 24 hours colourless crystals were obtained. The crystals were isolated and placed in a glovebox (0.098 g, 46%). The THF molecules were removed when the crystals were isolated *in vacuo*.

$^1\text{H}$  NMR (400.13 MHz,  $d_8$ -THF, 298 K)  $\delta$  3.07 [m, 4H,  $\text{N}(\text{CH}_2\text{CH}_2)_2\text{CH}_2$ ], 1.51 [m, 2H,  $\text{N}(\text{CH}_2\text{CH}_2)_2\text{CH}_2$ ], 1.24 [m, 4H,  $\text{N}(\text{CH}_2\text{CH}_2)_2\text{CH}_2$ ].

$^{13}\text{C}$  NMR (400.13 MHz,  $d_8$ -THF, 298 K)  $\delta$  57.3 [ $\text{N}(\text{CH}_2\text{CH}_2)_2\text{CH}_2$ ], 32.8 [ $\text{N}(\text{CH}_2\text{CH}_2)_2\text{CH}_2$ ], 28.7 [ $\text{N}(\text{CH}_2\text{CH}_2)_2\text{CH}_2$ ].

**Elemental analysis:** ( $\text{C}_5\text{H}_{10}\text{NNa}$ ) Calculated: C: 56.06 % H: 9.41 % N: 11.07 %. Found: C: 55.97 % H: 9.53 % N: 13.97 %.

## 2.4.2 General Experimental Procedure for Catalytic Hydroamination Reactions at NMR Tube Scale

Catalytic reactions were performed in a J. Young's NMR tube at NMR scale following the standard procedure. In a glovebox, the NMR tube was filled with 0.5 mmol of amine, 0.5 mmol of alkene or alkyne, 10 mol% of ferrocene (0.0095 g, 0.05 mmol) as internal standard and 0.609 g of solvent. The initial ratio of starting materials was calculated by integration in  $^1\text{H}$  NMR relative to the ferrocene. The precatalyst (0.025 mmol) was introduced and the reactions times were measured from this point in regular intervals of time until full conversion by  $^1\text{H}$  NMR spectrum (some reactions

were heated in a pre-heated oil bath). All the yields were calculated by integration of the products relative to the ferrocene in the  $^1\text{H}$  NMR spectrum.

- **Synthesis of 1-(1,2-diphenylvinyl)piperidine (6)**

$^1\text{H}$  NMR (400.13 MHz,  $d_8$ -THF, 298 K)  $\delta$  7.36-7.16 [m, 5H,  $H_{\text{ar}}$ ], 6.95-6.70 [m, 5H,  $H_{\text{ar}}$ ], 5.62 [s, 1H, C=CH], 2.90-2.82 [m, 4H,  $\text{N}(\text{CH}_2\text{CH}_2)_2\text{CH}_2$ ], 1.64-1.49 [m, 6H,  $\text{N}(\text{CH}_2\text{CH}_2)_2\text{CH}_2$ ].

$^{13}\text{C}$  NMR (400.13 MHz,  $d_8$ -THF, 298 K)  $\delta$  153.0 [C=C-N], 140.4 [ $C_{\text{q}}$ ], 139.3 [ $C_{\text{q}}$ ], 131.2 [CH], 129.2 [CH], 129.1 [CH], 128.7 [CH], 128.3 [CH], 124.7 [CH], 107.0 [C=CH], 51.2 [ $\text{N}(\text{CH}_2\text{CH}_2)_2\text{CH}_2$ ], 27.2 [ $\text{N}(\text{CH}_2\text{CH}_2)_2\text{CH}_2$ ], 25.4 [ $\text{N}(\text{CH}_2\text{CH}_2)_2\text{CH}_2$ ].

- **Synthesis of 1-(1,2-diphenylvinyl)pyrrolidine (7)**

$^1\text{H}$  NMR (400.13 MHz,  $d_8$ -THF, 298 K)  $\delta$  7.34-7.21 [m, 5H,  $H_{\text{ar}}$ ], 6.89-6.59 [m, 5H,  $H_{\text{ar}}$ ], 5.35 [s, 1H, C=CH], 3.07-2.95 [m, 4H,  $\text{N}(\text{CH}_2\text{CH}_2)_2$ ], 1.88-1.76 [m, 4H,  $\text{N}(\text{CH}_2\text{CH}_2)_2$ ].

$^{13}\text{C}$  NMR (400.13 MHz,  $d_8$ -THF, 298 K)  $\delta$  148.7 [C=C-N], 140.4 [ $C_{\text{q}}$ ], 139.2 [ $C_{\text{q}}$ ], 130.3 [CH], 129.1 [CH], 128.1 [CH], 127.9 [CH], 123.2 [CH], 100.7 (C=CH), 49.1 [ $\text{N}(\text{CH}_2\text{CH}_2)_2$ ], 25.6 [ $\text{N}(\text{CH}_2\text{CH}_2)_2\text{CH}_2$ ].

- **Synthesis of 1-(1,2-diphenylvinyl)morpholine (8)**

$^1\text{H}$  NMR (400.13 MHz,  $d_8$ -THF, 298 K)  $\delta$  7.37-7.21 [m, 5H,  $H_{\text{ar}}$ ], 6.99-6.71 [m, 5H,  $H_{\text{ar}}$ ], 5.63 [s, 1H, C=CH], 3.71-3.59 [m, 4H,  $\text{N}(\text{CH}_2\text{CH}_2)_2\text{O}$ ], 2.89-2.77 [m, 4H,  $\text{N}(\text{CH}_2\text{CH}_2)_2\text{O}$ ].

$^{13}\text{C}$  NMR (400.13 MHz,  $d_8$ -THF, 298 K)  $\delta$  151.9 [C=C-N], 139.7 [ $C_{\text{q}}$ ], 138.2 [ $C_{\text{q}}$ ], 132.3 [ $C_{\text{q}}$ ], 131.2 [CH], 129.2 [CH], 128.8 [CH], 128.2 [CH], 124.7 [CH], 107.0 [C=CH], 50.5 [ $\text{N}(\text{CH}_2\text{CH}_2)_2\text{O}$ ], 47.7 [ $\text{N}(\text{CH}_2\text{CH}_2)_2\text{O}$ ].

- **Synthesis of 1-(1,2-diphenylvinyl)dibutylamine (9)**

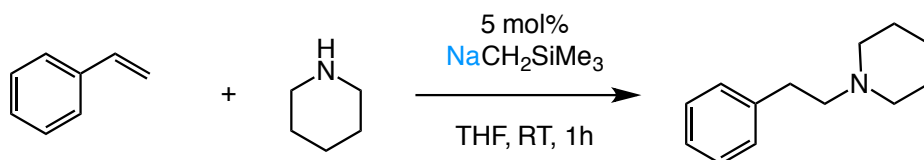
$^1\text{H}$  NMR (400.13 MHz,  $d_8$ -THF, 298 K)  $\delta$  7.31-7.16 [m, 5H,  $H_{\text{ar}}$ ], 6.89-6.80 [m, 2H,  $H_{\text{ar}}$ ], 6.78-6.69 [m, 1H,  $H_{\text{ar}}$ ], 6.66-6.57 [m, 2H,  $H_{\text{ar}}$ ], 5.51 [s, 1H, C=CH], 3.03-2.94 [t, 4H,  $\text{N}(\text{CH}_2\text{CH}_2\text{CH}_2\text{CH}_3)_2$ ], 1.58-1.46 [m, 4H,  $\text{N}(\text{CH}_2\text{CH}_2\text{CH}_2\text{CH}_3)_2$ ], 1.30-1.18 [m, 4H,  $\text{N}(\text{CH}_2\text{CH}_2\text{CH}_2\text{CH}_3)_2$ ], 0.91-0.8 [t, 4H,  $\text{N}(\text{CH}_2\text{CH}_2\text{CH}_2\text{CH}_3)_2$ ].

$^{13}\text{C}$  NMR (400.13 MHz,  $d_8$ -THF, 298 K)  $\delta$  149.7 [C=C-N], 140.1 [ $C_{\text{q}}$ ], 138.9 [ $C_{\text{q}}$ ], 131.0 [CH], 128.7 [ $C_{\text{ar}}$ ], 128.4 [ $C_{\text{ar}}$ ], 128.2 [ $C_{\text{ar}}$ ], 127.7 [ $C_{\text{ar}}$ ], 123.7 [ $C_{\text{ar}}$ ], 105.8 [C=CH], 49.8 [ $\text{N}(\text{CH}_2\text{CH}_2\text{CH}_2\text{CH}_3)_2$ ], 29.5 [ $\text{N}(\text{CH}_2\text{CH}_2\text{CH}_2\text{CH}_3)_2$ ], 21.0 [ $\text{N}(\text{CH}_2\text{CH}_2\text{CH}_2\text{CH}_3)_2$ ], 13.9 [ $\text{N}(\text{CH}_2\text{CH}_2\text{CH}_2\text{CH}_3)_2$ ].

### 2.4.3 General Procedure for Catalytic Hydroamination Reactions of Styrene Derivatives

To an oven dried Schlenk 5 mol% of  $[\text{Na}(\text{CH}_2\text{SiCH}_3)]$  (0.014 g, 0.13 mmol), the styrene derivative (2.5 mmol), the corresponding amine (2.63 mmol) and THF (3.13 mL) were added and stirred at room temperature during one hour. The final products were exposed to air and diluted with diethyl ether (20 mL). An oil was obtained after evaporating to dryness and was purified by chromatographic column (silica gel, hexane : ethyl acetate = 4 : 1).

- **Synthesis of 1-phenethylpiperidine (10)**<sup>[149]</sup>

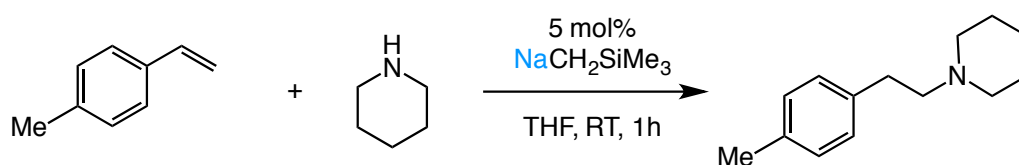


88% of isolated yield (0.4181 g) was obtained for compound **10**.

$^1\text{H}$  NMR (400.13 MHz,  $\text{CDCl}_3$ , 298 K)  $\delta$  7.35-7.39 [m, 2H,  $H_{\text{ar}}$ ], 7.28-7.31 [m, 3H,  $H_{\text{ar}}$ ], 2.90-2.94 [m, 2H,  $\text{PhCH}_2\text{CH}_2\text{N}$ ], 2.64-2.68 [m, 2H,  $\text{PhCH}_2\text{CH}_2\text{N}$ ], 2.57 [bs, 4H,  $\text{N}(\text{CH}_2\text{CH}_2)_2\text{CH}_2$ ], 1.74 [m, 4H,  $\text{N}(\text{CH}_2\text{CH}_2)_2\text{CH}_2$ ], 1.53-1.60 [m, 2H,  $\text{N}(\text{CH}_2\text{CH}_2)_2\text{CH}_2$ ].

$^{13}\text{C}$  NMR (400.13 MHz,  $\text{CDCl}_3$ , 298 K)  $\delta$  140.4 [ $\text{C}_q$ ], 128.4 [CH], 128 [CH], 125.8 [CH], 61.1 [ $\text{PhCH}_2\text{CH}_2\text{N}$ ], 54.5 [ $\text{N}(\text{CH}_2\text{CH}_2)_2\text{CH}_2$ ], 33.4 [ $\text{PhCH}_2\text{CH}_2\text{N}$ ], 25.8 [ $\text{N}(\text{CH}_2\text{CH}_2)_2\text{CH}_2$ ], 24.19 [ $\text{N}(\text{CH}_2\text{CH}_2)_2\text{CH}_2$ ].

- Synthesis of 1-(4-methylphenethyl)piperidine (**11**)<sup>[169]</sup>

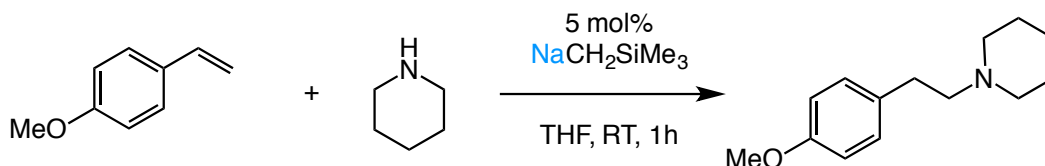


70 % of isolated yield (0.3534 g) was obtained for compound **11**.

$^1\text{H}$  NMR (400.13 MHz,  $\text{CDCl}_3$ , 298 K)  $\delta$  7.08 [s, 4H,  $H_{\text{ar}}$ ], 2.73-2.80 [m, 2H,  $\text{PhCH}_2\text{CH}_2\text{N}$ ], 2.49-2.57 [m, 2H,  $\text{PhCH}_2\text{CH}_2\text{N}$ ], 2.45 [br, 4H,  $\text{N}(\text{CH}_2\text{CH}_2)_2\text{CH}_2$ ], 2.30 [s, 3H,  $\text{CH}_3$ ], 1.58-1.66 [m, 4H,  $\text{N}(\text{CH}_2\text{CH}_2)_2\text{CH}_2$ ], 1.42-1.50 [m, 2H,  $\text{N}(\text{CH}_2\text{CH}_2)_2\text{CH}_2$ ].

$^{13}\text{C}$  NMR (400.13 MHz,  $\text{CDCl}_3$ , 298 K)  $\delta$  137.5 [ $\text{C}_q$ ], 135.2 [ $\text{C}_q$ ], 129.0 [CH], 128.5 [CH], 61.6 [ $\text{PhCH}_2\text{CH}_2\text{N}$ ], 54.6 [ $\text{N}(\text{CH}_2\text{CH}_2)_2\text{CH}_2$ ], 33.2 [ $\text{PhCH}_2\text{CH}_2\text{N}$ ], 25.9 [ $\text{N}(\text{CH}_2\text{CH}_2)_2\text{CH}_2$ ], 24.4 [ $\text{N}(\text{CH}_2\text{CH}_2)_2\text{CH}_2$ ], 20.9 [ $\text{CH}_3$ ].

- Synthesis of 1-(4-methoxyphenethyl)piperidine (**12**)

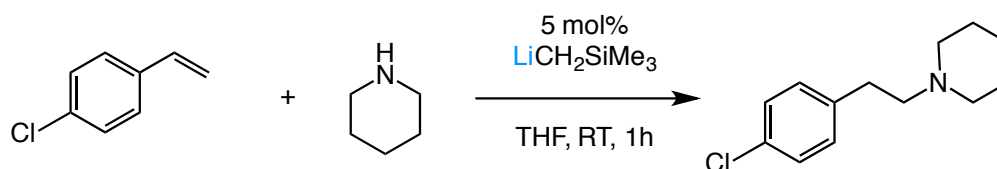


84 % of isolated yield (0.4618 g) was obtained for compound **12**.

$^1\text{H NMR}$  (400.13 MHz,  $\text{CDCl}_3$ , 298 K)  $\delta$  7.03-7.11 [m, 2H,  $H_{\text{ar}}$ ], 6.74-6.79 [m, 2H,  $H_{\text{ar}}$ ], 3.68 [s, 3H,  $\text{CH}_3$ ], 2.67-2.74 [m, 2H,  $\text{PhCH}_2\text{CH}_2\text{N}$ ], 2.43-2.51 [m, 2H,  $\text{PhCH}_2\text{CH}_2\text{N}$ ], 2.33-2.41 [br, 4H,  $\text{N}(\text{CH}_2\text{CH}_2)_2\text{CH}_2$ ], 1.52-1.61 [m, 4H,  $\text{N}(\text{CH}_2\text{CH}_2)_2\text{CH}_2$ ], 1.36-1.45 [m, 4H,  $\text{N}(\text{CH}_2\text{CH}_2)_2\text{CH}_2$ ].

$^{13}\text{C NMR}$  (400.13 MHz,  $\text{CDCl}_3$ , 298 K)  $\delta$  157.7 [ $\text{C}_q$ ], 132.4 [ $\text{C}_q$ ], 129.4 [CH], 113.6 [CH], 61.4 [ $\text{PhCH}_2\text{CH}_2\text{N}$ ], 54.9 [ $\text{CH}_3$ ], 54.4 [ $\text{N}(\text{CH}_2\text{CH}_2)_2\text{CH}_2$ ], 32.5 [ $\text{PhCH}_2\text{CH}_2\text{N}$ ], 25.8 [ $\text{N}(\text{CH}_2\text{CH}_2)_2\text{CH}_2$ ], 24.3 [ $\text{N}(\text{CH}_2\text{CH}_2)_2\text{CH}_2$ ].

• **Synthesis of 1-(4-chlorophenethyl)piperidine (13)** <sup>[149]</sup>

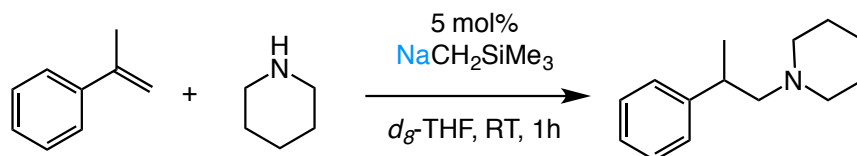


85 % of isolated yield (0.4736 g) was obtained for compound **13**.

$^1\text{H NMR}$  (400.13 MHz,  $\text{CDCl}_3$ , 298 K)  $\delta$  7.16-7.12 [d, 2H,  $J = 8.8$  Hz,  $H_{\text{ar}}$ ], 7.05-7.00 [d, 2H,  $J = 8.4$  Hz,  $H_{\text{ar}}$ ], 2.72-2.63 [m, 2H,  $\text{PhCH}_2\text{CH}_2\text{N}$ ], 2.46-2.40 [m, 2H,  $\text{PhCH}_2\text{CH}_2\text{N}$ ], 2.36 [br, 4H,  $\text{N}(\text{CH}_2\text{CH}_2)_2\text{CH}_2$ ], 1.59-1.48 [m, 4H,  $\text{N}(\text{CH}_2\text{CH}_2)_2\text{CH}_2$ ], 1.42-1.33 [m, 2H,  $\text{N}(\text{CH}_2\text{CH}_2)_2\text{CH}_2$ ].

$^{13}\text{C NMR}$  (400.13 MHz,  $\text{CDCl}_3$ , 298 K)  $\delta$  139.0 [ $\text{C}_q$ ], 131.5 [ $\text{C}_q$ ], 129.9 [ $\text{C}_{\text{ar}}$ ], 128.3 [ $\text{C}_{\text{ar}}$ ], 61.0 [ $\text{PhCH}_2\text{CH}_2\text{N}$ ], 54.3 [ $\text{N}(\text{CH}_2\text{CH}_2)_2\text{CH}_2$ ], 32.8 [ $\text{PhCH}_2\text{CH}_2\text{N}$ ], 25.9 [ $\text{N}(\text{CH}_2\text{CH}_2)_2\text{CH}_2$ ], 24.2 [ $\text{N}(\text{CH}_2\text{CH}_2)_2\text{CH}_2$ ].

- **Synthesis of 1-(2-phenylpropyl)piperidine (14)**<sup>[149]</sup>

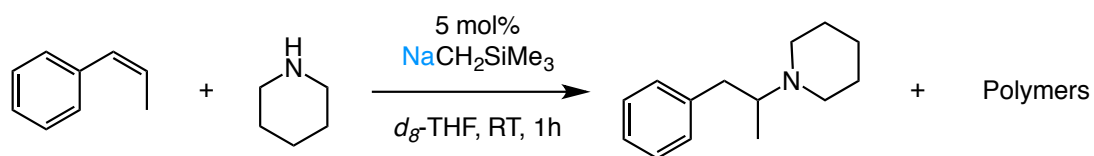


The reaction was performed in a J. Young's NMR tube adding 5 mol% of  $[\text{Na}(\text{CH}_2\text{SiCH}_3)]$  (0.014 g, 0.13 mmol), the styrene derivative (2.5 mmol), the corresponding amine (2.63 mmol) and in  $d_8\text{-THF}$  (0.609 g). 88 % of isolated yield (0.4512 g) was obtained for compound **14**.

$^1\text{H NMR}$  (400.13 MHz,  $\text{CDCl}_3$ , 298 K)  $\delta$  7.23-7.30 [m, 2H,  $H_{\text{ar}}$ ], 7.16-7.23 [m, 3H,  $H_{\text{ar}}$ ], 2.94 [sext., 1H,  $J = 32$  Hz,  $\text{PhCH}$ ], 2.35-2.49 [m, 4H,  $\text{N}(\text{CH}_2\text{CH}_2)_2\text{CH}_2$ ], 2.22-2.35 [br, 2H,  $\text{PhCH}(\text{CH}_3)\text{CH}_2\text{N}$ ], 2.33-2.41 [br, 4H,  $\text{N}(\text{CH}_2\text{CH}_2)_2\text{CH}_2$ ], 1.47-1.63 [m, 4H,  $\text{N}(\text{CH}_2\text{CH}_2)_2\text{CH}_2$ ], 1.34-1.46 [m, 2H,  $\text{N}(\text{CH}_2\text{CH}_2)_2\text{CH}_2$ ], 1.28 [d, 3H,  $J = 12$  Hz,  $\text{CH}_3$ ].

$^{13}\text{C NMR}$  (400.13 MHz,  $\text{CDCl}_3$ , 298 K)  $\delta$  146.6 [ $\text{C}_q$ ], 128.3 [CH], 127.2 [CH], 126.0 [CH], 67.2 [ $\text{PhCH}(\text{CH}_3)\text{CH}_2\text{N}$ ], 55.0 [ $\text{N}(\text{CH}_2\text{CH}_2)_2\text{CH}_2$ ], 37.6 [ $\text{PhCH}$ ], 26.2 [ $\text{N}(\text{CH}_2\text{CH}_2)_2\text{CH}_2$ ], 24.6 [ $\text{N}(\text{CH}_2\text{CH}_2)_2\text{CH}_2$ ], 20.0 [ $\text{CH}_3$ ].

- **Synthesis of 1-(1-phenylpropan-2-yl)piperidine (15)**<sup>[149]</sup>



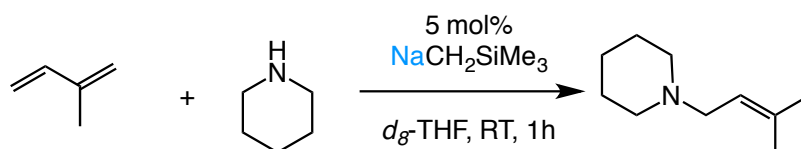
The reaction was performed in a J. Young's NMR tube adding 5 mol% of  $[\text{Na}(\text{CH}_2\text{SiCH}_3)]$  (0.014 g, 0.13 mmol), the styrene derivative (2.5 mmol), the corresponding amine (2.63 mmol) and in  $d_8\text{-THF}$  (0.609 g). 38 % of isolated yield (0.1932 g) was obtained for compound **15** and some polymerisation was observed.



**$^1\text{H}$  NMR (400.13 MHz,  $\text{CDCl}_3$ , 298 K)**  $\delta$  7.24-7.36 [m, 2H,  $H_{\text{ar}}$ ], 7.18-7.36 [m, 3H,  $H_{\text{ar}}$ ], 3.02-3.1 [dd, 1H,  $J = 4$  Hz,  $J = 12$  Hz,  $\text{PhCH}_2\text{CH}_2$ ], 2.78-2.89 [sext., 1H,  $J = 4$  Hz,  $\text{PhCH}_2\text{CH}$ ], 2.54-2.66 [m, 4H,  $\text{N}(\text{CH}_2\text{CH}_2)_2\text{CH}_2$ ], 2.38-2.47 [m, 1H,  $\text{PhCH}_2\text{CH}_2$ ], 1.60-1.70 [m, 4H,  $\text{N}(\text{CH}_2\text{CH}_2)_2\text{CH}_2$ ], 1.46-1.56 [m, 2H,  $\text{N}(\text{CH}_2\text{CH}_2)_2\text{CH}_2$ ], 0.98 [d, 3H,  $J = 8$ ,  $\text{CH}_3$ ].

**$^{13}\text{C}$  NMR (400.13 MHz,  $\text{CDCl}_3$ , 298 K)**  $\delta$  141.4 [ $\text{C}_q$ ], 129.3 [CH], 128.2 [CH], 125.7 [CH], 62.2 [ $\text{PhCH}_2\text{CH}(\text{CH}_3)\text{N}$ ], 49.8 [ $\text{N}(\text{CH}_2\text{CH}_2)_2\text{CH}_2$ ], 39.3 [ $\text{PhCH}_2\text{CH}(\text{CH}_3)\text{N}$ ], 26.7 [ $\text{N}(\text{CH}_2\text{CH}_2)_2\text{CH}_2$ ], 25.1 [ $\text{N}(\text{CH}_2\text{CH}_2)_2\text{CH}_2$ ], 14.3 [ $\text{CH}_3$ ].

- **Synthesis of 1-(3-methylbut-2-enyl)piperidine (16a)** <sup>[149]</sup>

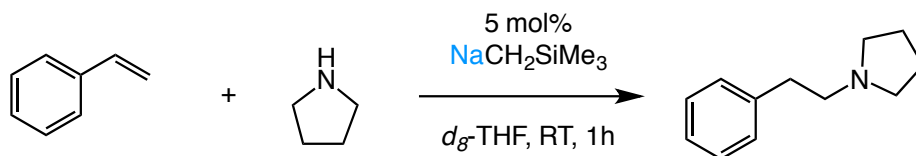


The reaction was performed in a J. Young's NMR tube adding 5 mol% of [ $\text{Na}(\text{CH}_2\text{SiCH}_3)$ ] (0.014 g, 0.13 mmol), the styrene derivative (2.5 mmol), the corresponding amine (2.63 mmol) and in  $d_8$ -THF (0.609 g). 51 % of isolated yield (0.195 g) was obtained for compound **16a**.

**$^1\text{H}$  NMR (400.13 MHz,  $\text{CDCl}_3$ , 298 K)**  $\delta$  5.23 [m, 1H,  $\text{NCH}_2\text{CH}=\text{C}(\text{CH}_3)_{\text{ab}}$ ], 2.78-2.89 [sext., 1H,  $J = 4$  Hz,  $\text{N}(\text{CH}_2\text{CH}_2)_2\text{CH}_2$ ], 2.24-2.40 [m, 4H,  $\text{N}(\text{CH}_2\text{CH}_2)_2\text{CH}_2$ ], 1.67 [m, 3H,  $\text{NCH}_2\text{CH}=\text{C}(\text{CH}_3)_{\text{ab}}$ ], 1.58 [s, 4H,  $\text{NCH}_2\text{CH}=\text{C}(\text{CH}_3)_{\text{ab}}$ ], 1.49-1.56 [m, 4H,  $\text{N}(\text{CH}_2\text{CH}_2)_2\text{CH}_2$ ], 1.33-1.43 [m, 2H,  $\text{N}(\text{CH}_2\text{CH}_2)_2\text{CH}_2$ ].

**$^{13}\text{C}$  NMR (400.13 MHz,  $\text{CDCl}_3$ , 298 K)**  $\delta$  134.5 [ $\text{NCH}_2\text{CH}=\text{C}(\text{CH}_3)_{\text{ab}}$ ], 121.59 [ $\text{NCH}_2\text{CH}=\text{C}(\text{CH}_3)_{\text{ab}}$ ], 56.8 [ $\text{NCH}_2\text{CH}=\text{C}(\text{CH}_3)_{\text{ab}}$ ], 54.8 [ $\text{N}(\text{CH}_2\text{CH}_2)_2\text{CH}_2$ ], 26.4 [ $\text{N}(\text{CH}_2\text{CH}_2)_2\text{CH}_2$ ], 24.6 [ $\text{N}(\text{CH}_2\text{CH}_2)_2\text{CH}_2$ ], 18.0 [ $\text{NCH}_2\text{CH}=\text{C}(\text{CH}_3)_{\text{ab}}$ ].

- **Synthesis of 1-phenethylpyrrolidine (17)**<sup>[149]</sup>

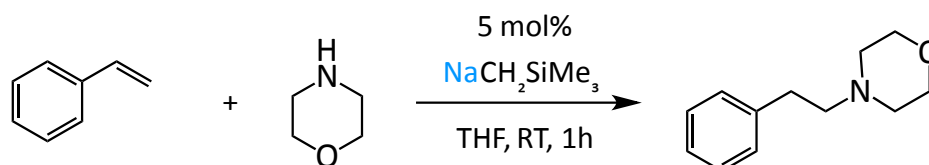


The reaction was performed in a J. Young's NMR tube adding 5 mol% of  $[\text{Na}(\text{CH}_2\text{SiCH}_3)]$  (0.014 g, 0.13 mmol), the styrene derivative (2.5 mmol), the corresponding amine (2.63 mmol) and in  $d_8\text{-THF}$  (0.609 g). 88 % of isolated yield (0.3889 g) was obtained for compound **17**.

**$^1\text{H}$  NMR (400.13 MHz,  $\text{CDCl}_3$ , 298 K)**  $\delta$  7.34-7.40 [m, 2H,  $H_{\text{ar}}$ ], 7.27-7.33 [m, 3H,  $H_{\text{ar}}$ ], 2.94 [m, 2H,  $\text{PhCH}_2\text{CH}_2\text{N}$ ], 2.80 [m, 2H,  $\text{PhCH}_2\text{CH}_2\text{N}$ ], 2.63-2.71 [m, 4H,  $\text{N}(\text{CH}_2\text{CH}_2)_2$ ], 1.86-1.95 [m, 4H,  $\text{N}(\text{CH}_2\text{CH}_2)_2$ ].

**$^{13}\text{C}$  NMR (400.13 MHz,  $\text{CDCl}_3$ , 298 K)**  $\delta$  140.4 [ $\text{C}_q$ ], 128.4 [CH], 128.2 [CH], 125.8 [CH], 58.2 [ $\text{PhCH}_2\text{CH}_2\text{N}$ ], 54.0 [ $\text{N}(\text{CH}_2\text{CH}_2)_2$ ], 35.8 [ $\text{PhCH}_2\text{CH}_2\text{N}$ ], 23.4 [ $\text{N}(\text{CH}_2\text{CH}_2)_2$ ].

- **Synthesis of 4-phenethylmorpholine (18)**<sup>[149]</sup>

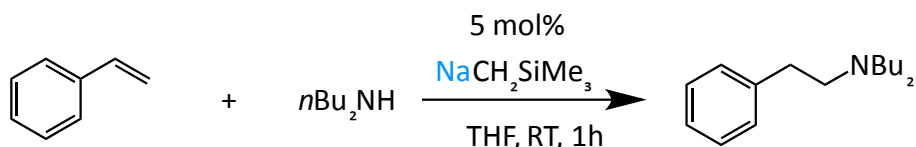


80 % of isolated yield (0.3835 g) was obtained for compound **18**.

**$^1\text{H}$  NMR (400.13 MHz,  $\text{CDCl}_3$ , 298 K)**  $\delta$  7.35-7.39 [m, 2H,  $H_{\text{ar}}$ ], 7.28-7.3 [m, 3H,  $H_{\text{ar}}$ ], 3.79 [t, 4H,  $J = 4$  Hz,  $\text{OCH}_2$ ], 2.88 [dd, 2H,  $J = 4$  Hz,  $J = 8$  Hz,  $\text{PhCH}_2\text{CH}_2\text{N}$ ], 2.65 [dd, 2H,  $J = 4$  Hz,  $J = 8$  Hz,  $\text{PhCH}_2\text{CH}_2\text{N}$ ], 2.54 [s, 4H,  $\text{N}(\text{CH}_2\text{CH}_2)_2\text{O}$ ].

**$^{13}\text{C}$  NMR (400.13 MHz,  $\text{CDCl}_3$ , 298 K)**  $\delta$  139.6 [ $\text{C}_q$ ], 128.0 [CH], 127.7 [CH], 125.4 [CH], 66.2 [ $\text{OCH}_2$ ], 60.2 [ $\text{PhCH}_2\text{CH}_2\text{N}$ ], 53.1 [ $\text{N}(\text{CH}_2\text{CH}_2)_2\text{O}$ ], 32.7 [ $\text{PhCH}_2\text{CH}_2\text{N}$ ].

- **Synthesis of N,N-dibutyl-benzeneethanamine (19)**<sup>[187]</sup>

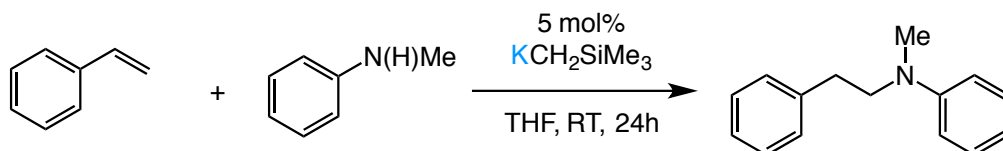


74 % of isolated yield (0.4330 g) was obtained for compound **19**.

<sup>1</sup>H NMR (400.13 MHz, CDCl<sub>3</sub>, 298 K) δ 7.34-7.40 [m, 2H, H<sub>ar</sub>], 7.27-7.32 [m, 3H, H<sub>ar</sub>], 2.83-2.89 [m, 2H, N(CH<sub>2</sub>CH<sub>2</sub>CH<sub>2</sub>CH<sub>3</sub>)<sub>2</sub>], 2.78-2.83 [m, 2H, N(CH<sub>2</sub>CH<sub>2</sub>CH<sub>2</sub>CH<sub>3</sub>)<sub>2</sub>], 2.60 [m, 4, PhCH<sub>2</sub>CH<sub>2</sub>N], 1.56 [m, 4H, N(CH<sub>2</sub>CH<sub>2</sub>CH<sub>2</sub>CH<sub>3</sub>)<sub>2</sub>], 1.45 [m, 4H, N(CH<sub>2</sub>CH<sub>2</sub>CH<sub>2</sub>CH<sub>3</sub>)<sub>2</sub>], 1.05 [m, 6H, N(CH<sub>2</sub>CH<sub>2</sub>CH<sub>2</sub>CH<sub>3</sub>)<sub>2</sub>].

<sup>13</sup>C NMR (400.13 MHz, CDCl<sub>3</sub>, 298 K) δ 140.9 [C<sub>q</sub>], 128.7 [CH], 128.2 [CH], 125.6 [CH], 56.5 [PhCH<sub>2</sub>CH<sub>2</sub>N], 53.7 [N(CH<sub>2</sub>CH<sub>2</sub>CH<sub>2</sub>CH<sub>3</sub>)<sub>2</sub>], 33.8 [PhCH<sub>2</sub>CH<sub>2</sub>N], 29.2 [N(CH<sub>2</sub>CH<sub>2</sub>CH<sub>2</sub>CH<sub>3</sub>)<sub>2</sub>], 20.8 [N(CH<sub>2</sub>CH<sub>2</sub>CH<sub>2</sub>CH<sub>3</sub>)<sub>2</sub>], 14.2 [N(CH<sub>2</sub>CH<sub>2</sub>CH<sub>2</sub>CH<sub>3</sub>)<sub>2</sub>].

- **Synthesis of N-methyl-N-phenylethylaniline (20)**<sup>[65]</sup>

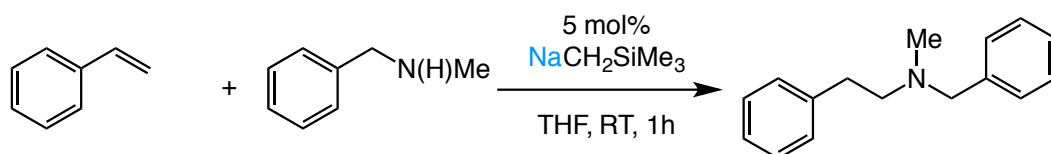


To an oven dried Schlenk 5 mol% of [K(CH<sub>2</sub>SiCH<sub>3</sub>)] (0.015 g, 0.13 mmol), the styrene derivative (2.5 mmol), the corresponding amine (2.63 mmol) and THF (3.13 mL) were added and stirred under reflux during 24 hours. 69 % of isolated yield (0.3661 g) was obtained for compound **20** after purification.

<sup>1</sup>H NMR (400.13 MHz, CDCl<sub>3</sub>, 298 K) δ 7.18-7.46 [m, 7H, H<sub>ar</sub>], 6.75-6.93 [m, 7H, H<sub>ar</sub>], 3.63 [m, 2H, PhCH<sub>2</sub>CH<sub>2</sub>N], 2.94 [s, 3H, CH<sub>3</sub>], 2.89-2.93 [m, 2H, PhCH<sub>2</sub>CH<sub>2</sub>N].

$^{13}\text{C}$  NMR (400.13 MHz,  $\text{CDCl}_3$ , 298 K)  $\delta$  148.6 [ $\text{C}_q$ ], 139.7 [ $\text{C}_q$ ], 129.4 [CH], 128.9 [CH], 128.6 [CH], 126.3 [CH], 116.4 [CH], 112.4 [CH], 54.6 [ $\text{PhCH}_2\text{CH}_2\text{N}$ ], 38.3 [ $\text{CH}_3$ ], 33.0 [ $\text{PhCH}_2\text{CH}_2\text{N}$ ].

- Synthesis of N-benzyl-N-methyl-2-phenylethanamine (**21**)<sup>[65]</sup>

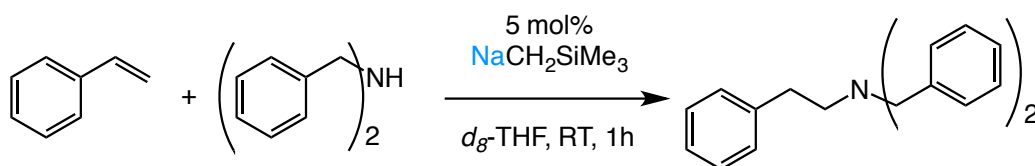


84 % of isolated yield (0.4761 g) was obtained for compound **21**.

$^1\text{H}$  NMR (400.13 MHz,  $\text{CDCl}_3$ , 298 K)  $\delta$  7.46-7.60 [m, 7H,  $H_{ar}$ ], 7.39-7.46 [m, 2H,  $H_{ar}$ ], 3.80 [s, 2H,  $\text{NCH}_2\text{Ph}$ ], 3.04-3.14 [m, 2H,  $\text{PhCH}_2\text{CH}_2\text{N}$ ], 2.87-2.97 [m, 2H,  $\text{PhCH}_2\text{CH}_2\text{N}$ ], 2.52 [s, 3H,  $\text{CH}_3$ ].

$^{13}\text{C}$  NMR (400.13 MHz,  $\text{CDCl}_3$ , 298 K)  $\delta$  140.5 [ $\text{C}_q$ ], 139.1 [ $\text{C}_q$ ], 128.9 [CH], 128.7 [CH], 128.3 [CH], 128.2 [CH], 126.9 [CH], 125.9 [CH], 62.3 [ $\text{NCH}_2\text{Ph}$ ], 59.2 [ $\text{PhCH}_2\text{CH}_2\text{N}$ ], 42.2 [ $\text{CH}_3$ ], 34.0 [ $\text{PhCH}_2\text{CH}_2\text{N}$ ].

- Synthesis of N,N-dibenzyl-2-phenylethanamine (**22**)<sup>[149]</sup>

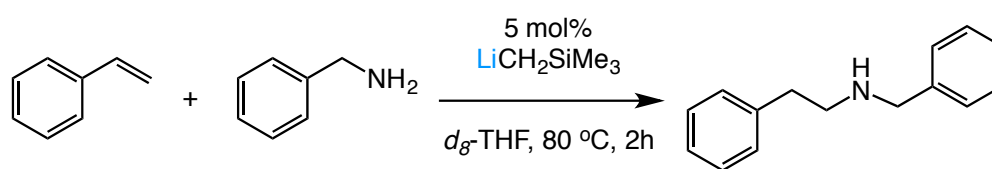


The reaction was performed in a J. Young's NMR tube adding 5 mol% of [ $\text{Na}(\text{CH}_2\text{SiCH}_3)$ ] (0.014 g, 0.13 mmol), the styrene derivative (2.5 mmol), the corresponding amine (2.63 mmol) and in  $d_8$ -THF (0.609 g). 72 % of isolated yield (0.54 g) was obtained for compound **22**. 28 % of the byproduct was also purified.

$^1\text{H}$  NMR (400.13 MHz,  $\text{CDCl}_3$ , 298 K)  $\delta$  7.15-7.44 [m, 13H,  $H_{\text{ar}}$ ], 7.06-7.14 [m, 2H,  $H_{\text{ar}}$ ], 3.66 [s, 4H,  $\{\text{Ph-CH}_2\}_2\text{N}$ ], 2.78-2.86 [m, 2H,  $\text{PhCH}_2\text{CH}_2\text{N}$ ], 2.71-2.78 [m, 2H,  $\text{PhCH}_2\text{CH}_2\text{N}$ ].

$^{13}\text{C}$  NMR (400.13 MHz,  $\text{CDCl}_3$ , 298 K)  $\delta$  140.7 [ $\text{C}_q$ ], 139.7 [ $\text{C}_q$ ], 128.9 [CH], 128.7 [CH], 128.2 [CH], 126.8 [CH], 125.7 [CH], 58.3 [ $\text{PhCH}_2\text{N}$ ], 54.9 [ $\text{PhCH}_2\text{CH}_2\text{N}$ ], 33.5 [ $\text{PhCH}_2\text{CH}_2\text{N}$ ].

- Synthesis of N-benzyl-2-phenylethanamine (**23**)<sup>[149]</sup>



The reaction was performed in a J. Young's NMR tube adding 5 mol% of  $[\text{Li}(\text{CH}_2\text{SiCH}_3)]$  (0.011 g, 0.13 mmol), the styrene derivative (2.5 mmol), the corresponding amine (2.63 mmol) and in  $d_8$ -THF (0.609 g). The mixture was heated at 80 °C during 2 hours. 65 % of isolated yield (0.3442 g) was obtained for compound **23**.

$^1\text{H}$  NMR (400.13 MHz,  $\text{CDCl}_3$ , 298 K)  $\delta$  7.20-7.39 [m, 10H,  $H_{\text{ar}}$ ], 3.83 [s, 2H,  $\text{NCH}_2\text{Ph}$ ], 2.89-2.96 [m, 2H,  $\text{PhCH}_2\text{CH}_2\text{N}$ ], 2.81-2.89 [m, 2H,  $\text{PhCH}_2\text{CH}_2\text{N}$ ], 1.53 [s, 1H,  $\text{NH}$ ].

$^{13}\text{C}$  NMR (400.13 MHz,  $\text{CDCl}_3$ , 298 K)  $\delta$  140.3 [ $\text{C}_q$ ], 139.9 [ $\text{C}_q$ ], 128.6 [CH], 128.3 [CH], 128.2 [CH], 127.9 [CH], 126.7 [CH], 126.0 [CH], 53.8 [ $\text{NCH}_2\text{Ph}$ ], 50.3 [ $\text{PhCH}_2\text{CH}_2\text{N}$ ], 36.4 [ $\text{PhCH}_2\text{CH}_2\text{N}$ ].

## Chapter 3 Hydroamination Reactions Using Alkali-Metal Magnesiate Precatalysts

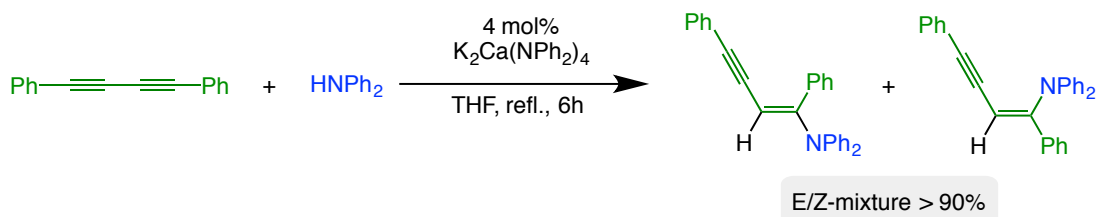
### 3.1 Introduction

#### 3.1.1 Hetero-Bimetallic Main Compounds in Catalysis

Bimetallic catalysis represents an alternative to the more conventional single-metal catalytic transformations in order to modify some reaction parameters, such as the selectivity or even the activity.<sup>[188,189]</sup> Key to the success of this mixed-metal catalysts is the proximity of those metals that allows them to work synergically, where normally one metal acts as a Lewis acid and the other one is part of an ate complex with the capability of behaving as a Lewis base.

Bimetallic catalysts have been known to date, combining different types of metals such as alkali-metals, lanthanides or transition metals.<sup>[189]</sup> Recent reports have been focusing on systems containing main group metals to promote catalytic reactions. For example, Westerhausen has demonstrated the synergic effect of bimetallic s-block metal catalysts. Potassium calciates such as  $[\text{K}_2\text{Ca}(\text{NPh}_2)_4]$  or  $[\text{K}_2\text{Ca}\{\{\text{N}(\text{H})\text{Dipp}\}_4\}]$  can efficiently catalyse hydroamination reactions of diphenylbutadiyne with a variety of anilines.<sup>[131-134]</sup> Exemplifying the cooperative effect of the ate compound as a catalyst, no reaction product is observed when

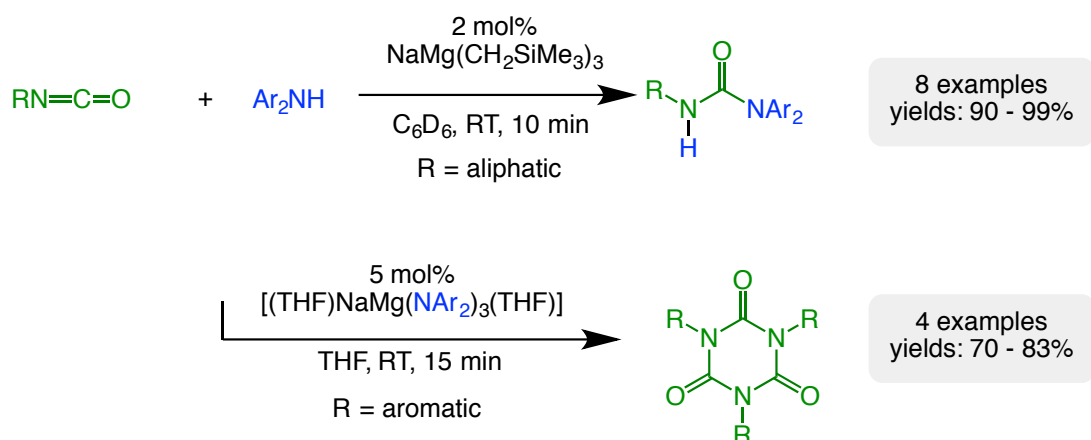
adding diphenylamine to 1,4-diphenylbutadiyne in presence of  $\text{Ca}(\text{NPh}_2)_2$  or  $\text{KNPh}_2$ . However, when the bimetallic calciate compound  $\text{K}_2\text{Ca}(\text{NPh}_2)_4$  is used as a catalyst the hydroamination products are formed in a >90% NMR yield (Z isomer 40.4%, isolated yield) (Scheme 3.1).<sup>[131]</sup>



Scheme 3.1: Hydroamination reaction of 1,4-diphenylbutadiyne and diphenylamine using  $[\text{K}_2\text{Ca}(\text{NPh}_2)_4]$  catalyst.<sup>[131]</sup>

### 3.1.1.1 Magnesiates in catalysis

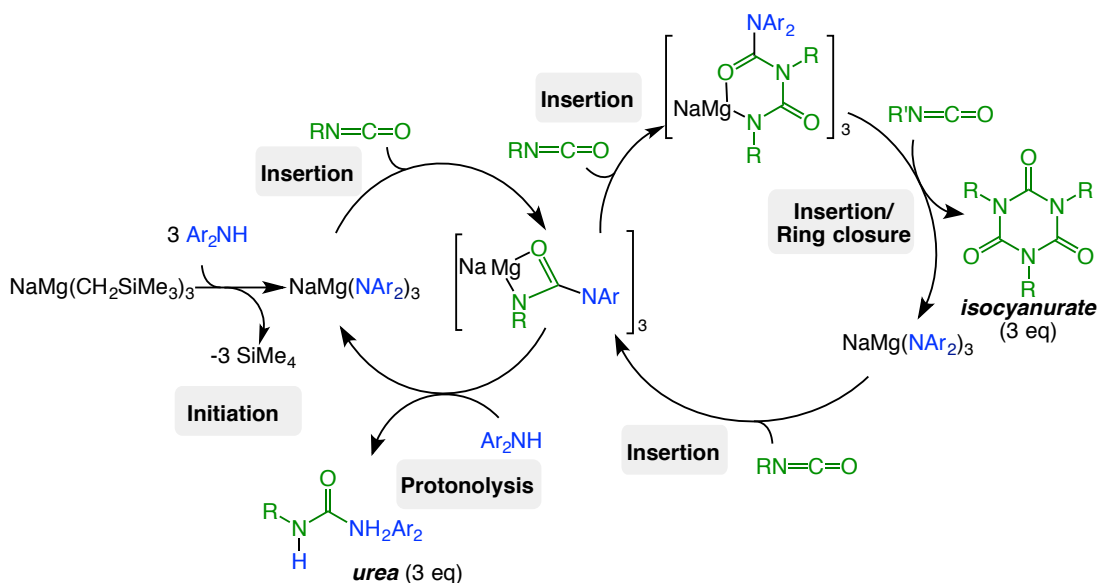
As previously mentioned in the introduction, alkali-metal magnesiates have already shown their properties as metallating agents and their enhanced nucleophilic power in a multitude of stoichiometric applications, surpassing in many occasions the performances of conventional single-metal reagents.<sup>[48,70]</sup> Opening new ground towards expanding the synthetic applications for mixed-metal reagents, our group has demonstrated that triorgano sodium magnesiate  $[\text{NaMg}(\text{CH}_2\text{SiMe}_3)_3]$ <sup>[128]</sup> has excellent catalytic capabilities to promote hydroamination/cyclotrimerization processes of isocyanates (Scheme 3.2).<sup>[129]</sup> These studies constitute the first example of magnesiate-mediated catalysed reactions.



Scheme 3.2: Sodium magnesiate-mediated hydroamination and trimerization reactions of isocyanates.<sup>[129]</sup>

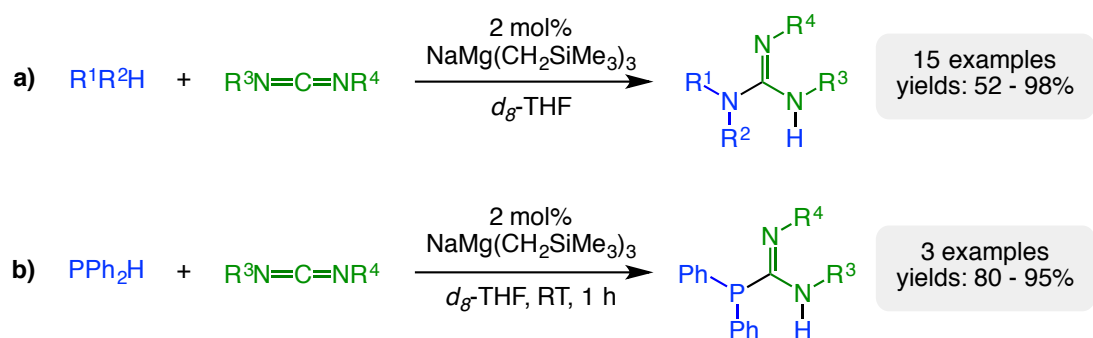
Stoichiometric studies have hinted that these reactions occur via similar mechanisms to those previously proposed in lanthanide chemistry for the hydroamination of isocyanates.<sup>[190]</sup> Thus, the homoalkyl magnesiate  $[\text{NaMg}(\text{CH}_2\text{SiMe}_3)_3]$  firstly deprotonates the amine to form an active tris(amido) species, which in turn undergoes nucleophilic addition to the unsaturated electrophile  $\text{RNCO}$  (Scheme 3.3). This nucleophilic addition can be favoured by coordination of  $\text{RNCO}$  to the Lewis acidic sodium centre, to form a tris(ureido)species which can then undergo protonolysis regenerating the nucleophilic amide magnesiate and liberating the hydroamination product.





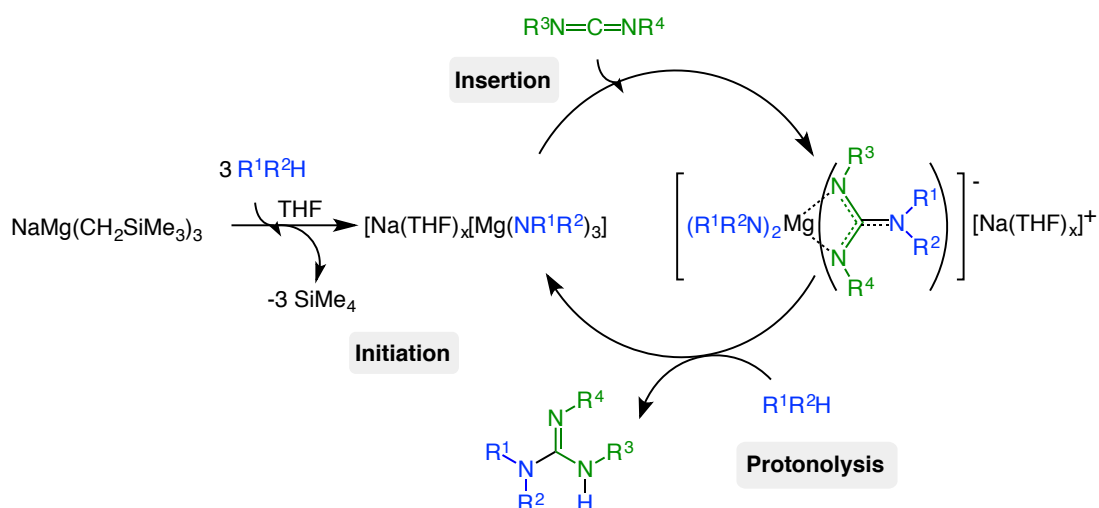
Scheme 3.3: Proposed catalytic cycle for sodium-magnesiate-mediated hydroamination and trimerization of isocyanates.<sup>[129]</sup>

Building on the catalytic applications of alkali-metal magnesiates, sodium magnesiate  $[\text{NaMg}(\text{CH}_2\text{SiMe}_3)_3]$  has also been reported by our group as an efficient catalyst for the guanylation and hydrophosphination of amines (Scheme 3.4).<sup>[130]</sup>



Scheme 3.4: Sodium magnesiate mediated-catalyzed a) guanylation and b) hydrophosphination of amines.<sup>[130]</sup>

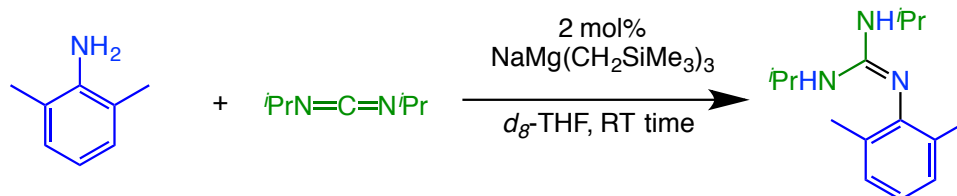
Stoichiometric and kinetic experiments provided mechanistic insights for these transformations and a catalytic cycle was suggested that is presented in Scheme 3.5.



Scheme 3.5: Proposed catalytic cycle for sodium-magnesiate-mediated-catalyzed guanylation of amines.<sup>[130]</sup>

An initial deprotonation of the ate compound forms a nucleophilic tris(amido) magnesiate that undergoes to insertion of the carbodiimide giving a sodium magnesiate guanidinate compound. By protonolysis of this second intermediate the guanidine product is obtained and the active sodium tris(amido) magnesiate is regenerated, which is the actual catalyst of the reaction.

Furthermore, these studies have shown that the catalytic activity of the mixed-metal complexes is better than its homometallic components. For example, the guanidination of 2,6-dimethylaniline with *N,N'*-diisopropylcarbodiimide is presented in Table 3.1 using different precatalysts.<sup>[130]</sup>

Table 3.1: Comparison of the different precatalytic species in the guanidination reaction of 2,6-dimethylaniline with *N,N'*-diisopropylcarbodiimide in *d*<sub>8</sub>-THF at RT.<sup>[130]</sup>

Entry	Precatalyst	Time (h)	Yield (%) <sup>[a]</sup>
1	[NaCH <sub>2</sub> SiMe <sub>3</sub> ]	0.25	72
2	[NaCH <sub>2</sub> SiMe <sub>3</sub> ]	1	84
3	[Mg(CH <sub>2</sub> SiMe <sub>3</sub> ) <sub>2</sub> ]	0.25	44
4	[Mg(CH <sub>2</sub> SiMe <sub>3</sub> ) <sub>2</sub> ]	16	99
5	[NaMg(CH <sub>2</sub> SiMe <sub>3</sub> ) <sub>3</sub> ]	0.25	99

<sup>[a]</sup> Yields determined by <sup>1</sup>H NMR using ferrocene as an internal standard.

As exemplified in Table 3.1 the sodium magnesiate complex [NaMg(CH<sub>2</sub>SiMe<sub>3</sub>)<sub>3</sub>] provides better catalytic activity than that of the monometallic components [NaCH<sub>2</sub>SiMe<sub>3</sub>] and [Mg(CH<sub>2</sub>SiMe<sub>3</sub>)<sub>2</sub>]. After 15 minutes of reaction the yield obtained for the guanidine product using [NaMg(CH<sub>2</sub>SiMe<sub>3</sub>)<sub>3</sub>] precatalyst is 99%, whereas for [NaCH<sub>2</sub>SiMe<sub>3</sub>] and [Mg(CH<sub>2</sub>SiMe<sub>3</sub>)<sub>2</sub>] is 72 and 44% respectively (Table 3.1 entry 5 vs entries 1 and 3).

The mechanistic studies on these transformations have shown that the key for the success of the catalytic process is the formation of a bifunctional catalyst which combines a Lewis acid (the Na cation) to which the unsaturated substrate can coordinate, being activated towards the nucleophilic attack of the magnesiate anion (Figure 3.1).

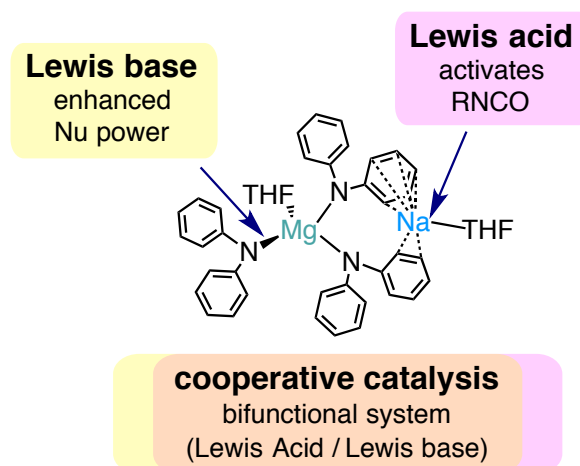


Figure 3.1: Bifunctional catalyst.

With the aim of expanding the scope of s-block cooperative catalysis in this chapter we report our findings assessing the ability of magnesiate compounds to promote intermolecular hydroamination reactions of alkenes and alkynes. A wide range of unsaturated substrates and primary and secondary amines have been studied in order to expand the scope of the catalytic approach, which allowed us to compare with the homometallic system described in Chapter 2. Additionally, structural and mechanistic studies have also been carried out to shed some light on the putative active species.

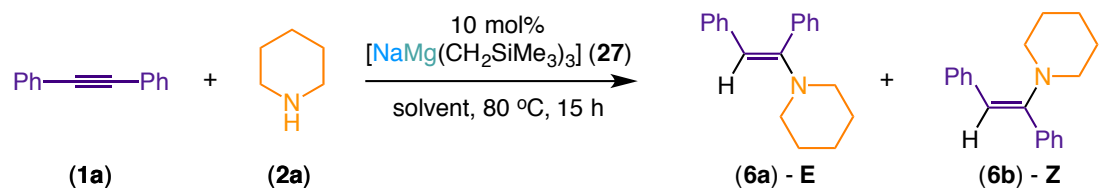
## 3.2 Results and Discussion

### 3.2.1 Optimisation of the Reaction Conditions

#### 3.2.1.1 Studies using Lower-Order Magnesiate Precatalysts

Similar to the monometallic systems described in Chapter 2, we first studied the reaction of diphenylacetylene (**1a**) and piperidine (**2a**) in different solvents and a 5 mol%  $\text{NaMg}(\text{CH}_2\text{SiMe}_3)_3$  (**27**) of precatalyst. The sodium magnesiate **27** was prepared by co-complexation of its homometallic components.<sup>[128]</sup> To investigate the role of the solvent, three different solvents with different coordinating abilities were employed ( $\text{CDCl}_3$ ,  $\text{C}_6\text{D}_6$  and  $d_8$ -THF in a 0.08 M concentration). All the reactions were performed in a J. Young's NMR tube using 10 mol% of  $\text{NaMg}(\text{CH}_2\text{SiMe}_3)_3$  (**27**) as precatalyst and heated at 80 °C during 15 hours.

Table 3.2: Hydroamination reaction of **1a** and **2a** in different solvents at 80 °C during 15 hours, using 10 mol% of precatalyst **27**.



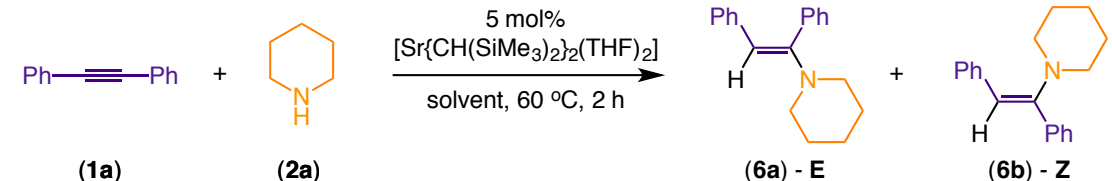
Entry	Solvent	Yield (%) <sup>[a]</sup>	E:Z <sup>[b]</sup>
1	$\text{CDCl}_3$	0	-
2	$\text{C}_6\text{D}_6$	42	90:10
3	$d_8$ -THF	100	63:37

<sup>[a]</sup> Yields determined by  $^1\text{H}$  NMR using ferrocene as an internal standard. <sup>[b]</sup> Determined by  $^1\text{H}$  NMR spectroscopy

As Table 3.2 shows, there exist a strong dependence of the solvent in the hydroamination reaction of the diphenylacetylene (**1a**) and the piperidine (**2a**). Using chlorinated solvent  $\text{CDCl}_3$ , no conversion is observed at 15 hours of reaction. Contrastingly, employing  $\text{C}_6\text{D}_6$  or  $d_8$ -THF compounds **6a** and **6b** are formed although the yield of the hydroamination process also showed a strong dependence with the solvent. Using  $\text{C}_6\text{D}_6$ , only 42% conversion is obtained after 15 hours whereas with the more coordinating ethereal solvent  $d_8$ -THF full conversion is observed. The solvent also affects the chemoselectivity of the process. Thus, in  $\text{C}_6\text{D}_6$  after 15 hours a 90:10 ratio of E:Z products is obtained whereas for  $d_8$ -THF, under these conditions, the ratio is 63:37.

Analogous solvent effect has been observed when **27** acts as catalyst for guanylation reactions.<sup>[130]</sup> Similarly, greater conversion of the guanidine product has been obtained when employing the more polar ethereal solvent  $d_8$ -THF in comparison with  $\text{C}_6\text{D}_6$ . Additionally, similar solvent dependence in intermolecular hydroamination reactions was also noticed by Hill in their studies using alkaline-earth metals as precatalysts.<sup>[149]</sup> In their work shown at Table 3.3, they report the study of the same reaction with the use of a 5 mol% of the strontium precatalyst  $[\text{Sr}\{\text{CH}(\text{SiMe}_3)_2\}_2(\text{THF})_2]$ .

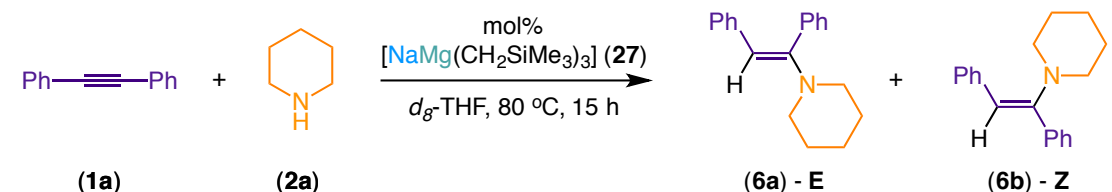
Table 3.3: Hydroamination reaction of **1a** and **2a** in different solvents at 60 °C during 2 hours, using 5 mol% of precatalyst  $[\text{Sr}\{\text{CH}(\text{SiMe}_3)_2\}_2(\text{THF})_2]$  reported by Hill.<sup>[149]</sup>



Entry	Solvent	Yield (%)	E:Z
1	<i>d</i> <sub>8</sub> -THF	100	91:9
2	C <sub>6</sub> D <sub>6</sub>	41	60:40
3	hexane	44	60:40

As a second step of the optimisation of the reaction conditions, different catalyst loads were tested in *d*<sub>8</sub>-THF (Table 3.4).

Table 3.4: Hydroamination reaction of **1a** and **2a** in *d*<sub>8</sub>-THF at 80 °C during 15 hours and using different amounts of **27** as precatalyst.



Entry	mol % ( <b>27</b> )	Yield (%) <sup>[a]</sup>	E:Z <sup>[b]</sup>
1	2	97	66:34
2	5	90	60:40
3	10	100	63:37

<sup>[a]</sup> Yields determined by <sup>1</sup>H NMR using ferrocene as an internal standard. <sup>[b]</sup> Determined by <sup>1</sup>H NMR spectroscopy

As presented in Table 3.4, the catalyst load can be reduced up to 2 mol% without significantly affecting the conversion or the selectivity of the reaction. However, in order to compare with the monometallic precatalysts  $[\text{MCH}_2\text{Si}(\text{Me})_3]$  [ $\text{M} = \text{Li}$ , **3**;  $\text{Na}$ , **4**; and  $\text{K}$ , **5**], 5 mol% of magnesiated precatalyst was used.

The effect of the alkali metal as a component of the bimetallic precatalyst (5 mol%) was also examined for the reaction of diphenylacetylene (**1a**) and the piperidine (**2a**). Comparing the results obtained of the  $[\text{MMg}(\text{CH}_2\text{SiMe}_3)_3]$  ( $\text{M} = \text{Li}$  (**26**),  $\text{Na}$  (**27**) and  $\text{K}$  (**28**)) with the bimetallic strontium precatalyst used by M. Hill,<sup>[149]</sup> longer times were required with the lithium, sodium or potassium lower order magnesiates (Table 3.5).

Table 3.5: Comparison of the different yields obtained in the hydroamination reaction of **1a** and **2a** in  $d_8$ -THF at 80 °C.

$\text{Ph}-\text{C}\equiv\text{C}-\text{Ph}$  +  $\xrightarrow[\text{d}_8\text{-THF, 80 }^\circ\text{C, time}]{\text{5 mol\% precatalyst}}$  +

**(1a)**                      **(2a)**                                      **(6a) - E**                      **(6b) - Z**

Entry	precatalyst	Time (h)	Yield (%) <sup>[a]</sup>	E:Z <sup>[b]</sup>
<b>1</b>	$[\text{Sr}\{\text{CH}(\text{SiMe}_3)_2\}_2(\text{THF})_2]$	2	100	91:9
<b>2</b>	$\text{LiMg}(\text{CH}_2\text{SiMe}_3)_3$ ( <b>26</b> )	18	49	86:14
<b>3</b>	$\text{NaMg}(\text{CH}_2\text{SiMe}_3)_3$ ( <b>27</b> )	18	98	70:30
<b>4</b>	$\text{KMg}(\text{CH}_2\text{SiMe}_3)_3$ ( <b>28</b> )	18	59	84:16

<sup>[a]</sup> Yields determined by  $^1\text{H}$  NMR using ferrocene as an internal standard. <sup>[b]</sup> Determined by  $^1\text{H}$  NMR spectroscopy

Full conversion was obtained by the low order sodium magnesiate precatalyst (**27**) when the reaction takes place at 80 °C in  $d_8$ -THF after 18 hours of heating (Table



3.5, entry 3). However, with Hill's strontium precatalyst, the reaction requires 2 hours to afford 100% yield in good selectivity.<sup>[149]</sup> As observed Table 3.5, precatalyst **27** has higher activity compared to the lithium and potassium congeners. Similar to Chapter 2 and the previous studies with group 2 catalysts<sup>[116]</sup> an alkali-metal effect has been observed, however in this case the reactivity is not proportional to the radius of the alkali-metal. Additionally, the selectivity towards the E product remains superior than Z when using **26**, **27** and **28**. However, a better selectivity is observed when using **26** (E:Z; 86:14) and **28** (E:Z; 84:16) compared to **27** (E:Z; 70:30) (Table 3.5, entries 2, 3 and 4).

### 3.2.1.2 Studies using higher-order magnesiate precatalysts

Encouraged by the initial results using homoleptic triorganomagnesiates **26**, **27** and **28** we next studied the ability of the higher order derivatives  $[(\text{TMEDA})_2\text{Li}_2\text{Mg}(\text{CH}_2\text{SiMe}_3)_4]^{[191]}$  (**29**)  $[(\text{TMEDA})_2\text{Na}_2\text{Mg}(\text{CH}_2\text{SiMe}_3)_4]^{[127]}$  (**30**) and  $[(\text{PMDETA})_2\text{K}_2\text{Mg}(\text{CH}_2\text{SiMe}_3)_4]^{[127]}$  (**31**). Previous studies assessing the reactivity of these compounds have shown that they can be significantly more activated within the context of deprotonative metallation<sup>[48]</sup> and Mg-halogen exchange<sup>[126]</sup> reactions than their lower-order derivatives.

The same hydroamination reaction of **1a** and **2a** was explored using the high order magnesiates as precatalysts.

Table 3.6: Comparison of different alkali-metal magnesiate precatalysts in the intermolecular hydroamination reaction of diphenylacetylene (**1a**) and piperidine (**2a**) in  $d_8$ -THF at RT.

Reaction scheme: Diphenylacetylene (**1a**) + Piperidine (**2a**)  $\xrightarrow[5 \text{ mol\% } [(L)_2M_2Mg(CH_2SiMe_3)_4] \text{ (29, 30 and 31)}]{d_8\text{-THF, RT, 3 h}}$  (6a) - E + (6b) - Z

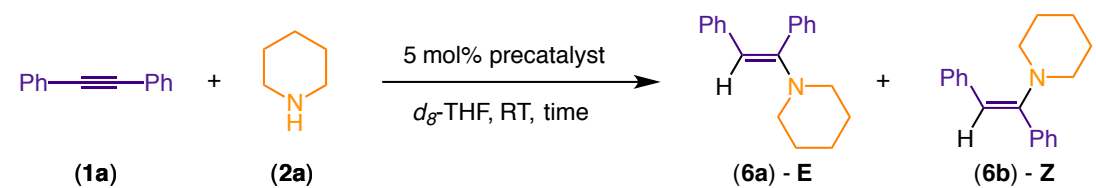
Entry	precatalyst	Yield (%) <sup>[a]</sup>	E:Z <sup>[b]</sup>
<b>1</b>	$[(TMEDA)_2Li_2Mg(CH_2SiMe_3)_4]$ ( <b>29</b> )	0	-
<b>2</b>	$[(TMEDA)_2Na_2Mg(CH_2SiMe_3)_4]$ ( <b>30</b> )	28	29:71
<b>3</b>	$[(PMDETA)_2K_2Mg(CH_2SiMe_3)_4]$ ( <b>31</b> )	100	93:7

<sup>[a]</sup> Yields determined by  $^1H$  NMR using ferrocene as an internal standard. <sup>[b]</sup> Determined by  $^1H$  NMR spectroscopy.

As shown in Table 3.6, there exist a dramatic alkali-metal effect with  $[(TMEDA)_2Li_2Mg(CH_2SiMe_3)_4]$  (**29**) being the slowest precatalyst, which in 3 hours of reaction can not achieve any conversion (Table 3.6, entry 1). Contrastingly, when the reaction is performed with the potassium magnesiate precatalyst  $[(PMDETA)_2K_2Mg(CH_2SiMe_3)_4]$  (**31**) 100% yield and excellent selectivity (E:Z; 93:7) is obtained. A similar trend in the alkali-metal effect regarding the reactivity and selectivity was found for the monometallic alkali-metal precatalysts explained in Chapter 2. This tendency is related again to the different aggregation state of the active species in solution that are formed at the first step of the reaction. The fact that these reactions can take place at room temperature, in contrast to the lower order magnesiates, is because they have an enhanced nucleophilic character.

The corresponding monometallic components of **31** were also tested as precatalysts for the hydroamination reaction of diphenylacetylene (**1a**) and piperidine (**2a**) (Table 3.7).

Table 3.7: Comparison of different precatalysts in the intermolecular hydroamination reaction of diphenylacetylene (**1a**) and piperidine (**2a**) in *d*<sub>8</sub>-THF at RT.



Entry	Precatalyst	Time	Yield (%) <sup>[a]</sup>	E:Z <sup>[b]</sup>
1	$[(\text{PMDETA})_2\text{K}_2\text{Mg}(\text{CH}_2\text{SiMe}_3)_4]$ ( <b>31</b> )	3	100	93:7
2	$\text{KCH}_2\text{SiMe}_3$ ( <b>5</b> )	0.25	100	92:8
3	$\text{Mg}(\text{CH}_2\text{SiMe}_3)_2$	24	0 <sup>[c]</sup>	-
4	$[(\text{PMDETA})_2\text{K}_2\text{Mg}(\text{CH}_2\text{SiMe}_3)_4]$ ( <b>31</b> ) + 10 mol% 18-crown-6	24	0 <sup>[c]</sup>	-

<sup>[a]</sup> Yields determined by <sup>1</sup>H NMR using ferrocene as an internal standard. <sup>[b]</sup> Determined by <sup>1</sup>H NMR spectroscopy. <sup>[c]</sup> 0% yield after heating at 80 °C for 24 hours.

When the single-metal  $\text{Mg}(\text{CH}_2\text{SiMe}_3)_2$  complex was used as a precatalyst no conversion was observed even heating the reaction at 80 °C during 24 hours (Table 3.7, entry 3). The same behaviour was found when using 5 mol% of  $[(\text{PMDETA})_2\text{K}_2\text{Mg}(\text{CH}_2\text{SiMe}_3)_4]$  (**31**) and adding 10 mol% of 18-crown-6, which is known to have a high affinity towards the potassium cations (Table 3.7, entry 4).<sup>[126]</sup> The fact that no conversion is observed when adding the crown ether, which can block the potassium coordination sites, suggests that the potassium atom has a key role and enables the coordination to the unsaturated molecule (Lewis acid

activation) and facilitates the nucleophilic addition bringing it into close proximity to the anionic amido magnesiate. Contrastingly, in the guanylation reactions catalysed by  $[\text{NaMg}(\text{CH}_2\text{SiMe}_3)_3]$  (**27**) the effect of the crown ether 15-crown-5 only shows a slight decrease on the reactivity, suggesting a secondary role of the alkali-metal in this processes.<sup>[130]</sup>

As demonstrated in Chapter 2, the alkali metal monometallic potassium precatalyst  $\text{KCH}_2\text{SiMe}_3$  (**5**) displays a higher reactivity than the bimetallic complex  $[(\text{PMDETA})_2\text{K}_2\text{Mg}(\text{CH}_2\text{SiMe}_3)_4]$  (**31**) (Table 3.7, entry 1 vs entry 2). Full conversion and excellent selectivity is achieved after 15 minutes when precatalyst **5** is used, whereas 3 hours are needed for **31**. These results differ from those obtained previously in the group for magnesiates in catalysis as reported in the introduction. In those reports,  $[\text{NaMg}(\text{CH}_2\text{SiMe}_3)_3]$  has a higher catalytic capability than its monometallic components  $\text{Na}(\text{CH}_2\text{SiMe}_3)$  or  $\text{Mg}(\text{CH}_2\text{SiMe}_3)_2$  in order to promote hydroamination/cyclotrimerization of isocyanates<sup>[129]</sup> or towards the guanylation of amines (Table 3.1).<sup>[130]</sup> However, in this system, the higher polarity of the K-N bonds in addition of the large size of the potassium atom, facilitates the  $\pi$ -coordination of the alkyne and activates it towards addition of the amido species.

### 3.2.2 Substrate Scope

Initial results of the reaction scope using different amines have been obtained. A variety of aliphatic and aromatic amines has been reacted with diphenylacetylene (**1a**) using potassium complex **31** as precatalyst (5 mol% of precatalyst in  $d_8$ -THF at room temperature) (Table 3.8).

Table 3.8: Intermolecular hydroamination of diphenylacetylene (**1a**) and a range of secondary amines (**2a-2c**, **2g-2h**) catalyzed by potassium precatalyst (**31**) in *d*<sub>8</sub>-THF at room temperature.

$$\text{Ph-C}\equiv\text{C-Ph} + \text{R}_2\text{NH} \xrightarrow[\text{d}_8\text{-THF, RT, time}]{\text{5 mol\% } [(\text{PMDETA})_2\text{K}_2\text{Mg}(\text{CH}_2\text{SiMe}_3)_4] \text{ (31)}} \text{Ph-CH=CH-Ph} + \text{Ph-CH=CH-NR}_2$$

(1a)
(2a-2c, 2g-2h)
(6a-8a) - E
(6b-8b) - Z

Entry	Amine	t (h)	Product	Yield (%) <sup>[a]</sup>	E:Z <sup>[b]</sup>
1	NH ( <b>2a</b> )	3	<b>6</b>	100	93:7
2	NH ( <b>2b</b> )	2	<b>7</b>	100	94:6
3	NH ( <b>2c</b> )	24	<b>8</b>	80	92:8
4	Bz <sub>2</sub> NH ( <b>2g</b> )	24	-	0 <sup>[c]</sup>	-
5	Ph <sub>2</sub> NH ( <b>2h</b> )	24	-	0 <sup>[c]</sup>	-

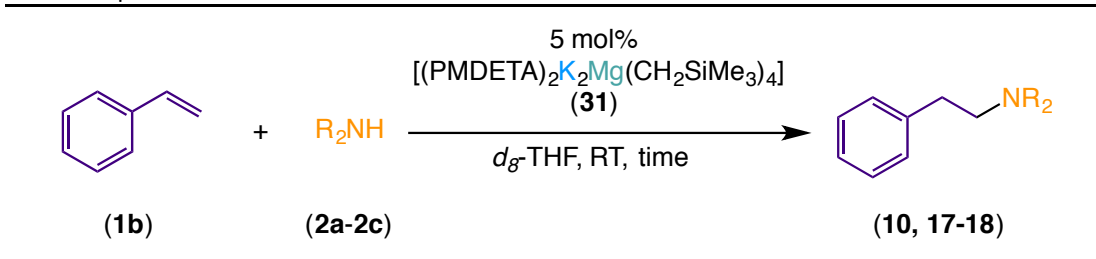
<sup>[a]</sup> Yields determined by <sup>1</sup>H NMR using ferrocene as an internal standard. <sup>[b]</sup> Determined by <sup>1</sup>H NMR integration of spectra. <sup>[c]</sup> 0% yield after heating at 80 °C for 24 hours.

Table 3.8 illustrates the results obtained when diphenylacetylene (**1a**) is reacted with a variety of amines. Similar to the monometallic precatalysts studied in Chapter 2, the reactivity of the cyclic amines piperidine (**2a**), pyrrolidine (**2b**) and morpholine (**2c**) (Table 3.8, entries 1 - 3) is superior to the aromatic dibenzylamine (**2g**) and diphenylamine (**2h**) (Table 3.8, entries 4 - 5), which do not form the hydroamination product. As observed in Chapter 2 and previous reports by Hill using the strontium precatalyst [Sr{CH(SiMe<sub>3</sub>)<sub>2</sub>]<sub>2</sub>(THF)<sub>2</sub>] the formation of the E isomer remains preferred over Z.

In order to obtain full conversion towards the hydroamination products **6** and **7**, when reacting diphenylacetylene (**1a**) with the six and five membered ring amines piperidine (**2a**) and pyrrolidine (**2b**), 3 and 2 hours at room temperature are required using precatalyst **31** (Table 3.8, entries 1 and 2). In comparison to the analogous reaction using precatalyst **5** [KCH<sub>2</sub>SiMe<sub>3</sub>] longer times are required. A much slower hydroamination reaction is observed when reacting diphenylacetylene (**1a**) with morpholine (**2c**), which requires 24 hours at room temperature to afford **8a** and **8b** (92:8) in 80% yield. As discussed in Chapter 2, these reactions are reported using transition metal catalysts such as nickel or gold, where long periods of time and high temperatures are required.<sup>[167,168]</sup>

The hydroamination reactions of diphenylacetylene (**1a**) with the bulky amines dibenzylamine (**2g**) and diphenylamine (**2h**) are not observed, even when the reaction is heated at 80 °C during 24 hours (Table 3.8, entries 4 and 5). However, NMR monitoring of the reaction indicates the formation of a KMg-amide, which suggests that this new complex is not nucleophilic enough to undergo to nucleophilic addition and initiate the catalytic cycle. These results are similar to the ones found when using precatalyst **5** [KCH<sub>2</sub>SiMe<sub>3</sub>], where no reaction is observed.

Initial findings of the reactivity of styrene and the cyclic amines namely piperidine (**2a**), pyrrolidine (**2b**) and morpholine (**2c**) have also been explored. The results obtained are displayed in Table 3.9, when using 5 mol% of **31** in *d*<sub>8</sub>-THF at room temperature.

Table 3.9: Intermolecular hydroamination of styrene (**1b**) with different amines (**2a-2c**) in  $d_8$ -THF at room temperature.

Entry	Amine	t (h)	Product	Yield (%) <sup>[a]</sup>
1	NH ( <b>2a</b> )	0.25	<b>10</b>	100
2	NH ( <b>2b</b> )	0.25	<b>17</b>	100
3	NH ( <b>2c</b> )	0.25	<b>18</b>	100

<sup>[a]</sup> Yields determined by <sup>1</sup>H NMR using ferrocene as an internal standard.

The hydroamination reactions between styrene (**1b**) and the six and five membered ring amines (**2a – 2c**) afford the *anti*-Markovnikov products **10**, **17** and **18** instantly (15 minutes) at room temperature and using 5 mol% of **31** in  $d_8$ -THF (Table 3.9, entries 1 - 3). This high catalytic activity is similar to the one obtained when using the sodium and potassium precatalysts **4** [NaCH<sub>2</sub>SiMe<sub>3</sub>] and **5** [KCH<sub>2</sub>SiMe<sub>3</sub>], obtaining full conversion towards compounds **10**, **17** and **18** using the same reaction conditions as in Table 3.9. In contrast, other reports have shown that high temperatures and long periods of times are required for these reactions. For example, LiN(SiMe<sub>3</sub>)<sub>2</sub> (5 mol%) with the presence of TMEDA (5 mol%) in C<sub>6</sub>D<sub>6</sub> at 120 - 150 °C, can afford compounds **10**, **17** and **18** after 1 – 3 hours in 61-82 % yields.<sup>[65]</sup>

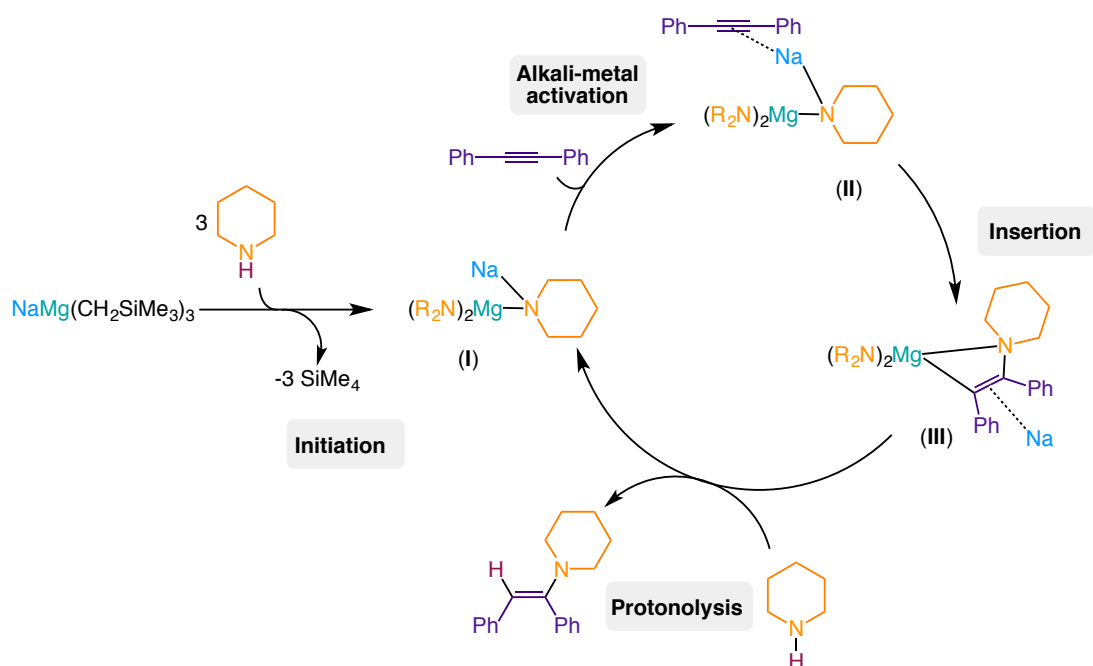
Group 2 catalysts such as  $[\text{Sr}\{\text{CH}(\text{SiMe}_3)_2\}_2(\text{THF})_2]$  achieve the hydroamination product **10** in 70% yield after 10 minutes at room temperature by using 5 mol% of the strontium precatalyst.<sup>[149]</sup> Further work on the reaction scope needs to be performed in order to assess if a different reactivity is obtained compared to the monometallic precatalysts studied in Chapter 2.

### 3.2.3 Study of the Catalytic Cycle

Analogous to Chapter 2 a series of stoichiometric studies have been performed in order to understand the constitution of the possible intermediates.

Previous studies on heavier alkali-earth metal chemistry by Hill assessing the ability of  $[\text{Sr}\{\text{CH}(\text{SiMe}_3)_2\}_2(\text{THF})_2]$ <sup>[149]</sup> to catalyse intermolecular hydroamination of alkenes and alkynes have revealed that they operate in a similar manner as early transition metal compounds.<sup>[192]</sup> Combining these results and those of Chapter 2, a similar catalytic cycle for the bimetallic magnesiate catalysts is suggested (Scheme 3.6).





Scheme 3.6: Proposed catalytic cycle for intermolecular hydroamination reactions *via* metal amide species catalysed by alkali-metal magnesiate catalysts.

Similar to Chapter 2, this process involves the deprotonation of the relevant amine, generating a nucleophilic amide intermediate (intermediate I in Scheme 3.6), where the alkali-metal  $\pi$ -engages with the C-C triple bond of the unsaturated organic molecule (intermediate II in Scheme 3.6), facilitating the insertion and generating intermediate III. Protonolysis of the addition product by the excess of amine can regenerate the nucleophilic active metal amide intermediate I and liberate the relevant hydroamination product.

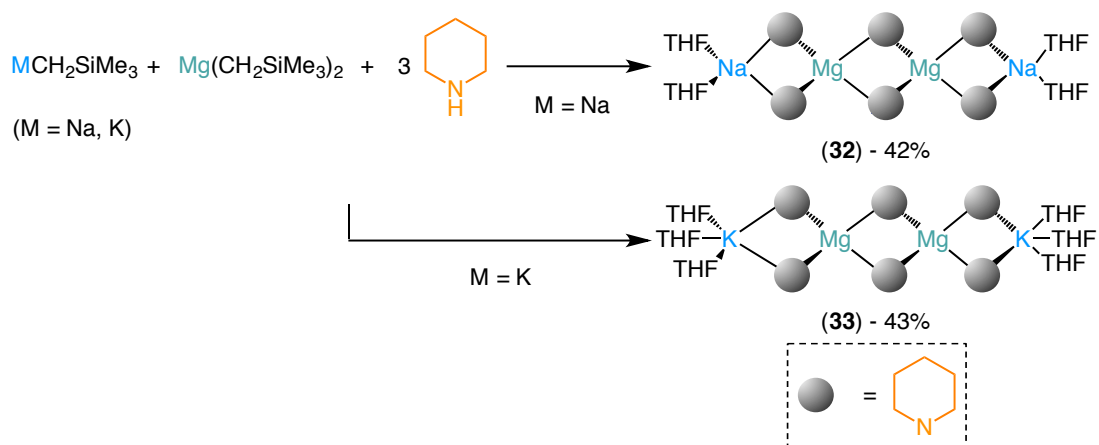
In order to shed some light on the possible intermediates involved in these catalytic processes, the stoichiometric reactions of magnesiates  $[\text{MMg}(\text{CH}_2\text{SiMe}_3)_3]$  ( $\text{M} = \text{Na}, \text{K}$ ) and  $[(\text{donor})_2\text{M}_2\text{Mg}(\text{CH}_2\text{SiMe}_3)_4]$  ( $\text{M} = \text{Na}, \text{K}$ ) were investigated with several amines. To prepare the homoleptic amido-alkali metal magnesiates, the relevant tri- and tetraorgano- derivatives were prepared by mixing the monometallic

compounds  $MCH_2SiMe_3$  and  $Mg(CH_2SiMe_3)_2$  in a 1:1 or 2:1 ratio respectively using hexane as a solvent. This approach allowed the isolation of compounds  $[(THF)_2\{NaMg(NC_5H_{10})_3\}]_2$  (**32**),  $[(THF)_3\{KMg(NC_5H_{10})_3\}]_2$  (**33**),  $[(TMEDA)_2\{Na_2Mg(NC_5H_{10})_4\}]$  (**34**) and  $[PMDTA)_2\{K_2Mg(NC_5H_{10})_4\}]$  (**35**), as crystalline solids all in relatively good yields.

### 3.2.3.1 Synthesis of homoleptic alkali-metal amide magnesiates

The amide active species were synthesized and characterized. The low order sodium and potassium amido-magnesiates (**32** and **33**, respectively) were characterized in the solid state by X-Ray crystallography and by NMR spectroscopic studies (including  $^1H$  DOSY NMR) in  $d_8$ -THF solutions.

Compounds **32** and **33** are the likely active catalyst species of the hydroamination reactions described. These compounds were obtained as colourless crystals by reaction of the precursors  $MCH_2SiMe_3$  ( $M = Na$  or  $K$ ),  $Mg(CH_2SiMe_3)_2$  and the corresponding amine piperidine, in 42 and 43% yield (Scheme 3.7). The X-Ray crystallographic studies confirmed the existence of the corresponding amides, which have also been characterized by  $^1H$  and  $^{13}C$  NMR spectroscopy.

Scheme 3.7: Synthesis of lower order sodium and potassium magnesiate amides **32** and **33**.

Lower order alkali-metal magnesiates **32** and **33** share the same structural motif in the solid state (Figure 3.2 and Figure 3.3), displaying a dimeric contacted ion-pair structure where the metals adopt a MMgMgM pseudo linear arrangement forming three fused four-membered rings orthogonal to each other. No precedent amide structures with the MMgMgM arrangement were found in the CCDC database, although a similar amido lithium zincate supported by the TMEDA donor  $[\{(\text{TMEDA})\text{LiZn}(\text{NMe}_2)_3\}_2]$ , reported by our group, follows the same architecture.<sup>[193]</sup>

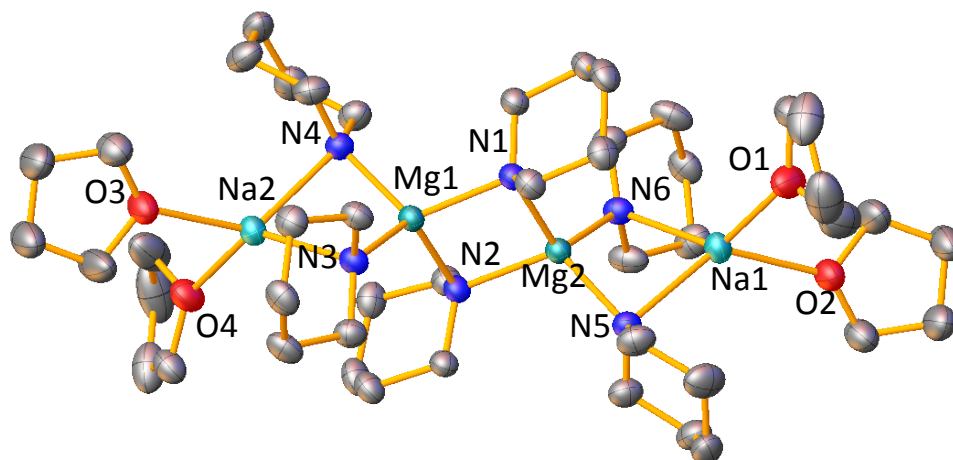


Figure 3.2: Molecular structure of **32** with 50% probability displacement ellipsoids. All hydrogen atoms have been omitted for clarity. Selected bond lengths (Å) and bond angles (°): Na1-N5 2.4719(16), Na1-N6 2.4445(17), Na1-O1 2.3480(17), Na1-O2 2.3625(15), Na2-N3 2.4635(17), Na2-N4 2.4607(16), Na2-O3 2.3519(15), Na2-O4 2.3429(16), Mg1-N1 2.1403(15), Mg1-N2 2.1224(15), Mg1-N3 2.0661(15), Mg1-N4 2.0773(16), Mg2-N1 2.1202(15), Mg2-N2 2.1352(15), Mg2-N5 2.0774(16), Mg2-N6 2.0733(15), O1-Na1-O2 81.62(6), O1-Na1-N6 129.76(6), O2-Na1-N6 122.56(6), O1-Na1-N5 117.61(6), O2-Na1-N5 130.77(6), N6-Na1-N5 81.29(5), O4-Na2-O3 84.46(6), O4-Na2-N4 117.11(6), O3-Na2-N4 128.70(6), O4-Na2-N3 132.81(6), O3-Na2-N3 119.46(6), N4-Na2-N3 80.82(5), N3-Mg1-N4 100.79(6), N3-Mg1-N2 117.72(6), N4-Mg1-N2 116.28(6), N3-Mg1-N1 116.20(6), N4-Mg1-N1 115.76(6), N2-Mg1-N1 91.19(6), N6-Mg2-N5 100.99(6), N6-Mg2-N1 117.33(6), N5-Mg2-N1 117.67(6), N6-Mg2-N2 114.82(6), N5-Mg2-N2 115.65(6), N1-Mg2-N2 91.39(6).

Compound **32** displays a dimeric contacted ion-pair structure where the metals adopt a pseudolinear [NaMgMgNa] arrangement (Na2⋯Mg1⋯Mg2, 158.48(3)° and Mg1⋯Mg2⋯Na1, 161.77(3)°). The Mg centres bind to four piperidine groups (average Mg-N internal, 2.13(1) Å and Mg-N external, 2.07(1) Å), whereas each sodium atom is attached to two amido groups (average Na-N, 2.46(1) Å) and two solvating molecules of THF. Both Na and Mg atoms exhibit a tetrahedral coordination (angles at Na1 and Na2 ranging from 80.82(5)° to 132.81(6)°; angles at Mg1 and Mg2 ranging from 91.19(6)° to 117.72(6)°). The Mg atoms bind to two bridging amido groups to form a [MgNMgN] planar four-membered ring (sum of angles, 359.92°), which is orthogonal to two adjacent [NaNMgN] rings (sum of

angles,  $347.88^\circ$  and  $349.88^\circ$ ). This core motif of three fused four-membered rings, comprising MMgMgM arrangement has been previously reported.<sup>[194,195]</sup>

As obtained in other bimetallic complexes, Mg-N bonds (Mg-N distances ranging from 2.0661(15) to 2.1403(15) Å, average Mg-N 2.10(3) Å) anchor the structure forming relatively short  $\sigma$  bonds, whereas Na is affixed to the  $\{\text{MgN}(\text{C}_5\text{H}_{10})_4\}$  structure forming elongated ancillary bonds (mean Na-N, 2.46(1) Å). This concept of anchoring/ancillary bonding has been previously described for bimetallic compounds.<sup>[162,196]</sup> Distances between Mg-N are slightly shorter than the analogous distances Mg-N( $\text{C}_5\text{H}_{10}$ ) of other reported structures (there are 14 entries in the CCDC database containing Mg-N( $\text{C}_5\text{H}_{10}$ ) distances ranging from 2.183(2)<sup>[197]</sup> to 2.349(2)<sup>[198]</sup> Å). Bimetallic sodium magnesiate amides also show similar Mg-N bond distances, where instead of piperidine, the similar TMP(H) amine is used. In this case the Mg-N(TMP) distance of  $[(\text{TMEDA})\text{Na}(\mu\text{-Bu})(\mu\text{-TMP})\text{Mg}(\text{TMP})]$  complex is 2.0791(17) Å.<sup>[199]</sup>

Using the same methodology, employing  $\text{KCH}_2\text{SiMe}_3$  instead of the Na alkyl, allowed the isolation of  $[(\text{THF})_3\{\text{KMg}(\text{NC}_5\text{H}_{10})_3\}]_2$  **33** in a 43% isolated yield.

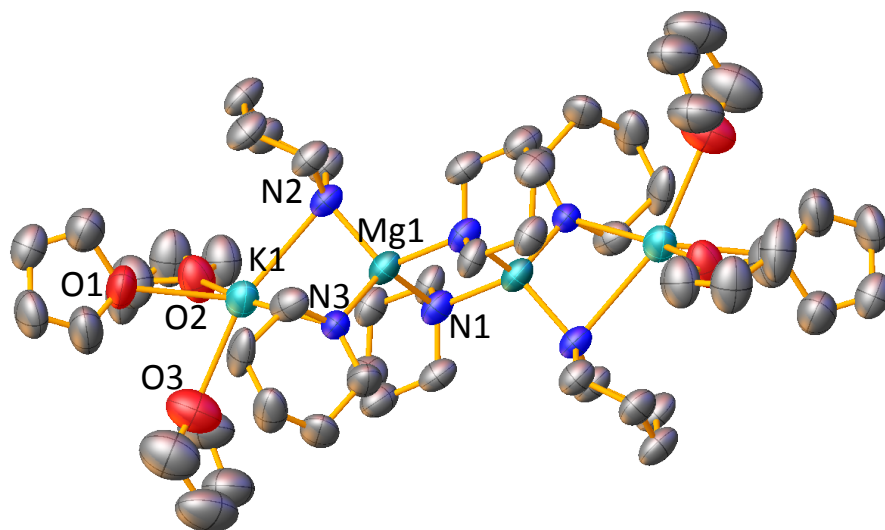


Figure 3.3: Molecular structure of **33** with 50% probability displacement ellipsoids. All hydrogen atoms have been omitted for clarity.

X-Ray crystallographic studies established the molecular structure of **33** comprising a dimeric structure following the same three fused four-membered rings framework in a MMgMgM arrangement, as the sodium analogue. Unfortunately, the resolution of the crystal was not good enough to compare bond lengths and angles for structure **33**, although similar Mg-N bond length values and shorter K-N distances compared to structure **32** would be expected.

Similar to the previous monometallic alkali-metal amides,  $^1\text{H}$  DOSY NMR studies were carried out for the Na amide **32**, in a 0.028 M  $d_8$ -THF solution. In all this Chapter the  $^1\text{H}$  DOSY NMR experiments were first calculated using internal calibration curves (ICC) method with the standards 1,2,3,4-tetraphenyl-naphthalene (TPhN), phenyl-naphthalene (PhN) and tetramethylsilane (TMS). However, since the concentration of the DOSY experiments are between the range allowed (15 to 50 mmol/L) for the more accurate DOSY-NMR using external calibration curves (ECC) reported by Stalke,<sup>[200]</sup> the  $^1\text{H}$  DOSY NMR experiments were recalculated using the

ECC approach and considering the TMS values as internal reference. The spectrum obtained for the  $^1\text{H}$  DOSY NMR of the amide **32** in  $d_8$ -THF solution is displayed in Figure 3.4

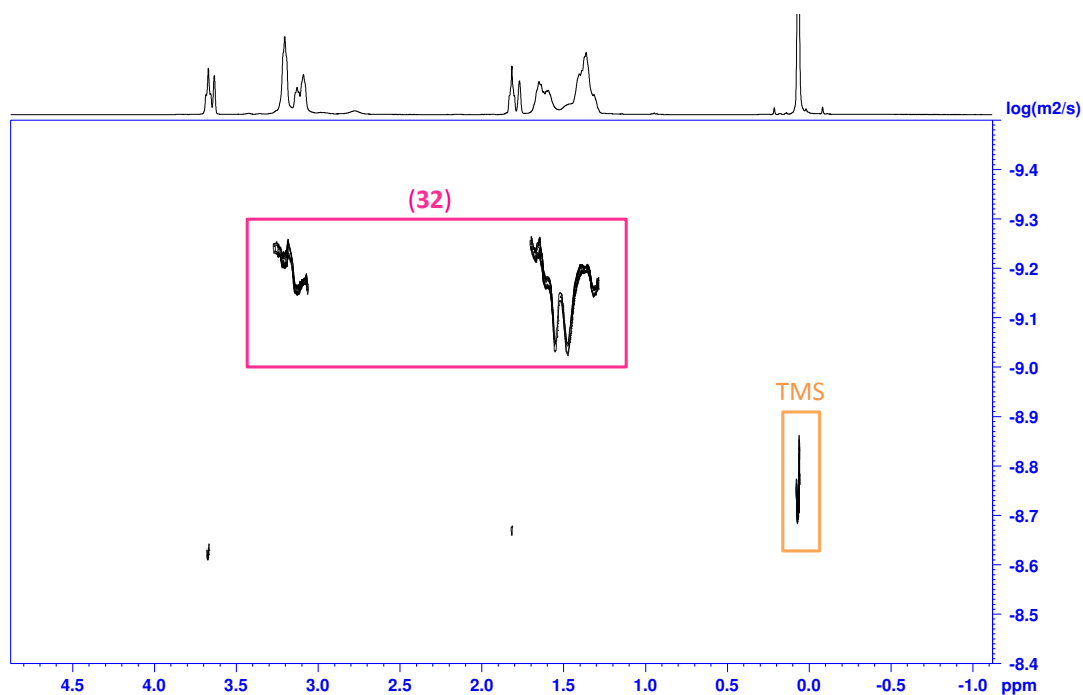


Figure 3.4:  $^1\text{H}$  DOSY experiment in  $d_8$ -THF of a mixture of compound **32** and the internal standard TMS.

The diffusion coefficient value obtained was  $D = 6.226 \cdot 10^{-10} \text{ m}^2/\text{s}$  when the sodium magnesiate amide **32** is dissolved in  $d_8$ -THF. Table 3.10 displays different possible aggregation states of **32** and the corresponding errors when the estimated formula weight is 694 g/mol obtained from the DOSY experiment.

Table 3.10: Possible sodium amide (**32**) species in  $d_8$ -THF solution and the corresponding molecular weights (MW) and errors. ( $D(\mathbf{32}) = 6.22\text{E-}10 \text{ m}^2/\text{s}$ ,  $D_{\text{TMS}} = 1.932\text{E-}9 \text{ m}^2/\text{s}$ ,  $\text{MW}_{\text{det}} = 694 \text{ g/mol}$ )

	monomer	dimer
<b>1 THF</b>		
<b>MW (g/mol)</b>	371.83	671.55
<b>Error (%)</b>	-46	-3
<b>2 THF</b>		
<b>MW (g/mol)</b>	443.93	742.66
<b>Error (%)</b>	-36	7
<b>3 THF</b>		
<b>MW (g/mol)</b>	516.04	814.76
<b>Error (%)</b>	-26	18
<b>4 THF</b>		
<b>MW (g/mol)</b>		887.87
<b>Error (%)</b>		28



Table 3.10 suggests different possible aggregation states of the magnesiate compound **32** considering the errors obtained for the estimated and real molecular weights. Considering the retention of a dimeric structure equal to the solid state an error of 28% is obtained. However varying the number of THF molecules, -3% of error is obtained when suggesting a dimer with one molecule of THF, and 7% for a dimer with 2 molecules of THF. The addition of another molecule of THF (dimer with 3 THF) would also be discarded from the  $^1\text{H}$  DOSY NMR results, since the error is 18%. Desaggregation to monomeric species seems unlikely due to the high errors obtained in the  $^1\text{H}$  DOSY NMR studies, ranging from -26 to -46, modifying the number of THF molecules.

The error in the molecular weight of solvent separated species  $[\text{Na}(\text{THF})_4]^+ [\text{Mg}(\text{NC}_5\text{H}_{10})_3]^-$  has also been calculated. The molecular weight corresponding to the  $[\text{Na}(\text{THF})_4]^+$  is not possible to calculate by  $^1\text{H}$  DOSY NMR since the THF is always in equilibrium solvation/desolvation. However, the molecular weight for  $[\text{Mg}(\text{NC}_5\text{H}_{10})_3]^-$  deviate -60% (MW =276.76 g/mol). These results suggest that the presence of a contact ion pair conformation solvated by THF is retained in  $d_8$ -THF solution. This approximation is in agreement with the cooperative behaviour of the catalyst, where both metals play an important role. No addition occurs when crown ether is used in the reaction. Presumably a crown ether could break this conformation by blocking the alkali-metal sites, preventing the coordination of the alkali-metal to the unsaturated molecule and therefore the insertion and the formation of the product.

Considering the retention of a dimeric structure equal to the solid state and varying the number of THF molecules, an error of -3% is obtained when suggesting a dimer with one molecule of THF, and 7% for a dimer with 2 molecules of THF.

In addition, equilibriums between dimers have also been considered, (Table 3.11) suggesting the possibility of equilibrium between dimers with one and two molecules of THF (2% error) when the sodium magnesiate amide is in THF solution.

Table 3.11: Possible equilibriums of dimeric amide (**32**) species in solution and the corresponding errors for MW<sub>det</sub>=694 g/mol.

Equilibrium between dimers	MW (g/mol)	Error (%)
$[\{\text{NaMg}(\text{NC}_5\text{H}_{10})_3\}]_2(\text{THF}) + \text{THF} \rightleftharpoons [\{\text{NaMg}(\text{NC}_5\text{H}_{10})_3\}]_2(\text{THF})_2$	707.605	2
$[\{\text{NaMg}(\text{NC}_5\text{H}_{10})_3\}]_2(\text{THF})_2 + \text{THF} \rightleftharpoons [\{\text{NaMg}(\text{NC}_5\text{H}_{10})_3\}]_2(\text{THF})_3$	779.71	12
$[\{\text{NaMg}(\text{NC}_5\text{H}_{10})_3\}]_2(\text{THF})_2 + 2\text{THF} \rightleftharpoons [\{\text{NaMg}(\text{NC}_5\text{H}_{10})_3\}]_2(\text{THF})_4$	815.765	18

Considering the results of the equilibriums between dimers displayed in Table 3.11, an equilibrium of sodium amido-magnesiate disolvated and trisolvated dimers in THF solution is suggested, since an error of 2% is obtained.

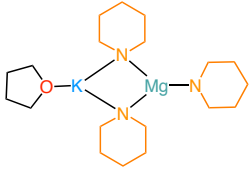
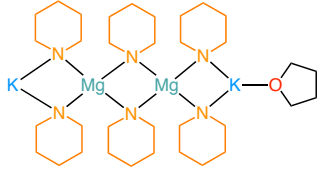
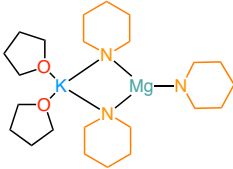
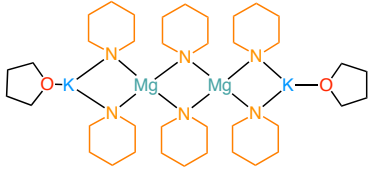
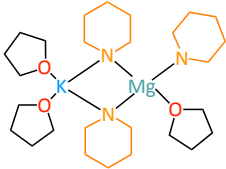
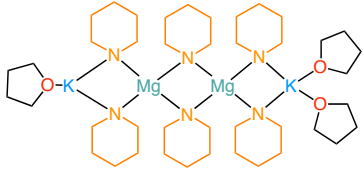
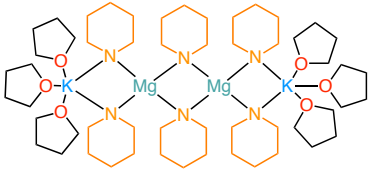
Similarly, <sup>1</sup>H DOSY NMR studies were carried out for the potassium amido-magnesiate analogue **33**, in a 0.028 M *d*<sub>8</sub>-THF solution using TMS as standard. The DOSY spectrum obtained is displayed in Figure 3.5.



Figure 3.5: <sup>1</sup>H DOSY experiment in *d*<sub>8</sub>-THF of a mixture of compound **33** and the internal standard TMS.

The diffusion coefficient value obtained in the <sup>1</sup>H DOSY NMR experiment was  $D = 6.0975 \cdot 10^{-10} \text{ m}^2/\text{s}$  for the potassium magnesiate **33**. The different aggregation states in *d*<sub>8</sub>-THF with the corresponding errors are presented in Table 3.12 when the estimated formula weight is 734 g/mol obtained from the DOSY experiment.

Table 3.12: Possible potassium amide (**33**) species in  $d_8$ -THF solution and the corresponding molecular weights (MW) and errors ( $D(\mathbf{33}) = 6.0975\text{E-}10 \text{ m}^2/\text{s}$ ,  $D_{\text{TMS}} = 1.956\text{E-}9 \text{ m}^2/\text{s}$ ,  $\text{MW}_{\text{det}} = 734 \text{ g/mol}$ ).

	monomer	dimer
<b>1 THF</b>		
<b>MW (g/mol)</b>	387.94	703.77
<b>Error (%)</b>	-47	-4
<b>2 THF</b>		
<b>MW (g/mol)</b>	460.04	775.87
<b>Error (%)</b>	-37	6
<b>3 THF</b>		
<b>MW (g/mol)</b>	532.15	847.98
<b>Error (%)</b>	-28	16
<b>6 THF</b>		
<b>MW (g/mol)</b>		1064.30
<b>Error (%)</b>		45%

Comparing the error obtained and the estimated with the real molecular weight,  $^1\text{H}$  DOSY NMR suggests that when the potassium amide **33** is dissolved in a THF solution a dimeric arrangement is retained in solution. The difference between the estimated and the real molecular weights for the monomeric species have bigger errors (-47 to -28%) than  $\pm 9\%$ , which is the maximum error predicted in the ECC-method. Both dimers with one and two THF molecules, display errors between the accepted range, -4 and 6%, which suggests the possibility of the existence of those species when **33** is dissolved in  $d_8$ -THF.

Similar as **32**, the solvent separated species  $[\text{K}(\text{THF})_6]^+ [\{\text{Mg}(\text{NC}_5\text{H}_{10})_3\}]^-$  have been calculated for **33**. The error obtained for the molecular weight of the anionic counterpart  $[\{\text{Mg}(\text{NC}_5\text{H}_{10})_3\}]^-$  differs 62% (MW = 276.73 g/mol). Coincidentally with the results for **32**,  $^1\text{H}$  DOSY NMR also suggests a contacted ion pair when potassium amide **33** is dissolved in  $d_8$ -THF, which would be in agreement with the cooperative effect of the bimetallic catalyst.

Equilibriums of the potassium amide dimers have also been calculated, and the errors obtained are displayed in Table 3.13.

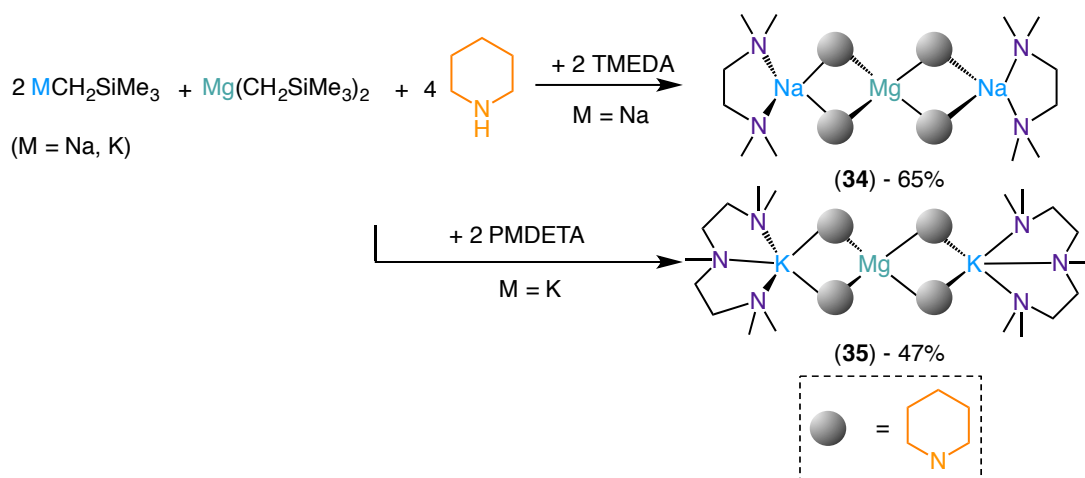
Table 3.13: Possible equilibriums of dimeric amide (**33**) species in solution and the corresponding errors for  $\text{MW}_{\text{est}} = 734$  g/mol.

Equilibrium between dimers	MW (g/mol)	Error (%)
$[\{\text{KMg}(\text{NC}_5\text{H}_{10})_3\}]_2(\text{THF}) + \text{THF} \rightleftharpoons [\{\text{KMg}(\text{NC}_5\text{H}_{10})_3\}]_2(\text{THF})_2$	739.82	1
$[\{\text{KMg}(\text{NC}_5\text{H}_{10})_3\}]_2(\text{THF})_2 + \text{THF} \rightleftharpoons [\{\text{KMg}(\text{NC}_5\text{H}_{10})_3\}]_2(\text{THF})_3$	811.925	11
$[\{\text{KMg}(\text{NC}_5\text{H}_{10})_3\}]_2(\text{THF})_2 + 2\text{THF} \rightleftharpoons [\{\text{KMg}(\text{NC}_5\text{H}_{10})_3\}]_2(\text{THF})_4$	847.98	16

From the errors obtained in the dimeric equilibriums suggested in Table 3.13, an equilibrium of monosolvated and disolvated potassium magnesiate dimers in THF solution is suggested, since the error obtained is 1%.

The results obtained in the  $^1\text{H}$  DOSY NMR studies for **32** and **33**, indicate that contacted ion pair conformation is retained in solution, which can be indicative in terms of synergic behaviour of the metals.

Following a similar procedure, the higher order alkali-metal magnesiates  $[(\text{TMEDA})_2\{\text{Na}_2\text{Mg}(\text{NC}_5\text{H}_{10})_4\}]$  **34** and  $[(\text{PMDETA})_2\{\text{K}_2\text{Mg}(\text{NC}_5\text{H}_{10})_4\}]$  **35** were prepared as colourless crystals in 65 and 47% yields respectively (Scheme 3.8). The amides were obtained by reaction of the precursors: 2 equivalents of  $\text{M}(\text{CH}_2\text{SiMe}_3)$  [M = Na or K] and one  $\text{Mg}(\text{CH}_2\text{SiMe}_3)_2$  that were treated with four equivalents of the corresponding amine piperidine and two of the donor (TMEDA or PMDETA) in hexane/toluene. The X-Ray crystallographic studies confirmed their existence, which have been characterised by  $^1\text{H}$  and  $^{13}\text{C}$  NMR spectroscopy as well as elemental analysis experiments. Unfortunately, no consistent results for the  $^1\text{H}$  DOSY NMR studies were obtained for species **34** and **35** in  $d_8$ -THF solution.

Scheme 3.8: Synthesis of higher order sodium and potassium magnesiate amides **34** and **35**.

Both compounds **34** and **35** display the same core architecture (Figure 3.6 and Figure 3.7). The amides present a monomeric contacted ion-pair structure with  $M \cdots Mg \cdots M$  arrangement where the central Mg atom coordinated to four anionic amide groups whereas each of the outer M atoms bind to two amido groups and a chelating TMEDA or PMDETA molecule. A search in the CCDC database revealed other bimetallic amides with lithium manganesate following the same motif,<sup>[201]</sup> and only two lithium higher order amido-magnesiate structures have been previously reported.<sup>[202,203]</sup>

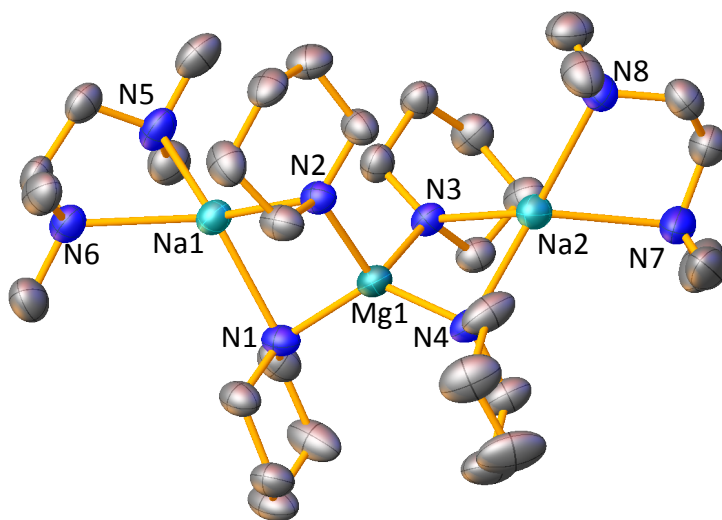


Figure 3.6: Molecular structure of **34** with 50% probability displacement ellipsoids. All hydrogen atoms have been omitted for clarity. Selected bond lengths (Å) and bond angles (°): Na1-N1 2.438(3), Na1-N2 2.455(3), Na1-N5 2.599(3), Na1-N6 2.564(6), Mg1-N1 2.068(3), Mg1-N2 2.088(3), Mg1-N3 2.081(3), Mg1-N4 2.055(3), Na2-N3 2.396(3), Na2-N4 2.439(3), Na2-N7 2.538(3), Na2-N8 2.497(3), N1-Na1-N2 81.83(9), N1-Na1-N6 124.32(14), N2-Na1-N6 127.98(13), N1-Na1-N5 126.47(10), N2-Na1-N5 132.17(11), N6-Na1-N5 71.55(13), N1-Mg1-N2 100.89(11), N3-Mg1-N2 105.07(11), N4-Mg1-N3 100.10(11), N4-Mg1-N1 128.67(12), N1-Mg1-N3 108.71(11), N4-Mg1-N2 111.55(11), N3-Na2-N4 81.93(10), N3-Na2-N8 126.86(10), N4-Na2-N8 137.83(11), N3-Na2-N7 128.07(11), N4-Na2-N7 116.70(10), N8-Na2-N7 72.45(10).

The mixed sodium/magnesium **34** presents a bent [Na-Mg-Na] arrangement (Na1⋯Mg1⋯Na2, 134.23(5)°). Each amide group in **34** is equivalent, acting as a bridge between Na and Mg atoms. Compound **34** can be envisaged as two four-membered ring [Na-N-Mg-N] (sum of internal angles, 349.5° and 349.7°) fused by their shared Mg vertex, which exhibits a tetrahedral coordination (angles around Mg ranging from 100.1(1)° to 128.7(1)°). Both terminal Na atoms coordinated to the chelate TMEDA ligand also present a tetrahedral coordination (angles around Na1 and Na2 ranging from 71.5(1)° to 137.8(1)°).

The Mg-N and Na-N bond distances have also been calculated and compared with amide **32** (Table 3.14).



Table 3.14: Comparison of the general features between compounds **32** and **34**.

Compound	Mg-N (Å)	Na-N (Å)
<b>32</b>	2.10(3)	2.108(2)
<b>34</b>	2.07(1)	2.075(1)

Both Mg-N and Na-N distances in **34** are relatively shorter to those found for the sodium lower order amido-magnesiate compound (Table 3.14). This structure also shows anchoring/ancillary bonding trend where the Mg-N distances (ranging from Mg1-N1 N4 2.055(3) to 2.088(3) Å, mean Mg-N 2.07(1) Å) are slightly shorter than other Mg-N(C<sub>5</sub>H<sub>10</sub>) reported in the literature (ranging from 2.183(2)<sup>[197]</sup> to 2.349(2)<sup>[198]</sup> Å).

Compound [PMDETA]<sub>2</sub>{K<sub>2</sub>Mg(NC<sub>5</sub>H<sub>10</sub>)<sub>4</sub>} **35** was also prepared as colourless crystals in 47% yield, using the same methodology as the sodium higher order amido-magnesiate, employing KCH<sub>2</sub>SiMe<sub>3</sub> instead of the Na.

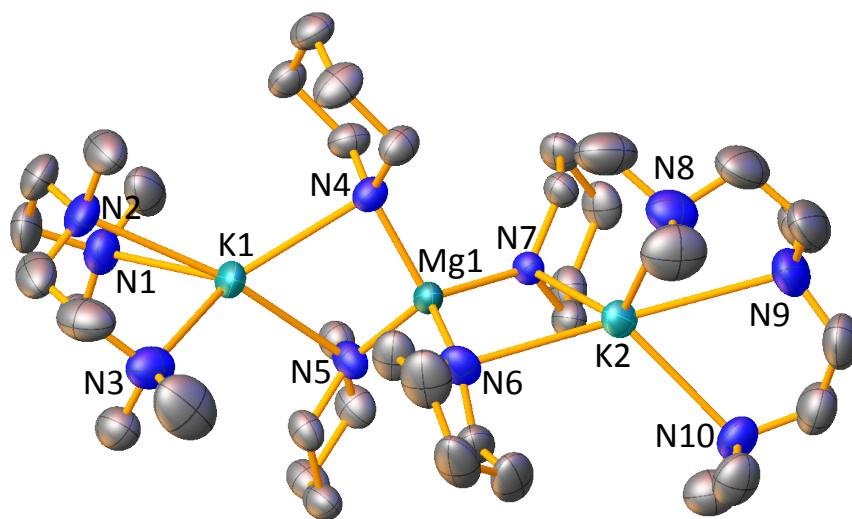


Figure 3.7: Molecular structure of higher order potassium magnesiate amide (**35**) with 50% probability displacement ellipsoids. All hydrogen atoms have been omitted for clarity.

X-Ray crystallographic studies established the molecular structure of **35** comprising a similar design as amide **34**. Compound **34** displays a contacted ion-pair structure with  $K \cdots Mg \cdots K$  arrangement where the central Mg atom is coordinated to four anionic amide groups whereas each of the outer K atoms bind to two amido groups and a chelating PMDETA molecule. Unfortunately, extensive disorder in the solid state structure prevents an accurate discussion of bonds and angles, however, similar Mg-N bond length values and shorter K-N distances compared to structure **34** would be expected.

Initial experiments have been performed in order to gain structural insights of intermediate **III** resulting from the insertion of diphenylacetylene in the Mg-N bond of **32** – **35**. Unfortunately, these attempts have been unsuccessful and no solid or crystals of the intermediate were obtained when reacting the amides **32-35** with diphenylacetylene (**1a**). The only product that has been obtained corresponds to the final hydroamination product, illustrating the instability of these species.

### 3.3 Conclusions

This chapter uncovers the catalytic applications of alkali-metal magnesiates for challenging intermolecular hydroamination reactions using the homoleptic alkali-metal magnesiate compounds  $[\text{MMg}(\text{CH}_2\text{SiMe}_3)_3]$  (M = Li (**26**), Na (**27**) and K (**28**)) and  $[(\text{donor})_2\text{M}_2\text{Mg}(\text{CH}_2\text{SiMe}_3)_4]$  (M = Li (**29**), Na (**30**) and K (**31**)).

Harsher reaction conditions (80 °C and longer reaction times) were required in some cases to overcome the kinetic barrier for the intermolecular hydroamination reactions studied when using alkali-metal lower order magnesiate compounds  $[\text{MMg}(\text{CH}_2\text{SiMe}_3)_3]$  (M = Li, Na, K). Higher order magnesiates  $[(\text{donor})_2\text{M}_2\text{Mg}(\text{CH}_2\text{SiMe}_3)_4]$  (M = Li, Na, K) exhibited a significantly better catalytic capability compared to their lower order congeners. Similarly as the monometallic precatalysts used in Chapter 2, a noticeable alkali-metal effect is observed for the higher order magnesiate precatalysts, however, this trend is not observed in the lower order magnesiates. Initial studies show the smooth hydroamination of styrene at room temperature in 15 minutes. This reactivity contrast sharply with  $[\text{Mg}(\text{CH}_2\text{SiMe}_3)_2]$ , which can not deprotonate these reactions. Thus, by pairing magnesium with an alkali-metal it is possible to install unique catalytic properties, activating the magnesium towards intermolecular hydroamination processes, showing similar efficiencies to those previously reported for heavier alkali-metal catalysts with calcium or strontium. Initial reactivity studies suggest that the role of the alkali-metal is to act as a potent Lewis acid, coordinating the unsaturated organic molecule to facilitate the addition of an amide anion. Further work expanding the reaction scope of these reactions needs to be performed.

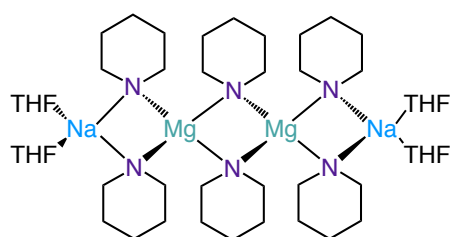
Similarly to the monometallic congeners described in Chapter 2, X-ray crystallography combined with  $^1\text{H}$  DOSY NMR experiments have been carried out

for the active alkali metal amido-magnesiates prepared. While a full kinetic study would shed more light on the processes involved in these transformations, these initial stoichiometric studies suggest similar mechanisms to those proposed for calcium or strontium catalysis. Collectively, these findings greatly add to the chemistry of cooperative bimetallics, expanding even more their synthetic potential, as efficient catalysts to access amines via hydroamination processes.

## 3.4 Experimental

### 3.4.1 Synthesis of Active Species

- Synthesis of  $[(\text{THF})_2\{\text{NaMg}(\text{NC}_5\text{H}_{10})_3\}]_2$  (**32**)



$[\text{Na}(\text{CH}_2\text{SiCH}_3)]$  (0.11 g, 1 mmol),  $[\text{Mg}(\text{CH}_2\text{SiCH}_3)_2]$  (0.22 g, 1 mmol) and hexane (10 mL) were added and stirred at room temperature during one hour. Piperidine (0.3 mL, 1 mmol) was added and the white

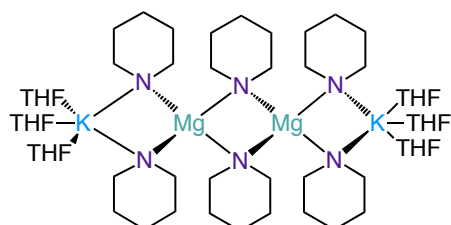
suspension was stirred during one hour more at room temperature. THF (0.32 mL) was added and the suspension was gently heated until a clear solution was obtained and was placed to the freezer ( $-33\text{ }^\circ\text{C}$ ). After 24 hours the white solid was filtered and placed in a glovebox (0.185 g, 42%).

$^1\text{H}$  NMR (400.13 MHz,  $\text{C}_6\text{D}_6$ , 298 K)  $\delta$  2.06-1.77 [br. m, 12H,  $\text{N}(\text{CH}_2\text{CH}_2)_2\text{CH}_2$ ], 1.74-1.46 [br m, 18H,  $\text{N}(\text{CH}_2\text{CH}_2)_2\text{CH}_2 + \text{N}(\text{CH}_2\text{CH}_2)_2\text{CH}_2$ ].

$^{13}\text{C}$  NMR  $\{^1\text{H}\}$  (100.62 MHz,  $\text{C}_6\text{D}_6$ , 298 K)  $\delta$  55.1 [CH,  $\text{N}(\text{CH}_2\text{CH}_2)_2\text{CH}_2$ ], 32.9 [CH,  $\text{N}(\text{CH}_2\text{CH}_2)_2\text{CH}_2$ ], 28.2 [CH,  $\text{N}(\text{CH}_2\text{CH}_2)_2\text{CH}_2$ ].

**Elemental analysis:** Due to the air and moisture sensitivity of the sample, elemental analysis experiments were unsuccessful.

- **Synthesis of  $[(\text{THF})_3\{\text{KMg}(\text{NC}_5\text{H}_{10})_3\}]_2$  (33)**



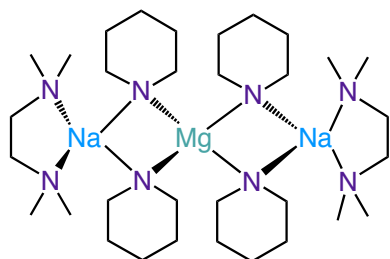
To an oven dried Schlenk  $[\text{K}(\text{CH}_2\text{SiCH}_3)]$  (0.13 g, 1 mmol),  $[\text{Mg}(\text{CH}_2\text{SiCH}_3)_2]$  (0.22 g, 1 mmol) and hexane (10 mL) were added and stirred at room temperature during one hour. Piperidine (0.3 mL, 1 mmol) was added and the white suspension was stirred during one hour more at room temperature. THF (3 mL) was added and the suspension was gently heated until solution that was placed to the fridge overnight. Colourless crystals were obtained. The crystals were isolated and placed in a glovebox (0.245 g, 43%).

$^1\text{H}$  NMR (400.13 MHz,  $\text{C}_6\text{D}_6$ , 298 K)  $\delta$  3.47-3.19 [br. m, 12H,  $\text{N}(\text{CH}_2\text{CH}_2)_2\text{CH}_2$ ], 1.42-1.55 [br. m, 6H,  $\text{N}(\text{CH}_2\text{CH}_2)_2\text{CH}_2$ ], 1.15-1.39 [br. m, 12H,  $\text{N}(\text{CH}_2\text{CH}_2)_2\text{CH}_2$ ].

$^{13}\text{C}$  NMR  $\{^1\text{H}\}$  (100.62 MHz,  $\text{C}_6\text{D}_6$ , 298 K)  $\delta$  55.5 [CH,  $\text{N}(\text{CH}_2\text{CH}_2)_2\text{CH}_2$ ], 32.0 [CH,  $\text{N}(\text{CH}_2\text{CH}_2)_2\text{CH}_2$ ], 28.4 [CH,  $\text{N}(\text{CH}_2\text{CH}_2)_2\text{CH}_2$ ].

**Elemental analysis:** Due to the air and moisture sensitivity of the sample, elemental analysis experiments were unsuccessful.

- **Synthesis of  $(\text{TMEDA})_2\text{Na}_2\text{Mg}(\text{NC}_5\text{H}_{10})_4$  (34)**



To an oven dried Schlenk  $[\text{Na}(\text{CH}_2\text{SiCH}_3)]$  (0.22 g, 2 mmol),  $[\text{Mg}(\text{CH}_2\text{SiCH}_3)_2]$  (0.20 g, 1 mmol) and hexane (10 mL) were added and stirred at room temperature during one hour. TMEDA (0.3 mL, 2 mmol) was added and the suspension was stirred during one hour. Piperidine (0.4 mL, 4 mmol) was added and the white suspension was stirred during one hour more at room temperature. The volume of the solution

was halved by evaporation in vacuum and toluene (2 mL) was added. The suspension was gently heated until solution that was placed in a hot water bath. After 24 hours colourless crystals were obtained, isolated and placed in a glovebox (0.415 g, 65%).

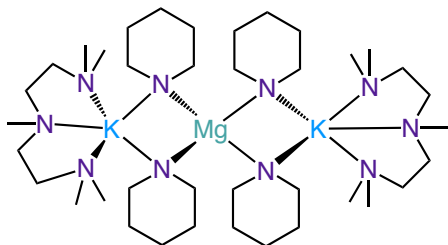
$^1\text{H NMR}$  (400.13 MHz,  $\text{C}_6\text{D}_6$ , 298 K)  $\delta$  3.51 [m, 16H,  $\text{N}(\text{CH}_2\text{CH}_2)_2\text{CH}_2$ ], 2.05 [m, 32H,  $\text{N}(\text{CH}_2\text{CH}_2)_2\text{CH}_2 + (\text{CH}_3)$  TMEDA], 1.83 [s, 8H,  $(\text{NCH}_2)$  TMEDA], 1.69 [m, 16H,  $\text{N}(\text{CH}_2\text{CH}_2)_2\text{CH}_2$ ].

$^{13}\text{C NMR}$   $\{^1\text{H}\}$  (100.62 MHz,  $d_8$ -THF, 298 K)  $\delta$  57.3 [ $(\text{CH}_2)$  TMEDA], 55.6 [ $\text{N}(\text{CH}_2\text{CH}_2)_2\text{CH}_2$ ], 46.2 [ $(\text{CH}_3)$  TMEDA], 32.8 [ $\text{N}(\text{CH}_2\text{CH}_2)_2\text{CH}_2$ ], 28.7 [ $\text{N}(\text{CH}_2\text{CH}_2)_2\text{CH}_2$ ].

**Elemental analysis:** ( $\text{C}_{32}\text{H}_{72}\text{MgN}_8\text{Na}_2$ ) *Calculated:* C: 60.12 % H: 11.35 % N: 17.53 %.

*Found:* C: 59.57 % H: 9.14 % N: 16.95 %.

• **Synthesis of  $[(\text{PMDETA})_2\text{K}_2\text{Mg}(\text{NC}_5\text{H}_{10})_4]$  (35)**



To an oven dried Schlenk [ $\text{K}(\text{CH}_2\text{SiCH}_3)$ ] (0.26 g, 2 mmol), [ $\text{Mg}(\text{CH}_2\text{SiCH}_3)_2$ ] (0.20 g, 1 mmol) and hexane (10 mL) were added and stirred at room temperature during one hour. PMDETA (0.4 mL, 2 mmol) was added and the

suspension was stirred during one hour. Piperidine (0.4 mL, 4 mmol) was added and a clear yellow solution was formed. After stirring for one hour at room temperature the solution was placed in the fridge. After 24 hours big yellow crystals were obtained, isolated and placed in a glovebox (0.3703 g, 47%).

$^1\text{H NMR}$  (400.13 MHz,  $\text{C}_6\text{D}_6$ , 298 K)  $\delta$  3.46 [m, 16H,  $\text{N}(\text{CH}_2\text{CH}_2)_2\text{CH}_2$ ], 2.09 [s, 30H,  $(\text{CH}_3)$  PMDETA], 2.08 [m, 8H,  $\text{N}(\text{CH}_2\text{CH}_2)_2\text{CH}_2$ ], 2.02 [s, 16H,  $(\text{NCH}_2)$  PMDETA], 1.78 [m, 16H,  $\text{N}(\text{CH}_2\text{CH}_2)_2\text{CH}_2$ ].

$^{13}\text{C}$  NMR  $\{^1\text{H}\}$  (100.62 MHz,  $d_8$ -THF, 298 K)  $\delta$  57.5 [CH<sub>2</sub> PMDETA], 56.1 [N(CH<sub>2</sub>CH<sub>2</sub>)<sub>2</sub>CH<sub>2</sub>], 55.8 [CH<sub>2</sub> PMDETA], 45.8 [(CH<sub>3</sub>)<sub>2</sub> PMDETA], 43.2 [(CH<sub>3</sub>) PMDETA], 32.4 [N(CH<sub>2</sub>CH<sub>2</sub>)<sub>2</sub>CH<sub>2</sub>], 29.0 [N(CH<sub>2</sub>CH<sub>2</sub>)<sub>2</sub>CH<sub>2</sub>].

**Elemental analysis:** (C<sub>38</sub>H<sub>86</sub>MgN<sub>10</sub>K<sub>2</sub>) *Calculated:* C: 57.02 % H: 10.83 % N: 17.50 %.  
*Found:* C: 58.30 % H: 11.44 % N: 17.18 %.

### 3.4.2 General Experimental Procedure for Catalytic Hydroamination Reactions at NMR Tube Scale

Catalytic reactions were performed in a J. Young's NMR tube at NMR scale following the standard procedure. In a glovebox, the NMR tube was filled with 0.6 mmol of amine, 0.5 mmol of alkene or alkyne, 10 mol% of ferrocene (0.0095 g, 0.05 mmol) as internal standard and 0.609 g of solvent. The initial ratio of starting materials was calculated by integration in  $^1\text{H}$  NMR relative to the ferrocene. The precatalyst (0.025 mmol) was introduced and the reactions times were measured from this point in regular intervals of time until full conversion by  $^1\text{H}$  NMR spectrum (some reactions were heated in a pre-heated oil bath). All the yields were calculated by integration of the products relative to the ferrocene in the  $^1\text{H}$  NMR spectrum.

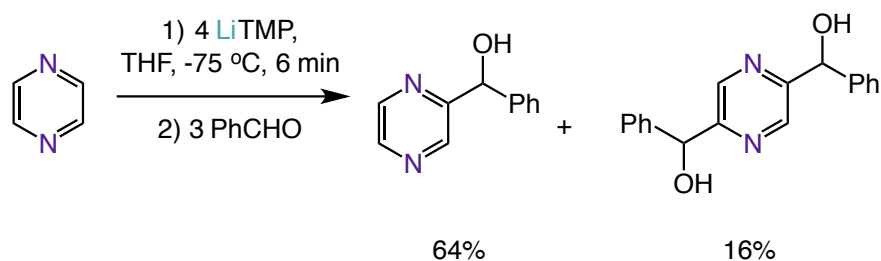
The characterisation of the organic hydroamination products formed is analogous to that reported in Chapter 2.



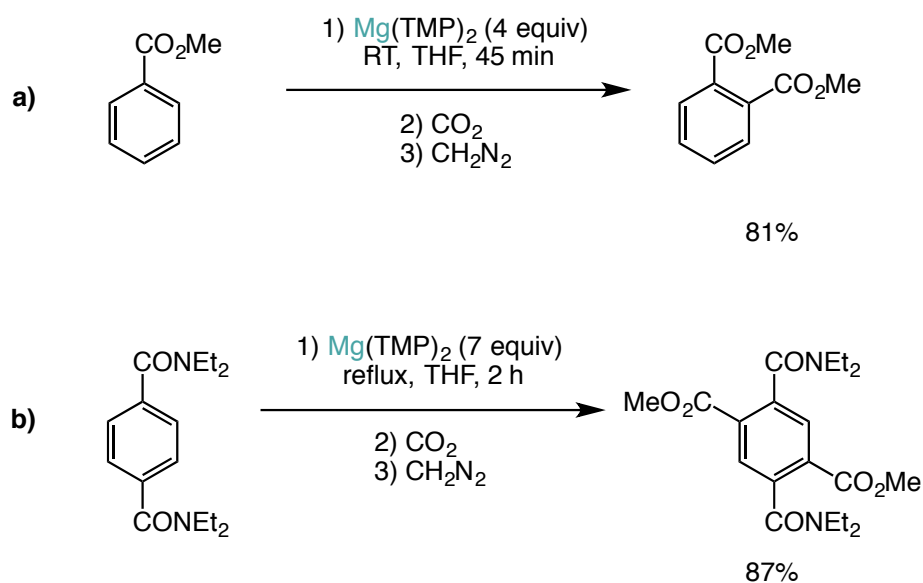
## Chapter 4 Regioselective Magnesiation of Heterocyclic Molecules

### 4.1 Introduction

Deprotonative metallation constitutes one of the most frequent and versatile synthetic methodologies for the functionalization of organic molecules.<sup>[2,39]</sup> Amongst the vast family of polar organometallic reagents, organolithiums are usually the reagents of choice, due to their high reactivity which stems primarily from the high polarity of their Li-C bonds.<sup>[204]</sup> However, these reagents also suffer from limited selectivity and poor functional group tolerance, which imposes in many cases the use of extremely low temperatures (e.g. -78 °C) in order to avoid competing side reactions.<sup>[62]</sup> For example, Scheme 4.1 shows an example of the harsh reaction conditions needed to deprotonate pyrazine when using LiTMP such as excess of base and -75 °C.

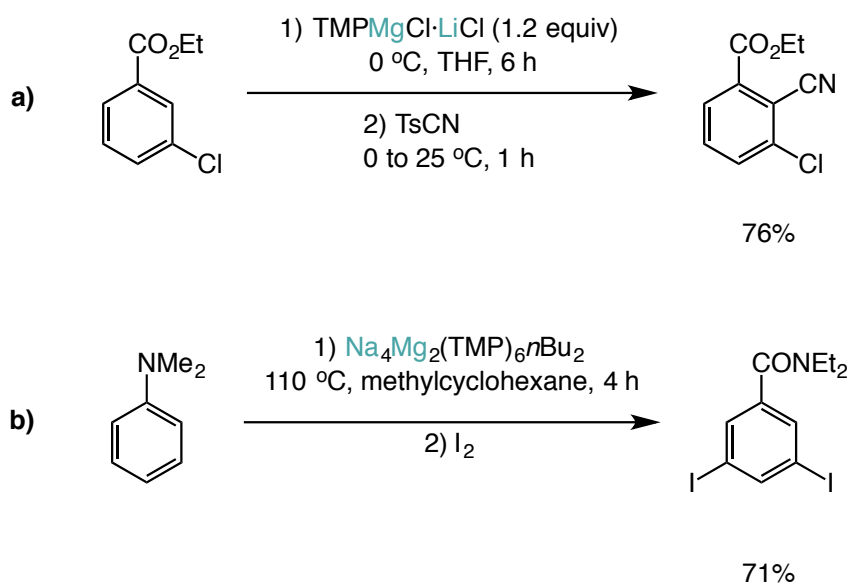
Scheme 4.1: Lithiation of diazine using LiTMP.<sup>[205]</sup>

Moving to lithium's diagonal partner in the periodic table, magnesium reagents can offer better selectivities and mild reaction conditions.<sup>[48,84,206]</sup> In particular, magnesium amides containing the basic and sterically demanding group TMP (2,2,6,6-tetramethylpiperidide) have proved to be effective regioselective bases that can execute the metallation of a wide range of substrates.<sup>[82,207–209]</sup> Moreover, due to their more limited reactivity, an excess of base is normally employed to ensure good yields, as shown in Scheme 4.2.<sup>[210,211]</sup>



Scheme 4.2: Examples of metallation using  $\text{Mg}(\text{TMP})_2$  base in excess. a) Metallation and subsequent quench of methyl benzoate at room temperature.<sup>[82]</sup> b) Dimetallation and subsequent quench of *N,N,N',N'*-tetraethylbenzene-1,4-dicarboxamide under reflux.<sup>[82]</sup>

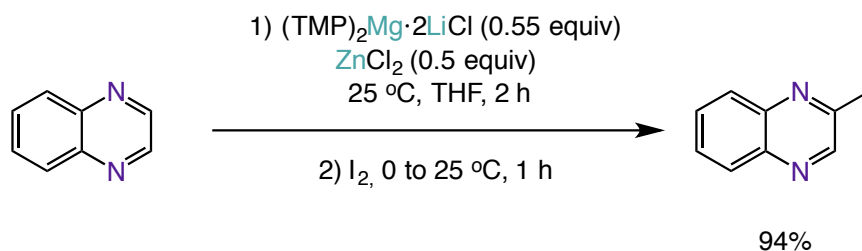
Notably, Knochel has pioneered the use of the LiCl-powered Turbo-Hauser base  $\text{TMPMgCl}\cdot\text{LiCl}$ , which allows the effective magnesiation of a myriad of functionalized aromatic or heterocyclic molecules, with excellent yields and under milder reaction conditions (0 °C - RT) (Scheme 4.3a).<sup>[70,87,212]</sup> Furthermore, O'Hara and Mulvey have recently shown that heterobimetallic reagents exhibit enhanced reactivities and unique selectivities, which cannot be replicated by their homometallic components. Remarkably, partnering  $\text{Mg}(\text{TMP})_2$  with  $\text{NaTMP}$  and  $\text{BuNa}$  results in the mixed-metal  $[\text{Na}_4\text{Mg}_2(\text{TMP})_6n\text{Bu}_2]$  base, which can surprisingly accomplish *meta-meta* deprotonation of aromatic substrates such as dimethylaniline (Scheme 4.3b).<sup>[124]</sup>



Scheme 4.3: Deprotonation reactions using mixed-metal bases. a) Metallation and subsequent quench of ethyl 3-chlorobenzoate using Turbo-Hauser base  $\text{TMPMgCl}\cdot\text{LiCl}$ .<sup>[70]</sup> b) *Meta-meta* deprotonation of dimethylaniline.<sup>[124]</sup>

Heterocyclic and (hetero)aromatic molecules are prevalent in vast numbers of pharmaceutical and biologically active molecules.<sup>[213–218]</sup> Thus the synthetic manipulation of these subunits, via careful control of the metallation process, is of critical importance. For example, metallation of  $\pi$ -deficient aza-heterocyclic substrates such as pyridines or diazines can be particularly problematic, in part due to the inherent lack of stability of the putative metallated intermediates,<sup>[219–221]</sup> rationalized in terms of the destabilizing electronic repulsion between the nitrogen lone pairs and the negative charge of the carbanion in the adjacent position to the nitrogen.<sup>[222]</sup> Importantly, such compounds also have a propensity to undergo nucleophilic addition reactions rather than metallation when exposed to polar organometallic reagents such as BuLi. A fact attributable to the electron-withdrawing effect of the nitrogen atoms, leaving a low lying LUMO and consequently a small HOMO/LUMO gap.<sup>[223]</sup> As a result, strict control of the

reaction conditions (low temperatures and short reaction times) as well as the use of bulky amide bases such as LiTMP or LDA (lithium diisopropylamide) are required in order to avoid unwanted addition reactions.<sup>[205]</sup> Even under these conditions the yields in metallation processes tend to be moderate.<sup>[224]</sup> Contrastingly, using TMPMgCl·LiCl as a base, Knochel has accomplished regioselective metallation of quinoxaline at 0 °C, however the reaction has to be carried out in the presence of ZnCl<sub>2</sub>, generating via salt metathesis, an organozinc intermediate *in situ*, which is substantially more stable than its magnesium analogue (Scheme 4.4).<sup>[225]</sup>



Scheme 4.4: Metallation of quinoxaline by using (TMP)<sub>2</sub>Mg·2LiCl and ZnCl<sub>2</sub> at mild reaction conditions.<sup>[225]</sup>

Recently our group has become interested in developing a new generation of monomeric magnesium bases containing the bulky  $\beta$ -diketiminato ligand (<sup>Dipp</sup>Nacnac = Ar\*NC(Me)CHC(Me)NAr\*; Ar\* = 2,6-*i*Pr<sub>2</sub>-C<sub>6</sub>H<sub>3</sub>).<sup>[106]</sup> These monomeric magnesium metallating manifolds are specifically designed in order to promote regioselective functionalization of sensitive molecules as well as trapping the sensitive anions formed. One of these bifunctional bases is [<sup>Dipp</sup>NacnacMg(TMP)] (**36**), which combines a basic (kinetically activated) TMP group and the sterically demanding  $\beta$ -diketiminato ligand (Figure 4.1).

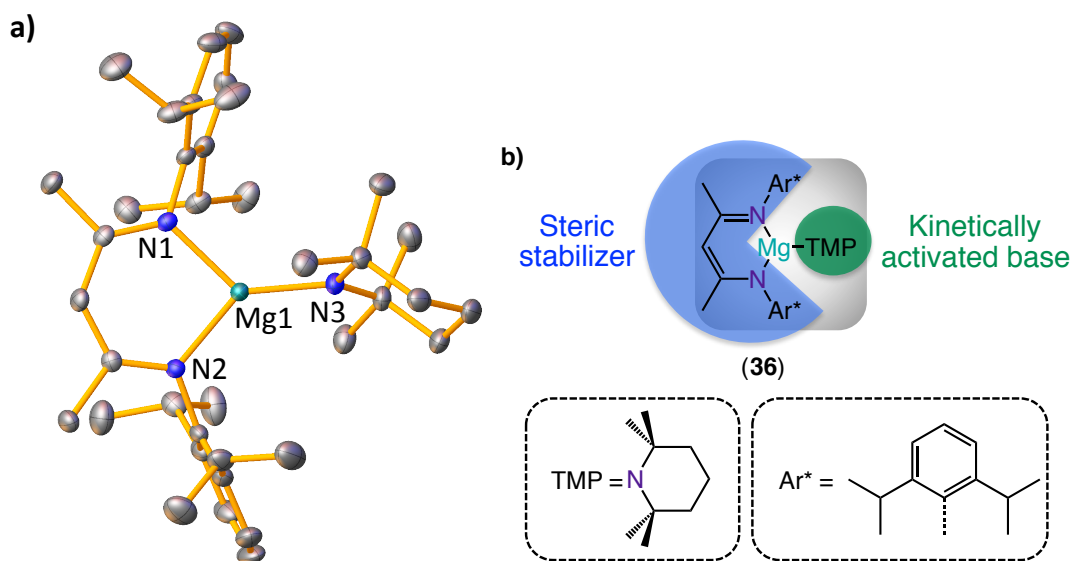


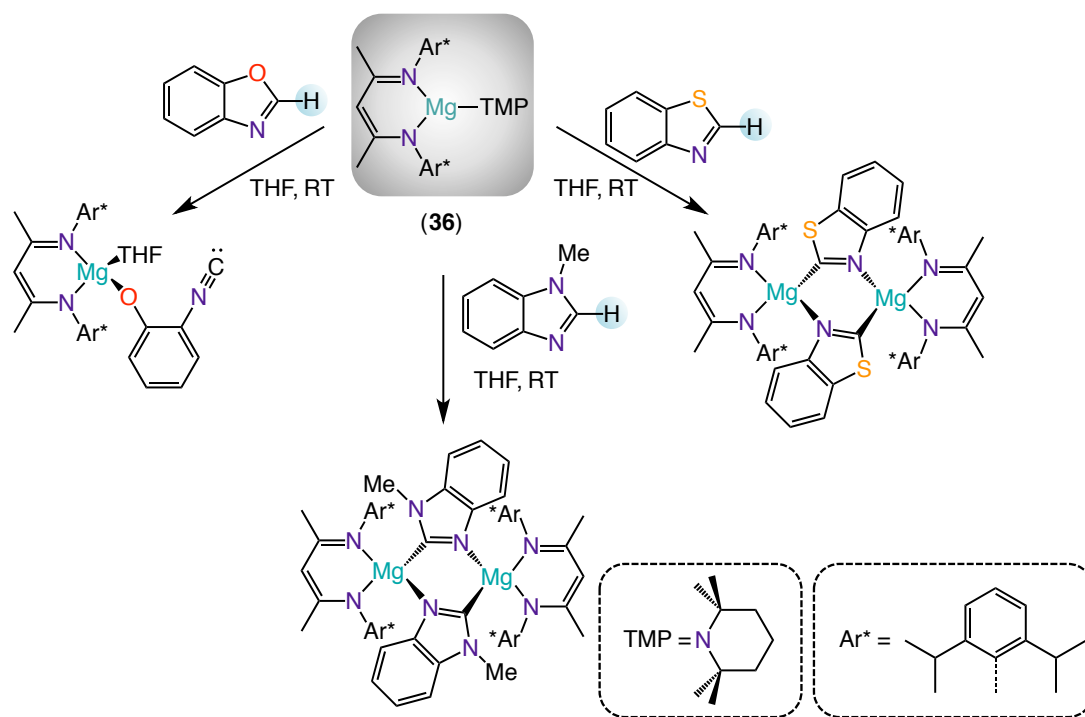
Figure 4.1: a) Molecular structure of **36** with 50% probability displacement ellipsoids. All hydrogen atoms have been omitted for clarity. b) Representation of the bifunctional base **36**.

Each component of the bimetallic compound **36** has a well-defined, but separate, role producing a very reactive magnesium metallating base. The steric congestion around the magnesium atom assists the formation of a kinetically activated monomeric base containing a terminal TMP group.<sup>[88]</sup> Additionally, the sterically demanding  $\beta$ -diketiminate ligand behaves as a trap of the anion formed by the deprotonation, which acting as a steric shield can confer an enhanced stability to the sensitive metallated fragments allowing their manipulation.

The utility of these  $\beta$ -diketiminate ligands has also been effectively demonstrated in a range of other applications such as stabilisers of Mg(I)-Mg(I) complexes.<sup>[101]</sup>  $\{(\text{Dipp})\text{Nacnac}\}\text{Mg}\}$  complexes have also been used as successful catalysts<sup>[113–117]</sup> or initiators for ring-opening polymerization reactions, among others.<sup>[226]</sup>

Preliminary studies revealed that the bifunctional magnesium amide base  $[\text{Dipp}\text{NacnacMg}(\text{TMP})]$  (**36**), containing the basic group TMP bonded terminally to

magnesium, can regioselectively  $\alpha$ -deprotonate benzothiazole and N-methyl benzimidazole at room temperature (Scheme 4.5).<sup>[106]</sup> In this regard the *modus operandi* of **36** involves kinetic activation by cleavage of the Mg-N(tmp) terminal bond which releases the active base and drives the Mg-H exchange process.<sup>[88]</sup> The  $\beta$ -diketiminate scaffold is observed to act as a steric stabilizer, protecting the new polar (and therefore reactive) Mg-C bonds. This protocol contrasts with previous studies using RMgCl or RLi reagents that require lower temperatures to avoid decomposition of the generated organometallic intermediate.<sup>[227]</sup>



Scheme 4.5: Deprotonation of benzoxazole, N-methyl benzimidazole and benzothiazole with base **36** at room temperature.

Stimulated by these initial findings, herein we expand the synthetic application of **36** by assessing its reactivity towards a range of relevant heterocyclic substrates including pyrazine, a particularly challenging substrate to deprotonate with single

metal reagents.<sup>[220,222]</sup> Trapping and structurally defining key organometallic intermediates has provided new insights into the way in which this magnesium base reagent operates.



## 4.2 Results and Discussion

The metalating ability of **36** ( $^{\text{Dipp}}\text{Nacnac} = \text{Ar}^*\text{NC}(\text{Me})\text{CHC}(\text{Me})\text{NAr}^*$ ;  $\text{Ar}^* = 2,6\text{-}^i\text{Pr}_2\text{-C}_6\text{H}_3$ ) was proved with a range of molecules such as heterocycles, triazoles and pyridine derivatives. Reactions were mainly carried out at room temperature, in THF, using equimolar amounts of **36** and the relevant organic substrate affording a variety of magnesiate compounds (**37** – **44**, **47**) in moderate to good crystalline yields (from 40 to 68%). Monitoring these reactions by NMR demonstrated that in many cases the reactions were quantitative. All the compounds were characterized by multinuclear NMR spectroscopy, elemental analysis and in some cases, their structures in the solid state were established by X-Ray crystallography.

### 4.2.1 Magnesiation of N/O-Heterocycles: Pyrazine and Benzofuran

We first looked at the deprotonation reactions between base **36** and the N/O-heterocyclic substrates pyrazine and benzofuran, with the former being less activated in terms of  $\text{pK}_a$  (39.3 for pyrazine and 32.7 for benzofuran in DMSO).<sup>[228]</sup> As previously mentioned, heterocyclic substrates are key building blocks in many pharmaceuticals and biologically active molecules. Interestingly, numerous natural products and pharmaceuticals contain diazines in their skeleton,<sup>[222]</sup> for example pyrazine can be found in the cancer chemopreventive compound Oltipraz.<sup>[229]</sup> Similarly, the benzofuran molecule can be found in natural products, molecular electronic and functional polymers.<sup>[230]</sup> It is also considered a biologically relevant heterocycle for being present in numerous of clinically approved drugs,<sup>[231]</sup> for instance, it is one of the key scaffolds needed for the synthesis of morphine.<sup>[217]</sup> Therefore, in order to form more complex molecules with this heterocyclic molecules, deprotonative metallation is one of the most common methodologies.<sup>[212]</sup>

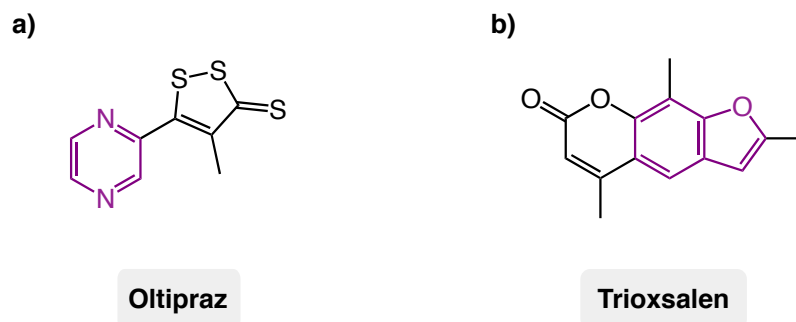
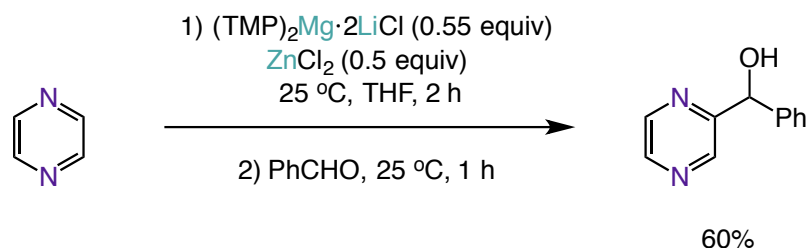


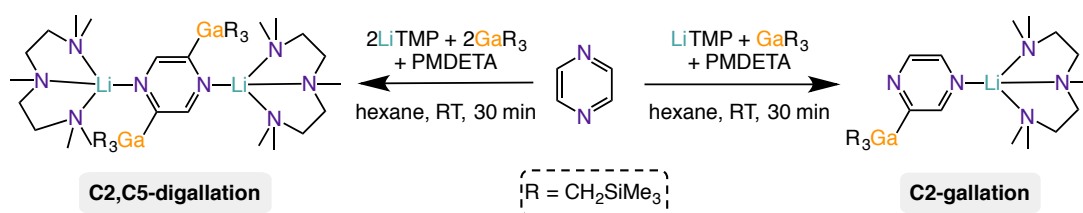
Figure 4.2: Examples of drugs containing pyrazine or benzofuran. a) Oltipraz, cancer chemopreventive. b) Trioxsalen, photosensitizer used to increase skin tolerance to sunlight and enhance pigmentation.

The smaller HOMO-LUMO gap coupled with the absence of directing groups in pyrazine, makes its regioselective deprotonation particularly challenging due to its tendency to undergo nucleophilic addition.<sup>[222]</sup> As shown in Scheme 4.1, cryogenic reaction conditions and short reaction times are required when LiTMP is employed. Such reactions afford the relevant metallated product after electrophilic interception, in yields ranging from 10 to 65%, along with small amounts (2 – 12%) of dimetallated product.<sup>[205]</sup> However, bimetallic combinations allow these reactions to be performed in milder reaction conditions, pairing Li with a softer metal such as Zn or Ga with different ligands. For example, when a mixture of 0.5 equivalents of  $\text{ZnCl}_2 \cdot \text{TMEDA}$  and 1.5 equivalents of LiTMP is reacted with pyrazine at room temperature during 2 hours, 2-iodopyrazine is obtained in 59% yield after electrophilic quench.<sup>[221]</sup> Knochel has also reported that the deprotonation of pyrazine using  $(\text{TMP})_2\text{Mg} \cdot 2\text{LiCl}$  requires the presence of  $\text{ZnCl}_2$  (0.5 equiv.) and can be achieved in 30 min at room temperature, in a 60% yield of the quenched compound.<sup>[225,232]</sup> In this reaction,  $\text{ZnCl}_2$  plays a key role, forming a zinc intermediate by transmetallation, which is much more stable than the corresponding magnesiate analogue (Scheme 4.6).



Scheme 4.6: Metallation of pyrazine by using  $(\text{TMP})_2\text{Mg}\cdot 2\text{LiCl}$  and  $\text{ZnCl}_2$  at mild reaction conditions.<sup>[225]</sup>

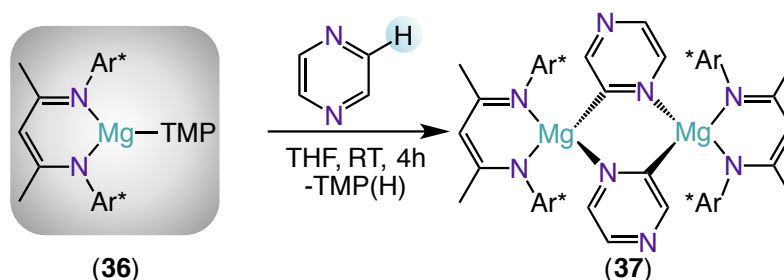
Our group has recently isolated an intermediate resulting from the regioselective 2,5-dizincation of this substrate using the mixed lithium zincate base  $[(\text{THF})\text{LiZn}(\text{TMP})^t\text{Bu}_2]$ .<sup>[220]</sup> Interestingly, using a single-metal organozinc reagent, such as  $\text{Zn}^t\text{Bu}_2$ , no metallation occurs and instead it forms a coordination adduct. Furthermore, the trans-metal-trapping reaction using LiTMP and the bulky trialkylgallium  $[\text{Ga}(\text{CH}_2\text{SiMe}_3)_3]$  proved to be effective towards the regioselective deprotonation of pyrazine at room temperature after 30 minutes in hexane.<sup>[233]</sup> In this system, using 1:1:1 stoichiometry the 2-monogallated pyrazine is obtained in quantitative yields, whereas a ratio of 2:2:1 affords the 2,5-disubstituted species in a 55% yield (Scheme 4.7).



Scheme 4.7: Deprotonation of pyrazine using LiTMP and a gallium alkyl trans-metal-trapping.<sup>[233]</sup>

The reaction between pyrazine and base **36** (1:1) in a THF solution at room temperature was first examined, which formed a dark green solution. Removal of

solvent *in vacuo* followed by slow cooling of hot toluene solution afforded a crop of light brown crystals of  $[\{({}^{\text{Dipp}}\text{Nacnac})\text{Mg}(\text{C}_4\text{H}_3\text{N}_2)\}_2]$  (**37**). A yield of 51% was isolated and an analysis of the filtrate showed that the C2-metallation of pyrazine is obtained quantitatively after 4 hours of reaction. The magnesiated compound **37** was characterized in the solid state (X-ray crystallography) and in solution ( $^1\text{H}$  and  $^{13}\text{C}$  NMR spectroscopy).



Scheme 4.8: Reactivity of **36** with pyrazine.

Crystallographic studies showed that the selective magnesiation of pyrazine was accomplished at room temperature, revealing the formation of a centrosymmetric dimer composed of two moieties of the  $\{({}^{\text{Dipp}}\text{Nacnac})\text{Mg}\}$  fragment, connected by two bridging asymmetric pyrazinyl rings (Figure 4.3). In compound **37**, the pyrazinyl anions are trapped by the  $\{({}^{\text{Dipp}}\text{Nacnac})\text{Mg}\}$  fragments, where the  $\beta$ -diketiminato ligand acts as a protective shelter towards the new Mg-C bonds. Additionally, molecular structure of **37** displays a dimeric motif with a Mg-N dative interaction between the  $\alpha$ -nitrogen of the pyrazinyl anion and the Mg atom of the neighbour unit. This dative interaction provides stabilization by minimising electronic repulsion between the lone pair of the nitrogen atom and the negative charge of the new carbanion formed.

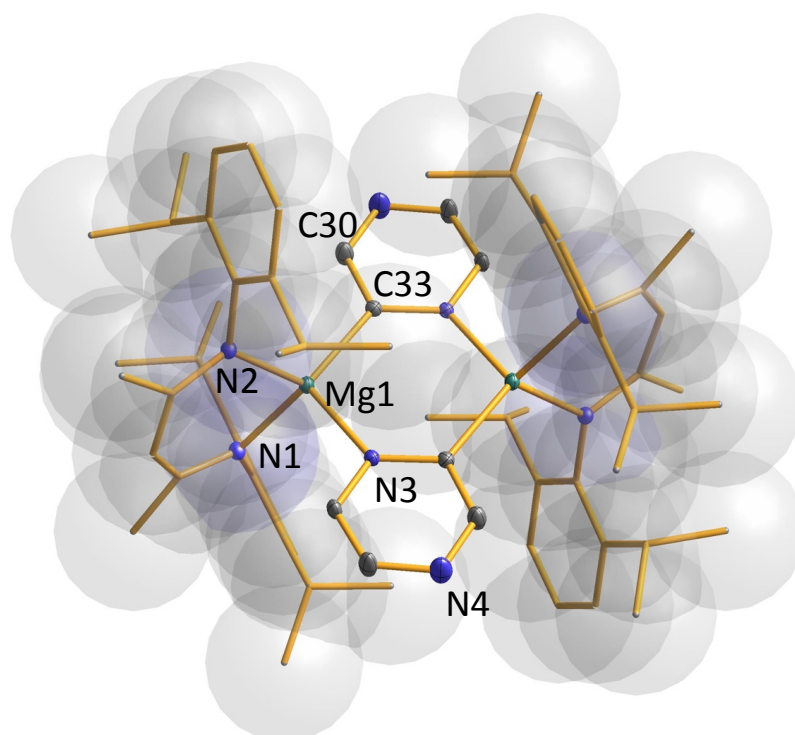


Figure 4.3: Molecular structure of **37** with 35% probability displacement ellipsoids. Carbon atoms of {<sup>Dipp</sup>Nacnac} framework are pictured as capped sticks with translucent space-filling van der Waals surfaces for a probe of 1.5 Å radius. All hydrogen atoms have been omitted for clarity. Selected bond lengths (Å) and bond angles (°): Mg1-N1 2.059(2), Mg1-N2 2.049(2), Mg1-N3 2.108(2), Mg1-C33 2.175(3), N1-Mg1-N2 93.07(9), N1-Mg1-C33 122.38(9), N2-Mg1-C33 120.37(9), N3-Mg1-N1 103.33(9), N3-Mg1-N2 105.17(8), N3-Mg1-C33 109.86(9).

A six-membered ring {MgCNMgCN} constitutes the core of the structure and both Mg atoms exhibit a distorted tetrahedral geometry (angles around to Mg ranging from 93.07(9)° to 122.38(9)°; mean: 108.56 °). Additionally, an approximate orthogonal disposition of the three-fused rings (dihedral angle 89.15°) is also present in **37**. The Mg-N distances [Mg1-N1 (2.059(2) Å) and Mg1-N2 (2.049(2) Å)] from the β-diketiminato ligand are shorter than the bond from the magnesium to the metallated pyrazine nitrogen Mg1-N3 [2.108(2) Å]. In agreement, similar Mg-N distances are observed in related β-diketiminato-Mg compounds containing neutral nitrogen donors such as pyridine or picoline [2.138(2) and 2.1282(13) Å].<sup>[234,235]</sup>

Since bond lengths can only give a first hint to the electronic properties of a molecule, Stalke has also reported charge density distribution experiments in order to quantify the contribution of related Mg-N interactions in the bonding present in  $[\text{Mg}\{(\text{pz}^*)_3\text{C}\}_2]$  ( $\text{pz}^*=3,5$ -dimethylpyrazolyl), where no charge transfer to the metal was observed.<sup>[236]</sup> Additionally, the bond distances of the magnesiated pyrazine, N3-C33 and C33-C30 [1.368(3) and 1.407(4) Å], are slightly more elongated than the corresponding values of free pyrazine [1.334 and 1.378 Å].<sup>[237]</sup> This could suggest an alternative description as a carbene dimer, similar to complementary studies by Boche that described the related metallated thiazole compounds as [3-metallathiazol-2-ylidenes] by comparative studies between these molecules and the corresponding free thiazole.<sup>[238]</sup> However, the N3-C33-C30 angle ( $114.83^\circ$ ) is smaller than the analogous angle in pyrazine ( $122.4^\circ$ ) and the Mg1-C33 distance (2.175(3) Å) is slightly shorter than that observed in Mg-N-heterocyclic carbenes [ranging from 2.200(2) to 2.288(5) Å].<sup>[106,239–244]</sup>

Pyrazine was also reacted with the butyl base  $[(^{\text{Dipp}}\text{Nacnac})\text{Mg}(n\text{Bu})(\text{THF})]$  proving the different reactivity pattern as the one observed for conventional bases such as BuLi or LiTMP (Figure 4.4).<sup>[1]</sup>

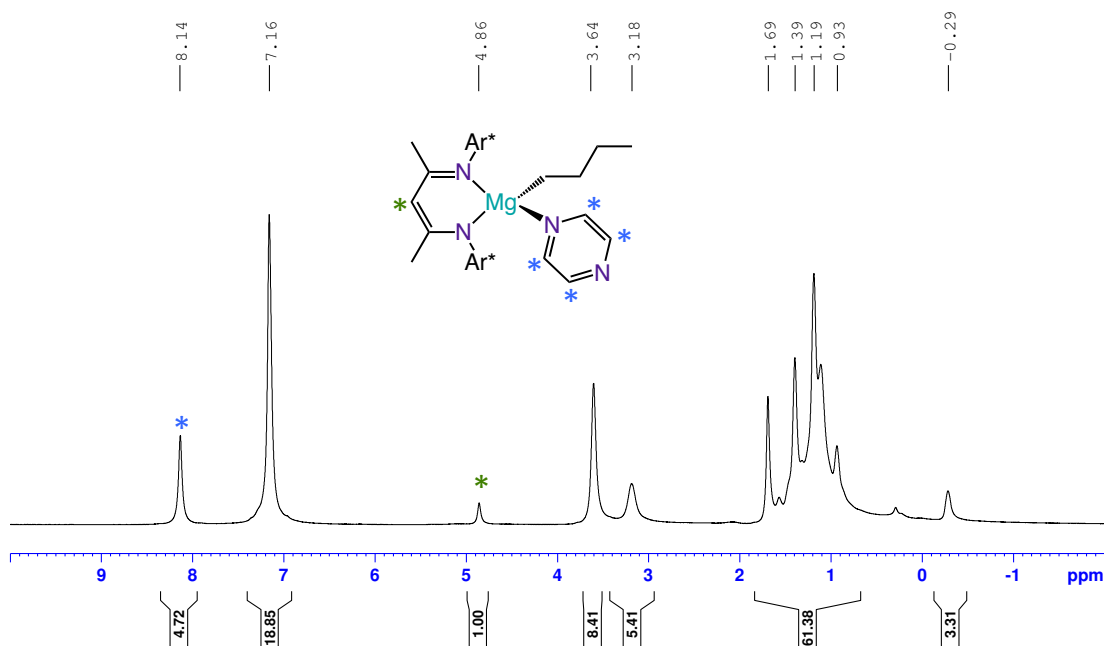


Figure 4.4:  $^1\text{H}$  NMR spectrum of  $[(\text{Dipp})\text{Nacnac}]\text{Mg}(\text{Bu})(\text{C}_4\text{H}_4\text{N}_2)$  in  $\text{C}_6\text{D}_6$ .

In Figure 4.4, the  $^1\text{H}$  NMR spectrum revealed a broad singlet at 8.14 ppm that has shifted to a lower field compared to free pyrazine (8.05 ppm) and suggests the presence of four equivalent protons of the pyrazine molecule coordinated to the magnesium centre. The broadening of the signals in the  $^1\text{H}$  NMR and the fact that there is only one signal for the pyrazine indicates a solvation/desolvation process.

The 2D  $^1\text{H}$  DOSY NMR experiment in  $\text{C}_6\text{D}_6$  with the presence of TMS (tetramethylsilane) as internal standard helped to rationalise the species in solution and is presented in Figure 4.5.

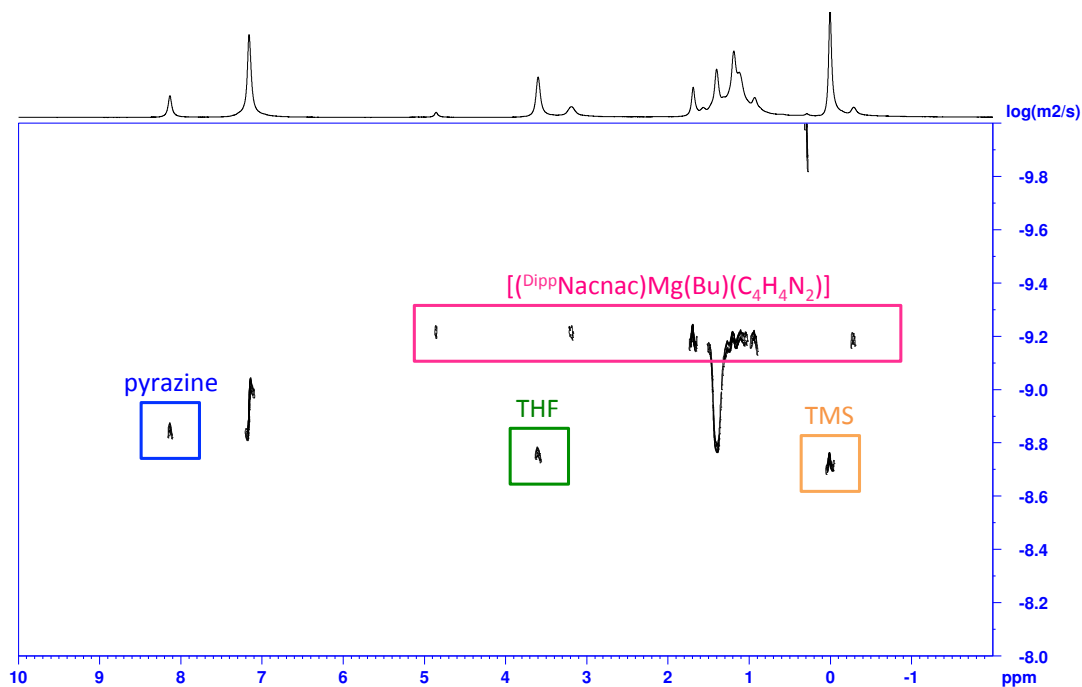


Figure 4.5:  $^1\text{H}$  DOSY NMR spectrum of  $[(^{\text{Dipp}}\text{Nacnac})\text{Mg}(\text{Bu})(\text{C}_4\text{H}_4\text{N}_2)]$  in  $\text{C}_6\text{D}_6$ .

This experiment confirmed the formation of the donor adduct  $[(^{\text{Dipp}}\text{Nacnac})\text{Mg}(\text{Bu})(\text{C}_4\text{H}_4\text{N}_2)]$  and the metallated compound **37** was not observed (Table 4.1).

Table 4.1: Possible species formed in  $\text{C}_6\text{D}_6$  and the corresponding diffusion coefficient ( $D$ ), molecular weights ( $MW$ ) and errors.

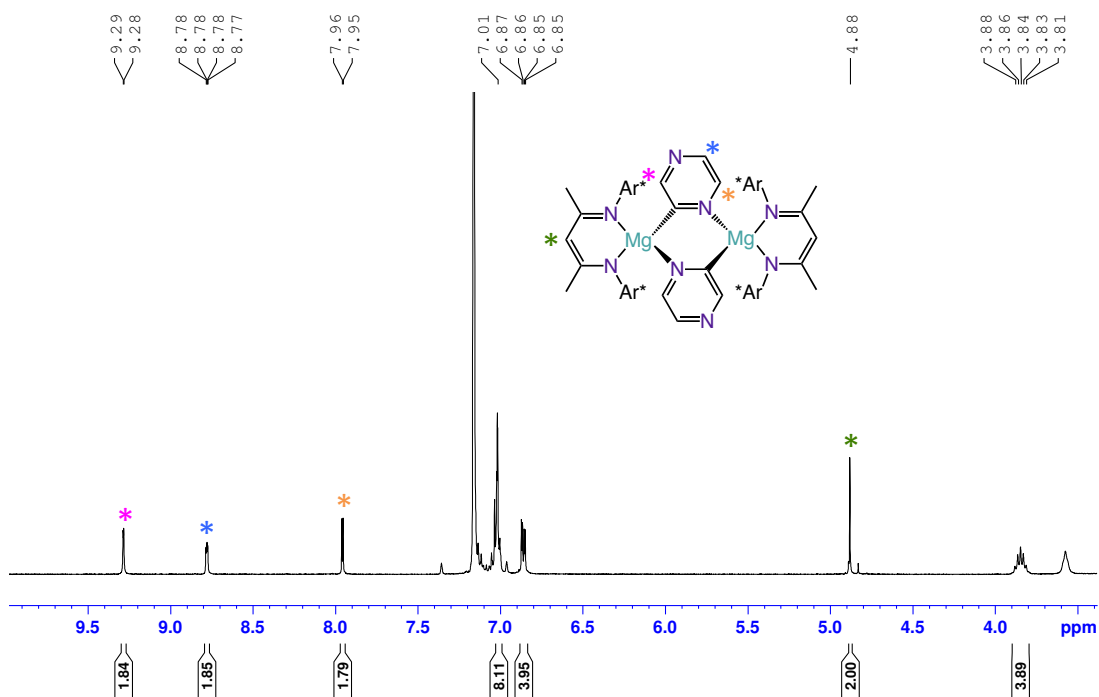
Compound	$D$ ( $\text{m}^2 \text{s}^{-1}$ )	$MW_{\text{calc}}$ ( $\text{g mol}^{-1}$ )	$MW_{\text{est}}$ ( $\text{g mol}^{-1}$ )	Error (%)
pyrazine	1.373E-9	80	151	47
THF	1.701E-9	72	107	33
$[(^{\text{Dipp}}\text{Nacnac})\text{Mg}(\text{Bu})(\text{C}_4\text{H}_4\text{N}_2)]$	5.7503E-10	579	615	6
$[(^{\text{Dipp}}\text{Nacnac})\text{Mg}(\text{Bu})(\text{THF})]$	5.7503E-10	571	615	7



Table 4.1 shows a comparison of the possible species formed in  $C_6D_6$ . The diffusion coefficient of pyrazine indicates an estimated molecular weight of  $151 \text{ g mol}^{-1}$ , larger (47% error) than free pyrazine ( $80 \text{ g mol}^{-1}$ ). Similarly, the molecular weight estimated for THF was  $107 \text{ g mol}^{-1}$ , which is also larger (33% error) than free THF ( $72 \text{ g mol}^{-1}$ ). However, the estimated molecular weight for both  $\beta$ -diketiminato complexes  $[(^{Dipp}Nacnac)Mg(Bu)(C_4H_4N_2)]$  and  $[(^{Dipp}Nacnac)Mg(Bu)(THF)]$  is  $615 \text{ g mol}^{-1}$  with an error of 6 and 7%, respectively. This result is consistent with the formation of a pyrazine donor adduct undergoing rapid solvation/desolvation.

These studies illustrate the different reactivity pattern between the TMP and the Bu bases, where **36** is kinetically more activated than  $[(^{Dipp}Nacnac)Mg(Bu)(THF)]$ . This, runs counter to the normal pattern exhibited by conventional bases, where, for example BuLi, is a stronger base than LiTMP.<sup>[1]</sup>

$^1H$  and  $^{13}C$  NMR spectroscopy was used to characterize **37** in deuterated benzene solution at room temperature and  $^1H$ - $^{13}C$  HSQC and  $^1H$  COSY experiments were conducted to facilitate the full assignment of the spectra.  $^1H$  NMR spectra of **37** showed three resonances at 9.29, 8.78 and 7.96 ppm, which are assigned to the metallated pyrazine, being consistent with the lack of symmetry in this aromatic ring (Figure 4.6). Those resonances clearly differ from the singlet at 8.05 ppm corresponding to the four equivalent protons in free pyrazine.

Figure 4.6:  $^1\text{H}$  NMR spectrum of **37** in  $\text{C}_6\text{D}_6$ .

The signal corresponding to the metallated carbon in **37** was not possible to identify due to the low solubility of the compound. However, three distinct resonances at 158.0, 145.1 and 142.2 ppm in the  $^{13}\text{C}$  NMR correspond to the magnesiated pyrazine that differ from the signal at 145.3 for the four equivalent carbon atoms of free pyrazine (Figure 4.7).

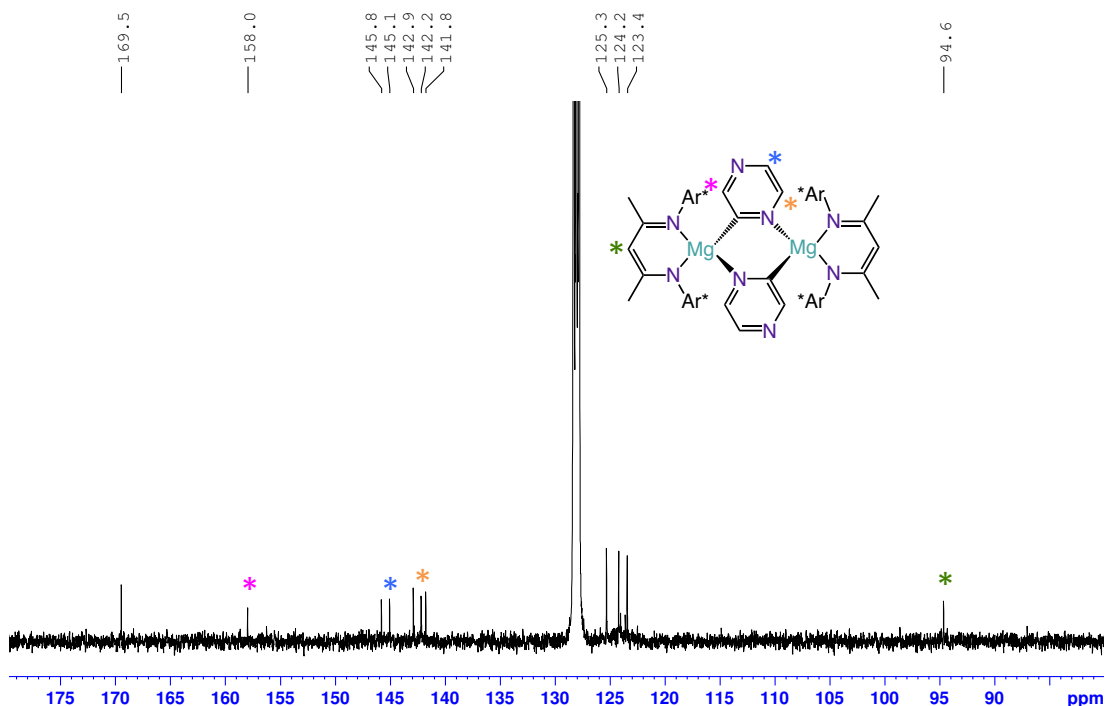


Figure 4.7:  $^{13}\text{C}$  NMR spectrum of **37** in  $\text{C}_6\text{D}_6$ .

Additionally, some resonances of the  $\beta$ -diketiminato ligand are used as a fingerprint of the different compounds and help to identify the formation of new products. The most informative signals in the  $^1\text{H}$  and  $^{13}\text{C}$  NMR correspond to the singlet resulting from the CH of the  $\{\text{DippNacnac}\}$  ligand backbone and the septuplets in the  $^1\text{H}$  NMR corresponding to the CH of the  $i\text{Pr}$  groups of the  $\text{Ar}^*$  substituents. In **37**, the singlet resulting from the CH of the  $\{\text{DippNacnac}\}$  ligand backbone has shifted from 4.86 in **36** to 4.88 ppm for **37** and two sets of new septuplets at 3.82 and 2.48 ppm correspond to the CH signals of the  $i\text{Pr}$  groups, differently from **36** (3.22 ppm). The CH of the  $\{\text{DippNacnac}\}$  ligand backbone in the  $^{13}\text{C}$  NMR spectrum has remained at 94.6 ppm.

We then moved to study the magnesiation reaction of benzofuran. Preparation of benzofuran derivatives with substituents at the C2 position appears to be well

documented, with reactions being performed by using lithium compounds at cryogenic temperatures ( $-78\text{ }^{\circ}\text{C}$ ),<sup>[245]</sup> and by mixed-metal compounds such as alkali-metal magnesiates, aluminates, cuprates or zincates.<sup>[126,246–248]</sup> In particular, magnesiation of benzofuran has been demonstrated at ambient temperatures using lithium magnesiates,<sup>[249]</sup> however no structural evidence of the magnesiated benzofuran is provided.

Solid-state characterization of metallated benzofuran intermediates has only been accomplished on a few occasions. Notably, iron N-heterocyclic carbenes such as  $\text{Cp}^*\text{Fe}\{\kappa^2\text{-(C,C)-L}^{\text{iPr}}\}$  ( $\text{L}^{\text{iPr}} = \text{CH}_2\text{CH}(\text{CH}_3)(3\text{-isopropyl-4,5-dimethylimidazol-2-ylidene-1-yl})$ ) are shown to promote C-H bond activation at room temperature at the 2-position of the benzofuran ring (Figure 4.8a).<sup>[250]</sup> The crystal structure of the dimer  $(2\text{-lithiobenzofuran-TMEDA})_2$  (TMEDA = N,N,N',N'-tetramethylethylenediamine) is also known, and can be readily isolated from the reaction between benzofuran and *n*-BuLi (1:1 ratio) in the presence of a chelating TMEDA ligand in diethyl ether at room temperature (Figure 4.8b).<sup>[251]</sup> However, the structural characterisation of any magnesiated intermediate has remained elusive.

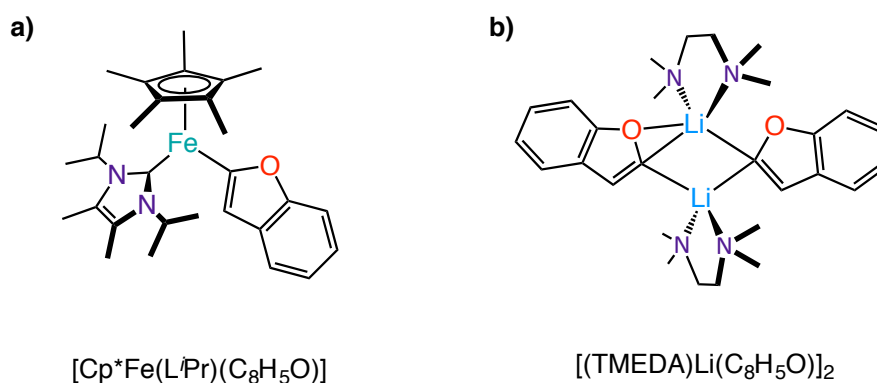
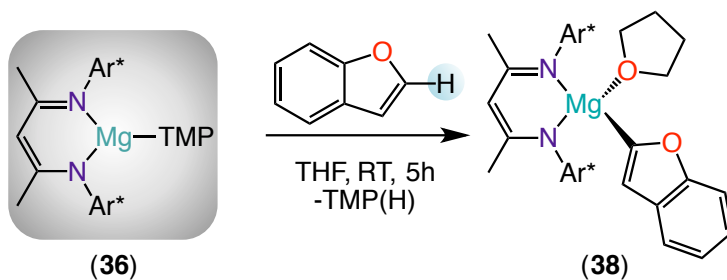


Figure 4.8: Examples of metallated benzofuran intermediates.

Moving to benzofuran heterocycle, we anticipated that its deprotonation at the C2 position would be possible due to the similarity, in terms of its  $\text{pK}_a$  value (32.7),<sup>[228]</sup>

with the previously deprotonated N-methyl benzimidazole (32.5)<sup>[106]</sup> by the same magnesium base **36**. Dissolving pure crystals of **36** in THF solution and adding an equivalent amount of benzofuran at room temperature resulted in the formation of  $[\{(\text{Dipp})\text{Nacnac}\}\text{Mg THF}\{\text{C}_8\text{H}_5\text{O}\}]$  (**38**) crude white solid after stirring for two hours at room temperature followed by removal of solvent *in vacuo*. Single colourless crystals of **38** suitable for X-ray diffraction studies, were grown from a hexane/toluene solution of **38** placed at  $-33\text{ }^\circ\text{C}$  (Scheme 4.9). Quantitative conversion after 5 hours at room temperature was observed by monitoring this reaction by  $^1\text{H}$  NMR spectroscopy and a 74% of isolated yield was obtained after 5 hours of reaction at room temperature.



Scheme 4.9: Reactivity of **36** with benzofuran.

Structural analysis of **38** revealed a monomeric structure containing benzofuran magnesiated at C2, which importantly represents the first structural study of a magnesiated benzofuran intermediate. Further inspection reveals that the Mg atom exists in a distorted tetrahedral geometry (angles around Mg ranging from  $93.60(6)^\circ$  to  $137.77(6)^\circ$ ; mean  $108.03^\circ$ ), where the  $\{(\text{Dipp})\text{Nacnac}\}\text{Mg}$  fragment coordinates to a terminal  $\alpha$ -metallated molecule of benzofuran and is solvated by a molecule of the THF (Figure 4.9).

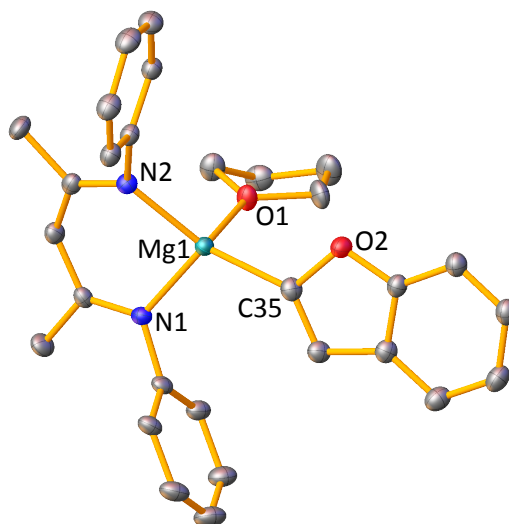


Figure 4.9: Molecular structure of **38** with 50% probability displacement ellipsoids. All hydrogen atoms and *i*Pr groups have been omitted for clarity. Selected bond lengths (Å) and bond angles (°): Mg1-N1 2.0573(15), Mg1-N2 2.0615(14), Mg1-O1 2.0282(12), Mg1-C35 2.1347(18), N1-Mg1-N2 93.60(6), N1-Mg1-C35 113.65(6), N2-Mg1-C35 137.77(6), O1-Mg1-N1 104.89(5), O1-Mg1-N2 103.26(5), O1-Mg1-C35 100.13(6).

In contrast to pyrazine or our previous dimers reported, resulting from the metallation of N-methyl benzimidazole and benzothiazole with **36**,<sup>[106]</sup> the crystal structure of **38** displays a monomeric arrangement reminiscent of that found in the ferrated benzofuran reported by Y. Ohki and K. Tatsumi (Figure 4.8a).<sup>[250]</sup> The Mg-C bond distance in **38** compares well with those found in related aryl magnesium complexes containing the  $\{(\text{D}^{\text{i}pp}\text{Nacnac})\text{Mg}\}$  fragment such as  $\{[(\text{D}^{\text{i}pp}\text{Nacnac})\text{Mg}\{(\text{OEt})_2(\text{Ph})\}]\}$  ([2.139(3) Å] vs [2.1347(18) Å] in **38**).<sup>[252]</sup> However, reflecting the monomeric constitution of **38**, the Mg-C distance is considerably shorter than other Mg-C(sp<sup>2</sup>) bond distances in magnesiated intermediates such as  $\{[\{(\text{THF})_3\text{Na}_2\}\{\text{TMEDA}\}\text{Mg}_2\}\{2\text{-C}_4\text{H}_3\text{O}\}_6\}_\infty$  [mean 2.18 Å]<sup>[253]</sup> or  $\{[(\text{TMEDA})_3\text{Na}_6\text{Mg}_3\text{-}(\text{CH}_2\text{SiMe}_3)(2,5\text{-C}_4\text{H}_2\text{O})_3(2\text{-C}_4\text{H}_3\text{O})_5]_2\}$  [mean 2.28 Å],<sup>[254]</sup> where the furan anions act as a bridging fragment in each case.

$^1\text{H}$  and  $^{13}\text{C}$  NMR spectroscopy also confirmed the formation of **38** and revealed that its solvating THF molecule can be removed under vacuum during the isolation of the crystals. The signal from the six *CH* aromatic protons corresponding to the Ar\* substituents appears at 7.13 in  $^1\text{H}$  NMR, which hampers the identification of the missing doublet resonance corresponding to the proton in the C2 position of the benzofuran that appears at the same chemical shift. However, in the  $^{13}\text{C}$  NMR spectrum of **38**, the metallated carbon (attached to Mg) has shifted to higher frequency (192.8 ppm) with respect to the related chemical shift of C2 of the free benzofuran (145.1 ppm). The diagnostic singlet resulting from the *CH* of the { $^{\text{Dipp}}$ Nacnac} ligand backbone has shifted from 4.86 ppm in **36** to 4.90 ppm and a new multiplet at 3.45 ppm appear for compound **38** corresponding to the four protons of the  $^i\text{Pr}$  groups.

#### 4.2.2 Magnesiation of Triazoles

Extending our metallation protocol with base **36**, we next turned our attention to the study of N-heterocyclic substrates from the triazole family namely 1-methyl-1,2,4-triazole and 1,5-diphenyl-1,2,3-triazole. 1-methyl-1,2,4-triazole is significantly more activated in terms of  $\text{pK}_a$  (34.0 at C3 and 28.5 at C5 for 1-methyl-1,2,4-triazole) than benzofuran (32.7) or pyrazine (39.3), in DMSO.<sup>[228,255]</sup>

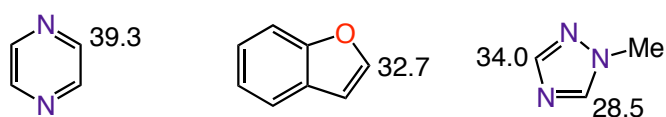


Figure 4.10: Experimental  $\text{pK}_a$  values of pyrazine, benzofuran and 1-methyl-1,2,4-triazole in DMSO.<sup>[228,255]</sup>

Triazole molecules and their benzo derivatives are attractive moieties in organic synthesis, material chemistry and organometallics.<sup>[70,256–260]</sup> Triazole scaffolds are

also typically known in medicinal chemistry to be part of antifungals,<sup>[261]</sup> although they are also present in other drugs such as anticonvulsant agents, for example (Figure 4.18).<sup>[262]</sup>

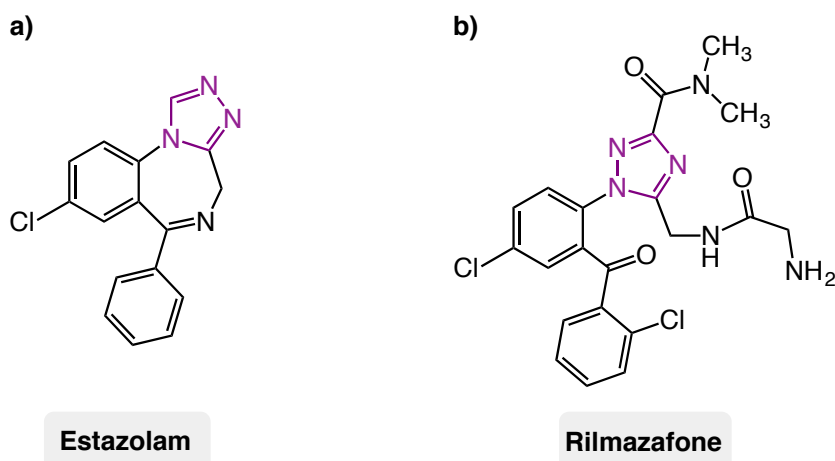
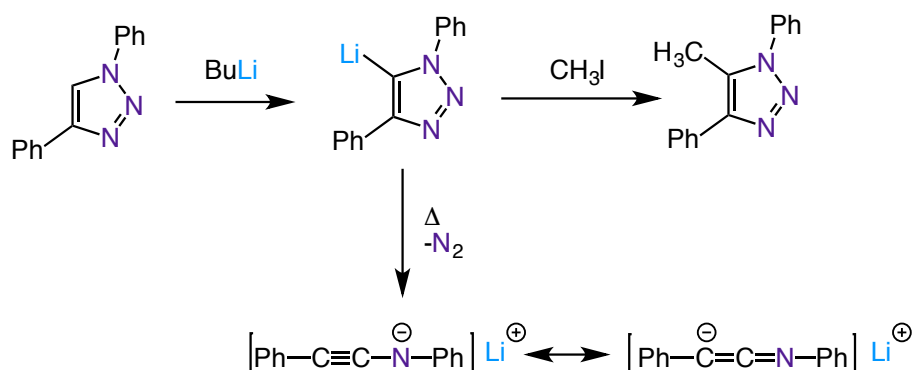


Figure 4.11: Examples of anticonvulsant agents containing triazole scaffolds. a) Estazolam, drug for sleep disorders. b) Rilmazafone, drug used to reduce anxiety.

Lithiation of five-membered heterocyclic triazoles is generally performed by *n*BuLi or LiTMP by strict control of the temperature (-78 to -20 °C), and the lithiated intermediates formed can be quenched with a variety of electrophiles.<sup>[263–265]</sup> However, at room temperature these intermediates tend to undergo fragmentation (Scheme 4.11).<sup>[266,267]</sup>



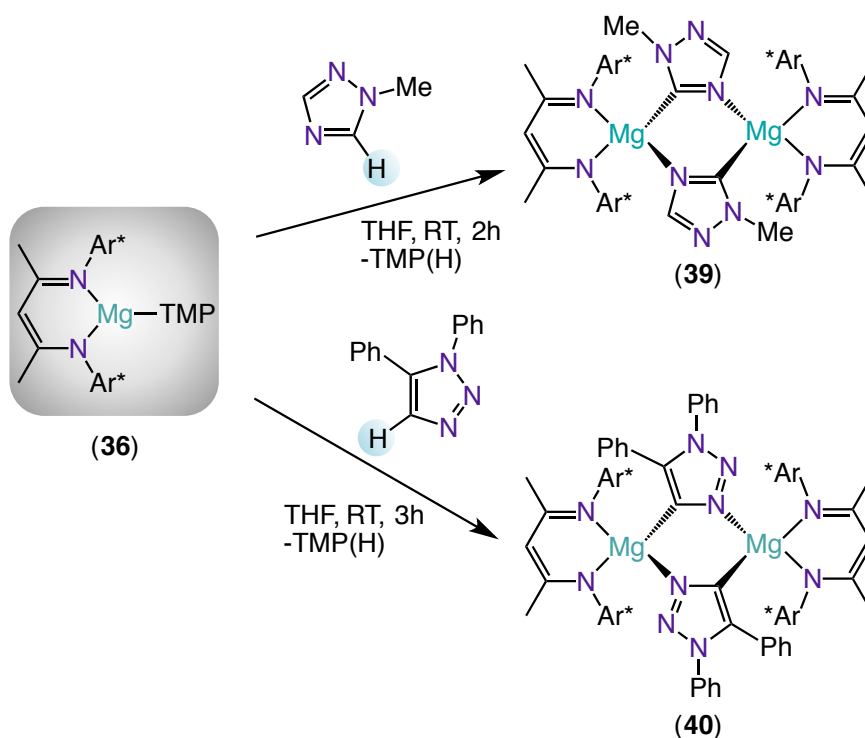
Scheme 4.10: Fragmentation reaction of 1,4-diphenyl-1,2,3-triazole.<sup>[266,267]</sup>

This decomposition reaction has been reported since the 1970s where, for example, 1,4-diphenyl-1,2,3-triazole decomposes to N-phenylalkynamide lithium complex while eliminating nitrogen.<sup>[266]</sup> Interestingly, lithiation at low temperatures of 1-methyl-1,2,4-triazole, 1,5-diphenyl-1,2,3-triazole has also been reported<sup>[268,269]</sup> Studies using mixed-metal bases have shown that 1-methyl-1,2,4-triazole can be metallated at room temperature. Thus, using potassium magnesiate  $[(\text{PMDETA})_2\text{K}_2\text{Mg}(\text{CH}_2\text{SiMe}_3)_4]$  (PMDETA = N,N,N',N'',N'''-pentamethyldiethylenetriamine) (2 equiv, 25 °C, 1 h), followed by addition of I<sub>2</sub>, forming the 5-iodo product in a 93% yield.<sup>[126]</sup> Furthermore, the same triazole can be zincated at the same position using lithium zincate  $[\text{Li}(\text{TMP})\text{Zn}(\text{tBu})_2]$  (2 equiv, 25 °C, 2 h), to give the same iodinated product in a 98% yield.<sup>[270]</sup>

Importantly, no structural or solution studies of the putative metallated intermediates of this heterocyclic substrate have been previously reported and a search in the CCDC database revealed that metallated examples of 1-methyl-1,2,4-triazole and 1,5-diphenyl-1,2,3-triazole have never been structurally characterized for s-block metals. The only structurally characterized examples of metallated triazoles, at the carbon atom, are known for triazoles containing the nitrogen atoms in consecutive positions. Moreover, most of the known complexes contain

transition metals such as gold or palladium,<sup>[271,272]</sup> which exist as precursors to N-heterocyclic carbenes and are formed by cycloaddition between azides with alkynes.<sup>[271,273–276]</sup>

Triazoles 1-methyl-1,2,4-triazole and 1,5-diphenyl-1,2,3-triazole were reacted with base **36** (1:1) in a THF solution at room temperature. Removal of solvent *in vacuo* followed by slow cooling of hot toluene solution afforded a crop of colourless crystals of  $[\{(\text{Dipp})\text{Nacnac}\}\text{Mg}(\text{C}_3\text{H}_4\text{N}_3)\}_2]$  (**39**) in a 66% yield from 1-methyl-1,2,4-triazole and  $[\{(\text{Dipp})\text{Nacnac}\}\text{Mg}(\text{C}_{14}\text{H}_{10}\text{N}_3)\}_2]$  (**40**) in a 45% yield from 1,5-diphenyl-1,2,3-triazole. Compounds **39** and **40** were characterized in the solid state (X-Ray crystallography) and in solution ( $^1\text{H}$  and  $^{13}\text{C}$  NMR spectroscopy).



Scheme 4.11: Reactivity of **36** with 1-methyl-1,2,4-triazole and 1,5-diphenyl-1,2,3-triazole.

X-Ray crystallography confirmed the C5- and C4-metallation of 1-methyl-1,2,4-triazole (Figure 4.12) and 1,5-diphenyl-1,2,3-triazole (Figure 4.13), respectively. The molecular structures of **39** and **40** present a strong resemblance to **37** and the previously reported metallated intermediates of benzothiazole and N-methyl benzimidazole.<sup>[106]</sup> Compounds **39** and **40** share the same structural motif in the solid state, displaying a centrosymmetric dimeric structure where the deprotonated substrates act as asymmetric bridges between two  $\{(\beta\text{-diketimate})\text{Mg}\}$  fragments. The structures are best described as three fused six-membered rings with a six-membered  $\{\text{MgCNMgCN}\}$  internal ring connected to, via shared Mg atoms, two outer  $\{\text{MgNCCCN}\}$  rings of the  $\{(\beta\text{-diketimate})\text{Mg}\}$  fragments.

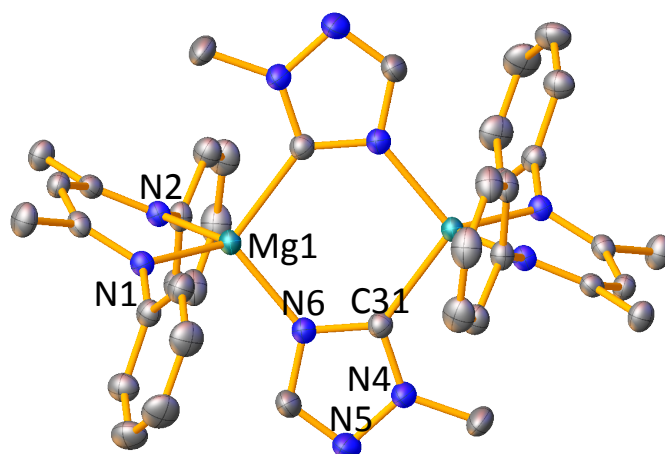


Figure 4.12: Molecular structure of **39** with 50% probability displacement ellipsoids. All hydrogen atoms and *t*-Pr groups have been omitted for clarity. Selected bond lengths (Å) and bond angles (°): Mg1-N1 2.064(1), Mg1-N2 2.077(1), Mg1-N6 2.075(1), Mg1-C31 2.195(1), N1-Mg1-N2 92.17(4), N1-Mg1-C31 116.71(5), N2-Mg1-C31 109.86(5), N6-Mg1-N1 115.53(5), N6-Mg1-N2 118.44(5), N6-Mg1-C31 104.43(5).

The Mg atoms of compound **39** (Figure 4.12) exhibits a distorted tetrahedral geometry (angles around to Mg ranging from 92.17(4)<sup>o</sup> to 118.44(5)<sup>o</sup>; mean, 109.13<sup>o</sup>) and form a  $\{\text{MgCNMgCN}\}$  planar six-membered ring, which exhibits an

approximately orthogonal disposition to two adjacent {MgNCCCN} rings (dihedral angle  $87.07^\circ$ ). The Mg-N distance values [Mg1-N1 (2.064(1) Å) and Mg1-N2 (2.077(1) Å)] from the  $\beta$ -diketiminate ligand in **39** lie in the same range as the coordinative bond from the magnesium to the nitrogen of the triazole anion [Mg1-N6 (2.075(1) Å)].

The structure of **40**, highly reminiscent of **39** shows that 1-methyl-1,2,4-triazole has been metallated at the C-4 position (Figure 4.13), although some bond parameters differ significantly.

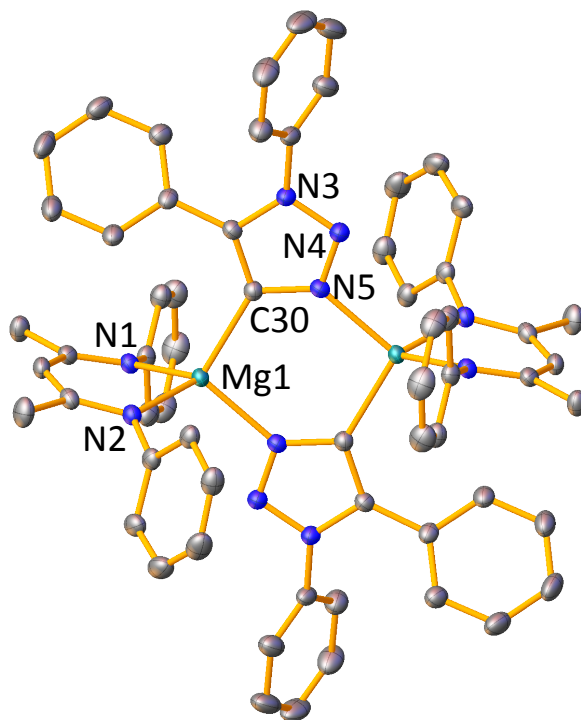


Figure 4.13: Molecular structure of **40** with 50% probability displacement ellipsoids. All hydrogen atoms and *i*Pr groups have been omitted for clarity. Selected bond lengths (Å) and bond angles ( $^\circ$ ): Mg1-N1 2.0785(11), Mg1-N2 2.0882(11), Mg1-N5 2.1139(12), Mg1-C30 2.1838(13), N1-Mg1-N2 90.93(4), N1-Mg1-C30 115.19(5), N2-Mg1-C30 118.14(5), N1-Mg1-N5 120.47(5), N2-Mg1-N5 111.59(5), N5-Mg1-C30 101.51(5).

In this case, the Mg-N distances [Mg1-N1 (2.0785(11) Å) and Mg1-N2 (2.0882(11) Å)] from the  $\beta$ -diketiminato ligand in **40** are slightly shorter than that of the bond from the magnesium to the nitrogen of the triazole anion Mg1-N5 (2.1139(12) Å). Additionally, the shorter Mg-C and longer Mg-N distance in **40** with respect to the analogous distances in **39** suggest that a larger coefficient of the electron density is localized on the carbon rather than the nitrogen atom.

A comparison of the general features of the dimeric compounds **37**, **39** and **40** reveals that the Mg-N distance of compound **40** is longer than that in **37** and **39** (Table 4.2). However, in all the cases considerably shorter Mg-N length compared to the one of the  $\beta$ -diketiminato-Mg compound reported by Hill, where pyridine is coordinated as a neutral N-donor to Mg (2.174(3) Å).<sup>[234]</sup> Furthermore, the longer Mg-C distance is observed for **39** (2.195(1) Å) and has a similar value to that reported in the magnesiated benzothiazole (2.193(2) Å).<sup>[106]</sup> Additionally, the Mg-N distances of the  $\beta$ -diketiminato ligand and that between the magnesium atoms appear to be slightly elongated for compound **40** (Table 4.2).

Table 4.2: Comparison of the general features between compounds **37**, **39** and **40**.

Compound	Mg-C (Å)	Mg-N (Å)	Mg-N <sub>Nacnac</sub> (Å)	Mg...Mg (Å)
<b>37</b>	2.175(3)	2.108(2)	2.059(2)/2.049(2)	3.827(1)
<b>39</b>	2.195(1)	2.075(1)	2.064(1)/2.077(1)	3.9811(6)
<b>40</b>	2.1838(13)	2.1139(12)	2.0785(11)/2.0882(11)	4.1025(7)

<sup>1</sup>H and <sup>13</sup>C NMR spectroscopy were used to characterize **39** and **40** in deuterated benzene solution at room temperature. Additionally <sup>1</sup>H-<sup>13</sup>C HSQC and COSY experiments were conducted to facilitate assignment of the spectra. A comparison of the <sup>1</sup>H NMR spectra of **39** and **40** with those of the heterocyclic substrates

reveals that the diagnostic resonances corresponding to the protons at the C5 position of free 1-methyl-1,2,4-triazole (7.94 ppm) and C4 position of free 1,5-diphenyl-1,2,3-triazole (7.72 ppm) have disappeared. The singlet resulting from the CH of the  $\beta$ -diketiminato ligand backbone resonates at 4.77 and 4.76 ppm for compounds **39** and **40**, respectively. Two sets of new septuplets corresponding to the CH signals of the <sup>i</sup>Pr groups of the Ar\* substituents appeared in each case (3.63 and 2.76 ppm for **39**; 3.78 and 3.04 ppm for **40**;). In the <sup>13</sup>C NMR spectrum of **39** the metallated carbon, attached to Mg, has shifted to higher frequency (184.9 ppm) with respect to the related chemical shift of C5 of the 1-methyl-1,2,4-triazole (152.3 ppm). Whereas the metallated quaternary carbon in **40** was not observed due to the limited solubility, which led to low intensity resonances in the <sup>13</sup>C NMR spectrum.

### 4.2.3 Magnesiation of Related Organic Substrates: Benzotriazole and Diphenylacetonitrile

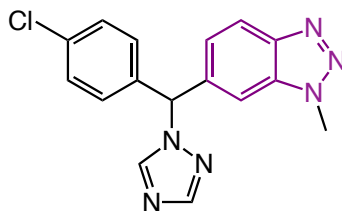
In parallel with these studies we have also assessed the reactivity of **36** with other related organic substrates, including benzotriazole and diphenylacetonitrile. In these cases the NH and CH protons of benzotriazole and diphenylacetonitrile are particularly acidic, with a pK<sub>a</sub> of 8.2 and 17.5 respectively.<sup>[277,278]</sup>



Figure 4.14: Experimental pK<sub>a</sub> values of benzotriazole and diphenylacetonitrile in DMSO.<sup>[277,278]</sup>

Between many applications, benzotriazole is known for its use as an effective corrosion inhibitor for copper and its alloys.<sup>[176]</sup> Benzotriazole derivatives can be

used as herbicides, insecticides<sup>[279]</sup> or in synthesis,<sup>[277]</sup> and is also present in the scaffold of some drugs, such as Vorozole.<sup>[280]</sup>



**Vorozole**

Figure 4.15: Vorozole, inhibitor containing benzotriazole scaffold.<sup>[280]</sup>

Crystal structures of metallated benzotriazole appeared to be well documented possibly due to the high acidity of the NH proton ( $pK_a = 8.2$ <sup>[277]</sup>). Most of these structures contain transition metals such as copper,<sup>[281]</sup> gold<sup>[282]</sup> or nickel<sup>[283]</sup> although structures with lanthanides such as dysprosium<sup>[284]</sup> are also known. Interestingly, a few examples of zincated complexes have also been reported showing deprotonation at the N-H. For example, the pentanuclear metal complex  $[Zn_5(C_6H_4N_3)_6(L)_3(Ac)] \cdot 0.5MeOH \cdot 0.5H_2O$  ( $L = p$ -aminobenzoate;  $Ac =$  acetate), which was prepared in a 56% yield after refluxing during 30 minutes<sup>[285]</sup> and the zinc complexes  $[Zn_5(\mu_3-OH)_2(\mu_2-OH)_2(L)_4(C_6H_4N_3)_2]_\infty$  and  $[Zn_4(L)_4(C_6H_4N_3)_4(bpy)_2]_\infty$  ( $L = 2$ -phenyl-4-quinolinecarboxylic acid;  $bpy = 4,4'$ -bipyridine) that were hydrothermally synthesised in a teflon-lined reactor heated to 160 °C for 72 hours, in 56% yield (Figure 4.16).<sup>[286]</sup>

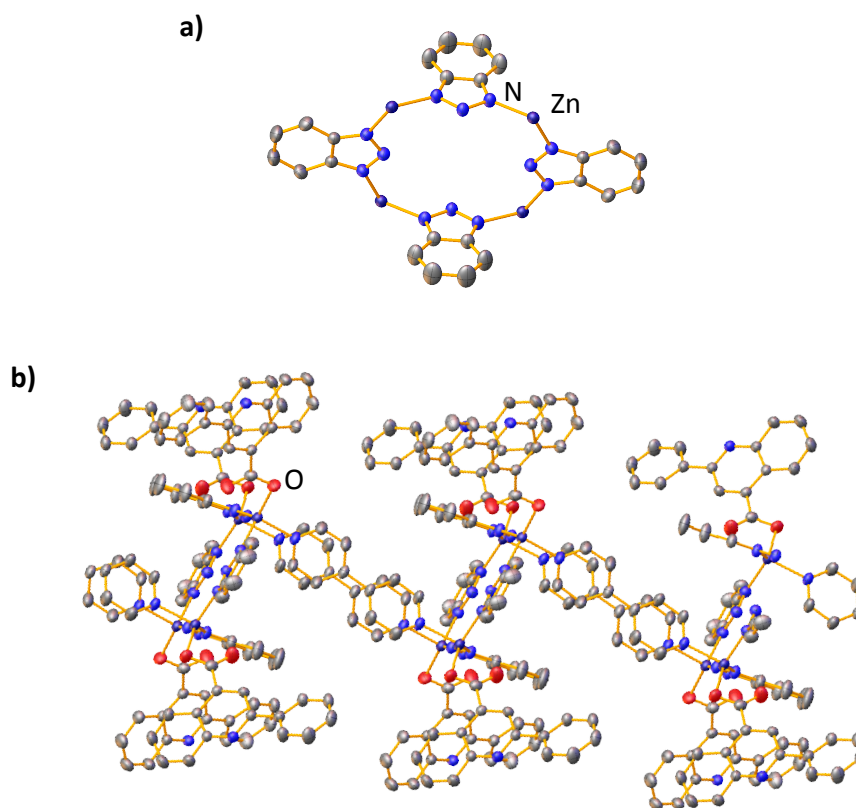


Figure 4.16: Molecular structure of  $[\text{Zn}_4(\text{L})_4(\text{C}_6\text{H}_4\text{N}_3)_4(\text{bpy})_2]_\infty$  ( $\text{L} = 2\text{-phenyl-4-quinolinecarboxylic acid}$ ) with 50% probability displacement ellipsoids. All hydrogen atoms have been omitted for clarity. a) View of the tetranuclear Zn(II) metallamacrocycle. b) View of the extended structure  $[\text{Zn}_4(\text{L})_4(\text{C}_6\text{H}_4\text{N}_3)_4(\text{bpy})_2]_\infty$ .<sup>[286]</sup>

Remarkably, an example of potassium amide ladder, which has previously been mentioned in the discussion of potassium amides in Chapter 2, has also been described (Figure 2.3). In order to perform such deprotonation the reaction mixture was cooled down with liquid nitrogen and further slow heating until 70 °C in order to crystalize the potassium compound  $[\{\text{KN}_3\text{C}_6\text{H}_4\}(\text{HMPA})]_\infty$ .<sup>[176]</sup> Furthermore, a mixed-metal compound  $[\text{HDMF}][\text{NaHg}_4(\text{C}_6\text{H}_4\text{N}_3)_6\text{I}_4]$  was also obtained at room temperature in 75% yield using slow diffusion of an aqueous solution of NaOH, solution of benzotriazole in DMF and aqueous solution of  $\text{HgI}_2$  during 4 days (Figure 4.17).<sup>[285]</sup>



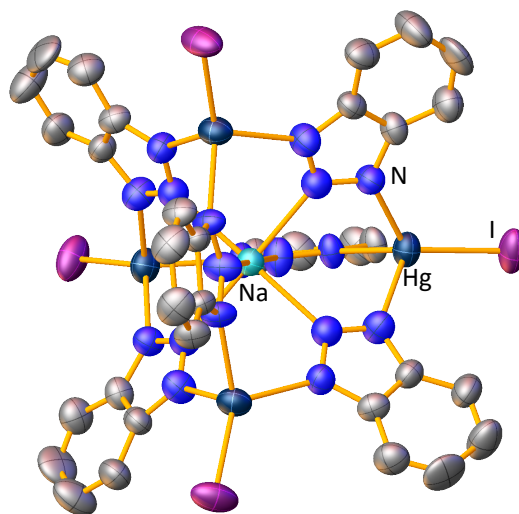
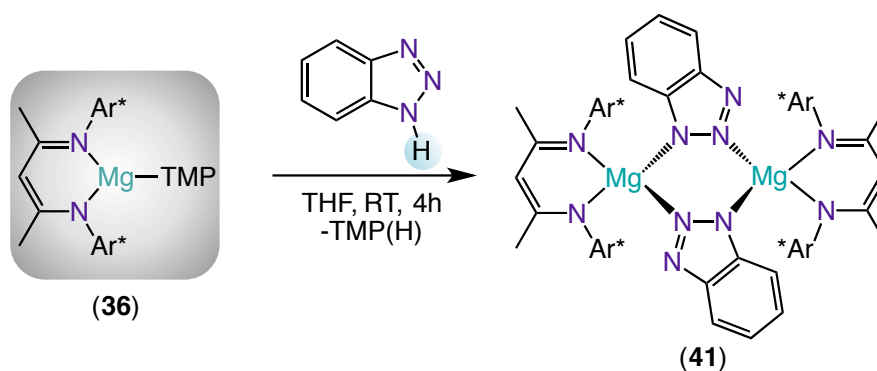


Figure 4.17: Example of a metallated benzotriazole, [HDMF][NaHg<sub>4</sub>(C<sub>6</sub>H<sub>4</sub>N<sub>3</sub>)<sub>6</sub>I<sub>4</sub>].<sup>[285]</sup>

Base **36** was treated with benzotriazole (1:1) in THF for 4 hours at room temperature. The solvent was removed and the yellow solid was dissolved in toluene, which gave a yellow suspension. After a filtration, colourless crystals of  $[\{(\text{Dipp})\text{Nacnac}\}\text{Mg}(\text{C}_6\text{H}_4\text{N}_3)]_2$  (**41**) were obtained in 55% isolated yield.



Scheme 4.12: Reactivity of **36** with benzotriazole.

X-Ray crystallography confirmed the N1-magnesiation of benzotriazole (Figure 4.18). **41** displays a centrosymmetric dimeric structure with two terminal  $\{\beta\}$ -

diketimate)Mg} fragments and two asymmetric benzotriazolyl ligands bridging via their N1 and N2 atoms (N3 and N4 in Figure 4.18).

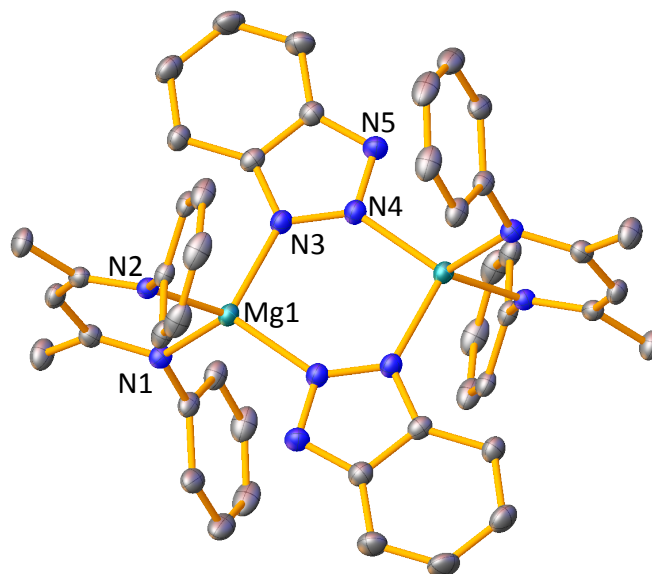


Figure 4.18: Molecular structure of **41** with 50% probability displacement ellipsoids. All hydrogen atoms and *t*Pr groups have been omitted for clarity. Selected bond lengths (Å) and bond angles (°): Mg1-N1 2.0262(12), Mg1-N2 2.0214(12), Mg1-N3 2.0678(13), Mg1-N4 2.0665(12), N1-Mg1-N3 110.26(5), N1-Mg1-N4 120.69(5), N2-Mg1-N1 95.21(5), N2-Mg1-N3 111.30(5), N2-Mg1-N4 118.55(5), N4-Mg1-N3 101.12(5).

Similar to **39** and **40**, the Mg atoms of metallated benzotriazole **41** also present a distorted tetrahedral geometry (angles around Mg ranging from  $95.21(5)^\circ$  to  $120.69(5)^\circ$ ; mean,  $109^\circ$ ), which forms a {MgNNMgNN} planar six-membered ring that exhibits an approximately orthogonal disposition to two adjacent {MgNCCCN} rings (dihedral angle  $88.72^\circ$ ). The Mg-N bonds from the N of the  $\beta$ -diketimate ligand [Mg1-N1 (2.0262(12) Å) and Mg1-N2 (2.0262(12) Å)] in compound **41** are slightly shorter compared to compounds **37-40** (distances ranging from 2.049(2) Å to 2.0882(11) Å; mean 2.067 Å). Additionally, they are also slightly shorter than the Mg-N bonds to the benzotriazolyl nitrogen atoms [Mg1-N3 (2.0678(13) Å) and Mg1-

N4 (2.0665(12) Å)]. Furthermore, the Mg-N distances to N3 and N4 appear to have similar length, which suggests that the negative charge of the benzotriazolyl molecule is delocalised in the benzotriazolyl nitrogen atoms, as well as being much shorter than the Mg-N distance of the neutral coordinated pyridine in [DippNacnacMg(NC<sub>5</sub>H<sub>5</sub>)(NC<sub>5</sub>H<sub>6</sub>)] [Mg-N (2.138(2) Å)].<sup>[234]</sup> The Mg...Mg distance [3.9754(6) Å] is elongated compared to compound **37** [3.827(1) Å] but slightly shorter than that of **39** and **40** [3.9811(6) and 4.1025(7) Å, respectively].

Within the benzotriazolyl ring, the N3-N4 bond resulted to be slightly elongated than N4-N5 in **41** [N3-N4 (1.3530(16) Å) and N4-N5 (1.3230(17) Å)]. Additionally, the N-N lengths in free benzotriazole appear to be slightly shorter [(1.345(2) Å) and (1.304(2) Å), respectively for free benzotriazole].<sup>[287]</sup>

In order to characterize compound **41** <sup>1</sup>H and <sup>13</sup>C NMR spectroscopy was performed in deuterated pyridine at room temperature, since low solubility and very weak signals were obtained in deuterated benzene or THF. Additionally <sup>1</sup>H-<sup>13</sup>C HSQC and COSY experiments were conducted to facilitate assignment of the spectra. The <sup>1</sup>H NMR reveals the disappearance of the CH aromatic protons of free benzotriazole (8.05 and 7.43 ppm) and new multiplets corresponding to the benzotriazolyl anion are displayed at 7.50 and 7.36 ppm. Additionally, the CH singlet backbone and CH multiplet of the <sup>i</sup>Pr groups of the β-diketimate ligand in **41** resonate at 5.2 and 3.23 ppm, respectively. In the <sup>13</sup>C NMR spectrum of **41** the significant carbon of the β-diketimate ligand CH backbone has a chemical shift at 95.3 ppm.

Moving to a non-heterocyclic molecule, base **36** was expected to deprotonate diphenylacetonitrile due to the high acidity of its CH proton (pK<sub>a</sub> = 17.5 in DMSO).<sup>[278]</sup> Nitrile groups with the presence of an acidic α-proton can undergo insertion or deprotonation under the appropriate reaction conditions.<sup>[288]</sup> These

metallated nitriles are relevant intermediates in synthetic chemistry since they are well known as being excellent nucleophiles.<sup>[289]</sup>

The deprotonated intermediates of diphenylacetonitrile have been previously characterised by X-Ray crystallography using transition metals such as iridium<sup>[290]</sup> or titanium,<sup>[291]</sup> as well as a ytterbium compound as a lanthanide example.<sup>[292]</sup> Interestingly, some recent reports have shown the importance of the metallation with zirconium in order to form low-membered metallacycles of group 4, which are interesting for their reactivity and stability.<sup>[291,293]</sup> Moreover, metallation of diphenylacetonitrile has also been achieved by alkali and alkaline-earth metal compounds.<sup>[294–297]</sup> The lithiated ketenimine dimer  $[\text{Ph}_2\text{C}=\text{C}=\text{NLi}(\text{Et}_2\text{O})_2]_2$  was reported by Neumüller and was crystalized from the deprotonation reaction of diphenylacetonitrile by *n*BuLi in diethyl ether at -78 °C (Figure 4.19a).<sup>[294]</sup> Fedushkin and Hill have also reported group 2 (magnesium and barium) diphenylketenimate complexes.<sup>[295–297]</sup> Thus, magnesium and barium complexes  $[\text{Mg}(\text{D}^{\text{ipp}}\text{BIAN})(\text{THF})_3]$ ,  $[\text{Mg}(\text{D}^{\text{tb}}\text{BIAN})(\text{THF})_2]$  and  $[\text{Ba}(\text{D}^{\text{ipp}}\text{BIAN})(\text{DME})_{2.5}]$  ( $\text{D}^{\text{ipp}}\text{BIAN}$  = 1,2-bis[(2,6-diisopropylphenyl)imino]acenaphthene;  $\text{D}^{\text{tb}}\text{BIAN}$  = 1,2-bis[(2,5-di-tert-butylphenyl)imino]acenaphthene; DME = Dimethoxyethane) react with diphenylacetonitrile to give the corresponding metallated ketenimine complexes at room temperature or -15 °C.<sup>[297]</sup> Similar reports have disclosed the magnesiation of diphenylacetonitrile by  $[\text{Mg}(\text{D}^{\text{ipp}}\text{BIAN})(\text{Me})]$  containing  $\text{D}^{\text{ipp}}\text{BIAN}$  radical anions at -70 °C and accompanied by the uncomitant elimination of methane (Figure 4.19b). Similarly, in Hill's catalytic hydroboration of nitriles using  $[\text{D}^{\text{ipp}}\text{NacnacMg}(\text{Bu})]$  and HBpin,  $[(\text{D}^{\text{ipp}}\text{NacnacMg})_2(\text{H}_2\text{BPin})(\text{N}=\text{C}=\text{CPh}_2)(\text{N}=\text{C}-\text{CHPh}_2)]$  was isolated instead, a result of magnesiation of the diphenylacetonitrile substrate rather than the expected hydroboration.<sup>[296]</sup>

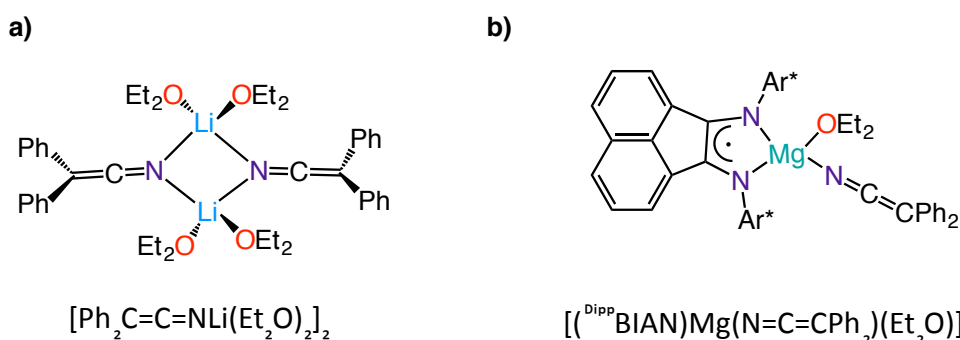
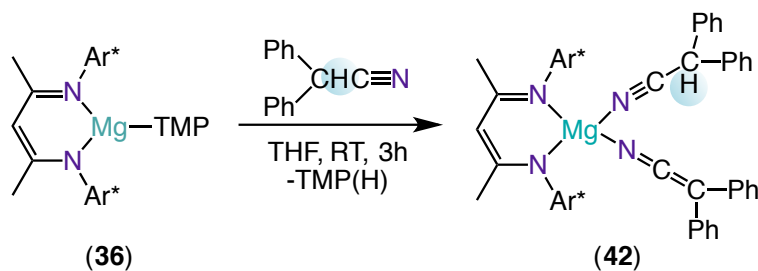


Figure 4.19: Examples of deprotonated diphenylacetoneimine. a) Lithiated ketenimine dimer  $[\text{Ph}_2\text{C}=\text{C}=\text{N}(\text{Et}_2\text{O})_2]_2$  reported by Neumüller.<sup>[294]</sup> b)  $[(^{\text{Dipp}}\text{BIAN})\text{Mg}(\text{N}=\text{C}=\text{CPh}_2)(\text{Et}_2\text{O})]$  by Fedushkin.<sup>[295]</sup>

Initially we reacted diphenylacetoneimine and **36** in  $d_8$ -THF in a J. Young's NMR tube and the  $^1\text{H}$  NMR was recorded. After 2 hours the  $^1\text{H}$  NMR spectrum showed complete consumption of diphenylacetoneimine indicating that metallation had occurred. Next, we repeated this reaction on a larger scale in a Schlenk flask to attempt to obtain suitable crystals for structural characterisation. Base **36** was reacted with one equivalent of diphenylacetoneimine at room temperature in THF. After stirring in THF for 3 hours the reaction solvent was removed and the residue was redissolved in a mixture of toluene and hexane. Unfortunately, the weak diffraction pattern of the crystals obtained for the deprotonation of diphenylacetoneimine prevented the determination of its molecular structure by X-Ray crystallography. However, the combination of different techniques including  $^1\text{H}$ ,  $^{13}\text{C}$ ,  $^1\text{H}$  DOSY NMR solution studies, IR spectroscopy and elemental analysis experiments helped to characterize the constitution of **42**, which is suggested in Scheme 4.13 and was obtained in a 40% yield when reacted with the correct stoichiometry (1:2).



Scheme 4.13: Metallation reaction of diphenylacetonitrile towards de formation of compound **42**.

NMR experiments were conducted at room temperature in deuterated benzene and additional  $^1\text{H}$ - $^{13}\text{C}$  HSQC experiment facilitated the assignment of the spectra. The  $^1\text{H}$  NMR analysis of **42** (Figure 4.20) reveals the indicative singlet corresponding to the *CH* proton of free diphenylacetonitrile (4.42 ppm) has shifted to 4.18 ppm suggesting the coordination of a diphenylacetonitrile molecule to the magnesium center. Furthermore, the diagnostic resonances corresponding to the *CH* of the  $\beta$ -diketiminato ligand backbone and the *CH* signal of the  $^i\text{Pr}$  groups in **42** have shifted to 4.89 and 3.40 ppm respectively, confirming the formation of the new compound. Additionally, several multiplets in the aromatic region appear to integrate as 26 protons, suggesting four phenyl groups and the six aromatic protons of the {<sup>Dipp</sup>Nacnac} ligand.

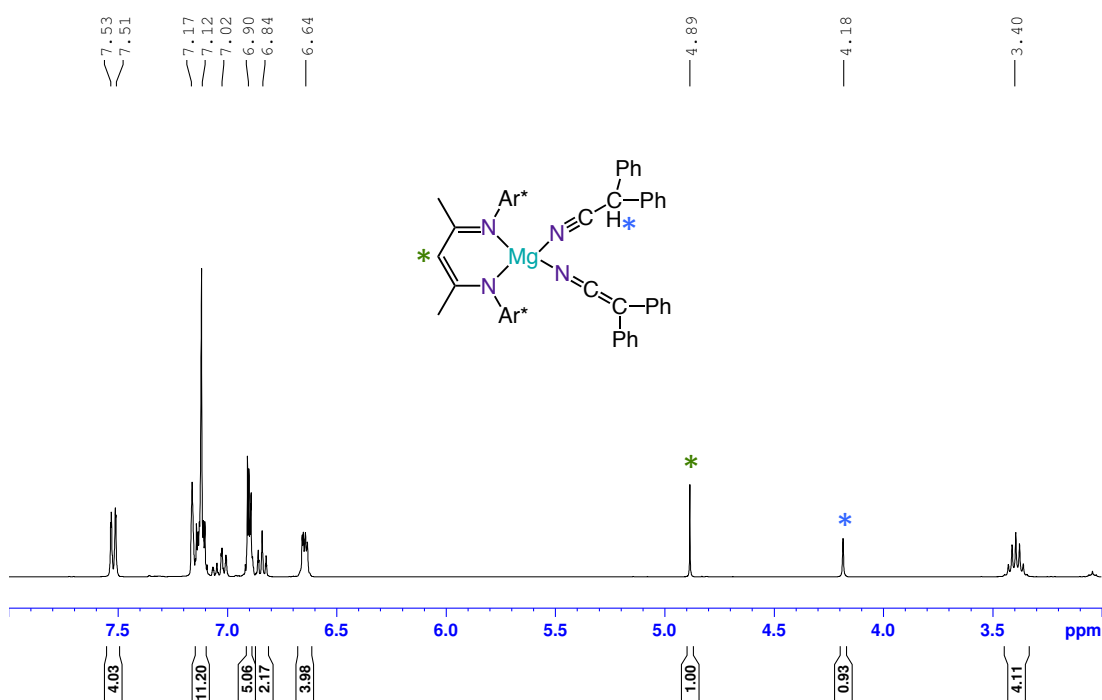


Figure 4.20:  $^1\text{H}$  NMR spectrum of **42** in  $\text{C}_6\text{D}_6$ .

The  $^{13}\text{C}$  NMR spectrum showed three resonances at 41.9 ppm corresponding to the  $\text{CPh}_2$  and at 53.4 and 153.1 ppm that can be assigned to the  $\text{C}=\text{C}=\text{N}$  carbons in the metallated nitrile. Hilmersson and Fleming have observed similarities in the  $^{13}\text{C}$  NMR signals with lithiated and magnesiated nitriles.<sup>[298]</sup> The  $^{13}\text{C}$  NMR resonances of the lithiated nitrile carbon vary modestly from 146.2 to 152.7 ppm depending on the solvent, although some examples of equilibrating lithiated acetonitriles resonate at 155.3 and 148.5 ppm.<sup>[298,299]</sup> In agreement with the  $^1\text{H}$  NMR obtained for **42**, two new signals resonate at 95.08 and 53.44 ppm, which correspond to the CH of the  $\beta$ -diketiminato ligand backbone and the CH proton of diphenylacetonitrile substrate that is coordinated to the magnesium, respectively.

$^1\text{H}$  DOSY NMR studies were also carried out in order to rationalise the constitution of **42** in order to predict the arrangement of the species in solution using ECC

technique reported by Stalke.<sup>[7,182,183]</sup> The experiment was performed in 40 mM of a C<sub>6</sub>D<sub>6</sub> solution using TMS as internal standard and the spectrum obtained is presented in Figure 4.21.

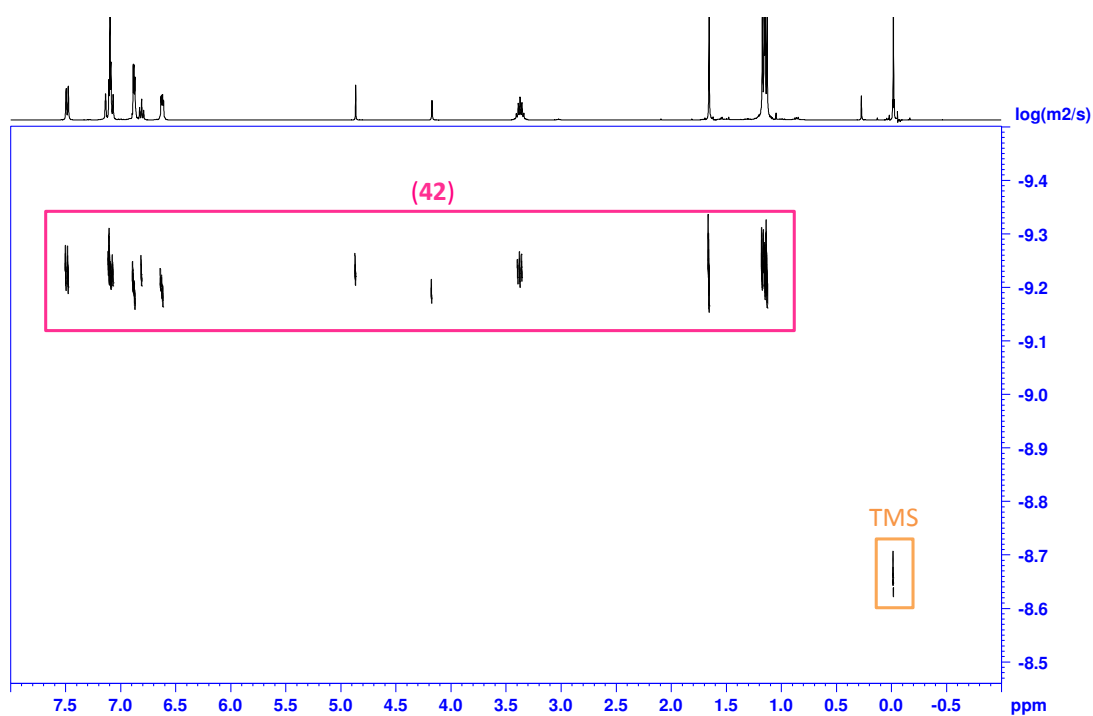


Figure 4.21: <sup>1</sup>H DOSY NMR spectrum of **42** in C<sub>6</sub>D<sub>6</sub>.

The <sup>1</sup>H DOSY NMR experiment indicates a molecular weight of 759 g mol<sup>-1</sup> for compound **42** when  $D = 5.919\text{E-}10 \text{ m}^2/\text{s}$  and  $D_{\text{TMS}} = 2.089\text{E-}9 \text{ m}^2/\text{s}$ . The results of the errors of the possible different species formed are presented in Table 4.3.



Table 4.3: Possible species formed in C<sub>6</sub>D<sub>6</sub> with the molecular weights (MW) and errors. (D(**42**)= 5.919E-10 m<sup>2</sup> s<sup>-1</sup>, D<sub>TMS</sub> = 2.089E-9 m<sup>2</sup> s<sup>-1</sup>, MW<sub>det</sub> = 759 g mol<sup>-1</sup>)

Compound	MW <sub>calc</sub> (g mol <sup>-1</sup> )	Error (%)
(a) [( <sup>Dipp</sup> Nacnac)Mg(N=C=CPh <sub>2</sub> )(N≡C-C(H)Ph <sub>2</sub> )]	827.46	9
(b) [( <sup>Dipp</sup> Nacnac)Mg(N=C=CPh <sub>2</sub> )]	634.21	-16
Equilibrium (a) and (b)	730.84	-4
Ph <sub>2</sub> CHC≡N	193.25	-75

According to the results obtained in the <sup>1</sup>H NMR DOSY experiment and considering the error limit in the range  $\leq \pm 9\%$ , [(<sup>Dipp</sup>Nacnac)Mg(N=C=CPh<sub>2</sub>)(N≡C-C(H)Ph<sub>2</sub>)] or a rapid solvation/desolvation equilibrium of the diphenylacetonitrile molecule could be the possible species in C<sub>6</sub>D<sub>6</sub> solution. However, the solvated/desolvated rapid equilibrium could potentially exist in solution since its error is significantly lower (4%).

The presence of the new band and 2100.7 cm<sup>-1</sup> in the IR confirmed the presence of ketenimido ligand that is assigned between 2000 and 2200 cm<sup>-1</sup> for  $\nu(\text{C}=\text{N})$  stretching mode in organometallic ketenimine complexes.<sup>[290,297]</sup> Another new band at 2283.5 cm<sup>-1</sup> was observed, appearing slightly shifted to higher wave numbers than that of diphenylacetonitrile (2243.3 cm<sup>-1</sup>) that is assigned to the  $\nu(\text{C}\equiv\text{N})$  of the (N≡C-CHPh<sub>2</sub>) moiety coordinated to the Mg in **42**.

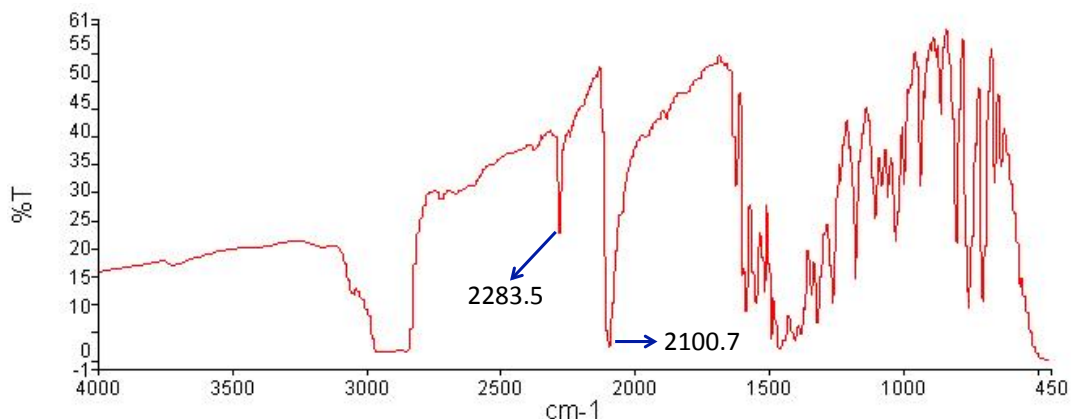


Figure 4.22: IR spectrum of **42** in Nujol.

Considering the previous results examined, the constitution of **42** suggests the presence of a diphenylketeniminate anion, generated by the deprotonation of the nitrile by **36**, forming a new Mg-N bond (similar to **41**) and a second non-diphenylacetonitrile molecule of substrate coordinated to the magnesium atom completing its coordination sphere. Similarly to the compounds presented above, **42** is stabilised by the bulky anionic  $\beta$ -diketiminato ligand. Hill, has previously reported a dinuclear magnesium complex with the presence of a diphenylketeniminate anion and a molecule of diphenylacetonitrile, which are supported by a bridging borate and  $\beta$ -diketiminato anionic ligand.<sup>[296]</sup>

#### 4.2.4 Magnesiation of Pyridine Derivatives

Building on these studies, we next attempted the deprotonation of a variety of pyridine derivatives namely: 2-picoline, 2-(2,4-difluorophenyl)pyridine and 4-methoxypyridine. Pyridines are important moieties in pharmaceuticals,<sup>[300]</sup> agrochemicals<sup>[301]</sup> and organic materials.<sup>[302]</sup> For example, the pyridine moiety appears in the skeleton of nicotine and pyridoxine (vitamin B<sub>6</sub>)<sup>[303]</sup> and 2-(2,4-

difluorophenyl)pyridine is a molecule that finds several applications as a precursor for organic light emitting diodes (OLEDs).<sup>[304]</sup>

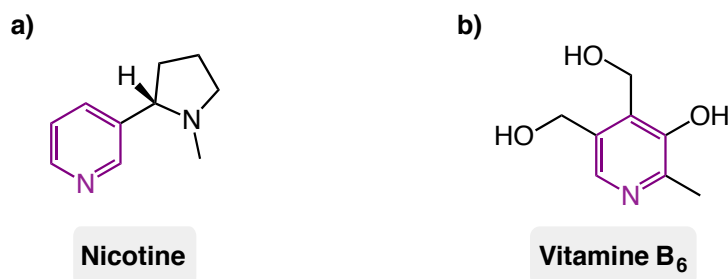
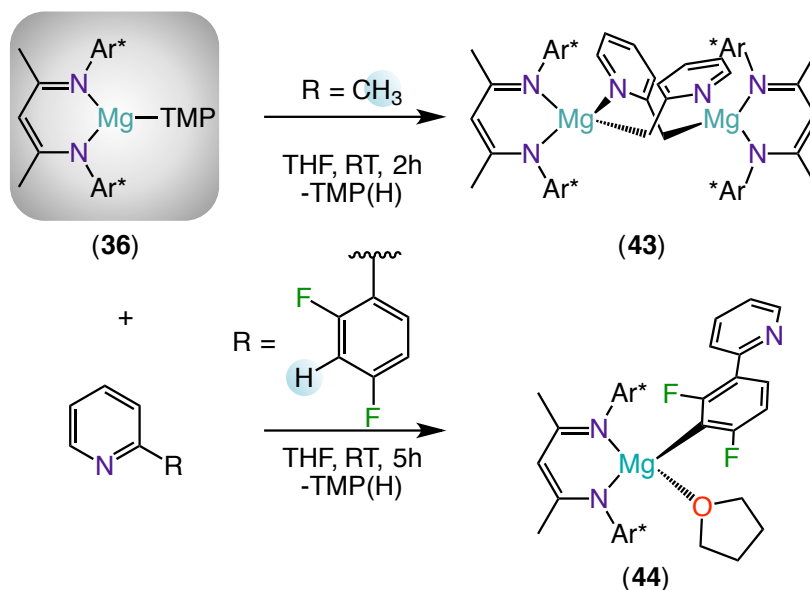


Figure 4.23: Examples of drugs containing pyridine.

Functionalisation of pyridines is an excellent tool to access to a wide variety of building blocks, where the metallation reaction is of crucial importance. These reactions can be performed by organometallic deprotonation, which is generally quantitative in short timescales and offers the possibility to attach different substituents and can be quenched by a variety of electrophiles.<sup>[305]</sup> Generally, alkyllithium derivatives have been one of the reagents of choice, however very low temperatures and a limitation of the scope is imposed due to the low compatibility between  $\pi$ -deficient heteroaromatics and the alkyllithium reagents that can generate nucleophilic side reactions. In this regard, different alternatives such as mixed-metal reagents have emerged.<sup>[303]</sup>

We first studied the magnesiation reaction of 2-picoline and 2-(2,4-difluorophenyl)pyridine. While in compounds **37** - **40** the metallation occurs in a C adjacent to one N atom of the heterocycle ( $\alpha$ -magnesiation), whilst these studies on C2 substituted pyridines revealed the formation of the regioselective lateral metallation products (Scheme 4.14).



Scheme 4.14: Lateral magnesiation of 2-substituted pyridines towards the formation of compounds **43** and **44**.

Stoichiometric reaction of **36** with 2-picoline and 2-(2,4-difluorophenyl)pyridine, in THF led to the isolation of colourless crystals of  $[[(\text{Dipp})\text{NacnacMg}(\text{C}_5\text{H}_6\text{N})]_2]$  (**43**) in a 67% yield and  $[(\text{Dipp})\text{NacnacMgTHF}(\text{C}_{11}\text{H}_6\text{F}_2\text{N})]$  (**44**) 68% crystalline yield, after recrystallization from a hexane/THF solution for **43** and toluene/THF for **44**. Monitoring these reactions by <sup>1</sup>H NMR in *d*<sub>8</sub>-THF demonstrated that formation of **43** and **44** occur quantitatively, without observing in solution other regioisomers. Synchrotron X-Ray diffraction studies confirmed the lateral magnesiation of these N-heterocyclic substrates, deprotonating at the methyl group of 2-picoline and at the C3 position of the fluoroaromatic ring of 2-(2,4-difluorophenyl)pyridine, for **43** and **44** respectively (Figure 4.24 and Figure 4.25). Additionally, NMR studies and elemental analysis helped to characterize the new magnesiated compounds.

Once more, a dimeric structure is obtained for the magnesiation of 2-picoline, reminiscent to those described above, where each of the newly formed 2-picolyl

anions in **43** bridge the two terminal  $\{(\beta\text{-diketiminate})\text{Mg}\}$  fragments via the methylene carbon and nitrogen atoms using their  $\text{CH}_2$  and N groups. The magnesium atoms in the previous dimeric compounds **37**, **39**, **40** and **41** were connected to each other via a three fused six-membered rings, however, in this case an internal eight-membered ring  $\{\text{MgCCNMgCCN}\}$  in a boat-type arrangement, is connected to the two terminal six-membered rings  $\{\text{MgNCCCN}\}$  of the  $\beta$ -diketiminate ligands in **43**. Furthermore in **43** both picolyl carbanion ligands point upwards in a splayed open arrangement (dihedral angle between the two pyridine-ring planes is  $73.38^\circ$ ), rather than lying approximately in the plane of the central ring, as in magnesiated pyrazine **37** or the metallated triazoles **39**, **40** and **41**. Presumably, this alternative geometry is a consequence of the steric requirement imposed by the bridging mode of the picolyl anion, which bonds to the two magnesium ions with non-adjacent carbon and nitrogen atoms and also results in the pronounced puckering of the central ring (Figure 4.24). A search of the CCDC for the picolyl anion acting as a  $\kappa\text{C}:\kappa\text{N}$  ligand reveals only one entry, corresponding to a palladium type dimer containing an 8-membered central ring resembling to that in **43**.<sup>[306]</sup>

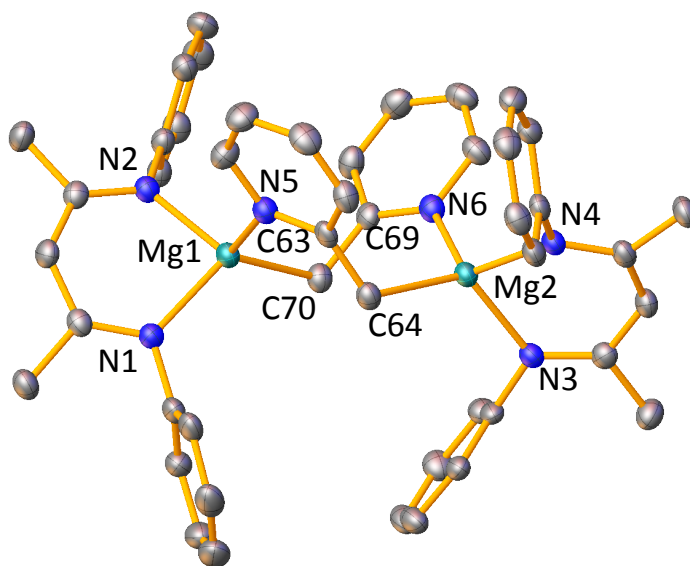
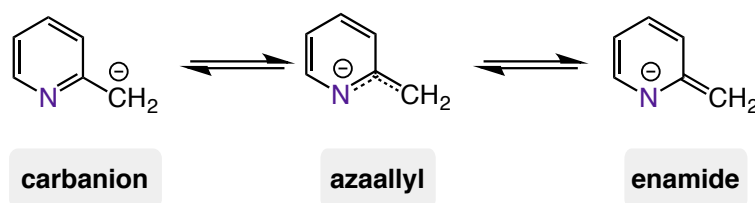


Figure 4.24: Molecular structure of **43** with 50% probability displacement ellipsoids. All hydrogen atoms and <sup>t</sup>Pr groups have been omitted for clarity. Selected bond lengths (Å) and bond angles (°): Mg1-N1 2.1021(16), Mg1-N2 2.1007(17), Mg1-N5 2.1208(17), Mg1-C70 2.2121(19), Mg2-N3 2.1013(17), Mg2-N4 2.0869(16), Mg2-N6 2.1321(18), Mg2-C64 2.2263(18), N1-Mg1-N2 92.44(6), N1-Mg1-C70 122.28(7), N2-Mg1-C70 112.21(7), N1-Mg1-N5 105.00(6), N2-Mg1-N5 111.80(7), N5-Mg1-C70 111.61(7), N3-Mg2-N4 90.56(6), N3-Mg2-C64 125.19(7), N3-Mg2-N6 103.42(6), N4-Mg2-C64 109.11(7), N4-Mg2-N6 120.86(7), N6-Mg2-C64 108.08(7).

A close inspection of the geometrical parameters of **43** revealed that the Mg atoms present a distorted tetrahedral geometry (angles around Mg1 ranging from 92.44(6)° to 122.28(7)°; mean: 108.83°; angles around Mg2 ranging from 90.56(6)° to 125.19(7)°; mean: 108.93°). The Mg-β-diketimate N distances in **43** (Mg1-N range 2.0869(16) - 2.1021(16) Å) are slightly shorter than the bond from the magnesium to the metallated picoline nitrogen (Mg1-N5 2.1208(17) and Mg2-N6 2.1321(18) Å). These Mg-N values are also shorter to those found in the coordination adducts [(<sup>Dipp</sup>Nacnac)Mg(Bu)(pyridine)] and [(<sup>Dipp</sup>Nacnac)Mg(Bu)(2-picoline)] (2.174(3) and 2.216(4) Å) reported by Hill.<sup>[234,235]</sup> Also, the N-C and C-C picolyl anion distances in **43** have been studied to establish the preferred bonding mode, since some structural and theoretical studies uncovering the diversity of

feasible electronic situations in 2-picolyl anions have previously been reported. These different bonding modes are the result of the delocalisation of the negative charge into the ring from the carbanion (Scheme 4.15).<sup>[307]</sup> For example, 2-picolyl lithium complexes form dimeric structures where the anions act as aza-allyl ligands having a simultaneously Li-C and Li-N interaction,<sup>[308]</sup> whereas lithium derivatives of  $\alpha$ C-substituted picolines have shown both azaallyl and enamido bonding modes.<sup>[309–311]</sup>



Scheme 4.15: Resonance stabilisation of the negative charge in 2-picolyl anions.<sup>[307]</sup>

In **43**, the N-C distances (N5-C63 1.383(2) and N6-C69 1.381(2) Å) are elongated compared to free 2-picoline (1.343 Å) but relatively close to standard  $Nsp^2-Csp^2$  single bonds (1.40 Å).<sup>[308]</sup> Moreover, the bonds to the methylene group (C63-C64 1.452(3) and C69-C70 1.453(3) Å) are slightly shorter than in 2-picoline (1.503(3) Å) but still close to a standard single bond ( $Csp^2-Csp^2$  1.466 and  $Csp^2=Csp^2$  1.335 Å).<sup>[308]</sup> These bond parameters detail that in **43**, the picolyl anions can be best described as carbanionic ligands, although some degree of delocalisation of the negative charge onto the N atom is also evident as indicated by the relatively short Mg-N bond distances.

Distinctively, the magnesiation of 2-(2,4-difluorophenyl)pyridine affords the monomeric compound **44** with a THF solvating molecule due to the remote location of the pyridyl N precluding the formation of dimers. In this case, the magnesiation takes place at the C3 atom in the fluorinated ring [i.e. C34 in Figure 4.25], which is

consistent with metallation at the most acidic site of the molecule, leaving the pyridine ring untouched (Figure 4.25). Previous reports have shown the same regioselectivity when organolithium bases are used, which have to be employed at low temperatures to avoid LiF elimination and benzyne formation.<sup>[312,313]</sup> **44** constitutes the first example where the metallated 2-(2,4-difluorophenyl)pyridine intermediate has been isolated and structurally characterized. This reactivity contrasts with those reported for transition metals such as Ir where 2-(2,4-difluorophenyl)pyridine undergoes cyclometallation, removing the H at the C5 position of the fluorinated ring.<sup>[314,315]</sup>

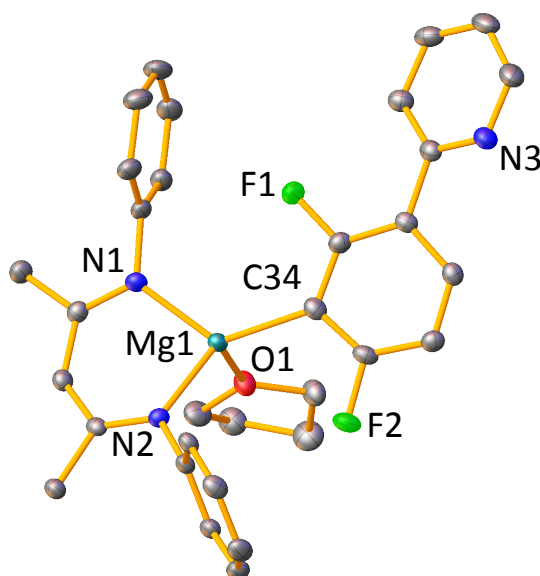


Figure 4.25: Molecular structure of **44** with 50% probability displacement ellipsoids. All hydrogen atoms and *i*Pr groups have been omitted for clarity. Selected bond lengths (Å) and bond angles (°): Mg1-N1 2.0548(12), Mg1-N2 2.0656(12), Mg1-C34 2.1499(14), Mg1-O1 2.0403(11), N1-Mg1-N2 94.10(5), N1-Mg1-C34 126.63(5), N2-Mg1-C34 126.47(5), N1-Mg1-O1 103.23(5), N2-Mg1-O1 102.56(5), O1-Mg1-C34 99.95(5).

The molecular structure of **44** displays a similar monomeric arrangement to that obtained for magnesiated benzofuran **38**. The Mg atom in **44** display a distorted



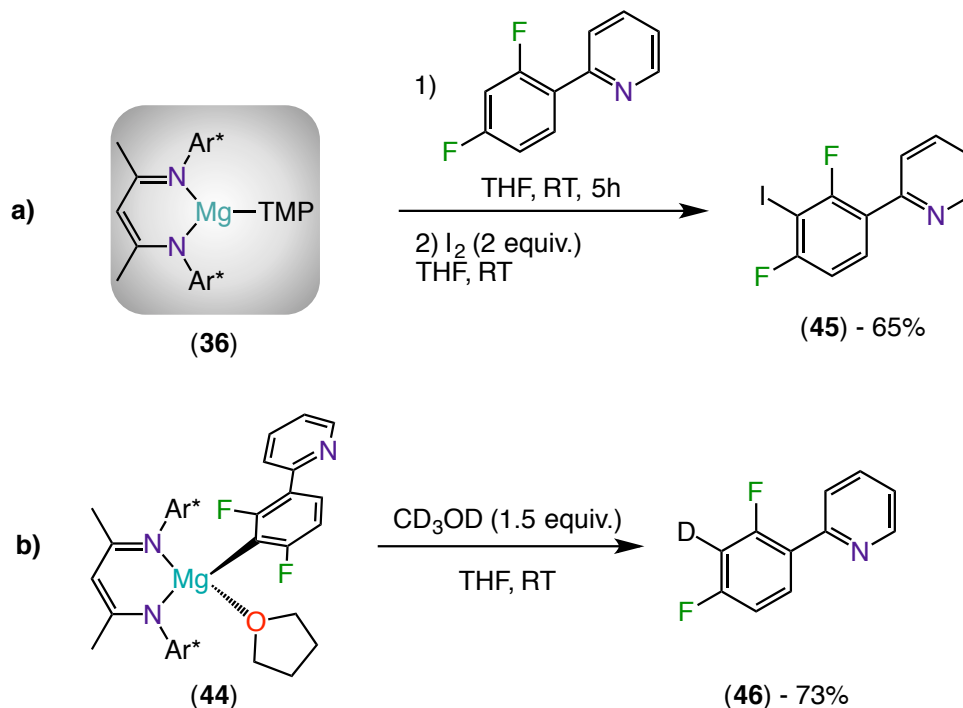
tetrahedral geometry (angles around to Mg1 ranging from 94.10(5)<sup>o</sup> to 126.63(5)<sup>o</sup>; mean: 107.39<sup>o</sup>) and the Mg-C bond distance [Mg1-C34 2.1499(14) Å] is slightly elongated compared to that in **38** [2.1347(18) Å] and the related  $\beta$ -diketiminato compound [ $\{(\text{Dipp})\text{Nacnac}\}\text{Mg}\{\text{OEt}_2\}(\text{Ph})\}$ ] ([2.139(3) Å].<sup>[252]</sup>

Compounds **43** and **44** were characterized by <sup>1</sup>H, <sup>13</sup>C NMR spectroscopy (and <sup>19</sup>F NMR for **44**) in deuterated benzene solution at room temperature. Further <sup>1</sup>H-<sup>13</sup>C HSQC, <sup>1</sup>H-<sup>1</sup>H COSY and <sup>13</sup>C {<sup>19</sup>F} (for **44**) NMR experiments facilitated the assignment of the metallated compound. Importantly, new multiplets corresponding to the protons of the picolyl ring of **43** have emerged at 7.79, 6.43, 5.86 and 4.87 ppm and the Mg-CH<sub>2</sub> protons are displayed at 1.63 and 1.28 ppm. Similarly, for compound **44** new aromatic multiplets corresponding to the fluoroaromatic ring resonate at 6.25 and 6.03 ppm and four new multiplets corresponding to the pyridine ring have emerged at 8.92, 7.07, 6.74 and 6.58 ppm. Interestingly, the resonances of the characteristic signals of the substrates are absent in the <sup>1</sup>H NMR spectrums of both products: the methyl group in free 2-picoline (2.40 ppm), for **43**; and the multiplet at 6.53 ppm corresponding to the CH proton of the C3 position of the fluorobenzene ring, for **44**. The diagnostic CH singlet resulting from the  $\beta$ -diketiminato ligand backbone resonates at 4.82 and 4.98 ppm, respectively. As well, four sets of broad multiplets corresponding to the CH signals of the <sup>i</sup>Pr groups of the Ar\* substituents have appeared (3.60, 3.26, 3.22 and 2.55 ppm for compound **43**; and 3.58, 3.36, 2.96 and 2.79 ppm, for **44**).

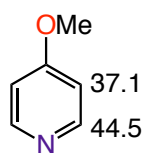
In the <sup>13</sup>C NMR spectrum, the magnesiated carbon Mg-CH<sub>2</sub> has shifted to higher frequency (35.5 ppm) compared to the related chemical shift of the methyl group in free 2-picoline (24.6 ppm) and new resonances of the magnesiated 2-picoline at 144.9, 135.5, 125.6, 122.0 and 110.8 ppm confirm the metallation of the substrate. The signal corresponding to the magnesiated C of the 2-(2,4-difluorophenyl)pyridine

fragment was not possible to assign in the  $^{13}\text{C}$  NMR of **44**, notwithstanding  $^{13}\text{C}\{^{19}\text{F}\}$  NMR experiments helped to assign most of the rest of the signals of the molecule. Additionally, the  $^{19}\text{F}$  NMR indicates the formation of the new metallated product with resonances at -77.6 and -82.0 ppm compared to -109.56 and -112.61 ppm in the substrate.

These findings show the potential of **36** to act as a regioselective base not only for N-heterocyclic substrates but also for substituted benzene and related ring systems. Initial reactivity studies of **44** with iodine and deuterated methanol demonstrated that the new C–Mg bonds in these systems are accessible to electrophiles, affording corresponding quenched products 2-(2,4-difluoro-3-iodophenyl)pyridine (**45**) and 2-(2,4-difluoro-3-deuteriophenyl)pyridine (**46**) in yields of 65 and 72% respectively, as a result of the incorporation of iodine or deuterium at the C3 position of the phenyl ring in 2-(2,4-difluorophenyl)pyridine (Scheme 4.16).

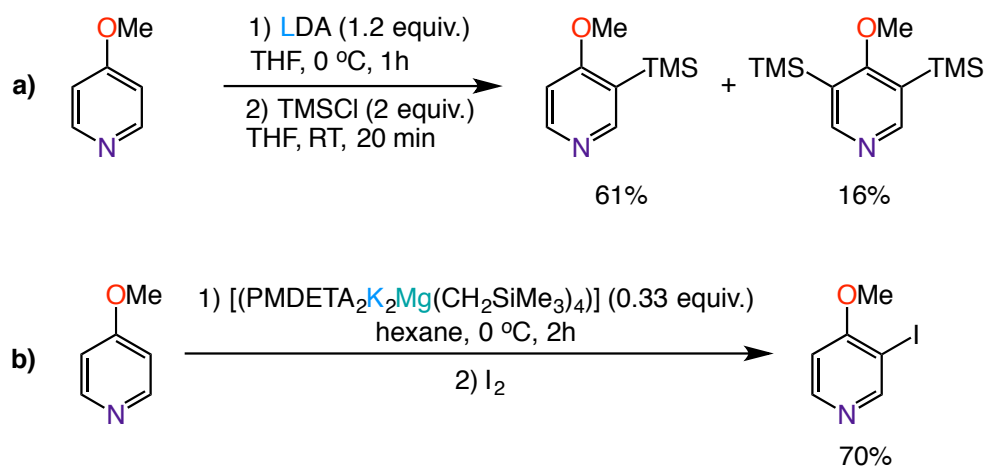
Scheme 4.16: Formation of the quenched products **45** and **46**.

Moving away from C2-substituted pyridines we next investigated the reactions of **36** towards 4-methoxypyridine. Mongin and co-workers have calculated the  $pK_a$  of this molecule in THF, where the proton in the 3 position is more acidic compared to that in position 2 (Figure 4.26).<sup>[303]</sup>

Figure 4.26: Calculated  $pK_a$  values of 4-methoxypyridine in THF.<sup>[303]</sup>

This molecule can be deprotonated using lithium derivatives such as LDA in THF in the presence of TMSCl at 0 °C, forming the 3-silylated derivative and the 3,5-disilylated product in 61 and 16% yields (Scheme 4.17a).<sup>[316]</sup> Additionally, other

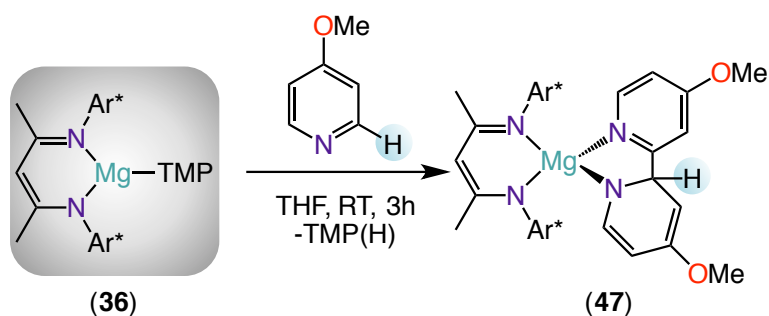
reports have shown that 4-methoxypyridine can convert to 70% yield of 3-iodo-4-methoxypyridine using  $[(\text{PMDETA})_2\text{K}_2\text{Mg}(\text{CH}_2\text{SiMe}_3)_4]$  in hexane at  $0\text{ }^\circ\text{C}$ <sup>[126]</sup> (Scheme 4.17b) or by using  $[\text{Li}(\text{TMP})\text{Zn}(\text{tBu})_2]$  in THF at room temperature.<sup>[270]</sup>



Scheme 4.17: Examples of deprotonation reactions of 4-methoxypyridine.

Interestingly, a search in the CCDC revealed only one metallated example of 4-methoxypyridine at the C2 position by a ruthenium complex.<sup>[317]</sup>

The reaction between **36** and 4-methoxypyridine resulted to the formation of dihydropyridine **47** in a 47% yield, where the dearomatization of the heterocycle follows a C-C coupling between an additional molecule of substrate (Scheme 4.18).

Scheme 4.18: Formation of dihydropyridine compound **47**.

Base **36** was reacted with 4-methoxypyridine (1:1) in THF over 3 hours at room temperature, which gave a dark red colour solution. Removal of solvent *in vacuo* followed by addition of a mixture of hexane and toluene afforded black crystals of  $[\{(\text{Dipp})\text{Nacnac}\}\text{Mg}(\text{C}_{12}\text{H}_{13}\text{N}_2\text{O}_2)]_2$  (**47**) (Figure 4.27). An isolated yield of 47% was obtained when the correct stoichiometry (1:2) was used. The magnesiated compound **47** was characterized in the solid state (X-ray crystallography) and in solution ( $^1\text{H}$  and  $^{13}\text{C}$  NMR spectroscopy). Monitoring the reaction by  $^1\text{H}$  NMR indicates that the reaction is quantitative after 3 hours.

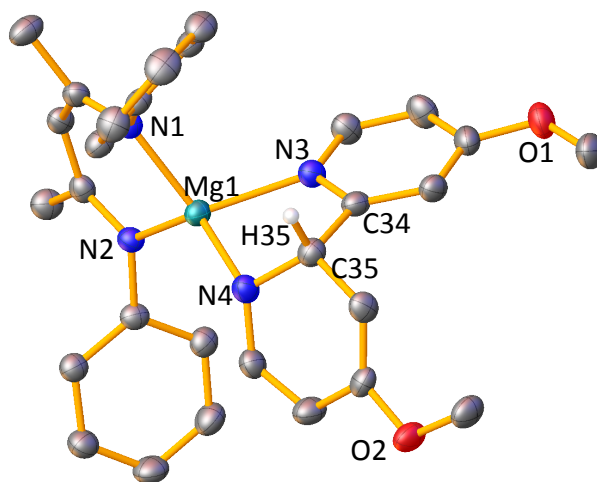
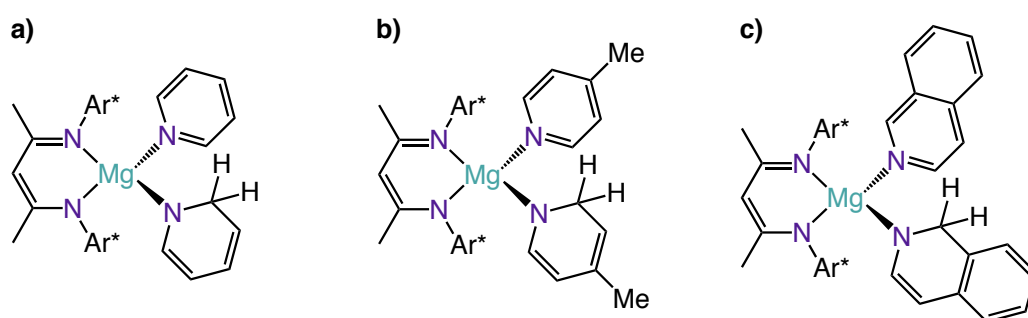


Figure 4.27: Molecular structure of **45** with 50% probability displacement ellipsoids. All hydrogen atoms except H35 and *i*Pr groups have been omitted for clarity. Selected bond lengths (Å) and bond angles (°): Mg1-N1 2.047(2), Mg1-N2 2.040(2), Mg1-N3 2.129(2), Mg1-N4 2.021(2), C34-C35 1.563(4), N1-Mg1-N2 93.58(9), N1-Mg1-N3 109.00(9), N1-Mg1-N4 124.12(9), N2-Mg1-N3 125.02(9), N2-Mg1-N4 125.34(9), N3-Mg1-N4 81.88(9).

Molecular structure of **47** displays a monomeric arrangement, where the {<sup>Dipp</sup>NacnacMg} fragment coordinates to a newly generated 2-dihydropyridine, resulting from a coupling reaction, which binds as a chelate through its two nitrogen atoms (N3 and N4 in Figure 4.27). The two molecules of 4-methoxypyridine have been coupled through the carbon adjacent to the nitrogen forming a new C-C bond with a value of 1.563(4) Å, consistent with a standard single bond distance (Csp<sup>2</sup>-Csp<sup>2</sup> 1.466 Å).<sup>[308]</sup> The magnesium atom displays a distorted tetrahedral geometry (angles around Mg1 ranging from 81.88(9) to 125.34(9)°; mean: 108.45°) probably imposed by the chelating nature of both N<sub>2</sub>-ligands present in **47**. A close inspection of the Mg-N distances in **47**, shows that for the β-diketiminato ligand they lie in the same range as the ones found for the other {<sup>Dipp</sup>NacnacMg} compounds described above [Mg1-N1 2.047(2) and Mg1-N2 2.040(2) Å vs Mg-N range 2.0214(12) to 2.1021(16) Å], whereas unsurprisingly the newly generated dihydropyridine Mg-N3

is significantly longer [2.129(2) Å] than Mg1-N4 [2.021(2) Å], reflecting the different nature.

Similar compounds of 1,2- and 1,4-dihydropyridine magnesium derivatives formed from dearomatisation of pyridine, 4-picoline and quinoline by a hydride transfer have been reported by Hill, and they have been isolated and characterised by X-Ray diffraction studies (Scheme 4.19).<sup>[234,235]</sup>



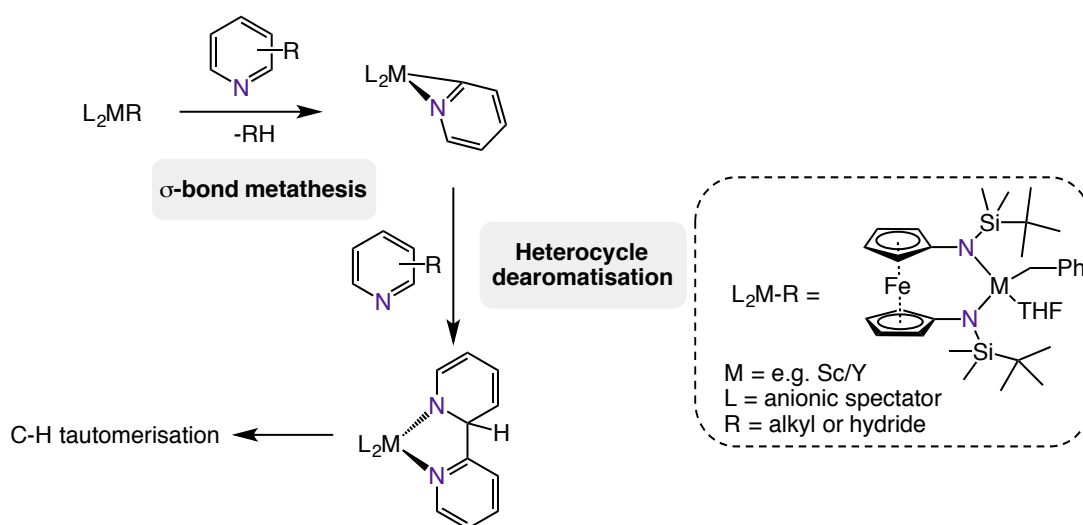
Scheme 4.19: 1,2-dihydropyridine magnesium complexes reported by Hill.<sup>[234,235]</sup>

Interestingly, these 1,2-dihydropyridine derivatives have similar Mg-N bond distances to those observed in **47** (Mg1-N3 2.129(2) vs 2.1289(19), 2.044(2), 2.1301(15) Å for pyridine, 4-picoline and quinoline derivatives respectively) and (Mg1-N4 2.021(2) vs 1.993(2), 1.993(3), 1.9926(16) Å for pyridine, 4-picoline and quinolone derivatives respectively).<sup>[234,235]</sup>

NMR studies also indicate the formation of the dihydropyridine compound **47**. The distinct singlet of the methoxy group in free 4-methoxypyridine has shifted from 3.12 ppm to two new singlets at 3.35 and 2.84 ppm. The singlet at 3.35 ppm also overlaps with the resonance corresponding to the dihydropyridyl  $sp^3$  proton. The distinctive signals at 3.35, 4.97-4.96, 5.24-5.22 and 6.94-6.93 ppm for the dihydropyridine ring protons demonstrate the loss of aromaticity of the ring, whereas the protons for the aromatic ring are displayed at 7.79-7.78, 6.57-6.56 and

6.26-6.23 ppm. The characteristic signals of the  $\{\text{Dipp}^{\text{Nacnac}}\}$  ligand are displayed in the  $^1\text{H}$  NMR at 4.93 ppm for the backbone and the broad multiplets at 3.62-3.47, 3.47-3.37, 3.30-3.08 ppm for the  $\text{CH}$  of the  $^i\text{Pr}$  groups illustrate the lack of symmetry in the molecule. Similarly, the non-aromatic signals of the  $\text{CH}$  from the dihydropyridine ring are displayed in the  $^{13}\text{C}$  NMR at 63.0, 72.9, 91.6 and 150.4 ppm and the characteristic  $\text{CH}$  of the  $\{\text{Dipp}^{\text{Nacnac}}\}$  backbone at 94.9 ppm.

Suzuki has previously reported diruthenium complexes that can catalyse dehydrogenative coupling of 4-substituted pyridines.<sup>[317]</sup> Structural studies of those complexes are reported, however, no dehydrogenation is observed. Contrastingly, Diaconescu has observed similar reactivity, to those of compound **47**, when reacting group 3 complexes supported by a ferrocene diamide ligand with heterocycles (Scheme 4.20).<sup>[318–320]</sup>

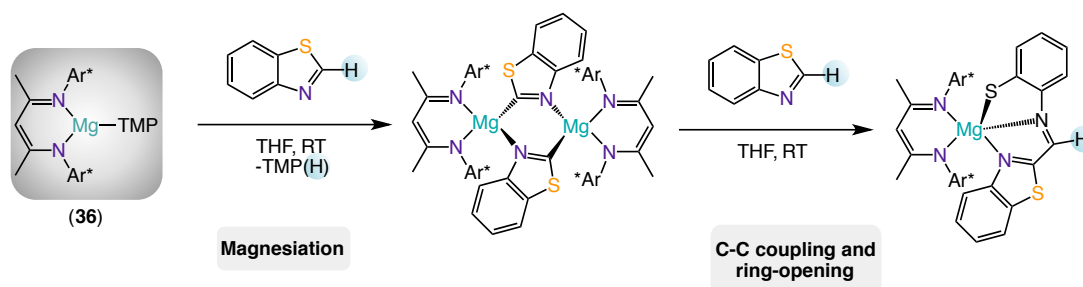


Scheme 4.20: Synthesis of group 3 complexes containing bipyridine ligands.<sup>[318–320]</sup>

In those studies, yttrium and scandium compounds can deprotonate and dearomatise heterocyclic molecules, followed by a C-C coupling between the relevant heterocycles forming a dihydropyridine coupled with the aromatic

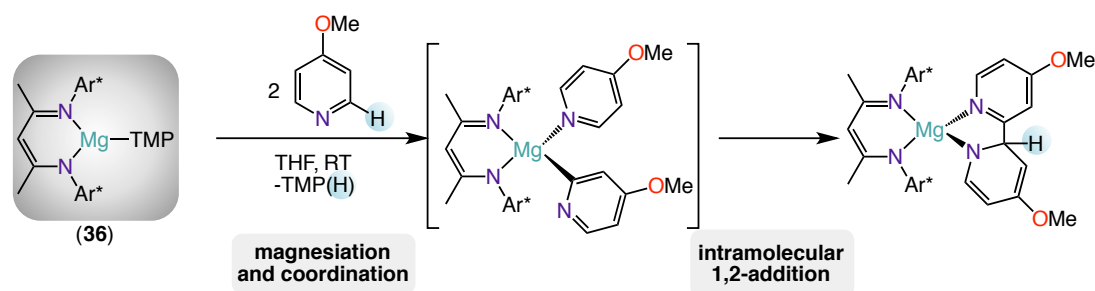


substrate. Related to this C-C bond forming process, our group has shown that when **36** is reacted with 2 equivalents of benzothiazole forms a coupled product, resulting from the nucleophilic addition of  $[(^{\text{Dipp}}\text{Nacnac})\text{Mg}(\text{C}_7\text{H}_4\text{SN})]_2$  to another molecule of benzothiazole (Scheme 4.21).<sup>[106]</sup> In this case the reaction takes place with the concomitant ring-opening of the five-membered heterocyclic ring.



Scheme 4.21: Reactivity of **36** with benzothiazole.<sup>[106]</sup>

A similar mechanism could be in operation here towards the formation of **47**, where the metallation of one equivalent of the 4-methoxypyridine takes place, whereas some of the unreacted substrate coordinates to the magnesium center. Facilitating an intramolecular nucleophilic addition, furnishing dihydropyridine product **47** (Scheme 4.22).

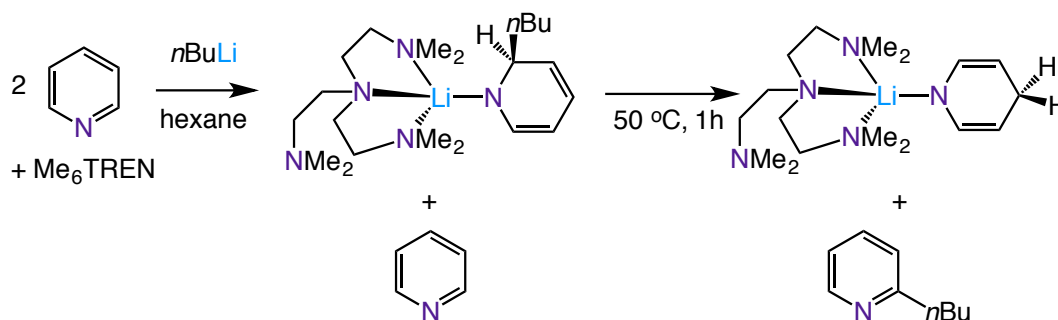


Scheme 4.22: Suggested mechanism for the formation of dihydropyridine compound **47**.

Presumably, the metallation reaction occurs after a first coordination of the 4-methoxypyridine bringing to close proximity the hydrogen at the 2 position to the TMP group and facilitating the deprotonation process.

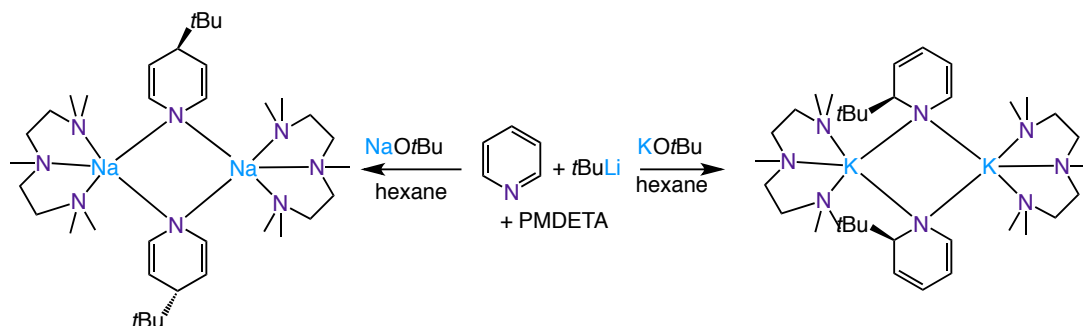
Dihydropyridines have been known since 1882, when they were first isolated.<sup>[218,321-323]</sup> This class of molecules are used in synthesis,<sup>[324,325]</sup> agrochemistry<sup>[326]</sup> and a broad range of medical applications.<sup>[215]</sup> They became particularly interesting after the discoveries of the isolation of the coenzyme nicotinamide adenine dinucleotide (NADH), responsible for reduction in several biological processes, and the studies of cardiovascular pharmaceutical molecules such as Nifedipine, a calcium channel blocker used to treat hypertension.<sup>[321,322]</sup> Despite its significant value in terms of applications, the isomeric kinetic 1,2-dihydropyridines have been less studied than the thermodynamic 1,4-dihydropyridines due to their more challenging preparation.<sup>[322]</sup>

Moreover, the reactivity of metallodihydropyridines, specially those of s-block dihydropyridines, have hardly been explored and only few examples of molecular structures of lithium 1,4-dihydropyridines are known.<sup>[327-329]</sup> Interestingly, Mulvey and Robertson have investigated the 1,2-nucleophilic addition of alkyllithiums to pyridine by varying the stoichiometry. In this report, they have been able to crystallise different lithio 1,2-dihydropyridines supported by different polydentate donor ligands. Additionally, they have demonstrated that these 1,2-alkyl isomers can react with any available pyridine in excess generating the thermodynamic lithio 1,4-dihydropyridine product and 2-alkylpyridine byproducts (Scheme 4.23).<sup>[330]</sup>



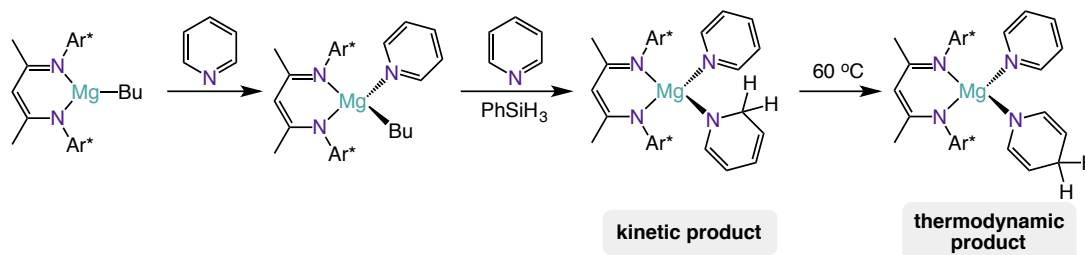
Scheme 4.23: Formation of 1-lithio-1,2- and 1-lithio-1,4-dihydropyridines.

Furthermore, they have also expanded the scope of group 1 dihydropyridines reporting the heavier alkali-metal sodium and potassium 1,2- and 1,4-dihydropyridines (Scheme 4.24).<sup>[331]</sup>

Scheme 4.24: Examples of synthesis of sodium and potassium dihydropyridines in the presence of PMDETA.<sup>[331]</sup>

Additionally, they have also demonstrated the potential applications of 1-lithium-2-alkyl-1,2-dihydropyridine as alternative dehydrogenation catalyst for the transformation of diamine boranes into cyclic 1,3,2-diazaborolidines.<sup>[67]</sup> Group 2 dihydropyridines have also been characterised for magnesium<sup>[234,235,332,333]</sup> and calcium<sup>[334,335]</sup> compounds, which have been used in hydroboration<sup>[114]</sup> and hydrosilylation<sup>[335]</sup> reactions.

Hill has reported 1,2- and 1,4-dihydropyridide magnesium derivatives formed from dearomatisation of pyridine, 4-picoline and quinoline by hydride transfer (Scheme 4.25).<sup>[234,235]</sup>



Scheme 4.25: Formation of 1,2- and 1,4-dihydropyridide magnesium derivatives.<sup>[234,235]</sup>

These complexes are prepared by mixing [<sup>Dipp</sup>NacnacMg(Bu)] with the different substituted pyridines or quinoline in the presence of PhSiH<sub>3</sub>. The mechanism to obtain the 1,2-dihydropyridide derivatives is suggested to be through the formation of an unobserved N-heterocycle-coordinated magnesium hydride and subsequent hydride transfer via C2-position of the heterocycle. Furthermore, the thermodynamic product 1,4-dihydropyridide derivative can be obtained when heating the reaction over 2 days at 60 °C by a hydride transfer to the C4-position.<sup>[235]</sup>

Since **47** is related to the synthetically useful parent bypyridine it was wondered if it could be a precursor of 4,4'-dimethoxy-2,2'-bipyridine. Exposure to air resulted in decolourisation of the purple dihydropyridine complex. The <sup>1</sup>H NMR spectrum revealed three new resonances corresponding to the aromatic protons of 4,4'-dimethoxy-2,2'-bipyridine. Also present in the spectrum are resonances indicative of [<sup>Dipp</sup>NacnacH]. Presumably Mg(OH)<sub>2</sub> also forms as a reaction byproduct (Figure 4.28). Thus the magnesium amide base provides a facile entry into C`C coupled bypyridine molecules.

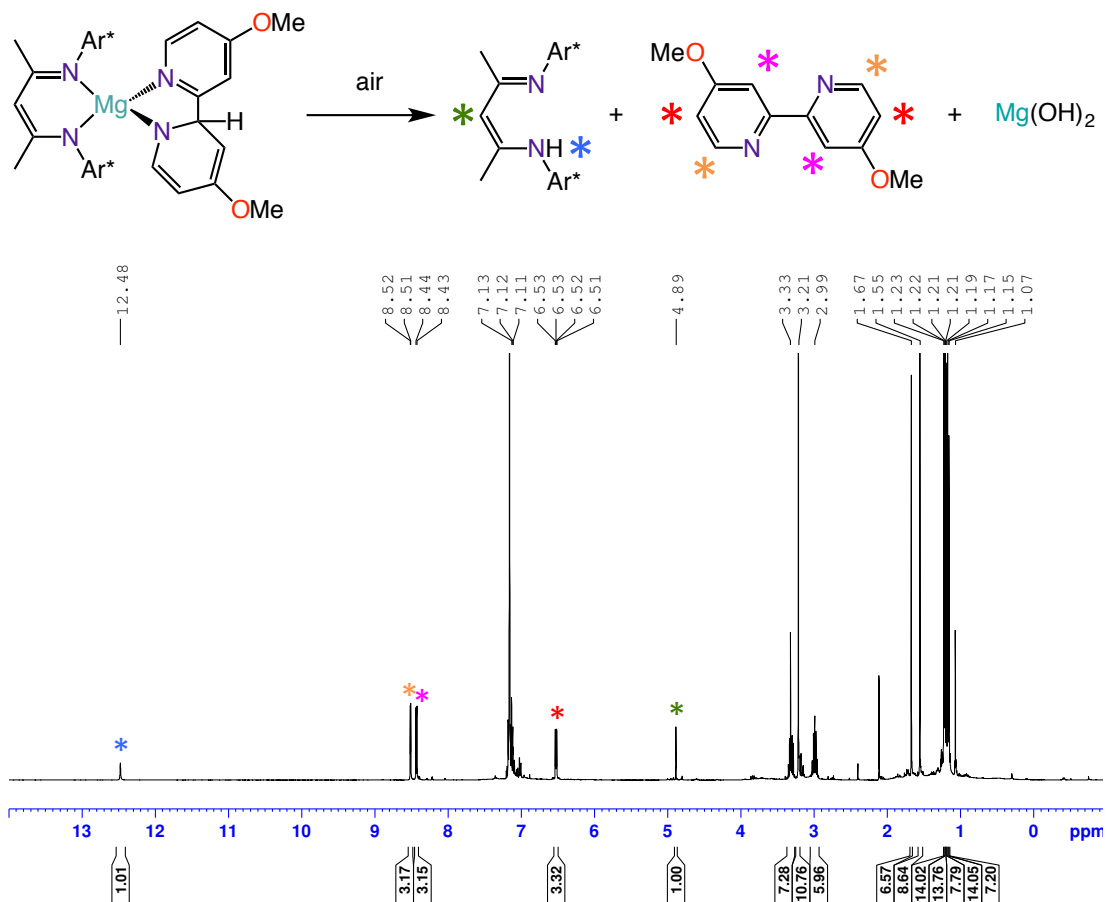


Figure 4.28: <sup>1</sup>H NMR spectrum of the 4,4'-dimethoxy-2,2'-bipyridine formation in C<sub>6</sub>D<sub>6</sub>.

These results show that when compound **47** was hydrolysed and exposed to air, forms the NH dihydropyridine that subsequently undergoes rearomatisation, forming quantitatively the corresponding bipyridine as well as [DippNacnacH] and Mg(OH)<sub>2</sub>. Snaith demonstrated that 1-lithium-2-butyl-1,2-dihydropyridine can hydrolyse with moisture forming N-H dihydropyridine, which can oxidise when exposed to air forming the rearomatised 2-butylpyridine.<sup>[336]</sup>

Similarly, preliminary results using pyridine and 4-picoline indicate similar reactivity to 4-methoxypyridine, showing the formation of coupled-dihydropyridines after a first deprotonation reaction.

### 4.3 Conclusions

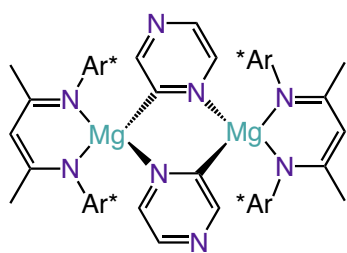
In this chapter, a systematic study of regioselective magnesiation reactions of a range of heterocyclic molecules has been performed. In these studies the organomagnesium base (**36**) has demonstrated its dual ability as an effective metallating reagent, and being able to trap and stabilize sensitive anions. This bifunctional base has been designed combining a basic kinetically activated TMP group that can successfully perform the magnesiation reactions and a bulky  $\beta$ -diketiminato anionic ligand, which can trap the sensitive anions formed.

Metallation of synthetically relevant heterocyclic molecules such as pyrazine, benzofuran, a variety of triazoles and pyridine derivatives at room temperature in THF has been achieved. Critical to this, the sterically bulky  $\beta$ -diketiminato ligand protects the highly reactive new Mg-C bond allowing the stabilization of compounds **37 – 44, 47** that exist as either a monomers or as dimers. NMR studies confirm that these species are stable in solution without showing any decomposition at room temperature. Further, preliminarily electrophilic quenches of the magnesiated compound **44** have been achieved forming compounds **45** and **46**, illustrating the potential use of this system to elaborate more diverse organic products. Finally, formation of dihydropyridine **47** and further rearomatisation opens a new entry point to the formation of bipyridine molecules.

## 4.4 Experimental

### 4.4.1 Synthesis of Active Species

- Synthesis of  $[\{(\text{Dipp}^{\text{Nacnac}})\text{Mg}(\text{C}_4\text{H}_3\text{N}_2)\}_2] \text{ (37)}$



To a solution of compound **36** (0.56 g, 1 mmol) in THF (10 mL), pyrazine (0.08 g, 1 mmol) was added. An immediate colour change from yellow to dark green was noted, and the solution was stirred for 2 hours at room temperature. The solvent was removed and 5 mL

of toluene was added. The resulting suspension was heated until obtain a solution that was left to cool in a hot water bath. This yielded the title compound after 24 hours as a light brown crystalline solid that was isolated and placed in a glovebox. In order to obtain a good yield of the compound, after 4 hours of reaction the solvent was removed and 10 mL of hexane were added obtaining a dark brown suspension. The resulting solid was isolated and placed in a glovebox (0.27 g, 51%).

$^1\text{H NMR}$  (400.13 MHz,  $\text{C}_6\text{D}_6$ , 298 K)  $\delta$  9.29-9.28 [d, 2H,  $J = 1.9$  Hz,  $\text{C}_4\text{H}_3\text{N}_2$ ], 8.78-8.77 [dd, 2H,  $J = 1.6$  Hz,  $J = 2.9$  Hz,  $\text{C}_4\text{H}_3\text{N}_2$ ], 7.96-7.95 [d, 2H,  $J = 3.0$  Hz,  $\text{C}_4\text{H}_3\text{N}_2$ ], 7.01 [br. s, 8H,  $\text{Ar}^*$  of  $\text{Dipp}^{\text{Nacnac}}$ ], 6.86-6.84 [m, 4H,  $\text{Ar}^*$  of  $\text{Dipp}^{\text{Nacnac}}$ ], 4.88 [s, 2H, CH of  $\text{Dipp}^{\text{Nacnac}}$ ], 3.88-3.80 [sept, 4H,  $J = 6.8$  Hz, CH,  $^i\text{Pr}$ ,  $\text{Ar}^*$  of  $\text{Dipp}^{\text{Nacnac}}$ ], 2.56-2.44 [m, 4H, CH,  $^i\text{Pr}$ ,  $\text{Ar}^*$  of  $\text{Dipp}^{\text{Nacnac}}$ ], 1.62 [s, 12H,  $\text{CH}_3$  of  $\text{Dipp}^{\text{Nacnac}}$ ], 1.56-1.54 [d, 12H,  $J = 6.8$  Hz,  $\text{CH}_3$ ,  $^i\text{Pr}$ ,  $\text{Ar}^*$  of  $\text{Dipp}^{\text{Nacnac}}$ ], 1.22-1.20 [d, 12H,  $J = 6.7$  Hz,  $\text{CH}_3$ ,  $^i\text{Pr}$ ,  $\text{Ar}^*$  of  $\text{Dipp}^{\text{Nacnac}}$ ], 0.97-0.96 [d, 12H,  $J = 6.8$  Hz,  $\text{CH}_3$ ,  $^i\text{Pr}$ ,  $\text{Ar}^*$  of  $\text{Dipp}^{\text{Nacnac}}$ ], -0.55--0.58 [d, 12H,  $J = 6.8$  Hz,  $\text{CH}_3$ ,  $^i\text{Pr}$ ,  $\text{Ar}^*$  of  $\text{Dipp}^{\text{Nacnac}}$ ].

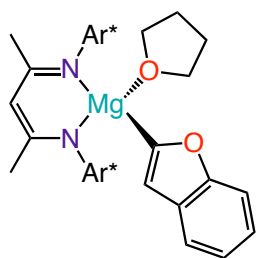
$^{13}\text{C NMR}$   $\{^1\text{H}\}$  (100.61 MHz,  $\text{C}_6\text{D}_6$ , 298 K)  $\delta$  169.5 [ $\text{C}_q$ ,  $\text{CHC}(\text{Me})$  of  $\text{Dipp}^{\text{Nacnac}}$ ], 158.0 [CH of  $\text{C}_4\text{H}_3\text{N}_2$ ], 145.8 [ $\text{C}_q$ ,  $^i\text{Pr}$ ,  $\text{Ar}^*$  of  $\text{Dipp}^{\text{Nacnac}}$ ], 145.1 [CH of  $\text{C}_4\text{H}_3\text{N}_2$ ], 142.9 [ $\text{C}_q$ ,  $^i\text{Pr}$ ,



Ar\* of <sup>Dipp</sup>Nacnac], 142.2 [CH of C<sub>4</sub>H<sub>3</sub>N<sub>2</sub>], 141.8 [C<sub>q</sub>, <sup>i</sup>Pr, Ar\* of <sup>Dipp</sup>Nacnac], 124.3 [CH, Ar\* of <sup>Dipp</sup>Nacnac], 124.2 [CH, Ar\* of <sup>Dipp</sup>Nacnac], 123.4 [CH, Ar\* of <sup>Dipp</sup>Nacnac], 94.0 [CH of <sup>Dipp</sup>Nacnac], 32.1 [CH, <sup>i</sup>Pr, Ar\* of <sup>Dipp</sup>Nacnac], 32.0 [CH, <sup>i</sup>Pr, Ar\* of <sup>Dipp</sup>Nacnac], 30.0 [CH, <sup>i</sup>Pr, Ar\* of <sup>Dipp</sup>Nacnac], 28.1 [CH, <sup>i</sup>Pr, Ar\* of <sup>Dipp</sup>Nacnac], 25.2 [CH<sub>3</sub>, <sup>i</sup>Pr, Ar\* of <sup>Dipp</sup>Nacnac], 24.5 [CH<sub>3</sub> of <sup>Dipp</sup>Nacnac], 24.3 [CH<sub>3</sub>, <sup>i</sup>Pr, Ar\* of <sup>Dipp</sup>Nacnac], 23.8 [CH<sub>3</sub>, <sup>i</sup>Pr, Ar\* of <sup>Dipp</sup>Nacnac], 23.5 [CH<sub>3</sub>, <sup>i</sup>Pr, Ar\* of <sup>Dipp</sup>Nacnac], (C<sub>q</sub> of C-Mg was not possible to assign).

**Elemental analysis:** (C<sub>66</sub>H<sub>88</sub>Mg<sub>2</sub>N<sub>8</sub>) *Calculated:* C: 76.07 % H: 8.51 % N: 10.75 %.  
*Found:* C: 75.81 % H: 8.81 % N: 9.81 %.

- **Synthesis of [(<sup>Dipp</sup>Nacnac)MgTHF{C<sub>8</sub>H<sub>5</sub>O}] (38)**



To a solution of compound **36** (0.56 g, 1 mmol) in THF (10 mL), benzofuran (0.11 mL, 1 mmol) was added. The dark yellow solution was stirred for 2 hours at room temperature. The solvent was removed and a mixture of 3 mL of hexane and 4 mL of toluene were added. The suspension was warmed until a solution was obtained, then placed at -33 °C. After 48 hours a crop of colourless crystals were isolated and placed in a glovebox (0.329g, 59%). In order to improve yield of the compound, after 5 hours of reaction the solvent was removed and 10 mL of hexane were added, the suspension was placed at -33 °C. The resulting solid was isolated and placed in a glovebox (0.413g, 74%).

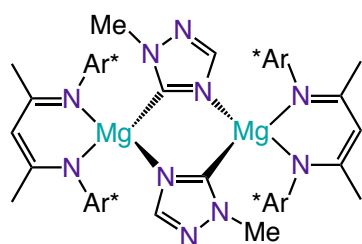
**<sup>1</sup>H NMR (400.13 MHz, C<sub>6</sub>D<sub>6</sub>, 298 K)** δ 7.56-7.53 [br. d, 1H, C<sub>8</sub>H<sub>5</sub>O], 7.46-7.43 [br. d, 1H, C<sub>8</sub>H<sub>5</sub>O], 7.13 [s, 6H, Ar\* of <sup>Dipp</sup>Nacnac], 7.11-7.02 [m, 2H, C<sub>8</sub>H<sub>5</sub>O], 6.64-6.63 [d, 1H, *J* = 4 Hz, C<sub>8</sub>H<sub>5</sub>O], 4.90 [s, 1H, CH], 3.45 [br. m, 4H, CH, <sup>i</sup>Pr, Ar\* of <sup>Dipp</sup>Nacnac], 1.72 [s, 6H, CH<sub>3</sub> of <sup>Dipp</sup>Nacnac], 1.22-1.20 [d, 12 H, *J* = 8 Hz, CH<sub>3</sub>, <sup>i</sup>Pr, Ar\* of <sup>Dipp</sup>Nacnac], 1.19-1.16 [br. m, 6H, CH<sub>3</sub>, <sup>i</sup>Pr, Ar\* of <sup>Dipp</sup>Nacnac], 1.13-1.05 [br. m, 6H, CH<sub>3</sub>, <sup>i</sup>Pr, Ar\* of <sup>Dipp</sup>Nacnac].

$^{13}\text{C}$  NMR  $\{^1\text{H}\}$  (100.62 MHz,  $\text{C}_6\text{D}_6$ , 298 K)  $\delta$  192.8 [ $\text{C}_q$ , Mg- $\text{C}_\alpha$  of  $\text{C}_8\text{H}_5\text{O}$ ], 168.9 [ $\text{C}_q$ ,  $\text{CHC}(\text{Me})$  of  $\text{Dipp}^{\text{Nacnac}}$ ], 159.9 [ $\text{C}_q$  of  $\text{C}_8\text{H}_5\text{O}$ ], 145.4 [ $\text{CH}$ ,  $\text{Ar}^*$  of  $\text{Dipp}^{\text{Nacnac}}$ ], 130.6 [ $\text{C}_q$  of  $\text{C}_8\text{H}_5\text{O}$ ], 125.5 [ $\text{CH}$ ,  $\text{Ar}^*$  of  $\text{Dipp}^{\text{Nacnac}}$ ], 124.0 [ $\text{CH}$ ,  $\text{Ar}^*$  of  $\text{Dipp}^{\text{Nacnac}}$ ], 121.2 [ $\text{CH}$  of  $\text{C}_8\text{H}_5\text{O}$ ], 120.9 [ $\text{CH}$  of  $\text{C}_8\text{H}_5\text{O}$ ], 119.6 [ $\text{CH}$  of  $\text{C}_8\text{H}_5\text{O}$ ], 119.1 [ $\text{CH}$  of  $\text{C}_8\text{H}_5\text{O}$ ], 110.4 [ $\text{CH}$  of  $\text{C}_8\text{H}_5\text{O}$ ], 94.7 [ $\text{CH}$  of  $\text{Dipp}^{\text{Nacnac}}$ ], 69.8 [ $\text{C}_q$ ,  $i\text{Pr}$ ,  $\text{Ar}^*$  of  $\text{Dipp}^{\text{Nacnac}}$ ], 28.4 [ $\text{CH}$ ,  $i\text{Pr}$ ,  $\text{Ar}^*$  of  $\text{Dipp}^{\text{Nacnac}}$ ], 25.2 [ $\text{CH}_3$ ,  $i\text{Pr}$ ,  $\text{Ar}^*$  of  $\text{Dipp}^{\text{Nacnac}}$ ], 25.0 [ $\text{CH}_3$ ,  $i\text{Pr}$ ,  $\text{Ar}^*$  of  $\text{Dipp}^{\text{Nacnac}}$ ], 24.6 [ $\text{CH}_3$ ,  $i\text{Pr}$ ,  $\text{Ar}^*$  of  $\text{Dipp}^{\text{Nacnac}}$ ], 24.1 [ $\text{CH}_3$ ,  $i\text{Pr}$ ,  $\text{Ar}^*$  of  $\text{Dipp}^{\text{Nacnac}}$ ].

**Elemental analysis:** ( $\text{C}_{37}\text{H}_{46}\text{MgN}_2\text{O}$ ) *Calculated:* C: 79.49 % H: 8.29 % N: 4.35 %.

*Found:* C: 79.53 % H: 9.06 % N: 4.70 %.

• **Synthesis of  $\{(\text{Dipp}^{\text{Nacnac}}\text{Mg}(\text{C}_3\text{H}_4\text{N}_3))_2\}$  (**39**)**



To a solution of **36** (0.56g, 1mmol) in THF (10 mL), 1-methyl-1,2,4-triazole (0.075 mL, 1mmol) was added. The yellow solution was stirred for 2 hours at room temperature and a solid precipitated. The solvent was removed and 10 mL of toluene were added. The

suspension was dissolved by gentle warming and was left in the fridge. After 48 hours a crop of colorless crystals were isolated and placed in a glovebox. Single crystals suitable for X-Ray analysis were obtained by heating the solution and cooling it down in a hot water bath. In order to obtain a good yield of the compound, after 2 hours of reaction the solvent was removed and 10 mL of hexane were added obtaining a suspension. The resulting solid was isolated and placed in a glovebox (0.35 g, 66%).

$^1\text{H}$  NMR (400.13 MHz,  $\text{C}_6\text{D}_6$ , 298 K)  $\delta$  8.10 [s, 2H,  $\text{N}(\text{Me})\text{NCHNC}$ ], 7.09-7.02 [m, 4H,  $\text{Ar}^*$  of  $\text{Dipp}^{\text{Nacnac}}$ ], 7.02-7.00 [dd, 4H,  $J = 1.6$  Hz,  $J = 7.7$  Hz,  $\text{Ar}^*$  of  $\text{Dipp}^{\text{Nacnac}}$ ], 6.91-6.86 [dd, 4H,  $J = 1.6$  Hz,  $J = 7.5$  Hz,  $\text{Ar}^*$  of  $\text{Dipp}^{\text{Nacnac}}$ ], 4.77 [s, 2H,  $\text{CH}$  of  $\text{Dipp}^{\text{Nacnac}}$ ], 3.97 [s, 6H,  $\text{N}(\text{CH}_3)\text{NCHNC}$ ], 3.66-3.59 [sept, 4H,  $J = 6.8$  Hz,  $\text{CH}$ ,  $i\text{Pr}$ ,  $\text{Ar}^*$  of

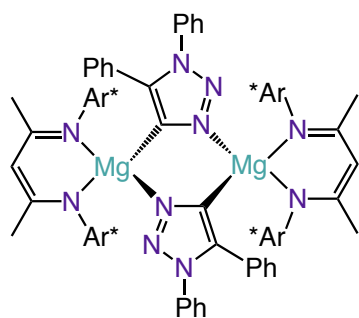
<sup>Dipp</sup>Nacnac], 2.79-2.72 [sept, 4H, *J* = 6.8 Hz, CH, <sup>*i*</sup>Pr, Ar\* of <sup>Dipp</sup>Nacnac], 1.54 [s, 12H, CH<sub>3</sub> of <sup>Dipp</sup>Nacnac], 1.44-1.42 [d, 12H, *J* = 7.0 Hz, CH<sub>3</sub>, <sup>*i*</sup>Pr, Ar\* of <sup>Dipp</sup>Nacnac], 1.19-1.17 [m, 12H, *J* = 6.7 Hz, CH<sub>3</sub>, <sup>*i*</sup>Pr, Ar\* of <sup>Dipp</sup>Nacnac], 1.03-1.01 [d, 12H, *J* = 6.9 Hz, CH<sub>3</sub>, <sup>*i*</sup>Pr, Ar\* of <sup>Dipp</sup>Nacnac], - 0.36- -0.38 [d, 12H, *J* = 6.8 Hz, CH<sub>3</sub>, <sup>*i*</sup>Pr, Ar\* of <sup>Dipp</sup>Nacnac].

<sup>13</sup>C NMR {<sup>1</sup>H} (100.61 MHz, C<sub>6</sub>D<sub>6</sub>, 298 K) δ 184.9 [C<sub>q</sub>, C<sub>α</sub> of C-Mg, C<sub>3</sub>H<sub>4</sub>N<sub>3</sub>], 168.9 [C<sub>q</sub>, CHC(Me) of <sup>Dipp</sup>Nacnac], 150.2 [CH of C<sub>3</sub>H<sub>4</sub>N<sub>3</sub>], 145.5 [C, Ar\* of <sup>Dipp</sup>Nacnac], 142.7 [of <sup>Dipp</sup>Nacnac], 141.7 [C, Ar\* of <sup>Dipp</sup>Nacnac], 129.3 [C, Ar\* of <sup>Dipp</sup>Nacnac] 125.3 [CH, Ar\* of <sup>Dipp</sup>Nacnac], 124.4 [CH, Ar\* of <sup>Dipp</sup>Nacnac], 123.4 [CH, Ar\* of <sup>Dipp</sup>Nacnac], 94.4 [CH of <sup>Dipp</sup>Nacnac], 38.8 [CH<sub>3</sub> of C<sub>3</sub>H<sub>4</sub>N<sub>3</sub>], 29.4 [CH, <sup>*i*</sup>Pr, Ar\* of <sup>Dipp</sup>Nacnac], 27.2 [CH, <sup>*i*</sup>Pr, Ar\* of <sup>Dipp</sup>Nacnac], 25.0 [CH<sub>3</sub>, <sup>*i*</sup>Pr, Ar\* of <sup>Dipp</sup>Nacnac], 24.4 [CH<sub>3</sub>, <sup>*i*</sup>Pr, Ar\* of <sup>Dipp</sup>Nacnac], 24.2 [CH<sub>3</sub> of <sup>Dipp</sup>Nacnac], 24.0 [CH<sub>3</sub>, <sup>*i*</sup>Pr, Ar\* of <sup>Dipp</sup>Nacnac], 22.4 [CH<sub>3</sub>, <sup>*i*</sup>Pr, Ar\* of <sup>Dipp</sup>Nacnac].

**Elemental analysis:** (C<sub>64</sub>H<sub>90</sub>Mg<sub>2</sub>N<sub>10</sub>) *Calculated:* C: 73.34 %, H: 8.66 %, N: 13.36 %.

*Found:* C: 73.59 %, H: 8.92 %, N: 13.68 %.

- **Synthesis of [({<sup>Dipp</sup>Nacnac}Mg(C<sub>14</sub>H<sub>10</sub>N<sub>3</sub>))<sub>2</sub>] (40)**



To a solution of **36** (0.28 g, 0.5 mmol) in THF (5 mL), 1,5-diphenyl-1,2,3-triazole (0.11 g, 0.5 mmol) was added. The yellow solution was stirred for 3 hours at room temperature where a precipitate appeared after this time. The solvent was removed and 10 mL of toluene were added. The resulting suspension was

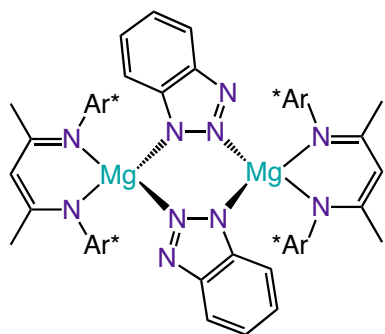
heated to give a dark yellow solution and was left to cool in a hot water bath. After 48 hours a crop of colourless crystals were isolated and placed in a glovebox (0.15 g, 45%).

**$^1\text{H}$  NMR (400.13 MHz,  $\text{C}_6\text{D}_6$ , 298 K)**  $\delta$  7.50-7.48 [br. d, 4H,  $J = 7.2$  Hz,  $\text{C}_{14}\text{H}_{10}\text{N}_3$ ], 7.15-6.95 [m, 28H,  $\text{C}_{14}\text{H}_{10}\text{N}_3$  + Ar\* of  $\text{DippNacnac}$ ], 4.76 [s, 2H, CH of  $\text{DippNacnac}$ ], 3.83-3.72 [sept, 4H,  $J = 6.8$  Hz, CH,  $i\text{Pr}$ , Ar\* of  $\text{DippNacnac}$ ], 3.10-3.00 [sept, 4H,  $J = 6.8$  Hz, CH,  $i\text{Pr}$ , Ar\* of  $\text{DippNacnac}$ ], 1.59 [s, 12H,  $\text{CH}_3$  of  $\text{DippNacnac}$ ], 1.25-1.23 [d, 12H,  $J = 6.8$  Hz,  $\text{CH}_3$ ,  $i\text{Pr}$ , Ar\* of  $\text{DippNacnac}$ ], 1.19-1.17 [d, 12H,  $J = 6.7$  Hz,  $\text{CH}_3$ ,  $i\text{Pr}$ , Ar\* of  $\text{DippNacnac}$ ], 1.00-0.98 [d, 12H,  $J = 6.8$  Hz,  $\text{CH}_3$ ,  $i\text{Pr}$ , Ar\* of  $\text{DippNacnac}$ ], 0.12-0.10 [d, 12H,  $J = 6.8$  Hz,  $\text{CH}_3$ ,  $i\text{Pr}$ , Ar\* of  $\text{DippNacnac}$ ].

**$^{13}\text{C}$  NMR  $\{^1\text{H}\}$  (100.61 MHz,  $\text{C}_6\text{D}_6$ , 343 K)**  $\delta$  168.3 [ $\text{C}_q$ ,  $\text{CHC}(\text{Me})$  of  $\text{DippNacnac}$ ], 147.2 [ $\text{C}_q$ , Ar], 147.0 [ $\text{C}_q$ , Ar], 143.3 [ $\text{C}_q$ , Ar], 143.0 [ $\text{C}_q$ , Ar], 138.7 [ $\text{C}_q$ , Ar], 130.4 [CH,  $\text{C}_{14}\text{H}_{10}\text{N}_3$ ], 129.0 [CH, Ar], 128.8 [CH, Ar], 127.4 [CH, Ar], 124.7 [CH, Ar], 124.4 [CH, Ar], 123.6 [CH, Ar], 96.6 [CH of  $\text{DippNacnac}$ ], 28.5 [CH,  $i\text{Pr}$ , Ar\* of  $\text{DippNacnac}$ ], 27.6 [CH,  $i\text{Pr}$ , Ar\* of  $\text{DippNacnac}$ ], 25.2 [ $\text{CH}_3$ ,  $i\text{Pr}$ , Ar\* of  $\text{DippNacnac}$ ], 25.1 [ $\text{CH}_3$  of  $\text{DippNacnac}$ ], 24.8 [ $\text{CH}_3$ ,  $i\text{Pr}$ , Ar\* of  $\text{DippNacnac}$ ], 24.7 [ $\text{CH}_3$ ,  $i\text{Pr}$ , Ar\* of  $\text{DippNacnac}$ ], 24.5 [ $\text{CH}_3$ , of  $\text{DippNacnac}$ ], ( $\text{C}_q$  of C-Mg was not possible to assign).

**Elemental analysis:** ( $\text{C}_{88}\text{H}_{102}\text{Mg}_2\text{N}_{10}$ ) *Calculated:* C: 77.99 % H: 7.76 % N: 10.58 %.  
*Found:* C: 78.36 % H: 7.89 % N: 10.17 %.

• **Synthesis of  $\{[(\text{DippNacnac})\text{Mg}(\text{C}_6\text{H}_4\text{N}_3)]_2\}$  (41)**



To a solution of **36** (0.56 g, 1 mmol) in THF (5 mL), benzotriazole (0.120 g, 1 mmol) was added. The yellow solution was stirred for 4 hours at room temperature where a precipitate appeared after this time. The solvent was removed and the yellow solid was dissolved in toluene, which gave a yellow suspension.

After, a filtration was performed and colourless crystals of  $\{[(\text{DippNacnac})\text{Mg}(\text{C}_6\text{H}_4\text{N}_3)]_2\}$  (**41**) were obtained. In order to obtain a good yield of the compound, after 4 hours of reaction the solvent was removed and 10 mL of

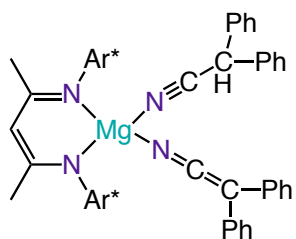
hexane were added obtaining a suspension. The resulting solid was isolated and placed in a glovebox (0.31 g, 55%).

**$^1\text{H}$  NMR (400.13 MHz,  $d_5$ -pyr, 298 K)**  $\delta$  7.51-7.48 [br. m, 4H,  $\text{C}_6\text{H}_4\text{N}_3$ ], 7.36-7.24 [br. m, 16H,  $\text{C}_6\text{H}_4\text{N}_3$  +  $\text{Ar}^*$  of  $\text{Dipp}^{\text{Nacnac}}$ ], 5.20 [s, 2H, CH of  $\text{Dipp}^{\text{Nacnac}}$ ], 3.26-3.17 [m, 8H, CH,  $i$ Pr,  $\text{Ar}^*$  of  $\text{Dipp}^{\text{Nacnac}}$ ], 1.89 [s, 12H,  $\text{CH}_3$  of  $\text{Dipp}^{\text{Nacnac}}$ ], 1.17-1.15 [d, 24H,  $J = 6.8$  Hz,  $\text{CH}_3$ ,  $i$ Pr,  $\text{Ar}^*$  of  $\text{Dipp}^{\text{Nacnac}}$ ], 0.66-0.64 [d, 24H,  $J = 6.8$  Hz,  $\text{CH}_3$ ,  $i$ Pr,  $\text{Ar}^*$  of  $\text{Dipp}^{\text{Nacnac}}$ ], 1.00-0.98 [d, 12H,  $J = 6.8$  Hz,  $\text{CH}_3$ ,  $i$ Pr,  $\text{Ar}^*$  of  $\text{Dipp}^{\text{Nacnac}}$ ].

**$^{13}\text{C}$  NMR  $\{^1\text{H}\}$  (100.61 MHz,  $d_5$ -pyr, 343 K)**  $\delta$  170.3 [ $\text{C}_q$ ,  $\text{CHC}(\text{Me})$  of  $\text{Dipp}^{\text{Nacnac}}$ ], 145.8 [ $\text{C}_q$ , Ar], 145.7 [ $\text{C}_q$ , Ar], 143.3 [ $\text{C}_q$ , Ar], 125.9 [CH,  $\text{C}_6\text{H}_4\text{N}_3$ ], 124.5 [CH, Ar], 123.5 [CH, Ar], 117.2 [CH,  $\text{C}_6\text{H}_4\text{N}_3$ ], 95.3 [CH of  $\text{Dipp}^{\text{Nacnac}}$ ], 28.9 [CH,  $i$ Pr,  $\text{Ar}^*$  of  $\text{Dipp}^{\text{Nacnac}}$ ], 24.6 [ $\text{CH}_3$  of  $\text{Dipp}^{\text{Nacnac}}$ ], 24.5 [ $\text{CH}_3$ ,  $i$ Pr,  $\text{Ar}^*$  of  $\text{Dipp}^{\text{Nacnac}}$ ]. ( $\text{C}_q$  of C-Mg was not possible to assign).

**Elemental analysis:** ( $\text{C}_{70}\text{H}_{90}\text{Mg}_2\text{N}_{10}$ ) *Calculated:* C: 75.06 % H: 8.10 % N: 12.50 %. *Found:* C: 73.65 % H: 7.71 % N: 11.36 %.

- **Synthesis of  $\{[\{\text{Dipp}^{\text{Nacnac}}\text{Mg}(\text{C}_{14}\text{H}_{11}\text{N})(\text{C}_{14}\text{H}_{10}\text{N})\}]\}$  (42)**



To a solution of **36** (0.28 g, 0.5 mmol) in THF (5 mL), diphenylacetonitrile (0.197 g, 0.5 mmol) was added. The yellow solution was stirred for 3 hours at room temperature and a bright yellow colour was obtained. The solvent was removed and the residue was redissolved in a

mixture of 2 mL of toluene and 2 mL hexane. The resulting solid was isolated and placed in a glovebox (0.16 g, 40%).

**$^1\text{H}$  NMR (400.13 MHz,  $\text{C}_6\text{D}_6$ , 298 K)**  $\delta$  7.53-7.51 [d, 4H,  $J = 10$  Hz,  $\text{C}_{28}\text{H}_{21}\text{N}_2$ ], 7.14-7.09 [br. m, 11H,  $\text{Ar}^*$  of  $\text{Dipp}^{\text{Nacnac}}$  +  $\text{C}_{28}\text{H}_{21}\text{N}_2$ ], 6.93-6.89 [br. m, 5H,  $\text{C}_{28}\text{H}_{21}\text{N}_2$ ], 6.87-6.81 [br. m, 2H,  $\text{C}_{28}\text{H}_{21}\text{N}_2$ ], 6.68-6.61 [br. m, 4H,  $\text{C}_{28}\text{H}_{21}\text{N}_2$ ], 4.89 [s, 1H, CH of

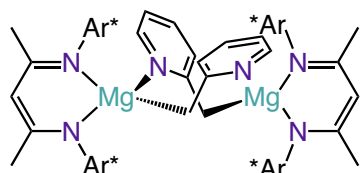
<sup>Dipp</sup>Nacnac], 4.18 [s, 1H, CH, N≡C-C(H)Ph<sub>2</sub> of C<sub>28</sub>H<sub>21</sub>N<sub>2</sub>], 3.40 [sept., 4H, J = 4.5 Hz, CH, <sup>i</sup>Pr, Ar\* of <sup>Dipp</sup>Nacnac], 1.68 [s, 6H, CH<sub>3</sub> of <sup>Dipp</sup>Nacnac], 1.20-1.18 [d, 12H, J = 8 Hz, CH<sub>3</sub>, <sup>i</sup>Pr, Ar\* of <sup>Dipp</sup>Nacnac], 1.17-1.15 [d, 12H, J = 8 Hz, CH<sub>3</sub>, <sup>i</sup>Pr, Ar\* of <sup>Dipp</sup>Nacnac].

<sup>13</sup>C NMR {<sup>1</sup>H} (150.90 MHz, C<sub>6</sub>D<sub>6</sub>, 298 K) δ 169.87 [C<sub>q</sub>, CHC(Me) of <sup>Dipp</sup>Nacnac], 153.13 [C<sub>q</sub>, N=C=CPh<sub>2</sub> of C<sub>28</sub>H<sub>21</sub>N<sub>2</sub>], 144.17 [C<sub>q</sub>], 143.11 [C<sub>q</sub>], 142.43 [C<sub>q</sub>], 133.22 [C<sub>q</sub>], 129.62 [CH of of C<sub>28</sub>H<sub>21</sub>N<sub>2</sub>], 128.91 [CH of Ar\* of <sup>Dipp</sup>Nacnac], 125.84 [CH, Ar\* of <sup>Dipp</sup>Nacnac], 124.34 [CH, of C<sub>28</sub>H<sub>21</sub>N<sub>2</sub>], 124.25 [CH, of C<sub>28</sub>H<sub>21</sub>N<sub>2</sub>], 119.74 [CH of C<sub>28</sub>H<sub>21</sub>N<sub>2</sub>], 95.08 [CH of <sup>Dipp</sup>Nacnac], 53.44 [C<sub>q</sub>, N=C=CPh<sub>2</sub> of C<sub>28</sub>H<sub>21</sub>N<sub>2</sub>], 41.94 [CH, N≡C-C(H)Ph<sub>2</sub> of C<sub>28</sub>H<sub>21</sub>N<sub>2</sub>], 28.48 [CH, <sup>i</sup>Pr, Ar\* of <sup>Dipp</sup>Nacnac], 25.05 [CH<sub>3</sub>, <sup>i</sup>Pr, Ar\* of <sup>Dipp</sup>Nacnac], 24.65 [CH<sub>3</sub>, <sup>i</sup>Pr, Ar\* of <sup>Dipp</sup>Nacnac], 24.01 [CH<sub>3</sub> of <sup>Dipp</sup>Nacnac].

**Elemental analysis:** (C<sub>56</sub>H<sub>60</sub>MgN<sub>4</sub>) *Calculated:* C: 82.69 % H: 7.44 % N: 6.89 %. *Found:* C: 82.31 % H: 7.62 % N: 6.82 %.

**IR (Nujol, cm<sup>-1</sup>)** 2283.5 (ν (C≡N)), 2100.7 (ν (C=C=N)).

• **Synthesis of [({<sup>Dipp</sup>Nacnac})Mg(C<sub>5</sub>H<sub>6</sub>N)]<sub>2</sub> (**43**)**



To a solution of compound **36** (0.56 g, 1 mmol) in THF (10 mL), 2-picoline (0.1 mL, 1 mmol) was added. The yellow solution turned to strong orange colour and was stirred for 2 hours at room temperature. The

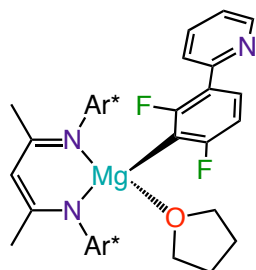
solvent was removed and 2 mL of hexane and 4 mL of THF were added. The resulting suspension was heated to solution and was placed at -33 °C. This yielded the title compound after 24 hours as colourless crystals. In order to obtain a good yield of the compound, after 2 hours of reaction the solvent was removed and 10 mL of hexane were added. The suspension was heated and placed at -15 °C. The resulting solid was isolated after 2 days and placed in a glovebox (0.35 g, 67%).

**$^1\text{H}$  NMR (600.13 MHz,  $\text{C}_6\text{D}_6$ , 298 K)**  $\delta$  7.79-7.78 [d, 2H,  $J = 5.4$  Hz,  $\text{C}_6\text{H}_6\text{N}$ ], 7.28-7.17 [br. m, 2H,  $\text{Ar}^*$  of  $\text{DippNacnac}$ ], 7.15-6.90 [br. m, 10H,  $\text{Ar}^*$  of  $\text{DippNacnac}$ ], 6.45-6.40 [br. td, 2H,  $\text{C}_6\text{H}_6\text{N}$ ], 5.88-5.84 [br. t, 2H,  $J = 6.2$  Hz,  $\text{C}_6\text{H}_6\text{N}$ ], 4.87-4.86 [br. d, 2H,  $J = 8.2$  Hz,  $\text{C}_6\text{H}_6\text{N}$ ], 4.82 [s, 2H,  $\text{CH}$  of  $\text{DippNacnac}$ ], 3.60 [br. m, 2H,  $\text{CH}$ ,  $i\text{Pr}$ ,  $\text{Ar}^*$  of  $\text{DippNacnac}$ ], 3.26 [br. m, 2H,  $\text{CH}$ ,  $i\text{Pr}$ ,  $\text{Ar}^*$  of  $\text{DippNacnac}$ ], 3.22 [br. m, 2H,  $\text{CH}$ ,  $i\text{Pr}$ ,  $\text{Ar}^*$  of  $\text{DippNacnac}$ ], 2.55 [br. m, 2H,  $\text{CH}$ ,  $i\text{Pr}$ ,  $\text{Ar}^*$  of  $\text{DippNacnac}$ ], 1.68 [br. s, 6H,  $\text{CH}_3$  of  $\text{DippNacnac}$ ], 1.63 [br. s, 2H,  $\text{CH}_2$  of  $\text{C}_6\text{H}_6\text{N}$ ], 1.60 [br. s, 6H,  $\text{CH}_3$  of  $\text{DippNacnac}$ ], 1.49 [br. m, 6H,  $\text{CH}_3$ ,  $i\text{Pr}$ ,  $\text{Ar}^*$  of  $\text{DippNacnac}$ ], 1.28 [br. s, 2H,  $\text{CH}_2$  of  $\text{C}_6\text{H}_6\text{N}$ ], 1.26-1.09 [br. m, 18H,  $\text{CH}_3$ ,  $i\text{Pr}$ ,  $\text{Ar}^*$  of  $\text{DippNacnac}$ ], 1.09-1.01 [br. m, 6H,  $\text{CH}_3$ ,  $i\text{Pr}$ ,  $\text{Ar}^*$  of  $\text{DippNacnac}$ ], 1.01-0.93 [br. m, 6H,  $\text{CH}_3$ ,  $i\text{Pr}$ ,  $\text{Ar}^*$  of  $\text{DippNacnac}$ ], 0.93-0.80 [br. m, 6H,  $\text{CH}_3$ ,  $i\text{Pr}$ ,  $\text{Ar}^*$  of  $\text{DippNacnac}$ ], 0.23 [br. m, 6H,  $\text{CH}_3$ ,  $i\text{Pr}$ ,  $\text{Ar}^*$  of  $\text{DippNacnac}$ ].

**$^{13}\text{C}$  NMR  $\{^1\text{H}\}$  (150.90 MHz,  $\text{C}_6\text{D}_6$ , 298 K)**  $\delta$  176.8 [ $\text{C}_q$ ,  $\text{CHC}(\text{Me})$  of  $\text{DippNacnac}$ ], 144.9 [ $\text{CH}$  of  $\text{C}_6\text{H}_6\text{N}$ ], 135.5 [ $\text{CH}$  of  $\text{C}_6\text{H}_6\text{N}$ ], 125.6 [ $\text{CH}$ ,  $\text{Ar}^*$  of  $\text{DippNacnac}$ ], 124.8 [ $\text{CH}$ ,  $\text{Ar}^*$  of  $\text{DippNacnac}$ ], 124.5 [ $\text{CH}$ ,  $\text{Ar}^*$  of  $\text{DippNacnac}$ ], 124.3 [ $\text{CH}$ ,  $\text{Ar}^*$  of  $\text{DippNacnac}$ ], 123.4 [ $\text{CH}$ ,  $\text{Ar}^*$  of  $\text{DippNacnac}$ ], 122.0 [ $\text{CH}$  of  $\text{C}_6\text{H}_6\text{N}$ ], 110.8 [ $\text{CH}$  of  $\text{C}_6\text{H}_6\text{N}$ ], 95.1 [ $\text{CH}$  of  $\text{DippNacnac}$ ], 35.5 [ $\text{Mg-CH}_2$  of  $\text{C}_6\text{H}_6\text{N}$ ], 29.3 [ $\text{CH}$ ,  $i\text{Pr}$ ,  $\text{Ar}^*$  of  $\text{DippNacnac}$ ], 28.7 [ $\text{CH}$ ,  $i\text{Pr}$ ,  $\text{Ar}^*$  of  $\text{DippNacnac}$ ], 28.0 [ $\text{CH}$ ,  $i\text{Pr}$ ,  $\text{Ar}^*$  of  $\text{DippNacnac}$ ], 25.7 [ $\text{CH}_3$ ,  $\text{DippNacnac}$ ], 25.5 [ $\text{CH}_3$ ,  $\text{DippNacnac}$ ], 25.4 [ $\text{CH}_3$ ,  $\text{DippNacnac}$ ], 25.1 [ $\text{CH}_3$ ,  $\text{DippNacnac}$ ], 24.9 [ $\text{CH}_3$ ,  $\text{DippNacnac}$ ], 24.5 [ $\text{CH}_3$ ,  $\text{DippNacnac}$ ], 24.3 [ $\text{CH}_3$ ,  $\text{DippNacnac}$ ], 23.8 [ $\text{CH}_3$ ,  $\text{DippNacnac}$ ], 23.5 [ $\text{CH}_3$ ,  $\text{DippNacnac}$ ], 14.34 [ $\text{CH}_3$ ,  $i\text{Pr}$ ,  $\text{Ar}^*$  of  $\text{DippNacnac}$ ].

**Elemental analysis:** ( $\text{C}_{66}\text{H}_{88}\text{Mg}_2\text{N}_8$ ) *Calculated:* C: 78.71 % H: 8.87 % N: 7.87 %.  
*Found:* C: 77.39 % H: 8.52 % N: 7.35 %.

• **Synthesis of [(<sup>Dipp</sup>Nacnac)MgTHF(C<sub>11</sub>H<sub>6</sub>F<sub>2</sub>N)] (44)**



To a solution of **36** (0.56 g, 1 mmol) in THF (5 mL), 2-(2,4-difluorophenyl)pyridine (0.2 g, 1mmol) was added. The dark yellow solution was stirred for 5 hours at room temperature. The solvent was removed and a 1 mL of THF was added. The suspension was dissolved by heating and was placed at -30 °C.

After 48 hours a crop of colorless crystals were isolated, washed with hexane and placed in a glovebox (0.43 g, 68%). Single crystals suitable for X-Ray analysis were obtained by a mixture of 1 mL of hexane and 1 mL of toluene at -30 °C. The THF molecule was removed when the crystals were isolated *in vacuo*.

**<sup>1</sup>H NMR (400.13 MHz, C<sub>6</sub>D<sub>6</sub>, 298 K)** δ 8.96-8.88 [br. dd, 1H, *J* = 0.8 Hz, *J* = 5.4 Hz, C<sub>11</sub>H<sub>6</sub>F<sub>2</sub>N], 7.36-7.32 [br. dd, 1H, *J* = 1.2 Hz, *J* = 8.1, Ar\* of <sup>Dipp</sup>Nacnac], 7.23-7.17 [br. m, 1H, Ar\* of <sup>Dipp</sup>Nacnac], 7.14-7.00 [m, 3H, Ar\* of <sup>Dipp</sup>Nacnac + 1H, C<sub>11</sub>H<sub>6</sub>F<sub>2</sub>N], 6.93-6.86 [br. m, 1H, Ar\* of <sup>Dipp</sup>Nacnac], 6.75-6.73 [br.d, 1H, C<sub>11</sub>H<sub>6</sub>F<sub>2</sub>N], 6.62-6.54 [br. td, 1H, C<sub>11</sub>H<sub>6</sub>F<sub>2</sub>N], 6.28-6.20 [br. m, 1H, C<sub>11</sub>H<sub>6</sub>F<sub>2</sub>N], 6.06-6.00 [dd, 1H, *J* = 3.6 Hz, *J* = 8.0 Hz, C<sub>11</sub>H<sub>6</sub>F<sub>2</sub>N], 4.98 [s, 1H, CH of <sup>Dipp</sup>Nacnac], 3.65-3.50 [sept, 1H, *J* = 6.4 Hz, CH, <sup>i</sup>Pr, Ar\* of <sup>Dipp</sup>Nacnac], 3.45-3.30 [sept, 1H, *J* = 6.7 Hz, CH, <sup>i</sup>Pr, Ar\* of <sup>Dipp</sup>Nacnac], 3.00-2.90 [sept, 1H, *J* = 6.7 Hz, CH, <sup>i</sup>Pr, Ar\* of <sup>Dipp</sup>Nacnac], 2.84-2.73 [sept, 1H, *J* = 6.4 Hz, CH, <sup>i</sup>Pr, Ar\* of <sup>Dipp</sup>Nacnac], 1.84 [s, 3H, CH<sub>3</sub> of <sup>Dipp</sup>Nacnac], 1.81 [s, 3H, CH<sub>3</sub> of <sup>Dipp</sup>Nacnac], 1.54-1.52 [d, 3 H, *J* = 6.8 Hz, CH<sub>3</sub>, <sup>i</sup>Pr, Ar\* of <sup>Dipp</sup>Nacnac], 1.31-1.30 [d, 3H, *J* = 6.8 Hz, CH<sub>3</sub>, <sup>i</sup>Pr, Ar\* of <sup>Dipp</sup>Nacnac], 1.25-1.24 [d, 3H, *J* = 6.8 Hz, CH<sub>3</sub>, <sup>i</sup>Pr, Ar\* of <sup>Dipp</sup>Nacnac], 1.14-1.11 [br. m, 6H, CH<sub>3</sub>, <sup>i</sup>Pr, Ar\* of <sup>Dipp</sup>Nacnac], 0.82-0.80 [d, 3H, *J* = 6.8 Hz, CH<sub>3</sub>, <sup>i</sup>Pr, Ar\* of <sup>Dipp</sup>Nacnac], 0.53-0.51 [d, 3H, *J* = 6.7 Hz, CH<sub>3</sub>, <sup>i</sup>Pr, Ar\* of <sup>Dipp</sup>Nacnac], 0.22-0.21 [d, 3H, *J* = 6.7 Hz, CH<sub>3</sub>, <sup>i</sup>Pr, Ar\* of <sup>Dipp</sup>Nacnac].

**<sup>13</sup>C NMR {<sup>1</sup>H} (100.61 MHz, C<sub>6</sub>D<sub>6</sub>, 298 K)** δ 169.3 [C<sub>q</sub>, CHC(Me) of <sup>Dipp</sup>Nacnac], 168.5 [C<sub>q</sub>, CHC(Me) of <sup>Dipp</sup>Nacnac], 158.9 [C<sub>q</sub>, C<sub>11</sub>H<sub>6</sub>F<sub>2</sub>N], 148.9 [C<sub>11</sub>H<sub>6</sub>F<sub>2</sub>N], 146.7 [C<sub>q</sub>, Ar\* of



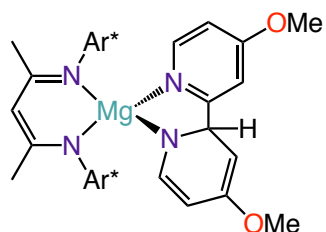
<sup>Dipp</sup>Nacnac], 143.1 [C<sub>q</sub>, Ar\* of <sup>Dipp</sup>Nacnac], 142.9 [C<sub>q</sub>, Ar\* of <sup>Dipp</sup>Nacnac], 142.5 [C<sub>q</sub>, Ar\* of <sup>Dipp</sup>Nacnac], 141.7 [C<sub>q</sub>, Ar\* of <sup>Dipp</sup>Nacnac], 137.8 [C<sub>11</sub>H<sub>6</sub>F<sub>2</sub>N], 129.3 [C<sub>q</sub>], 128.6 [C<sub>11</sub>H<sub>6</sub>F<sub>2</sub>N], 125.3 [CH, Ar\* of <sup>Dipp</sup>Nacnac], 124.2 [CH, Ar\* of <sup>Dipp</sup>Nacnac], 123.9 [CH, Ar\* of <sup>Dipp</sup>Nacnac], 123.4 [C<sub>11</sub>H<sub>6</sub>F<sub>2</sub>N], 123.1 [CH, Ar\* of <sup>Dipp</sup>Nacnac], 122.0 [C<sub>11</sub>H<sub>6</sub>F<sub>2</sub>N], 109.5-109.1 [CH, d, J = 38.8 Hz, C<sub>11</sub>H<sub>6</sub>F<sub>2</sub>N], 93.9 [CH of <sup>Dipp</sup>Nacnac], 30.3 [CH, <sup>i</sup>Pr, Ar\* of <sup>Dipp</sup>Nacnac], 29.5 [CH, <sup>i</sup>Pr, Ar\* of <sup>Dipp</sup>Nacnac], 28.3 [CH, <sup>i</sup>Pr, Ar\* of <sup>Dipp</sup>Nacnac], 28.1 [CH, <sup>i</sup>Pr, Ar\* of <sup>Dipp</sup>Nacnac], 25.3 [CH<sub>3</sub>, <sup>i</sup>Pr, Ar\* of <sup>Dipp</sup>Nacnac], 25.2 [CH<sub>3</sub> of <sup>Dipp</sup>Nacnac], 24.8 [CH<sub>3</sub>, <sup>i</sup>Pr, Ar\* of <sup>Dipp</sup>Nacnac], 24.7 [CH<sub>3</sub>, of <sup>Dipp</sup>Nacnac], 24.6 [CH<sub>3</sub>, <sup>i</sup>Pr, Ar\* of <sup>Dipp</sup>Nacnac], 24.5 [CH<sub>3</sub>, <sup>i</sup>Pr, Ar\* of <sup>Dipp</sup>Nacnac], 24.0 [CH<sub>3</sub>, <sup>i</sup>Pr, Ar\* of <sup>Dipp</sup>Nacnac], 23.8 [CH<sub>3</sub>, <sup>i</sup>Pr, Ar\* of <sup>Dipp</sup>Nacnac], 23.5 [CH<sub>3</sub>, <sup>i</sup>Pr, Ar\* of <sup>Dipp</sup>Nacnac], 22.8 [CH<sub>3</sub>, <sup>i</sup>Pr, Ar\* of <sup>Dipp</sup>Nacnac].

<sup>13</sup>C NMR {<sup>19</sup>F} (100.61 MHz, C<sub>6</sub>D<sub>6</sub>, 298 K) δ 171.6-171.27 [C<sub>q</sub>, dd, J = 12.5 Hz, J = 43.6 Hz, C-F of C<sub>11</sub>H<sub>6</sub>F<sub>2</sub>N], 166.9-166.7 [C<sub>q</sub>, d, J = 11.5 Hz, C-F of C<sub>11</sub>H<sub>6</sub>F<sub>2</sub>N], 132.3 [C<sub>q</sub>], 119.0-118.9 [C<sub>q</sub>, d, J = 10 Hz, C<sub>11</sub>H<sub>6</sub>F<sub>2</sub>N], (C<sub>q</sub> of C-Mg was not possible to assign).

<sup>19</sup>F NMR (376.40 MHz, C<sub>6</sub>D<sub>6</sub>, 298 K) δ -77.6 [s, C<sub>11</sub>H<sub>6</sub>F<sub>2</sub>N], -82.0 [s, C<sub>11</sub>H<sub>6</sub>F<sub>2</sub>N].

**Elemental analysis:** (C<sub>37</sub>H<sub>46</sub>MgN<sub>2</sub>O) *Calculated:* C: 76.00 % H: 7.49 % N: 6.65 %.  
*Found:* C: 76.22 % H: 7.75 % N: 6.51 %.

• **Synthesis of [(<sup>Dipp</sup>Nacnac)Mg(C<sub>12</sub>H<sub>13</sub>N<sub>2</sub>O<sub>2</sub>)] (47)**



To a solution of **36** (0.28 g, 0.5 mmol) in THF (5 mL), 4-methoxypyridine (0.105 mL, 1 mmol) was added. The solution turned to dark red and was stirred for 3 hours at room temperature. The solvent was removed and a mixture of 2 mL of hexane and 2 mL of toluene was added and was placed at -30 °C. After 48 hours a crop of black crystals were isolated, washed with hexane and placed in a glovebox (0.154 g, 47%).

**$^1\text{H}$  NMR (400.13 MHz,  $\text{C}_6\text{D}_6$ , 298 K)**  $\delta$  8.79-7.78 [d, 1H,  $J = 6.2$  Hz,  $\text{C}_{12}\text{H}_{13}\text{N}_2\text{O}_2$ ], 7.13-7.00 [br. m, 6H, Ar\* of  $\text{D}^{\text{ipp}}$ Nacnac], 6.94-6.93 [d, 1H,  $J = 6.1$  Hz,  $\text{C}_{12}\text{H}_{13}\text{N}_2\text{O}_2$ ], 6.57-6.56 [d, 1H,  $J = 2.5$  Hz,  $\text{C}_{12}\text{H}_{13}\text{N}_2\text{O}_2$ ], 6.26-6.23 [dd, 1H,  $J = 6.2$  Hz,  $J = 2.6$  Hz,  $\text{C}_{12}\text{H}_{13}\text{N}_2\text{O}_2$ ], 5.24-5.22 [dd, 1H,  $J = 6.3$  Hz,  $J = 2.2$  Hz,  $\text{C}_{12}\text{H}_{13}\text{N}_2\text{O}_2$ ], 4.97-4.96 [d, 1H,  $J = 2.8$  Hz,  $\text{C}_{12}\text{H}_{13}\text{N}_2\text{O}_2$ ], 4.93 [s, 1H, CH of  $\text{D}^{\text{ipp}}$ Nacnac], 3.62-3.47 [br. m, 1H, CH,  $i$ Pr, Ar\* of  $\text{D}^{\text{ipp}}$ Nacnac], 3.47-3.37 [br. m, 1H, CH,  $i$ Pr, Ar\* of  $\text{D}^{\text{ipp}}$ Nacnac], 3.35 [s, 3H,  $\text{CH}_3$  OMe of  $\text{C}_{12}\text{H}_{13}\text{N}_2\text{O}_2$ ], 3.35 [br m, 3H,  $\text{CH}_3$  OMe of  $\text{C}_{12}\text{H}_{13}\text{N}_2\text{O}_2$  + 1H, CH of  $\text{C}_{12}\text{H}_{13}\text{N}_2\text{O}_2$ ], 3.30-3.08 [br. m, 2H, CH,  $i$ Pr, Ar\* of  $\text{D}^{\text{ipp}}$ Nacnac], 2.84 [s, 3H,  $\text{CH}_3$  OMe of  $\text{C}_{12}\text{H}_{13}\text{N}_2\text{O}_2$ ], 1.73 [s, 6H,  $\text{CH}_3$  of  $\text{D}^{\text{ipp}}$ Nacnac], 1.50-1.34 [br. d, 6 H,  $\text{CH}_3$ ,  $i$ Pr, Ar\* of  $\text{D}^{\text{ipp}}$ Nacnac], 1.31-1.30 [br. d, 12H,  $\text{CH}_3$ ,  $i$ Pr, Ar\* of  $\text{D}^{\text{ipp}}$ Nacnac], 0.83-0.72 [br. d, 3HCH $_3$ ,  $i$ Pr, Ar\* of  $\text{D}^{\text{ipp}}$ Nacnac], 0.67-0.53 [br. d, 3HCH $_3$ ,  $i$ Pr, Ar\* of  $\text{D}^{\text{ipp}}$ Nacnac].

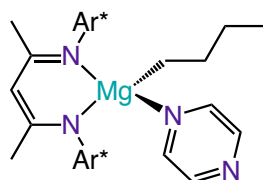
**$^{13}\text{C}$  NMR  $\{^1\text{H}\}$  (100.61 MHz,  $\text{C}_6\text{D}_6$ , 298 K)**  $\delta$  172.3 [ $\text{C}_q$ ], 169.5 [ $\text{C}_q$ ], 168.1 [ $\text{C}_q$ ], 161.2 [ $\text{C}_q$ ], 150.4 [CH,  $\text{C}_{12}\text{H}_{13}\text{N}_2\text{O}_2$ ], 147.1 [CH,  $\text{C}_{12}\text{H}_{13}\text{N}_2\text{O}_2$ ], 144.8 [ $\text{C}_q$ ], 142.8 [ $\text{C}_q$ ], 142.1 [ $\text{C}_q$ ], 124.2 [CH, Ar\* of  $\text{D}^{\text{ipp}}$ Nacnac], 123.6 [ $\text{C}_q$ , Ar\* of  $\text{D}^{\text{ipp}}$ Nacnac], 110.7 [CH,  $\text{C}_{12}\text{H}_{13}\text{N}_2\text{O}_2$ ], 106.5 [CH,  $\text{C}_{12}\text{H}_{13}\text{N}_2\text{O}_2$ ], 94.9 [CH of  $\text{D}^{\text{ipp}}$ Nacnac], 91.6 [CH,  $\text{C}_{12}\text{H}_{13}\text{N}_2\text{O}_2$ ], 72.9 [CH,  $\text{C}_{12}\text{H}_{13}\text{N}_2\text{O}_2$ ], 63.0 [CH,  $\text{C}_{12}\text{H}_{13}\text{N}_2\text{O}_2$ ], 54.8 [OCH $_3$ ,  $\text{C}_{12}\text{H}_{13}\text{N}_2\text{O}_2$ ], 53.4 [OCH $_3$ ,  $\text{C}_{12}\text{H}_{13}\text{N}_2\text{O}_2$ ], 29.2 [CH,  $i$ Pr, Ar\* of  $\text{D}^{\text{ipp}}$ Nacnac], 29.0 [CH,  $i$ Pr, Ar\* of  $\text{D}^{\text{ipp}}$ Nacnac], 28.2 [CH,  $i$ Pr, Ar\* of  $\text{D}^{\text{ipp}}$ Nacnac], 28.1 [CH,  $i$ Pr, Ar\* of  $\text{D}^{\text{ipp}}$ Nacnac], 25.4 [CH $_3$ ,  $i$ Pr, Ar\* of  $\text{D}^{\text{ipp}}$ Nacnac], 24.5 [CH $_3$ ,  $i$ Pr, Ar\* of  $\text{D}^{\text{ipp}}$ Nacnac], 24.4 [CH $_3$  of  $\text{D}^{\text{ipp}}$ Nacnac], 24.1 [CH $_3$  of  $\text{D}^{\text{ipp}}$ Nacnac].

**Elemental analysis:** ( $\text{C}_{41}\text{H}_{54}\text{MgN}_4\text{O}_2$ ) *Calculated:* C: 74.70 % H: 8.26 % N: 8.50 %.

*Found:* C: 75.02 % H: 8.07 % N: 8.01 %.

#### 4.4.2 DOSY NMR Studies

- Reaction of  $[(^{\text{Dipp}}\text{Nacnac})\text{Mg}(\text{Bu})(\text{THF})]$  with pyrazine

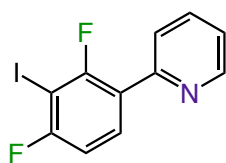


In a J. Young's NMR tube, pyrazine (20  $\mu\text{L}$  of a 1.78 M solution of pyrazine in  $\text{C}_6\text{D}_6$ , 0.035 mmol) was added to a solution of  $[(^{\text{Dipp}}\text{Nacnac})\text{Mg}(\text{Bu})(\text{THF})]$  (0.020 g, 0.035 mmol) in  $\text{C}_6\text{D}_6$  (0.6 mL). The solution changed colour to brown. 5  $\mu\text{L}$  of TMS (tetramethylsilane) were added in order to use as internal standard in the DOSY experiment.<sup>[7]</sup>

$^1\text{H}$  NMR (400.13 MHz,  $\text{C}_6\text{D}_6$ , 298 K)  $\delta$  8.14 [br s, 4H,  $\text{C}_4\text{H}_4\text{N}_2$ ], 7.16 [br s, 6H,  $\text{Ar}^*$  of  $^{\text{Dipp}}\text{Nacnac}$ ], 4.86 [br s, 1H, CH of  $^{\text{Dipp}}\text{Nacnac}$ ], 3.18 [br s, 4H, CH,  $i\text{Pr}$ ,  $\text{Ar}^*$  of  $^{\text{Dipp}}\text{Nacnac}$ ], 2.01-0.66 [br m, 60H,  $\text{CH}_3$  of  $^{\text{Dipp}}\text{Nacnac}$  and Bu], -0.29 [br s, 2H,  $\text{Mg}-\text{CH}_2$  of Bu].

#### 4.4.3 Preliminary Electrophilic Quenching Studies

- Reaction of 2-(2,4-difluoro-3-iodophenyl)pyridine (**45**)



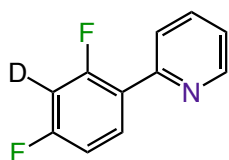
To a solution of **36** (0.56 g, 1 mmol) in THF (5 mL), 2-(2,4-difluorophenyl)pyridine (0.2 g, 1mmol) was added. The dark yellow solution was stirred for 5 hours at room temperature. A solution of iodine (0.51 g, 2 mmol) in THF (4 mL) was then added and the yellow solution turned to a brown suspension that was stirred overnight at room temperature. After this time the suspension was opened to air. Water (40 mL) was added and the solution was extracted with diethylether (30 ml x 2). The ether solution was washed with water (40 mL), sat.  $\text{Na}_2\text{S}_2\text{O}_3$  aq (40 mL) and brine (40 mL). The solution was then dried over  $\text{Na}_2\text{SO}_4$ , and the filtrate was evaporated *in vacuo*. Ferrocene (0.019 g) was added as an internal standard and the mixture was

dissolved in  $\text{CDCl}_3$ . The  $^1\text{H}$  NMR spectrum suggests the presence of a 65% of compound **45** since the integration versus ferrocene revealed 35% of presence of 2-(2,4-difluorophenyl)pyridine and the signals corresponding to the iodinated product **45** are overlapping with the 2-(2,4-difluorophenyl)pyridine signals.

$^1\text{H}$  NMR (400.13 MHz,  $\text{CDCl}_3$ , 298 K)  $\delta$  8.74-8.73 [br. d, 1H,  $J = 4$  Hz,  $\text{C}_{11}\text{H}_6\text{F}_2\text{IN}$ ], 8.14-8.00 [m, 1H,  $\text{C}_{11}\text{H}_6\text{F}_2\text{IN}$ ], 7.80-7.69 [m, 2H,  $\text{C}_{11}\text{H}_6\text{F}_2\text{IN}$ ], 7.27-7.10 [m, 1H,  $\text{C}_{11}\text{H}_6\text{F}_2\text{IN}$ ], 7.06-6.98 [m, 1H,  $\text{C}_{11}\text{H}_6\text{F}_2\text{IN}$ ].

$^{19}\text{F}$  NMR (376.40 MHz,  $\text{CDCl}_3$ , 298 K)  $\delta$  -90.8 [s,  $\text{C}_{11}\text{H}_6\text{F}_2\text{IN}$ ], -93.6 [s,  $\text{C}_{11}\text{H}_6\text{F}_2\text{IN}$ ].

- **Synthesis of 2-(2,4-difluoro-3-deuteriophenyl)pyridine (46)**



To a solution of **44** (0.63 g, 1 mmol) in THF (5 mL),  $\text{d}_4$ -methanol (0.06 mL, 1.5 mmol) was added. The mixture turned to a beige suspension that was stirred overnight at room temperature. The suspension was then filtered and washed with dichloromethane and the filtrate was evaporated *in vacuo*.  $\text{CHCl}_3$  was then added to perform the deuterium NMR experiments. After this, the solvent was removed, ferrocene (0.019 g) was added as an internal standard and the mixture was dissolved in  $\text{CDCl}_3$ . The integration versus ferrocene revealed a 72% of compound **46**.

$^1\text{H}$  NMR (400.13 MHz,  $\text{CDCl}_3$ , 298 K)  $\delta$  8.61 [br. s, 1H,  $\text{C}_{11}\text{H}_6\text{F}_2\text{DN}$ ], 8.04-7.09 [br. m, 1H,  $\text{C}_{11}\text{H}_6\text{F}_2\text{DN}$ ], 7.70-7.54 [br. m, 2H,  $\text{C}_{11}\text{H}_6\text{F}_2\text{DN}$ ], 7.16-6.95 [m, 1H,  $\text{C}_{11}\text{H}_6\text{F}_2\text{DN}$ ], 6.96-6.87 [m, 1H,  $\text{C}_{11}\text{H}_6\text{F}_2\text{DN}$ ].

$^{19}\text{F}$  NMR (376.40 MHz,  $\text{CDCl}_3$ , 298 K)  $\delta$  -109.3 [ $\text{C}_{11}\text{H}_6\text{F}_2\text{DN}$ ], -112.8 [ $\text{C}_{11}\text{H}_6\text{F}_2\text{DN}$ ].

## Chapter 5 Deprotonation and C-F Activation of Fluorinated Aromatic Molecules

### 5.1 Introduction

Fluorine is the most electronegative element in the periodic table, which makes the C-F bond one of the strongest in organic chemistry ( $105.4 \text{ kcal mol}^{-1}$ ).<sup>[337]</sup> The high electronegativity of the F atom also makes the  $\text{C}^{\delta(+)}\text{-F}^{\delta(-)}$  bond highly polarised with the electron density on the fluorine atom. Consequently, the C-F bond has a significant electrostatic character, rather than electron sharing typical of the covalent bond, which provides interesting properties such as electrostatic/dipole interaction with its environment. Molecules with C-F bonds have a broad range of applications in materials, pharmaceuticals, agrochemicals and fine chemicals.<sup>[337–341]</sup>

Particularly, fluorinated aromatic substrates are ubiquitous in many important applications in pharmaceuticals and materials as part of more complex molecular scaffolds.<sup>[341–345]</sup> For example, Januvia is one of the medicines for diabetes that contains a trifluoroaromatic core, as well as the insecticide Transfluthrin that contains the substituted 1,2,4,5-tetrafluorobenzene in its skeleton (Figure 5.1).<sup>[346]</sup>

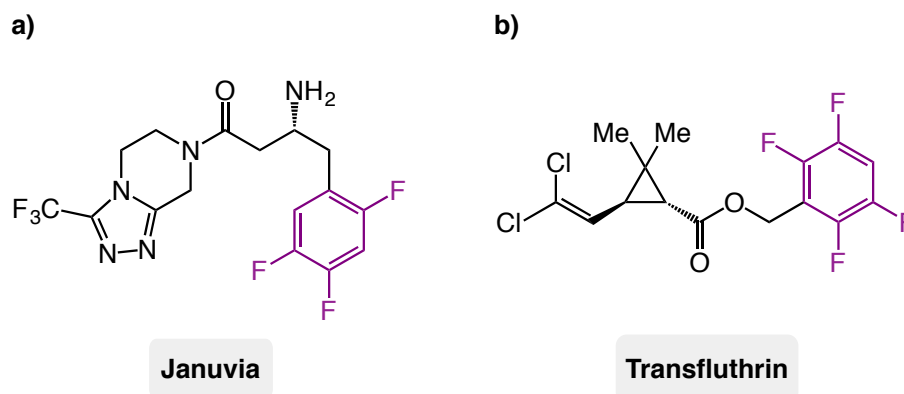
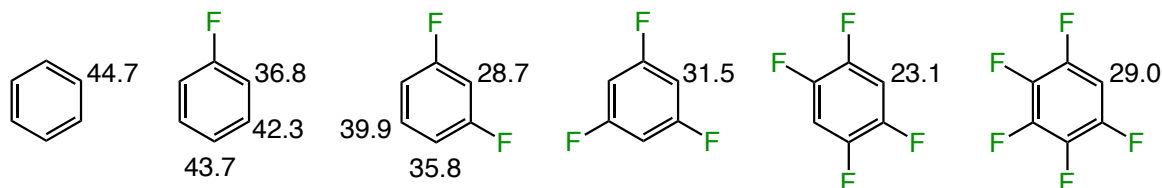


Figure 5.1: Examples of applications of fluoroaromatic molecules. a) Januvia, oral medicine for diabetes. b) Transfluthrin, pyrethroid insecticide.

In this context, C-H and C-F activation of fluoroarenes constitute two of the main methods to access these complex architectures. These reactions display an increasing interest for chemists due to the high inertness of C–F and C–H bonds, which generally require the use of transition metal complexes in order to perform these challenging transformations.<sup>[347–350]</sup>

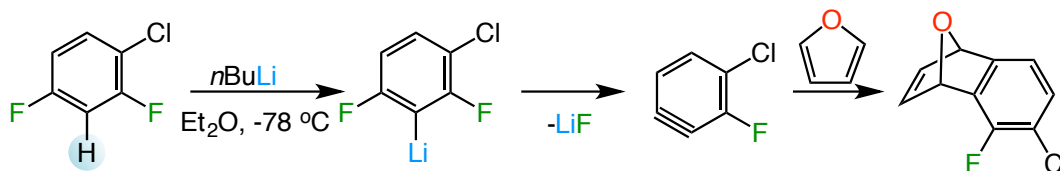
### 5.1.1 C-H metallation of fluoroaromatics

Deprotonative metallation of fluoroaromatic compounds is a basic tool for functionalization in order to form more complex scaffolds. The high electronegativity of the fluorine atom and therefore the strong polarisation of the C-F bond, leads to an increase in the acidity of the protons in *ortho* positions relative to the fluorine. Figure 5.6 compares the predicted  $pK_a$  values of a series of fluoroaromatic molecules with benzene, exemplifying how the fluorine substituents can tune the acidity of those substrates and therefore their reactivity.<sup>[228]</sup>

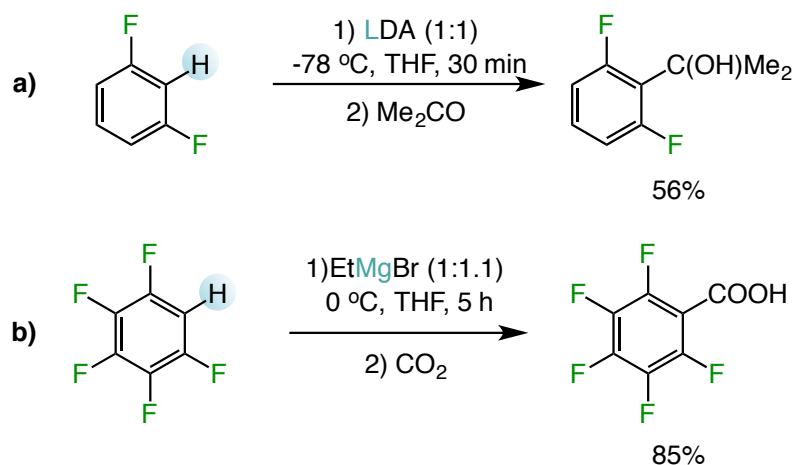
Figure 5.2: Theoretical prediction of acidities  $pK_a$  of benzene derivatives.<sup>[228]</sup>

The repetitive introduction of the same substituent in a molecule does not always lead to an additive effect<sup>[351]</sup> and both kinetic and thermodynamic effects need to be considered.<sup>[352]</sup> Schlosser has extensively studied the addition of substituent effects and the deprotonation energies of different fluoroaromatics in the gas phase when deprotonated with LDA and *sec*-butyllithium.<sup>[351,353]</sup> These studies show a linear relationship between the differential free activation energies  $\Delta\Delta G^\ddagger$  and the relative deprotonation energies  $\Delta\Delta G_g^\circ$  that increases with the number of fluorine atoms in the molecule.

C-H activation reactions of fluoroaromatics are normally performed by transition metal compounds.<sup>[348–350,354–356]</sup> However, these substrates can also be deprotonated by organolithium reagents at extremely low temperatures ( $-78^\circ\text{C}$ ) in order to avoid competing nucleophilic substitution reactions or formation of LiF (Scheme 5.1).<sup>[357,358]</sup>

Scheme 5.1: Example of LiF elimination and further benzyne trapping, after first deprotonation with *n*BuLi.<sup>[358]</sup>

For example, lithiation of 1,3-difluorobenzene by an equimolar amount of LDA at  $-78\text{ }^{\circ}\text{C}$  in THF during 30 minutes and subsequent trapping with acetone, leads to 2-(2,6-difluorophenyl)propan-2-ol in a 56 % yield (Scheme 5.2a). In some cases Grignard reagents have also been employed, where the deprotonation reaction displays priority over the nucleophilic substitution, in THF at  $0\text{ }^{\circ}\text{C}$ .<sup>[359]</sup> For instance, the deprotonation of pentafluorobenzene can be achieved with different Grignard reagents such as ethylmagnesium bromide, methylmagnesium iodide or isopropylmagnesium chloride, in THF at  $0\text{ }^{\circ}\text{C}$ . Moderate to good yields (25 - 85%) were obtained after 5 hours of reaction and consecutive carbonation reaction (Scheme 5.2b).<sup>[359]</sup>

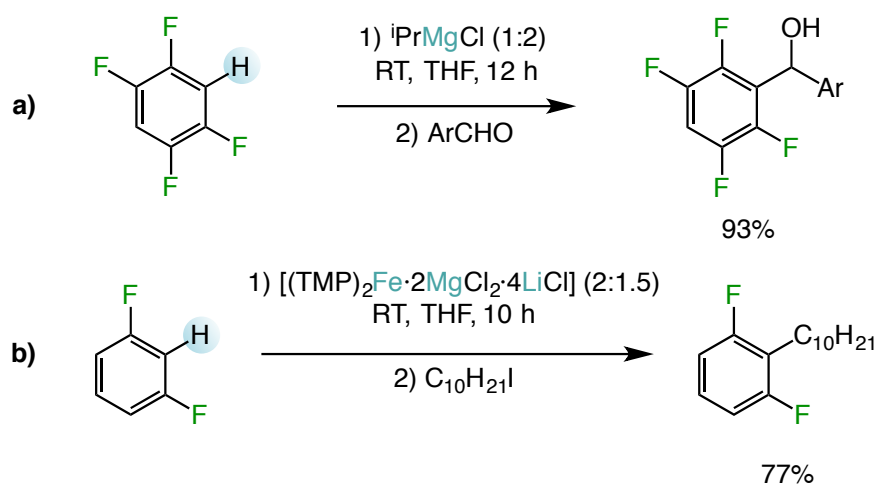


Scheme 5.2: Examples of metallation of fluoroaromatics using different bases. a) Metallation and subsequent quench of 1,3-difluorobenzene with LDA.<sup>[357]</sup> b) Metallation and subsequent quench of pentafluorobenzene with  $\text{EtMgBr}$ .<sup>[359]</sup>

Recent studies by Huang have also shown a new approach to access polyfluoroaryl carbinols via addition to aldehydes using Grignard reagents at room temperature.<sup>[346]</sup> These studies have shown that 1,2,4,5-tetrafluorobenzene can be deprotonated by  $^i\text{PrMgCl}$  followed by addition of 2-naphthaldehyde (2.25:1.25:1), which leads to the monoaddition product in a 93% yield at room temperature after



12 hours (Scheme 5.3a).<sup>[346]</sup> Knochel has also reported the ferration of 1,3-difluorobenzene by the mixed-metal base  $[(\text{TMP})_2\text{Fe}\cdot 2\text{MgCl}_2\cdot 4\text{LiCl}]$  (2:1.5), which leads to the formation of the corresponding alkylated fluorobenzene in 77% yield after 10 hours at room temperature and further quench using 1-iododecane (Scheme 5.3b).<sup>[360]</sup>



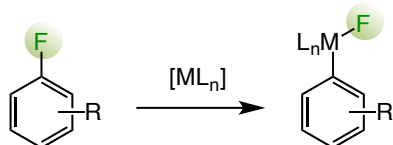
Scheme 5.3: Examples of metallation of fluoroaromatics using different bases. a) Metallation and subsequent quench of 1,2,4,5-tetrafluorobenzene with  $i\text{PrMgCl}$ .<sup>[346]</sup> b) Metallation and subsequent quench of 1,3-difluorobenzene with a mixed-metal base.<sup>[360]</sup>

## Fluoroaromatics in C-F Activation

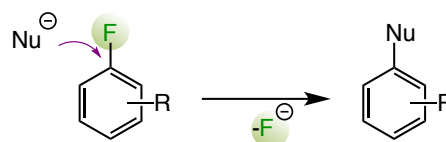
Cleavage of a C-F bond is an excellent approach to derivatisation of reactive polyfluorinated building blocks and to design new fluorine-containing molecules. In partially fluorinated aromatic molecules C-H and C-F activation are competitive processes, where C-F bond is stronger than C-H ( $105.4$  vs  $98.8$  Kcal mol<sup>-1</sup>, for C-F and C-H respectively).<sup>[337]</sup> Therefore, C-F bond functionalization is a very challenging process, which has particular interest to access new synthetically relevant molecules. As well, this process is attractive for the transformation of C-F to C-<sup>18</sup>F for the preparation of <sup>18</sup>F-labelled molecules used in medical imaging.<sup>[361]</sup> Several

methods exist to activate C-F bonds such as oxidative addition, hydrodefluorination, nucleophilic substitution or defluorination via benzyne, among others (Scheme 5.4).<sup>[350,362]</sup>

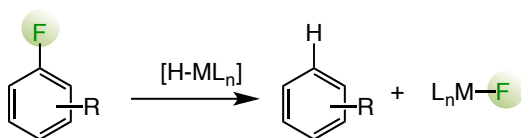
**a) Oxidative addition of low-valent metals**



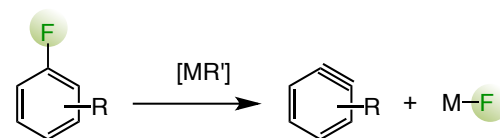
**c) Nucleophilic substitution**



**b) Hydrodefluorination**



**d) Defluorination via benzyne**

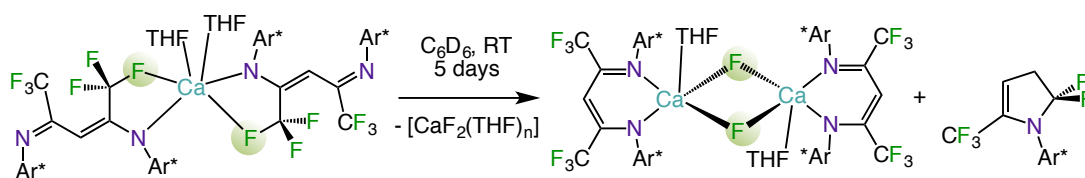


Scheme 5.4: C-F bond activation pathways.

Interestingly, the use of directing groups such as carbonyl, nitril, pyridyl, etc. facilitates the C-F bond activation of the fluorine atom in the *ortho* position in the presence of competing C-H bonds.<sup>[363–368]</sup>

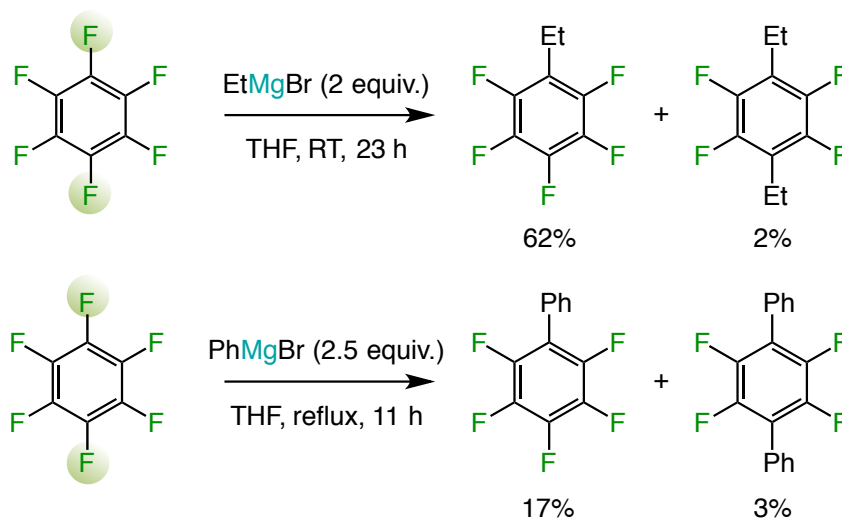
Typically, transition metals such as nickel, platinum, rhodium or palladium have been employed for C-F activation reactions,<sup>[349,362,369]</sup> although in the recent years, main group reagents such as boron, aluminium, silicon or magnesium complexes have also attracted particular interest.<sup>[370]</sup> To date, the most studied transformation is C-F borylation, however catalysts with rhodium or nickel are also required in these transformations.<sup>[348,371–373]</sup> Alternatively, reactions using low valent aluminium (I),<sup>[374,375]</sup> silicon (II),<sup>[376,377]</sup> germanium (II)<sup>[378]</sup> and Mg(I)<sup>[368]</sup> have recently emerged.<sup>[370]</sup>

Focusing on group 2 reagents, Hill has reported the C-F bond cleavage by solution decomposition of a calcium  $\beta$ -diketiminate complex with a N,F-chelated binding mode via an heteroleptic calcium fluoride intermediate (Scheme 5.5).<sup>[170]</sup>

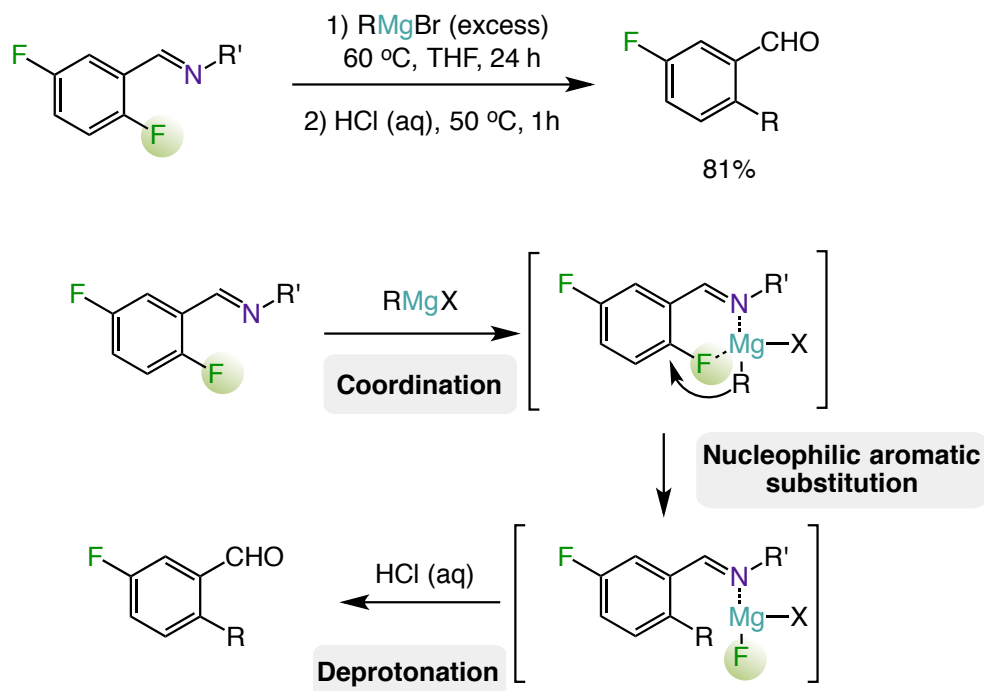


Scheme 5.5: C-F bond cleavage from the decomposition of a calcium  $\beta$ -diketiminate complex.<sup>[170]</sup>

Notably, C-F cleavage reactions can also be achieved using Grignard reagents in absence of metal catalysts.<sup>[368,379,380]</sup> In 1964 Harper reported C-F activation reactions by Grignard reagents.<sup>[359]</sup> Hexafluorobenzene is reacted with different Grignard reagents in THF at room temperature (except for PhMgBr that needs to be refluxed). Moderate yields (17 – 62%) are obtained for monosubstituted products and in some cases side products are also produced. In these studies it has been demonstrated that the reactivity of the Grignard reagents decreases following the order: allyl or benzyl > alkyl > aryl, and the use of alkyl substituents avoids the formation of side products (Scheme 5.6).

Scheme 5.6: C-F activation reactions by Grignard reagents.<sup>[359]</sup>

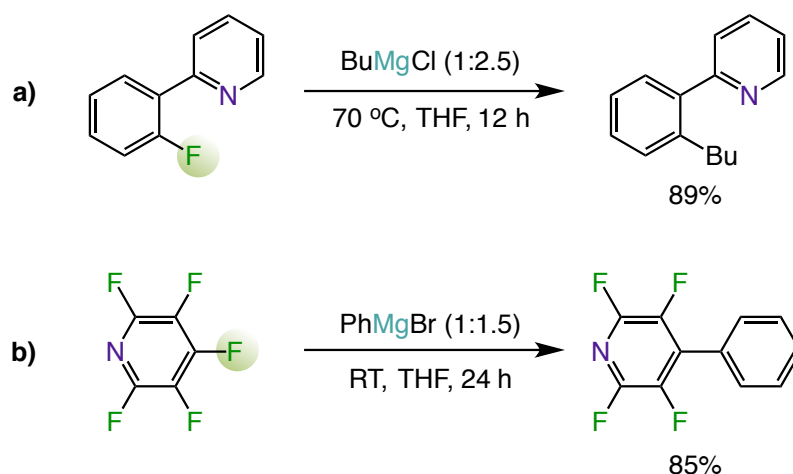
More recently in 2014, Li reported the *ortho*-alkylation and arylation of the C-F bonds of polyfluoroaryl imines. These compounds are treated with variety of Grignard reagents in excess at high temperatures (50 - 80 °C), obtaining high yields of the quenched products (49 - 93%) (Scheme 5.7).<sup>[368]</sup> A suggested mechanism is also reported where the imine substituent plays a key role in the reaction pathway, anchoring the Grignard reagent and facilitating the nucleophilic aromatic substitution (Scheme 5.7c).



Scheme 5.7: *Ortho*-alkylation of fluoroaryl imine with Grignard reagents and suggested mechanism.<sup>[368]</sup>

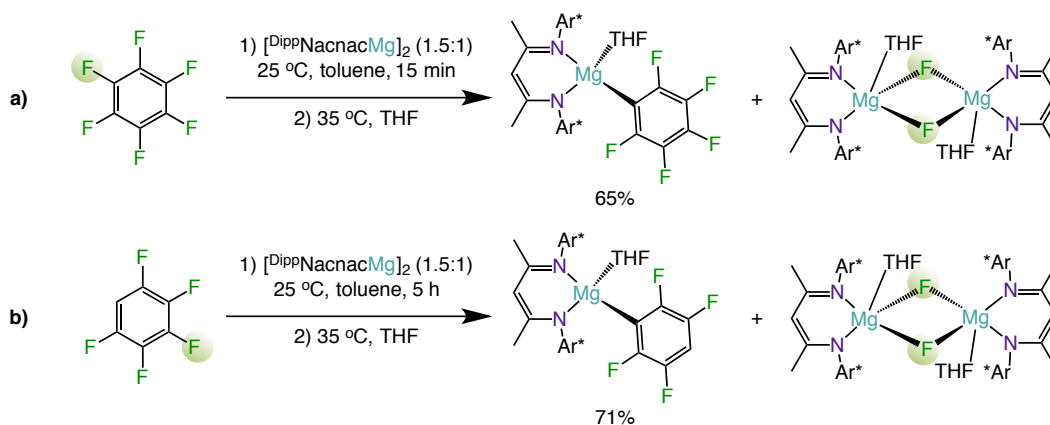
Recent studies have also demonstrate that cross-coupling reactions involving C-F bond cleavage can be performed with Grignard reagents in the absence of transition-metal complexes.<sup>[369,381,382]</sup> Cao has reported a new transition-metal free methodology for alkylation and arylation reactions of polyfluoroarenes via pyridine-directed regioselective nucleophilic aromatic substitution.<sup>[381]</sup> High isolated yields (83 to 90%) of the *ortho*-alkylation or phenylation were obtained by reacting Grignard reagents such as BuMgCl, EtMgCl, PhMgBr and MeMgCl (2.5 equiv.) with a variety of fluoropyridine derivatives in THF under reflux during 6-24 hours (Scheme 5.8a). Additionally, they suggest a possible reaction mechanism where the coordination of the magnesium to the pyridine nitrogen plays a key role to the nucleophilic aromatic substitution and formation of C-C bond. Furthermore, Li has shown that alkyl and aryl Grignard reagents can react with perfluorinated arenes at

room temperature (except for hexafluorobenzene where 60 °C is needed) in moderate to good yields (57 to 99%) in THF during 24 hours (Scheme 5.8b).<sup>[382]</sup> In these studies they found that an increase of the temperature reduces the selectivity and the yields of the coupled products, since homocoupled Grignard byproducts are obtained.



Scheme 5.8: a) Coupling reaction of 2-(2-fluorophenyl)pyridine with BuMgCl at 70 °C.<sup>[381]</sup> b) Coupling reaction of pentafluoropyridine with PhMgBr at room temperature.<sup>[382]</sup>

Remarkably, Crimmin has recently developed a new methodology using a  $\beta$ -diketiminato Mg(I) complex.<sup>[383]</sup> In these studies the C-F bonds of a series of fluoroarenes are added to the Mg(I)-Mg(I) bond of the  $[\text{Dipp}^{\text{NacnacMg}}]_2$  complex generating the corresponding magnesium fluoride and aryl products. (Scheme 5.9) These reactions can be executed at room temperature with a variety of perfluorinated and partially fluorinated arenes, in different periods of time depending on the fluoroarene reagent (15 min to 7 days).

Scheme 5.9: C-F bond functionalization with  $[\text{DippNacnacMg}]_2$  at room temperature.<sup>[383]</sup>

High NMR yields are obtained for these reactions (80 – 95%) and the isolation of the aryl complexes derived as a byproduct of the  $[\text{DippNacnacMgF}]$  can be recrystallized and isolated in a range of moderate yields (38 – 54%). Additionally, some of the magnesium fluoroaryl complexes have been crystallographically characterised, exhibiting a monomeric structure as shown in Figure 5.3.

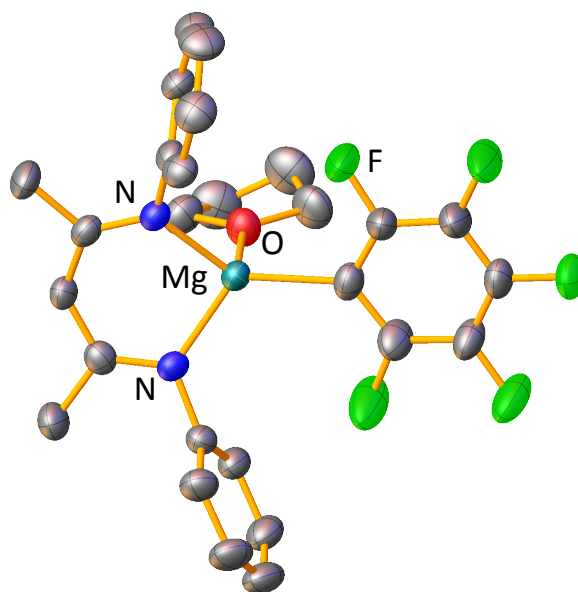
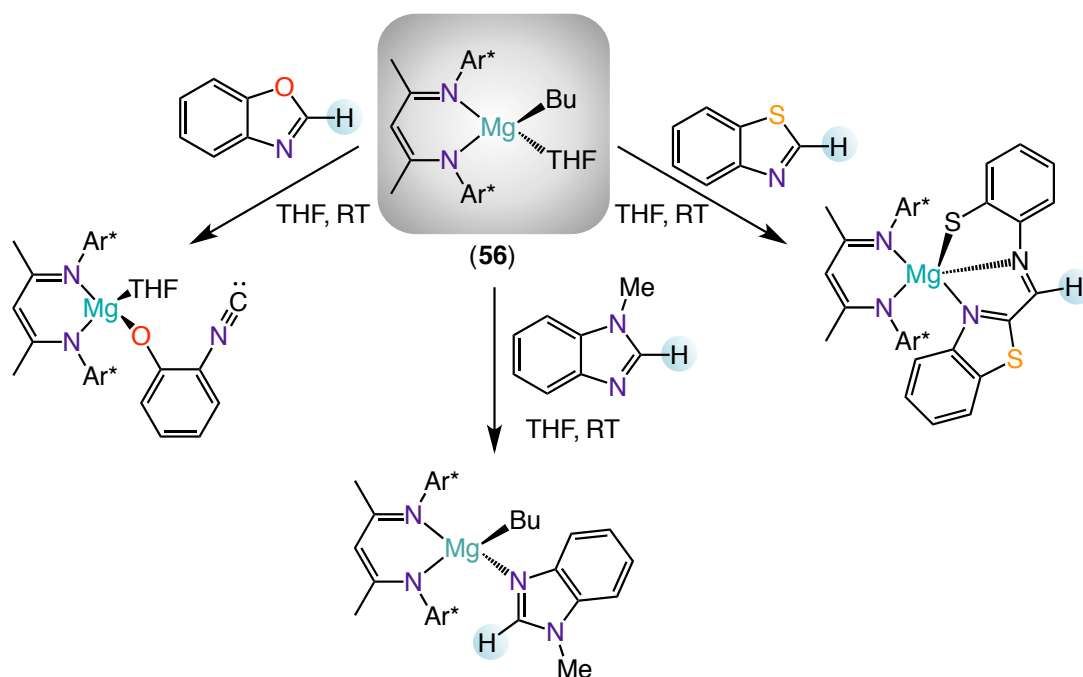


Figure 5.3: Molecular structure of magnesium fluoroaryl compound supported by  $\{\text{Dipp}\}\text{Nacnac}$  ligand with 50% probability displacement ellipsoids. All hydrogen atoms and  $^i\text{Pr}$  groups have been omitted for clarity.<sup>[383]</sup>

Encouraged by the work previously reported by our group illustrating the different behaviour of bases  $[\text{Dipp}\text{NacnacMg}(\text{TMP})]$  (**36**) and  $[\text{Dipp}\text{NacnacMg}(\text{THF})\text{Bu}]$  (**56**),<sup>[106]</sup> in this chapter we expand the substrate scope to a range of fluorinated aromatic molecules with a variety of fluorine substituents. For instance, the reactions of base **36** or **56** with benzoxazole led to deprotonation followed by ring opening in both cases (Scheme 4.5 and Scheme 5.10). In contrast, the reactions of **36** and **56** with the less acidic substrates benzothiazole and benzimidazole take place differently (Scheme 4.5 vs Scheme 5.10). In both cases, the  $[\text{Dipp}\text{NacnacMg}(\text{TMP})]$  (**36**) deprotonates the substrates in the C2 position forming dimeric structures (Scheme 4.5). The reaction of benzothiazole and  $[\text{Dipp}\text{NacnacMg}(\text{THF})\text{Bu}]$  (**56**) results to a cascade reaction where one equivalent of substrate is magnesiated by the base and a second non-deprotonated substrate is coordinated and undergoes to ring opening (Scheme 5.10). As well, when benzimidazole is treated with **56** the substrate coordinates to the Mg atom acting as a nitrogen donor (Scheme 5.10). In this



regard, the divergent behaviour of the bases can be justified by the enhanced kinetic activation by cleavage of the Mg-N(tmp) terminal bond in **36** vs Mg-C(Bu) bond of **56** (Scheme 4.5 vs Scheme 5.10).



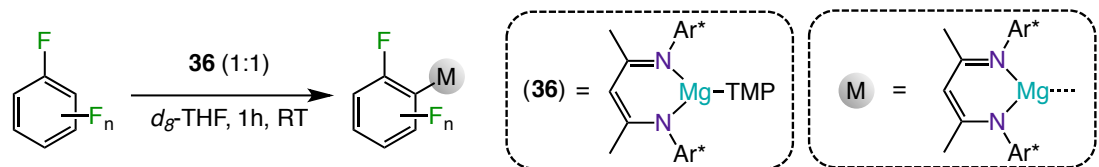
Scheme 5.10: Reactivity of benzoxazole, N-methyl benzimidazole and benzothiazole with base **56** at room temperature.<sup>[106]</sup>

Building on these studies, this chapter assesses the ability of [DippNacnacMg(TMP)] (**36**) and [DippNacnacMg(THF)Bu] (**56**) to functionalise fluoroaromatic molecules via C-F or C-H activation.

## 5.2 Results and Discussion

### 5.2.1 Magnesium of Fluorinated Aromatic Substrates

We studied the stoichiometric deprotonation reactions using [<sup>Dipp</sup>NacnacMg(TMP)] (**36**), of five fluorinated aromatic compounds with varying number of fluorine substituents in order to understand the behaviour of these compounds under the effect of the magnesium base. As mentioned above, the deprotonation of these fluoroaromatics have been previously reported by using bases such as organolithiums,<sup>[357]</sup> Grignard reagents<sup>[346,359]</sup> or bimetallic bases,<sup>[360]</sup> apart from the more usually used transition metals.<sup>[348,349,354–356]</sup> The metallation reaction of a family of fluorinated aromatic substrates with **36** (1:1) was first studied using NMR spectroscopy. All of the reactions were monitored by NMR spectroscopy and the yields were calculated using ferrocene as internal standard. A combination of <sup>19</sup>F and <sup>1</sup>H NMR, in particular the *CH* signal from the β-diketiminate fragment, were very diagnostic for the formation of the new compounds. Table 5.1 shows the corresponding yields obtained after 1 hour of reaction at room temperature relative to ferrocene.

Table 5.1: Reactivity of base **36** with fluorobenzene derivatives (1:1) after 1 hour, in  $d_8$ -THF at room temperature.

Entry	n	product	Yield (%) <sup>[a,b]</sup>
1	0		0 <sup>[c]</sup>
2	1		74 <sup>[d]</sup> (66)
3	2		78 <sup>[d]</sup> (43)
4	3		100 (66)
5	4		100 (56)

<sup>[a]</sup> Yields determined by  $^1\text{H}$  NMR using ferrocene as an internal standard after 1h at RT. <sup>[b]</sup> Isolated yields in parenthesis after 2h at RT. <sup>[c]</sup> No reaction after 24h heating at 80 °C. <sup>[d]</sup> Full conversion after 2h at RT.

Previously Schlosser has carried out interesting kinetic studies assessing the reactivity of fluoroarenes towards *sec*-BuLi, by analysing the relationship between the free activation energies and the gas-phase deprotonation energies in order to predict the relative rates of metallation.<sup>[351,353,384]</sup> According to these studies, we expected fluorobenzene to be the most difficult substrate to deprotonate ( $pK_a$  values: 36.8, 42.3 and 43.7).<sup>[228]</sup> In agreement, we found that after heating fluorobenzene and **36** for 24 hours at 80 °C, there is no reaction as evidenced by the presence of both starting materials in the  $^1\text{H}$  and  $^{19}\text{F}$  NMR spectra. Notably,  $^{19}\text{F}$  NMR monitoring of the reaction shows that the signal for fluorobenzene at -112.3 ppm does not change over time. We next attempted the reactions with 1,3-difluorobenzene and 1,3,5-trifluorobenzene. The reactions of **36** towards 1,3-difluorobenzene and 1,3,5-trifluorobenzene were also monitored by  $^1\text{H}$  and  $^{19}\text{F}$  NMR. Monomagnesiation of 1,3-difluorobenzene by **36** takes place at room temperature in 2 hours. However, after 1 hour of reaction at room temperature 74% of yield relative to ferrocene internal standard is observed. During the course of the reaction the diagnostic singlet of the  $\beta$ -diketiminato *CH* at 4.92 ppm begins to decrease, while at the same time a new signal belonging to the metallated compound **48** begins to emerge at 4.97 ppm. Two new sets of multiplets appeared, ranging from 6.85 to 6.93 ppm and from 6.42 to 6.38 ppm with a relative 2:1 ratio, which can be attributed to the *meta* and *para* protons of the *CH* aryl groups (Figure 5.4). Consistent with these  $^1\text{H}$  NMR studies, a new signal at -82.2 ppm in the  $^{19}\text{F}$  NMR confirmed the formation of the new product **48**, at a significant different chemical shift to that observed for free 1,3-difluorobenzene at 109.1 ppm.

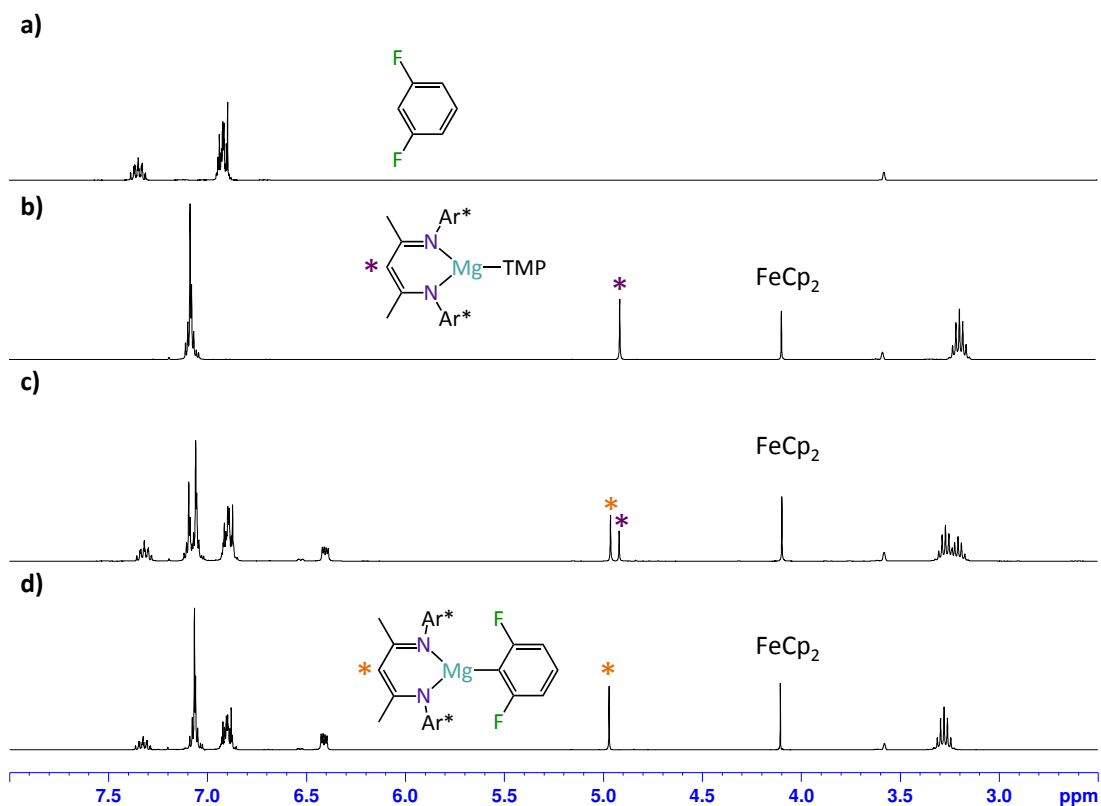
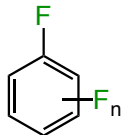
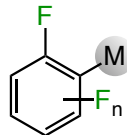


Figure 5.4: a)  $^1\text{H}$  NMR spectrum of 1,3-difluorobenzene in  $d_8$ -THF. b)  $^1\text{H}$  NMR spectrum of base **36** in  $d_8$ -THF. c)  $^1\text{H}$  NMR spectrum for the reaction of **36** (0.2 mmol) and 1 equivalent of  $\text{C}_6\text{H}_4\text{F}_2$  (0.2 mmol) at RT in  $d_8$ -THF after 30 min, mixture of **36** and **48**. d)  $^1\text{H}$  NMR spectrum for the reaction of **36** (0.2 mmol) and 1 equivalent of  $\text{C}_6\text{H}_4\text{F}_2$  (0.2 mmol) at RT in  $d_8$ -THF after 2 hours, formation of **48**.

Similarly, **36** effectively metallates 1,3,5-trifluorobenzene, 1,2,4,5-tetrafluorobenzene and pentafluorobenzene. The former in 2 hours at room temperature affording complete conversion of the starting materials to the metallated product **49**. The latter two substrates were quantitatively deprotonated in one hour at room temperature, affording the deprotonated products **50** and **51**. Metallation was confirmed by multinuclear NMR spectroscopy in a similar way to **48**. The most diagnostic singlet, the *CH* of the  $\beta$ -diketiminato fragment appeared in the  $^1\text{H}$  NMR (4.92 (**49**), 5.01 (**50**) and 5.02 ppm (**51**)). New resonances were observed in the  $^{19}\text{F}$  and  $^{13}\text{C}$  NMR corresponding to the formation

of the new magnesiated fluoroaromatic products. Table 5.2 shows a comparison of the different chemical shifts in the  $^{19}\text{F}$  NMR resonances between the fluorinated aromatic substrates and the magnesiated compounds **48-51**. When introducing the magnesium atom, the resonances corresponding to the fluorine atoms in the  $^{19}\text{F}$  NMR are more deshielded. Additionally, for the metallated complexes **49-51**, multiple new resonances have emerged illustrating the unsymmetrical fluorine atoms in the molecule.

Table 5.2: Comparison of  $^{19}\text{F}$  NMR in THF between the fluorinated substrates and the metallated species **48-51**.

		$\delta^{19}\text{F}$ NMR ( $d_8$ -THF)	
Entry	n	 $\delta^{19}\text{F}$ NMR	 $\delta^{19}\text{F}$ NMR
<b>1</b>	1	-109.1	-82.2
<b>2</b>	2	-106.7	-82.0 / -116
<b>3</b>	3	-139.0	-113.5 / -140.0
<b>4</b>	4	-140.3 / -156.4 / -164.3	-112.8 / -160.3 / -163.6

In order to estimate the constitution of the magnesiated species of compounds (**48** - **51**) in solution,  $^1\text{H}$  DOSY NMR studies were performed. In this case, the magnesiation reaction of 1,3,5-trifluorobenzene with **36** was studied using Stalke's DOSY methodology mentioned in Chapter 2.<sup>[200]</sup> Using this technique, the estimated size (in terms of molecular weight) of the species formed in the metallation reaction of 1,3,5-trifluorobenzene with **36** was obtained, corresponding to the solution

constitution of **49**. The experiment was carried out in 40 mM of a  $d_8$ -THF solution using tetramethylsilane (TMS) as internal standard (Figure 5.5).

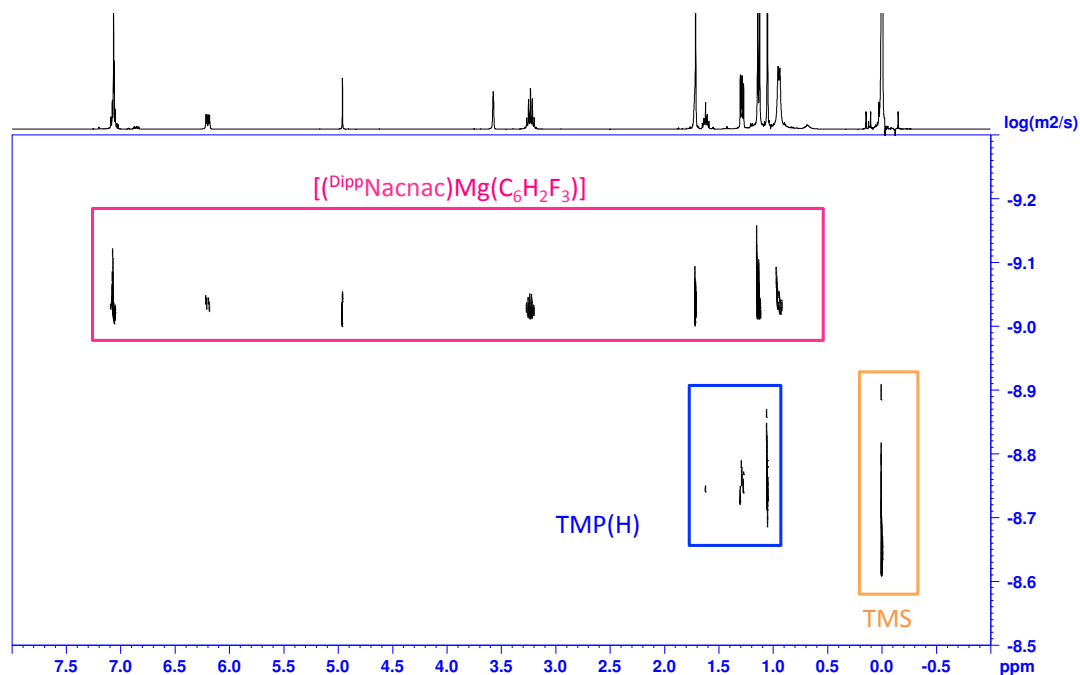


Figure 5.5:  $^1\text{H}$  DOSY NMR spectrum of the reaction of **49** in  $d_8$ -THF and TMS as internal standard.

The findings estimate a molecular weight of  $524 \text{ g mol}^{-1}$  with an error of 9% for the anticipated monomeric compound where the magnesium atom is coordinated to the  $\beta$ -diketimate fragment and to the terminal trifluorobenzene ligand (Table 5.3). A higher aggregation state, such as a dimeric unit as observed in some of the structures from Chapter 4 (**37**, **39** – **41** and **43**), would be inconsistent with the obtained results, as the error value would increase to 118%. Similarly, a THF solvated magnesium  $\beta$ -diketimate complex would increase the error value to 23%. A lower error of 16% would be obtained for an equilibrium of solvation/desolvation of THF, however, the error of the predicted MW in ECC DOSY method has a

maximum of  $\pm 9\%$  which would indicate that this equilibrium is not present in solution.

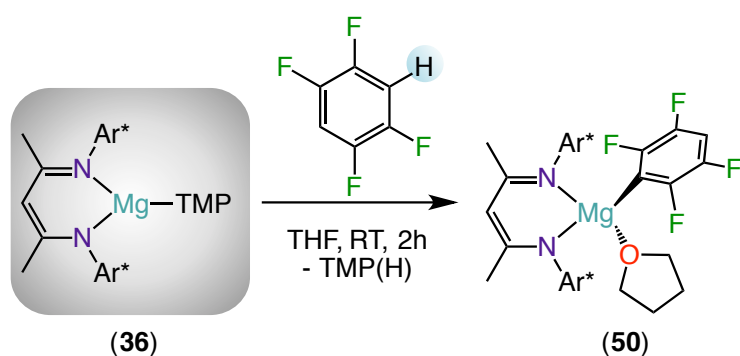
Table 5.3: Possible species formed in  $d_8$ -THF and the corresponding diffusion coefficient (D), molecular weights (MW) and errors  $MW_{\text{est}}=524 \text{ g mol}^{-1}$ .

Compound	D ( $\text{m}^2 \text{s}^{-1}$ )	MW <sub>calc</sub> ( $\text{g mol}^{-1}$ )	Error (%)
$[(^{\text{Dipp}}\text{Nacnac})\text{Mg}(\text{C}_6\text{H}_2\text{F}_3)]$ (a)	1.373E-9	572	9
$[(^{\text{Dipp}}\text{Nacnac})\text{Mg}(\text{C}_6\text{H}_2\text{F}_3)(\text{THF})]$ (b)	5.7503E-10	644	23
$[(^{\text{Dipp}}\text{Nacnac})\text{Mg}(\text{C}_6\text{H}_2\text{F}_3)_2]$ (c)	5.7503E-10	1144	118
(a) $\rightleftharpoons$ (b)	5.7503E-10	608	16

This experiment suggests that **49** in  $d_8$ -THF solution exists as a monomer without THF solvation (Table 5.3).

Structural insights on the molecular structure of these magnesiated intermediate were gained by performing an X-Ray crystallographic study on **50**. **36** was reacted with one equivalent of 1,2,4,5-tetrafluorobenzene during 2 hours at room temperature in THF. When reducing the solvent to 1 mL of THF, colourless crystals formed corresponding to compound  $[(^{\text{Dipp}}\text{Nacnac})\text{MgTHF}(\text{C}_6\text{HF}_4)]$  (**50**) that was isolated in a 75 % yield (Scheme 5.11).



Scheme 5.11: Reactivity of **36** with 1,2,4,5-tetrafluorobenzene.

The molecular structure of **50** confirmed the monometallation of 1,2,4,5-tetrafluorobenzene. Elemental analysis is in good agreement with the solid-state structure without THF molecule that is removed *in vacuo*. Additionally, the recorded NMR data ( $^1\text{H}$ ,  $^{13}\text{C}$  and  $^{19}\text{F}$ ) is also in good agreement with those of the control reactions in a J. Young's NMR tube (Table 5.1).

Few examples of monometallation of 1,2,4,5-tetrafluorobenzene have been structurally reported, where transition metals such as ruthenium,<sup>[385]</sup> rhodium,<sup>[386]</sup> gold<sup>[387]</sup> nickel<sup>[388]</sup> or platinum<sup>[389]</sup> are generally used in C-H activation processes. In these transition metal examples an excess of the fluorinated substrate is generally required and in some cases the reaction takes place at high temperatures or under irradiation. Additionally, rare examples of crystallographically characterized magnesium fluoroaryl compounds have been reported in the literature, although Crimmin has recently shown some  $\{(\text{Dipp})\text{Nacnac}\}\text{Mg}\}$  fluoroaryl examples obtained by C-F activation.<sup>[383]</sup>

X-Ray characterisation of compound **50** revealed a monomeric structure where, the  $\{(\text{Dipp})\text{Nacnac}\}\text{Mg}\}$  fragment coordinates to a terminal magnesiated tetrafluorobenzene moiety and is solvated by a molecule of the THF, a similar motif

to those described for compounds **39** and **44** in Chapter 4 for the metallation of benzofuran and 2-(2,4-difluorophenyl)pyridine (Figure 5.6). Interestingly, the monomeric arrangement of compound **44** is consistent with the results obtained in the solution studies by  $^1\text{H}$  DOSY NMR (Table 5.3), although a THF molecule is solvating in the solid state. Importantly, it represents the first magnesiated 1,2,4,5-tetrafluorobenzene intermediate structurally characterised.

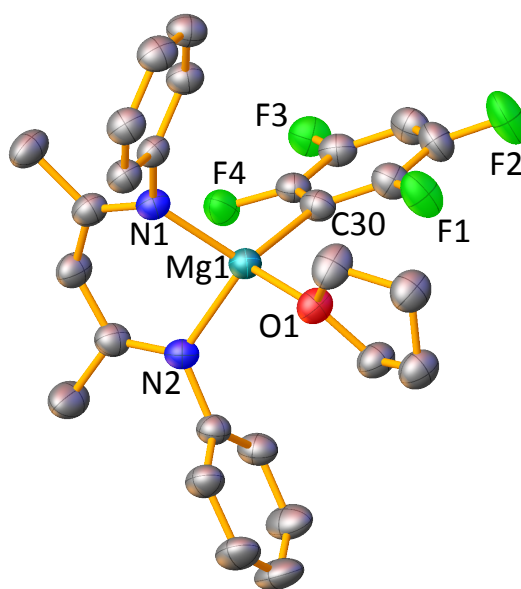


Figure 5.6: Molecular structure of **50** with 50% probability displacement ellipsoids. All hydrogen atoms and  $^i\text{Pr}$  groups have been omitted for clarity. Selected bond lengths ( $\text{\AA}$ ) and bond angles ( $^\circ$ ): Mg1-N1 2.0326(16), Mg1-N2 2.0414(16), Mg1-C30 2.1705(19), Mg1-O1 2.0286(14), N1-Mg1-N2 94.23(7), N1-Mg1-C30 116.68(7), N2-Mg1-C30 117.74(7), N1-Mg1-O1 114.95(6), N2-Mg1-O1 106.01(6), O1-Mg1-C30 106.75(7).

The Mg atom of compound **50** displays a distorted tetrahedral geometry (angles around Mg ranging from  $94.23(7)^\circ$  to  $117.74(7)^\circ$ ; mean  $109.07^\circ$ ). The Mg1-C30 distance [ $2.1705(19) \text{\AA}$ ] is between the range of the Mg-C distances of the similar  $\{(\text{Dipp})\text{Nacnac}\}\text{Mg}$  fluoroaryl examples reported by Crimmin [Mg-C bond lengths ranges from  $2.1381(15)$  to  $2.176(2) \text{\AA}$ ].<sup>[383]</sup> A close inspection of the Mg-F distance of

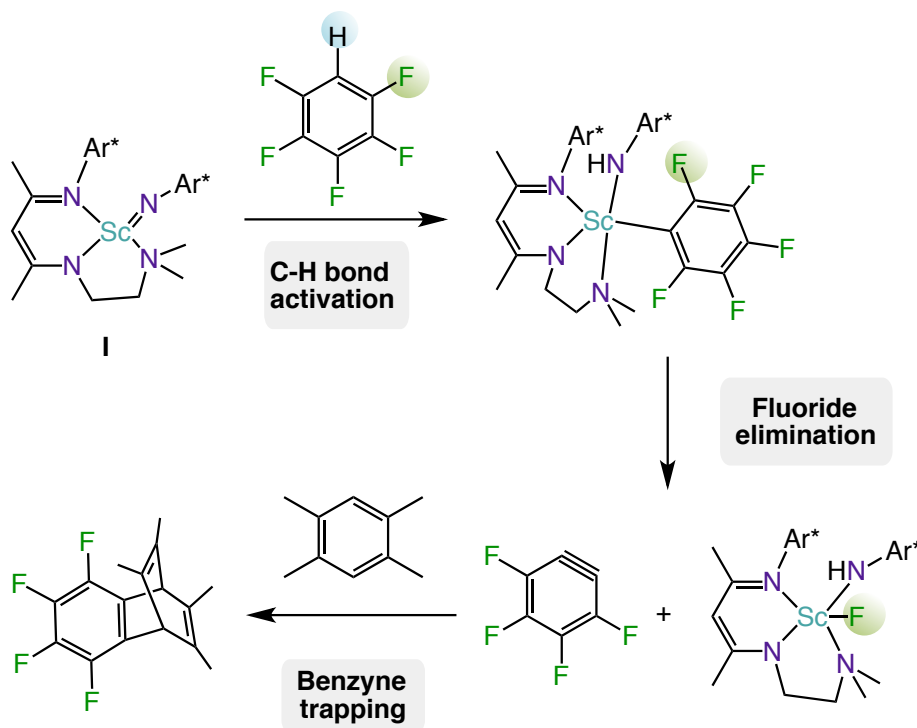
the *ortho*-fluorine atoms F1 and F4 indicates that F4 is slightly closer than F1 [Mg1-F1 (3.3214 Å) vs Mg1-F4 (3.2773 Å)], however this distance is still too long to suggest any type of long distance Mg...F interaction.

Compounds [(<sup>Dipp</sup>Nacnac)Mg(C<sub>6</sub>H<sub>3</sub>F<sub>2</sub>)] (**48**), [(<sup>Dipp</sup>Nacnac)Mg(C<sub>6</sub>H<sub>2</sub>F<sub>3</sub>)] (**49**) and [(<sup>Dipp</sup>Nacnac)Mg(C<sub>6</sub>F<sub>5</sub>)] (**51**) were prepared and isolated as solids in 66, 43 and 63% yields. The three compounds have been characterised by NMR and elemental analysis techniques. (See experimental section for details) The NMR experiments were performed in *d*<sub>8</sub>-THF and the spectrums recorded are in agreement with those obtained during the control reactions in Table 5.1. Notably, the crystal structure of compound [(<sup>Dipp</sup>Nacnac)Mg(C<sub>6</sub>F<sub>5</sub>)(THF)] (**51**) has previously been reported by Crimmin by reacting Mg(I) complex [(<sup>Dipp</sup>Nacnac)Mg]<sub>2</sub> with hexafluorobenzene (1:1.5) in toluene via C-F bond activation process (Scheme 5.9).<sup>[383]</sup> This structure of [(<sup>Dipp</sup>Nacnac)Mg(C<sub>6</sub>F<sub>5</sub>)(THF)] is displayed in Figure 5.3c and is analogous to that described for **50**.

In order to test the stability of complexes **48-51**, different temperature studies have been performed. Interestingly, NMR has revealed no decomposition when a solution of compound **49** in *d*<sub>8</sub>-THF was cooled down to -33 °C for 24 hours or heated to 80 °C for 3 days. Furthermore, base **36**, 1,3,5-trifluorobenzene and durene or 1,3-diphenylisobenzofuran (1:1:1) were reacted in a J. Young's NMR tube in *d*<sub>8</sub>-THF. <sup>1</sup>H and <sup>19</sup>F NMR experiments indicated that the only reaction observed is the metallation of 1,3,5-trifluorobenzene and the trapping reagents (durene or 1,3-diphenylbenzofuran) remained intact even on heating the tube to 80 °C for 5 hours. Remarkably, the β-diketimate anionic ligand plays a key role towards the stabilisation of the magnesiated fluoroderivatives complexes **48-51** protecting the new anion formed and preventing the formation of any decomposition product such as [<sup>Dipp</sup>NacnacMgF]<sub>2</sub>.

These results contrast with the recent work by Chen, who has reported the metallation of fluoroarenes using a scandium imido intermediate (compound **I** in Scheme 5.12) generated from the reaction between  $[\text{LSc}=\text{NAr}^*(\text{DMAP})]$  and 9-BBN (DMAP = 4-dimethylaminopyridine;  $\text{L} = [\text{MeC}(\text{NAr}^*)\text{CHC}(\text{Me})(\text{NCH}_2\text{CH}_2\text{NMe})]^-$  and 9-BBN = 9-borabicyclononane).

The scandium intermediate is supported with a bulky anionic ligand and contains a terminal imido group. When the scandium complex is reacted with a fluoroaromatic molecule such as fluorobenzene, 1,4-difluorobenzene, 1,3,5-trifluorobenzene or pentafluorobenzene, it undergoes fluoride elimination and benzyne formation (Scheme 5.12).<sup>[390]</sup>

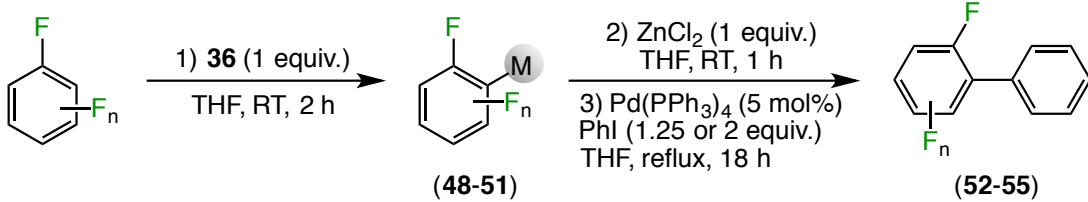
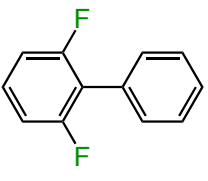
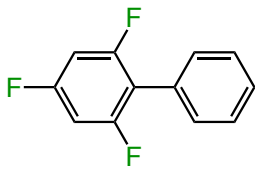


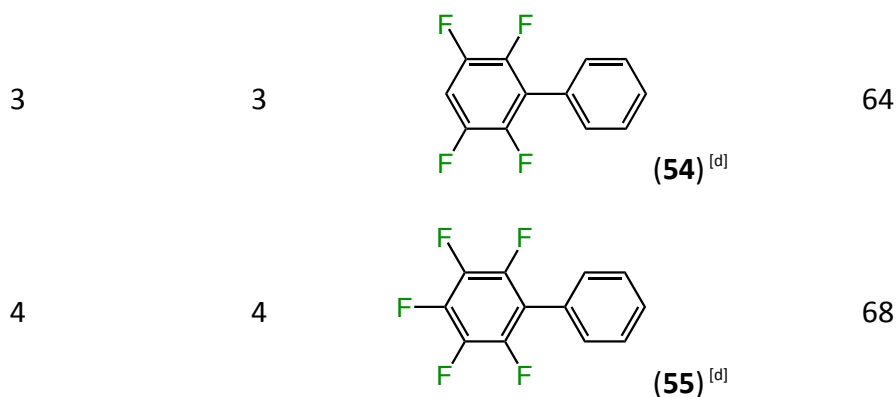
Scheme 5.12: C-H bond activation followed by fluoride elimination and benzyne trapping.<sup>[390]</sup>

DFT calculations of the dehydrofluorination reaction of pentafluorobenzene demonstrate that a first metallation reaction takes place followed by *ortho* C-F abstraction, which is more energetically demanding. The fluoride elimination is facilitated by the interaction between scandium and the fluorine that are in close proximity when the metallation takes place. As well, the trapping of the benzyne products were performed by adding durene, which undergoes a [2+2] cycloaddition with the benzyne species formed.

Exemplifying the synthetic utility of **48-51**, their reactivity was assessed in Negishi cross-coupling reactions with iodobenzene as an electrophilic coupling partner. The magnesiated fluoroaromatic complexes **48-51** were prepared in situ using the protocol outlined in Table 5.4, followed by transmetalation with ZnCl<sub>2</sub> (1 equiv.) and coupling with PhI (slight excess) catalysed by Pd(PPh<sub>3</sub>)<sub>4</sub> (5 mol%).

Table 5.4: Negishi cross-coupling reactions of **48-51** with iodobenzene.

			
Entry	n	product	Yield (%)
1	1	 <b>(52)</b> <sup>[a,b]</sup>	64 <sup>[c]</sup>
2	2	 <b>(53)</b> <sup>[a]</sup>	62

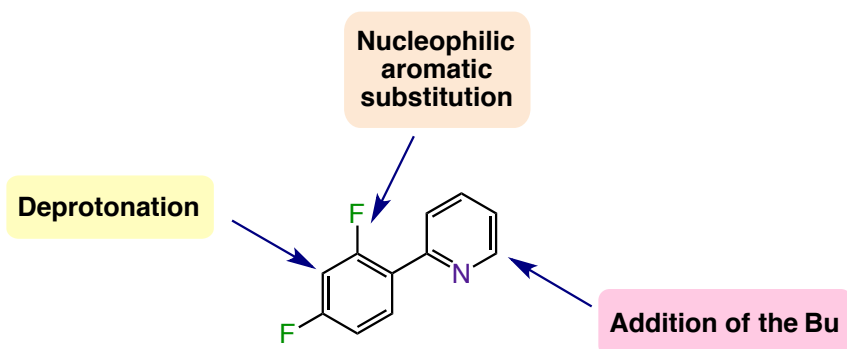


<sup>[a]</sup> 2 equiv. of IPh <sup>[b]</sup> 10 mol% Pd(PPh<sub>3</sub>)<sub>4</sub>. <sup>[c]</sup> Starting from isolated sample of **48**. <sup>[d]</sup> 1.25 equiv. of IPh.

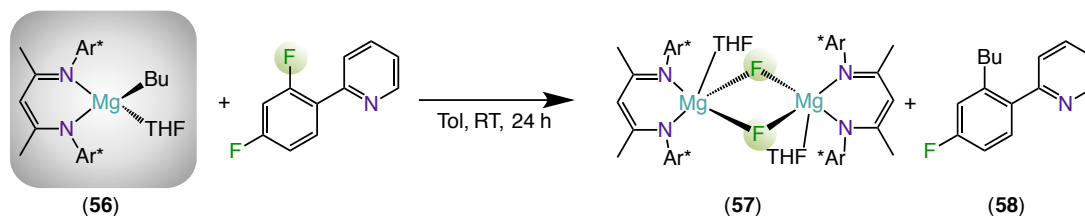
The different coupled complexes **52-55** have been purified and characterised by <sup>1</sup>H, <sup>13</sup>C and <sup>19</sup>F NMR experiments in CDCl<sub>3</sub> and are consistent with those reported in the literature.<sup>[391]</sup>

### 5.2.2 C-F Activation of Fluoroarenes Using [<sup>Dipp</sup>NacnacMg(THF)Bu] Base

We next studied the reaction of [<sup>Dipp</sup>NacnacMg(THF)Bu] (**56**) complex towards fluoroarene complexes, looking first at the reaction with 2-(2,4-difluorophenyl)pyridine, where different pathways can be predicted (Scheme 5.13).

Scheme 5.13: Possible reactions pathways when reacting **56** with 2-(2,4-difluorophenyl)pyridine.

The reaction between 2-(2,4-difluorophenyl)pyridine and  $[\text{Dipp}^{\text{Nacnac}}\text{Mg}(\text{THF})\text{Bu}]$  (**56**) (1:1) at room temperature, in THF does not lead to any product after 1 day and the starting materials are recovered. Contrastingly, when refluxing this mixture, a precipitate of colourless crystals is formed at the bottom of the Schlenk after 24 hours of reaction. Analysis of the crystalline solid by X-Ray and NMR experiments determined the formation of  $[\text{Dipp}^{\text{Nacnac}}\text{MgF}(\text{THF})]_2$  (**57**). Additionally, the filtrate solution was also analysed by NMR experiments indicating the formation of 2-(2-butyl-4-fluorophenyl)pyridine (**58**). However, this reaction is not complete and the presence of starting materials is observed. Further studies in order to optimise the reaction conditions indicate that 92% of compound **58** is achieved in milder reaction conditions (room temperature in 24 hours) when using toluene as a solvent (Scheme 5.14).

Scheme 5.14: Reactivity of **56** with 2-(2,4-difluorophenyl)pyridine.

This solvent effect could be related to a competitive coordination to the magnesium between the THF and the substrate, which would not occur when using toluene as a solvent.

Crystallographic studies and NMR spectroscopy confirmed the formation of products **57** and **58**. The crystalline solid was filtered and dissolved in  $C_6D_6$ .  $^{19}F$  NMR displays the diagnostic signal at -187.8 ppm corresponding to  $[^{Dipp}NacnacMgF(THF)]_2$  which differs drastically from the  $^{19}F$  NMR resonances of the 2-(2,4-difluorophenyl)pyridine substrate (-109.5 and -112.6) or the metallated product  $[(^{Dipp}Nacnac)MgTHF(C_{11}H_6F_2N)]$  (**44**) (-77.6 and -82.0 ppm) (Figure 5.7).

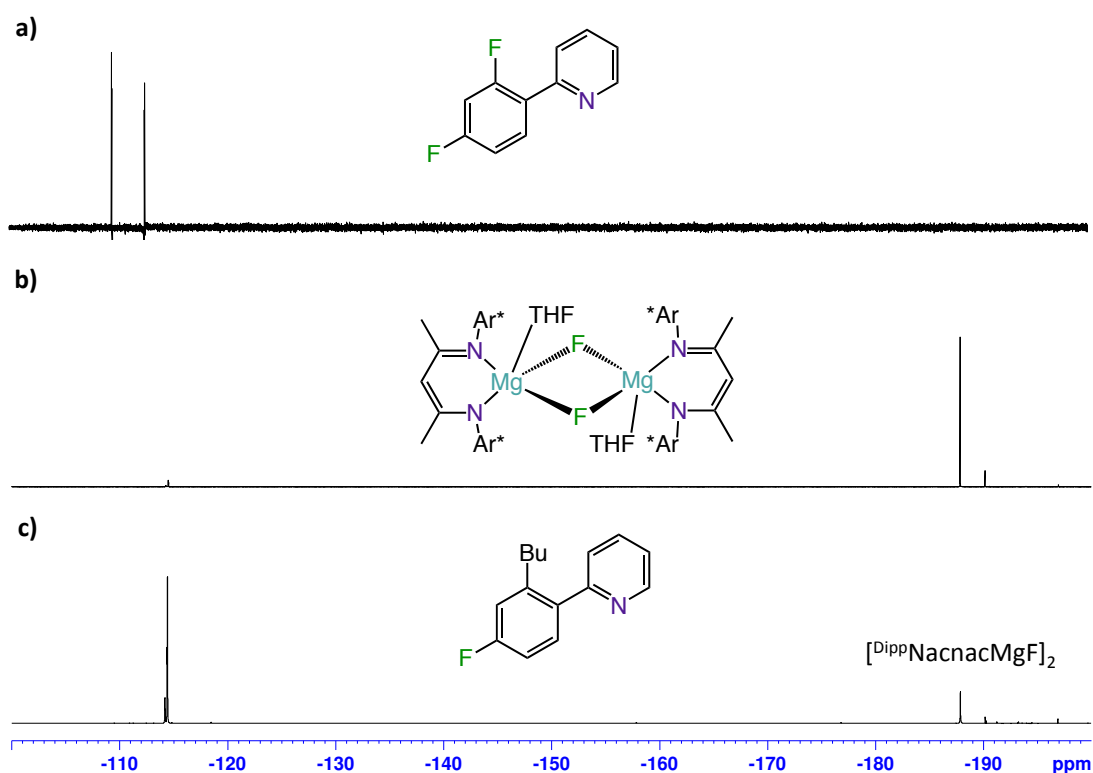


Figure 5.7: a)  $^{19}F$  NMR spectrum of 2-(2,4-difluorophenyl)pyridine in  $C_6D_6$ . b)  $^{19}F$  NMR spectrum of **57** in  $C_6D_6$ . c)  $^{19}F$  NMR spectrum of **58** in  $C_6D_6$  (presence of an impurity of **57**).



In addition, the diagnostic signals of the CH of the {<sup>Dipp</sup>Nacnac} ligand backbone and the multiplets of the <sup>i</sup>Pr groups have shifted to 4.83 and 3.01 ppm, compared to 4.80 and 3.30 ppm for base **56** in <sup>1</sup>H NMR. X-Ray crystallography also confirmed the formation of **57**, which agrees with the one reported by Roesky (Figure 5.8).<sup>[392]</sup>

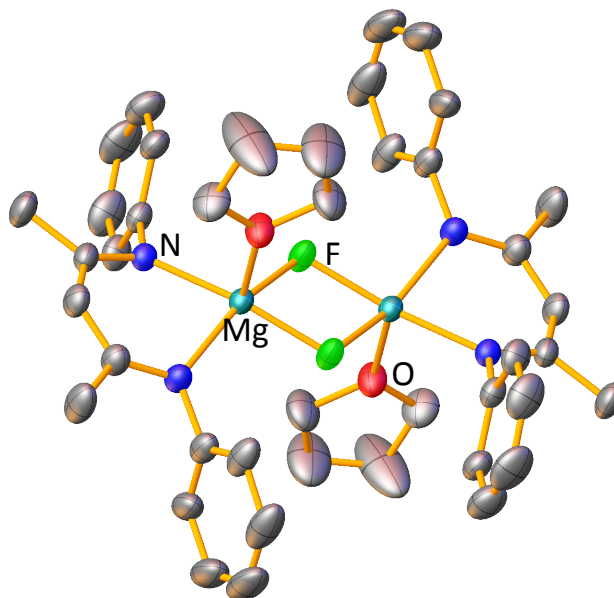
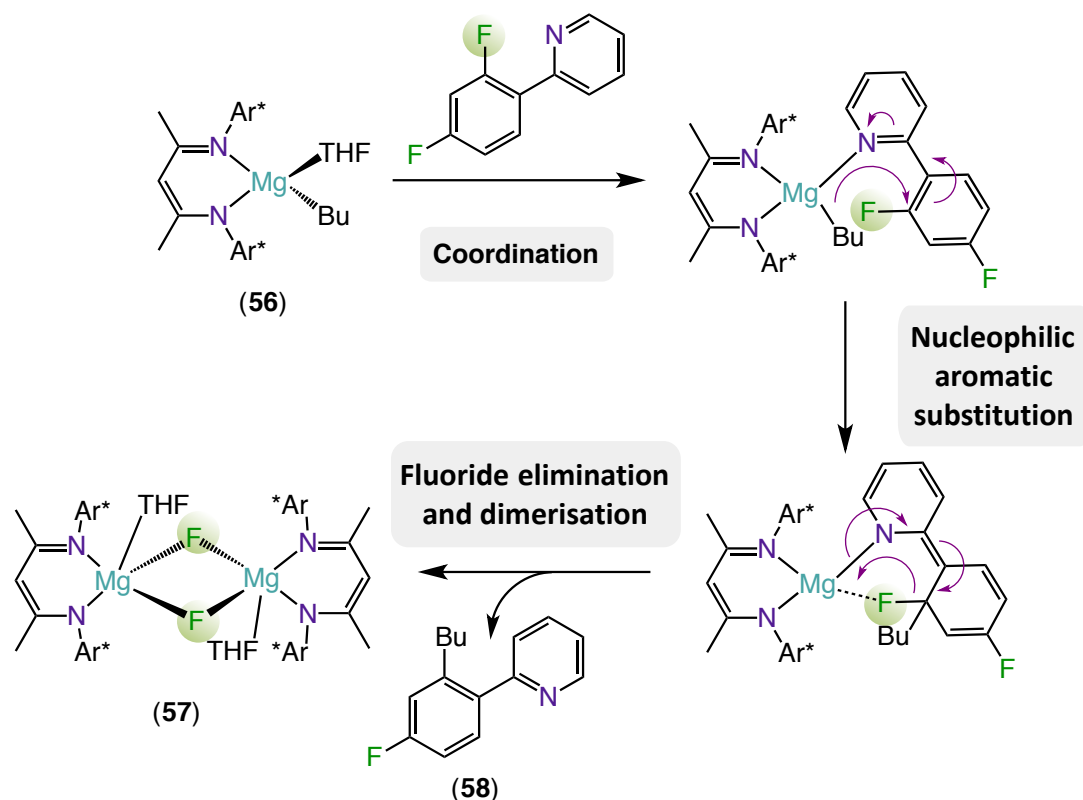


Figure 5.8: Molecular structure of **57** with 50% probability displacement ellipsoids. All hydrogen atoms and <sup>i</sup>Pr groups have been omitted for clarity.<sup>[392]</sup>

The filtrate of the reaction was also treated. Removal of solvent *in vacuo* followed by addition of C<sub>6</sub>D<sub>6</sub> and 9.5 mg of ferrocene (internal standard) provided a yield of 92% for product **58**, calculated by integration relative to the internal standard in the <sup>1</sup>H NMR. Organic workup and column chromatography purification followed by <sup>1</sup>H, <sup>13</sup>C and <sup>19</sup>F NMR experiments in CDCl<sub>3</sub>, confirmed the formation of 2-(2-butyl-4-fluorophenyl)pyridine (**58**) by comparison with published data.<sup>[381]</sup>

As illustrated in Scheme 5.8, alkylation of a variety of polyfluoroarenes has been previously achieved from the reaction of 2-(2,4-difluorophenyl)pyridine and Grignard reagents such as BuMgCl (2.5 equivalents) in THF under reflux conditions

(6 to 24 hours), where the *ortho*-position of the pyridine group plays a key role in the suggested mechanism of the reaction and favours the nucleophilic aromatic substitution to the fluorine in *ortho* position.<sup>[381]</sup> A similar process could be in operation for **58** (Scheme 5.15).

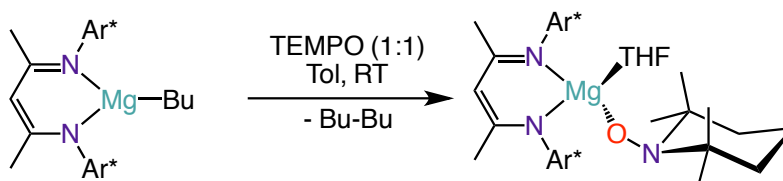


Scheme 5.15: Suggested mechanism for the formation of **58**.

Alternatively, a radical pathway could also be in operation. In order to assess if the reaction is inhibited when using the TEMPO (2,2,6,6-tetramethyl-1-piperidinyloxy) radical, base **56**, 2-(2,4-difluorophenyl)pyridine and TEMPO were added in a J. Young's NMR tube in toluene. After 24 hours at room temperature colourless crystals were formed at the bottom of the tube which were filtered and characterised by NMR studies confirming the formation of  $[\text{Dipp}^{\text{NacnacMgF}}(\text{THF})_2]_2$

(**57**). Additionally, the analysis of the filtrate by NMR also indicates the formation of 2-(2-butyl-4-fluorophenyl)pyridine (**58**). These results indicate that addition of radical scavenger TEMPO does not affect the outcome of the reaction affording **57** and **58** in the same yields as describe above, which supports that this reaction does not involve the formation of radical species.

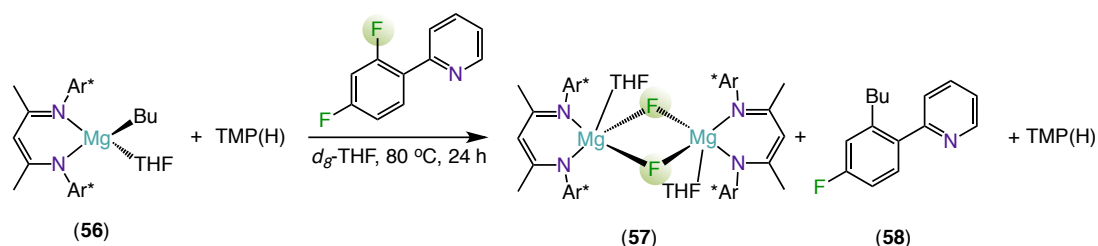
Hill has shown that when [<sup>Dipp</sup>NacnacMg(Bu)] is reacted with the nitroxyl radical TEMPO a new compound [<sup>Dipp</sup>NacnacMg(TEMPO)THF] is obtained, alongside octane (Scheme 5.16).<sup>[393]</sup>



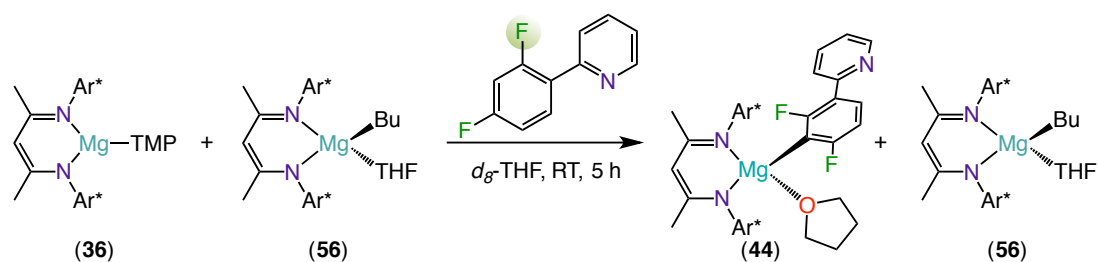
Scheme 5.16: Reaction of [<sup>Dipp</sup>NacnacMg(Bu)] with TEMPO radical.<sup>[393]</sup>

Interestingly, recent studies by Hill have shown that the butyl complex **56** reacts at room temperature in toluene with TEMPO to form the tempoxide complex depicted in Scheme 5.16 with the subsequent elimination of octane. The presence of this tempoxide complex [<sup>Dipp</sup>NacnacMg(TEMPO)THF] could not be detected by NMR analysis of the crude product from the reaction of **56** with 2-(2,4-difluorophenyl)pyridine in the presence of TEMPO, indicating that under the conditions investigated **56** reacts preferentially with the aromatic substrate than with the radical scavenger.

In order further probe the reactivity of the base **56** under different conditions, two additional reactions were performed. To investigate a possible ligand exchange reaction, base **56** was reacted with TMP(H) and 2-(2,4-difluorophenyl)pyridine in equimolar amounts in a J. Young's NMR tube in *d*<sub>8</sub>-THF (Scheme 5.17).

Scheme 5.17: Formation of **57** and **58** in the presence of TMP(H).

$^1\text{H}$  and  $^{19}\text{F}$  NMR experiments indicate that no reaction occurred after 24 hours at room temperature. Heating the J. Young's NMR tube to 80 °C during 24 hours leads to a precipitate of colourless crystals, which is attributed to the formation of  $[\text{Dipp}^{\text{Ni}}\text{NacnacMgF}(\text{THF})]_2$  (**57**) as indicated by the resonance displayed at 188.9 ppm in the  $^{19}\text{F}$  NMR spectrum and without detecting formation of the metallation product **44**. This indicates that the butyl group does not exchange with the TMP ligand, otherwise metallated product would have been observed. A second, competition experiment was also performed between an equimolar mixture of base **36** and **56** with 2-(2,4-difluorophenyl)pyridine in a J. Young's NMR tube in  $d_8$ -THF (Scheme 5.18).

Scheme 5.18: Formation of **44** when reacting **36** and **56** with 2-(2,4-difluorophenyl)pyridine in  $d_8$ -THF at room temperature.

NMR spectroscopy analysis indicate the preferential formation of the metallated product  $[(\text{Dipp}^{\text{Ni}}\text{Nacnac})\text{MgTHF}(\text{C}_{11}\text{H}_6\text{F}_2\text{N})]$  (**44**) occurs at room temperature. The

remaining resonances in the  $^1\text{H}$  NMR spectrum correspond to unreacted butyl base **56**.

Preliminary studies with the more challenging hexafluorobenzene and magnesium complexes **36** and **56** have been examined in a J. Young's NMR tube. Hexafluorobenzene was treated with base **36** (1:1) in  $d_8$ -THF. Reaction control by NMR ( $^1\text{H}$  and  $^{19}\text{F}$ ) experiments confirmed that no reaction occurs even heating at 80 °C during 24 hours and the singlet at 164.6 ppm corresponding to hexafluorobenzene remains intact. When hexafluorobenzene is reacted with butyl complex **56**, colourless crystals at the bottom of the tube were formed and a new resonance at 188.9 ppm in the  $^{19}\text{F}$  NMR is displayed corresponding to the formation of compound  $[\text{Dipp}^{\text{NacnacMgF}}(\text{THF})]_2$  (**57**). In this case, no reaction occurs using  $d_8$ -Tol, even heating 80 °C during 24 hours. Further experiments need to be performed in order to investigate the other products produced in this reaction and optimise the reaction conditions.

### 5.3 Conclusions

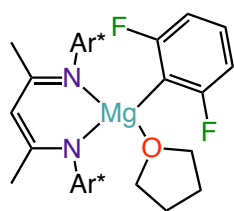
This chapter illustrated the different reactivities assessed by the monomeric bases  $[\text{DippNacnacMg(TMP)}]$  (**36**) and  $[\text{DippNacnacMg(THF)Bu}]$  (**56**) when reacted with a variety of fluoroaromatic molecules. These studies clearly demonstrated that the base **36** can regioselective deprotonate 1,3-difluorobenzene, 1,3,5-trifluorobenzene, 1,2,4,5-tetrafluorobenzene and pentafluorobenzene quantitatively at room temperature with no presence of side-products. Furthermore, the sensitive fluoroaryl anions can be trapped and stabilised by the sterically demanding  $\beta$ -diketiminato ligand preventing any further benzyne formation reaction via  $[\text{DippNacnacMgF}]$  elimination, as well as being thermally stable at elevated temperatures (80 °C). Therefore, the stabilization of the magnesiated compounds **48** – **51** has been accomplished and X-Ray crystallography studies confirmed that compound **50** exists as a monomer in the solid state and  $^1\text{H}$  DOSY NMR studies suggest that the magnesiated species also exists as monomers in solution. Preliminary reactivity studies have also illustrated that these compounds can undergo to Negishi cross-coupling with iodobenzene.

When employing the kinetically more retarded butyl base **56** with 2-(2,4-difluorophenyl)pyridine, nucleophilic aromatic substitution occurs affording compounds  $[\text{DippNacnacMgF(THF)}]_2$  (**57**) and 2-(2-butyl-4-fluorophenyl)pyridine (**58**). This dramatic change of reactivity clearly contrasts with the deprotonation product obtained by **36**.

## 5.4 Experimental

### 5.4.1 Synthesis of Active Species

- Synthesis of [(<sup>Dipp</sup>Nacnac)Mg(C<sub>6</sub>H<sub>3</sub>F<sub>2</sub>)(THF)] (**48**)



To a solution of **36** (0.56 g, 1 mmol) in THF (5 mL), 1,3-difluorobenzene (0.1 mL, 1 mmol) was added. The yellow solution was stirred for 2 hours at room temperature. The solvent was concentrated to 1 mL and 2 mL of hexane were added. The resulting yellow solution was stored at -15 °C. After 48 hours a white solid precipitated, and was isolated and placed in a glovebox (0.417 g, 66%).

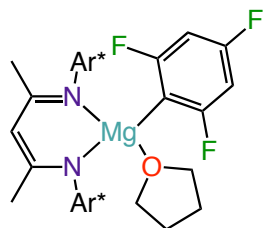
<sup>1</sup>H NMR (400.13 MHz, *d*<sub>8</sub>-THF, 298 K) δ 7.06 [s, 6H, Ar\* of <sup>Dipp</sup>Nacnac], 6.89 [q, 1H, *J* = 7.6 Hz, C<sub>6</sub>H<sub>3</sub>F<sub>2</sub>], 6.42-6.38 [dd, 2H *J* = 3.6 Hz, *J* = 8.4 Hz, C<sub>6</sub>H<sub>3</sub>F<sub>2</sub>], 4.97 [s, 1H, CH of <sup>Dipp</sup>Nacnac], 3.27 [m, 4H, CH, <sup>i</sup>Pr, Ar\* of <sup>Dipp</sup>Nacnac], 1.72 [s, 6H, CH<sub>3</sub> of <sup>Dipp</sup>Nacnac], 1.33-1.27 [m, 4H, CH, <sup>i</sup>Pr, Ar\* of <sup>Dipp</sup>Nacnac], 1.15-1.10 [d, 12 H, *J* = 4, CH<sub>3</sub>, <sup>i</sup>Pr, Ar\* of <sup>Dipp</sup>Nacnac], 0.98-0.90 [d, 12H, *J* = 8 CH<sub>3</sub>, <sup>i</sup>Pr, Ar\* of <sup>Dipp</sup>Nacnac].

<sup>13</sup>C NMR {<sup>1</sup>H} (100.62 MHz, *d*<sub>8</sub>-THF, 298 K) δ 173.5-170.9 [dd, *J* = 230, *J* = 30, C<sub>6</sub>H<sub>3</sub>F<sub>2</sub>], 168.9 [C<sub>q</sub>, CHC(Me) of <sup>Dipp</sup>Nacnac], 146.1 [C, Ar\* of <sup>Dipp</sup>Nacnac], 143.1 [C, Ar\* of <sup>Dipp</sup>Nacnac], 128.7 [t, *J* = 8, C<sub>6</sub>H<sub>3</sub>F<sub>2</sub>], 125.3 [CH, Ar\* of <sup>Dipp</sup>Nacnac], 123.9 [CH, Ar\* of <sup>Dipp</sup>Nacnac], 108.9-108.5 [dd, *J* = 35, *J* = 4, C<sub>6</sub>H<sub>3</sub>F<sub>2</sub>], 95.3 [CH of <sup>Dipp</sup>Nacnac], 49.9 [CH, <sup>i</sup>Pr, Ar\* of <sup>Dipp</sup>Nacnac], 28.4 [CH, <sup>i</sup>Pr, Ar\* of <sup>Dipp</sup>Nacnac], 24.6 [CH<sub>3</sub>, <sup>i</sup>Pr, Ar\* of <sup>Dipp</sup>Nacnac], 24.5 [CH<sub>3</sub>, <sup>i</sup>Pr, Ar\* of <sup>Dipp</sup>Nacnac], 19.1 [CH<sub>3</sub>, <sup>i</sup>Pr, Ar\* of <sup>Dipp</sup>Nacnac].

<sup>19</sup>F NMR {<sup>1</sup>H} (376.40 MHz, *d*<sub>8</sub>-THF, 298 K) δ -82.2 [s, C<sub>6</sub>H<sub>3</sub>F<sub>2</sub>].

**Elemental analysis:** (C<sub>39</sub>H<sub>52</sub>F<sub>2</sub>MgN<sub>2</sub>O) *Calculated:* C: 74.69 % H: 8.36 % N: 4.47 %.  
*Found:* C: 74.55 % H: 8.26 % N: 4.55 %.

• **Synthesis of [(<sup>Dipp</sup>Nacnac)Mg(C<sub>6</sub>H<sub>2</sub>F<sub>3</sub>)(THF)] (49)**



To a solution of **36** (0.28 g, 0.5 mmol) in THF (5 mL), 1,3,5-trifluorobenzene (0.05 mL, 0.5 mmol) was added. The yellow solution was stirred for 2 hours at room temperature. The solvent was removed and 5 mL of hexane were added obtaining a yellow solution that was stored at -70 °C. After 48 hours a white solid precipitated, and was isolated and placed in a glovebox (0.14 g, 43%).

**<sup>1</sup>H NMR (400.13 MHz, *d*<sub>8</sub>-THF, 298 K)** δ 7.07 [s, 6H, Ar\* of <sup>Dipp</sup>Nacnac] 6.22-6.19 [dd, *J* = 9.8, *J* = 3.4 Hz, 2H, C<sub>6</sub>H<sub>2</sub>F<sub>3</sub>], 4.97 [s, 1H, CH of <sup>Dipp</sup>Nacnac], 3.62 [m, 4H, OCH<sub>2</sub>, THF], 3.29-3.19 [sept, 4H, *J* = 6.8 Hz, CH, <sup>*i*</sup>Pr, Ar\* of <sup>Dipp</sup>Nacnac], 1.77 [m, 4H, CH<sub>2</sub>, THF], 1.72 [s, 6H, CH<sub>3</sub> of <sup>Dipp</sup>Nacnac], 1.15-1.13 [d, 12H, *J* = 6.8 Hz, CH<sub>3</sub>, <sup>*i*</sup>Pr, Ar\* of <sup>Dipp</sup>Nacnac], 0.96-0.95 [d, 12H, *J* = 5.9 Hz, CH<sub>3</sub>, <sup>*i*</sup>Pr, Ar\* of <sup>Dipp</sup>Nacnac].

**<sup>13</sup>C NMR {<sup>1</sup>H} (100.62 MHz, *d*<sub>8</sub>-THF, 298 K)** 169.1 [C<sub>q</sub>, CHC(Me) of <sup>Dipp</sup>Nacnac], 146.0 [CH, Ar\* of <sup>Dipp</sup>Nacnac], 143.1 [CH, Ar\* of <sup>Dipp</sup>Nacnac], 125.4 [CH, Ar\* of <sup>Dipp</sup>Nacnac], 124.0 [CH, Ar\* of <sup>Dipp</sup>Nacnac], 95.3 [CH of <sup>Dipp</sup>Nacnac], 68.0 [OCH<sub>2</sub>, THF], 28.4 [CH, <sup>*i*</sup>Pr, Ar\* of <sup>Dipp</sup>Nacnac], 26.3 [CH<sub>2</sub>, THF], 24.6 [CH<sub>3</sub>, <sup>*i*</sup>Pr, Ar\* of <sup>Dipp</sup>Nacnac], 24.4 [CH<sub>3</sub>, <sup>*i*</sup>Pr, Ar\* of <sup>Dipp</sup>Nacnac] (C<sub>q</sub> of C-Mg and C<sub>6</sub>H<sub>2</sub>F<sub>3</sub> were not possible to assign).

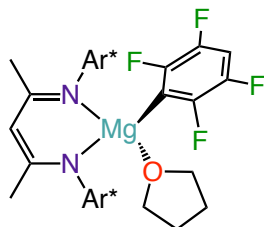
**<sup>19</sup>F NMR {<sup>1</sup>H} (376.40 MHz, *d*<sub>8</sub>-THF, 298 K)** δ -82.0 [br, 2F, C<sub>6</sub>H<sub>2</sub>F<sub>3</sub>], -116 [s, 1F, C<sub>6</sub>H<sub>2</sub>F<sub>3</sub>].

**Elemental analysis:** (C<sub>35</sub>H<sub>43</sub>F<sub>3</sub>MgN<sub>2</sub>) *Calculated:* C: 72.61 % H: 7.97 % N: 4.34 %.

*Found:* C: 72.38 % H: 8.42 % N: 5.47 %.



• **Synthesis of [(<sup>Dipp</sup>Nacnac)Mg(C<sub>6</sub>HF<sub>4</sub>)(THF)] (50)**



To a solution of **36** (0.28 g, 0.5 mmol) in THF (5 mL), 1,2,4,5-tetrafluorobenzene (0.056 mL, 0.5 mmol) was added. The yellow solution was stirred for 1 hour at room temperature. The solvent was reduced to 1 mL of THF and the solution was stored at -70 °C. After 48 hours a crop of colorless crystals

yielded the title compound as colourless crystals. In order to obtain a good yield of the compound, after 1 hour of reaction the solvent was removed and 5 mL of hexane were added. A white solid precipitated, and was isolated and placed in a glovebox (0.22 g, 66%).

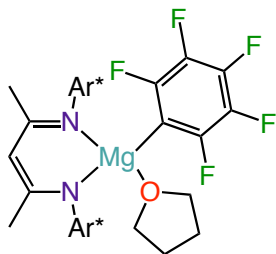
<sup>1</sup>H NMR (400.13 MHz, *d*<sub>8</sub>-THF, 298 K) δ 7.10 [s, 6H, Ar\* of <sup>Dipp</sup>Nacnac] 6.78-6.70 [m, 1H, C<sub>6</sub>HF<sub>4</sub>], 5.01 [s, 1H, CH of <sup>Dipp</sup>Nacnac], 3.62 [m, 4H, OCH<sub>2</sub>, THF], 3.28-2.18 [sept, 4H, *J* = 6.8 Hz, CH, <sup>i</sup>Pr, Ar\* of <sup>Dipp</sup>Nacnac], 1.77 [m, 4H, CH<sub>2</sub>, THF], 1.74 [s, 6H, CH<sub>3</sub> of <sup>Dipp</sup>Nacnac], 1.15-1.14 [d, 12 H, *J* = 6.8 Hz, CH<sub>3</sub>, <sup>i</sup>Pr, Ar\* of <sup>Dipp</sup>Nacnac], 0.96-0.94 [d, 12H, *J* = 6.4 Hz, CH<sub>3</sub>, <sup>i</sup>Pr, Ar\* of <sup>Dipp</sup>Nacnac].

<sup>13</sup>C NMR {<sup>1</sup>H} (100.62 MHz, *d*<sub>8</sub>-THF, 298 K) δ 169.4 [C<sub>q</sub>, CHC(Me) of <sup>Dipp</sup>Nacnac], 145.9 [C, Ar\*], 143.2 [C, Ar\*], 125.6 [CH, Ar\* of <sup>Dipp</sup>Nacnac], 124.2 [CH, Ar\* of <sup>Dipp</sup>Nacnac], 104.0 [C<sub>6</sub>HF<sub>4</sub>], 95.5 [CH of <sup>Dipp</sup>Nacnac], 28.4 [CH, <sup>i</sup>Pr, Ar\* of <sup>Dipp</sup>Nacnac], 26.3 [CH<sub>3</sub>, <sup>i</sup>Pr, Ar\* of <sup>Dipp</sup>Nacnac], 24.2 [CH<sub>3</sub>, <sup>i</sup>Pr, Ar\* of <sup>Dipp</sup>Nacnac], (C<sub>q</sub> of C-Mg was not possible to assign).

<sup>19</sup>F NMR {<sup>1</sup>H} (376.40 MHz, *d*<sub>8</sub>-THF, 298 K) δ -113.5 [br, 2F, C<sub>6</sub>HF<sub>4</sub>], -140.0 [m, 2F, C<sub>6</sub>HF<sub>4</sub>].

**Elemental analysis:** (C<sub>35</sub>H<sub>42</sub>F<sub>4</sub>MgN<sub>2</sub>) *Calculated:* C: 70.64 % H: 7.60 % N: 4.22 %.  
*Found:* C: 70.75 % H: 7.48 % N: 4.60 %.

• **Synthesis of [(<sup>Dipp</sup>Nacnac)Mg(C<sub>6</sub>F<sub>5</sub>)(THF)] (51)**



To a solution of **36** (0.28 g, 0.5 mmol) in THF (5 mL), pentafluorobenzene (0.056 mL, 0.5 mmol) was added. The yellow solution was stirred for 1 hour at room temperature. The solvent was removed and 10 mL of hexane were added obtaining a yellow suspension that was stored at -30 °C.

After 48 hours a white solid precipitated, and was isolated and placed in a glovebox (0.19 g, 56%).

**<sup>1</sup>H NMR (400.13 MHz, *d*<sub>8</sub>-THF, 298 K)** δ 7.10 [s, 6H, Ar\* of <sup>Dipp</sup>Nacnac], 5.02 [s, 1H, CH of <sup>Dipp</sup>Nacnac], 3.61 [m, 4H, OCH<sub>2</sub>, THF], 3.25-3.15 [sept, 4H, *J* = 6.8 Hz, CH, <sup>i</sup>Pr, Ar\* of <sup>Dipp</sup>Nacnac], 1.77 [m, 4H, CH<sub>2</sub>, THF], 1.74 [s, 6H, CH<sub>3</sub> of <sup>Dipp</sup>Nacnac], 1.16-1.14 [d, 12H, *J* = 7.9 Hz, CH<sub>3</sub>, <sup>i</sup>Pr, Ar\* of <sup>Dipp</sup>Nacnac], 0.97-0.95 [d, 12H, *J* = 7.1 Hz, CH<sub>3</sub>, <sup>i</sup>Pr, Ar\* of <sup>Dipp</sup>Nacnac].

**<sup>13</sup>C NMR {<sup>1</sup>H} (100.62 MHz, *d*<sub>8</sub>-THF, 298 K)** δ 169.6 [C<sub>q</sub>, CHC(Me) of <sup>Dipp</sup>Nacnac], 145.7 [CH, Ar\* of <sup>Dipp</sup>Nacnac], 143.1 [CH, Ar\* of <sup>Dipp</sup>Nacnac], 125.7 [CH, Ar\* of <sup>Dipp</sup>Nacnac], 124.2 [CH, Ar\* of <sup>Dipp</sup>Nacnac], 95.5 [CH of <sup>Dipp</sup>Nacnac], 68.1 [OCH<sub>2</sub>, THF], 28.5 [CH, <sup>i</sup>Pr, Ar\* of <sup>Dipp</sup>Nacnac], 26.2 [CH<sub>2</sub>, THF], 24.7 [CH<sub>3</sub>, <sup>i</sup>Pr, Ar\* of <sup>Dipp</sup>Nacnac], 24.5 [CH<sub>3</sub>, <sup>i</sup>Pr, Ar\* of <sup>Dipp</sup>Nacnac], 24.2 [CH<sub>3</sub>, <sup>i</sup>Pr, Ar\* of <sup>Dipp</sup>Nacnac], (C<sub>q</sub> of C-Mg and C<sub>6</sub>F<sub>5</sub> were not possible to assign).

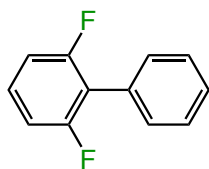
**<sup>19</sup>F NMR {<sup>1</sup>H} (376.40 MHz, *d*<sub>8</sub>-THF, 298 K)** δ -112.8 [br, C<sub>6</sub>F<sub>5</sub>], -160.3 [s, C<sub>6</sub>H<sub>2</sub>F<sub>3</sub>], -163.6 [s, C<sub>6</sub>H<sub>2</sub>F<sub>3</sub>].

**Elemental analysis:** (C<sub>35</sub>H<sub>41</sub>F<sub>5</sub>MgN<sub>2</sub>) *Calculated:* C: 68.77 % H: 7.25 % N: 4.11 %.  
*Found:* C: 68.86 % H: 7.27 % N: 4.26 %.

## 5.4.2 General Experimental Procedure for Negishi Cross-Coupling Reactions

To an oven dried Schlenk **36** (0.56 g, 1 mmol) and the fluoroaromatic derivative (1 mmol) were dissolved in THF (5 mL) during 2 hours at room temperature. ZnCl<sub>2</sub> (0.14 g, 1 mmol) was then added and the solution was stirred at room temperature during one hour. 5 mol% of Pd(PPh<sub>3</sub>)<sub>4</sub> (0.058 g) and iodobenzene (1.25 or 2 mmol) were added and the solution was refluxed during 18 hours. After this time the solution was opened to air. NH<sub>4</sub>Cl was added and the solution was extracted with ethyl acetate (30 mL x 2) and brine (20 mL x 3). The solution was then dried over MgSO<sub>4</sub>, and the filtrate was evaporated *in vacuo*. The compound was purified by chromatographic column (silica gel, petroleum ether 40 – 60 °C).

- **Synthesis of 2,6-difluorobiphenyl (52)**<sup>[391]</sup>



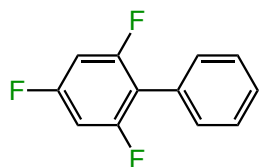
The reaction was performed starting from **48** (0.627 g, 1 mmol). 10 mol% of Pd(PPh<sub>3</sub>)<sub>4</sub> (0.1167 g) and iodobenzene (0.416 g, 2 mmol) were also employed. 64% isolated yield (0.122 g) was obtained for compound **52**.

<sup>1</sup>H NMR (400.13 MHz, CDCl<sub>3</sub>, 298 K) δ 7.53-7.41 [m, 5H, C<sub>6</sub>H<sub>5</sub>], 7.34-7.26 [m, 1H, CHCH<sub>2</sub>CF of C<sub>6</sub>H<sub>3</sub>F<sub>2</sub>], 7.06-6.98 [m, 2H, CHCF of C<sub>6</sub>H<sub>3</sub>F<sub>2</sub>].

<sup>13</sup>C NMR {<sup>1</sup>H} (100.6 MHz, CDCl<sub>3</sub>, 298 K) δ 161.6-159.0 [dd, J = 10.8 Hz, J = 249.9, C<sub>q</sub>, CF of C<sub>6</sub>H<sub>3</sub>F<sub>2</sub>], 130.3 [CH], 129.0 [CH], 128.3 [CH], 127.3 [CH], 118.6 [C<sub>q</sub>, CCF of C<sub>6</sub>H<sub>3</sub>F<sub>2</sub>], 111.6-111.9 [m, CH, CHCF of C<sub>6</sub>H<sub>3</sub>F<sub>2</sub>].

<sup>19</sup>F NMR {<sup>1</sup>H} (376.40 MHz, CDCl<sub>3</sub>, 298 K) δ -114.5 [s, 2F].

- **Synthesis of 2,4,6-trifluorobiphenyl (53)**<sup>[391]</sup>



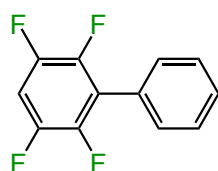
In this reaction 2 equivalents of iodobenzene (0.416 g, 2 mmol) were employed. 62% isolated yield (0.129 g) was obtained for compound **53**.

**<sup>1</sup>H NMR (400.13 MHz, CDCl<sub>3</sub>, 298 K)** δ 7.51-7.39 [m, 5H, C<sub>6</sub>H<sub>5</sub>], 6.81-6.71 [m, 2H, C<sub>6</sub>H<sub>2</sub>F<sub>3</sub>].

**<sup>13</sup>C NMR {<sup>1</sup>H} (100.6 MHz, CDCl<sub>3</sub>, 298 K)** δ 161.7 [C<sub>q</sub>, CF of C<sub>6</sub>H<sub>2</sub>F<sub>3</sub>], 130.4 [CH of C<sub>6</sub>H<sub>5</sub>], 128.5 [CH of C<sub>6</sub>H<sub>5</sub>], 100.9-100.3 [m, CH of C<sub>6</sub>H<sub>2</sub>F<sub>3</sub>]. The weak signal of the sample prevented assignment of the rest of the carbon atoms.

**<sup>19</sup>F NMR (376.40 MHz, CDCl<sub>3</sub>, 298 K)** δ -109.0 [m, 2F, C<sub>6</sub>H<sub>2</sub>F<sub>3</sub>], -101.3 [t, 1F, *J* = 6.5 Hz C<sub>6</sub>H<sub>2</sub>F<sub>3</sub>].

- **Synthesis of 2,3,5,6-tetrafluorobiphenyl (54)**<sup>[391]</sup>



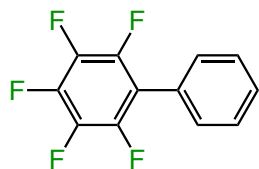
In this reaction 1.25 equivalents of iodobenzene (0.260 g, 1.25 mmol) were employed. 64% isolated yield (0.145 g) was obtained for compound **54**.

**<sup>1</sup>H NMR (400.13 MHz, CDCl<sub>3</sub>, 298 K)** δ 7.56-7.41 [m, 5H, C<sub>6</sub>H<sub>5</sub>], 7.13-7.01 [m, 1H, C<sub>6</sub>HF<sub>4</sub>].

**<sup>13</sup>C NMR {<sup>1</sup>H} (100.6 MHz, CDCl<sub>3</sub>, 298 K)** δ 130.3 [CH of C<sub>6</sub>H<sub>5</sub>], 129.4 [CH of C<sub>6</sub>H<sub>5</sub>], 128.8 [CH of C<sub>6</sub>H<sub>5</sub>], 105.2-104.7 [m, CH of C<sub>6</sub>HF<sub>4</sub>]. The weak signal of the sample prevented assignment of the rest of the carbon atoms.

**<sup>19</sup>F NMR (376.40 MHz, CDCl<sub>3</sub>, 298 K)** δ -139.2 [m, 2F, C<sub>6</sub>HF<sub>4</sub>], -143.9 [m, 2F, C<sub>6</sub>HF<sub>4</sub>].

- **Synthesis of 2,3,4,5,6-pentafluorobiphenyl (55)**<sup>[391]</sup>



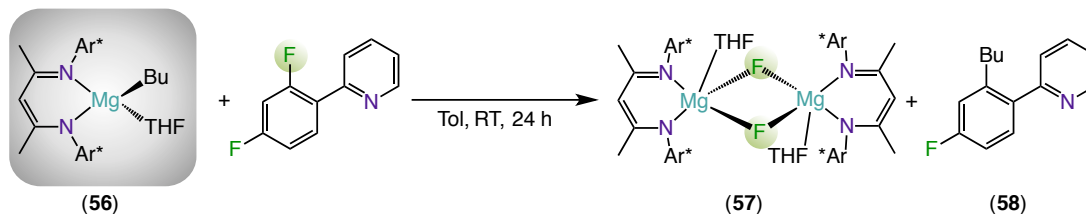
In this reaction 1.25 equivalents of iodobenzene (0.260 g, 1.25 mmol) were employed. 68% isolated yield (0.166 g) was obtained for compound **55**.

<sup>1</sup>H NMR (400.13 MHz, CDCl<sub>3</sub>, 298 K) δ 7.54-7.39 [m, 5H, C<sub>6</sub>H<sub>5</sub>].

<sup>13</sup>C NMR {<sup>1</sup>H} (100.6 MHz, CDCl<sub>3</sub>, 298 K) δ 130.3 [CH of C<sub>6</sub>H<sub>5</sub>], 129.4 [CH of C<sub>6</sub>H<sub>5</sub>], 128.9 [CH of C<sub>6</sub>H<sub>5</sub>]. The weak signal of the sample prevented assignment of the rest of the carbon atoms.

<sup>19</sup>F NMR {<sup>1</sup>H} (376.40 MHz, CDCl<sub>3</sub>, 298 K) δ -143.2 [m, C<sub>6</sub>F<sub>5</sub>], -155.6 [m, C<sub>6</sub>F<sub>5</sub>], -162.2 [m, C<sub>6</sub>F<sub>5</sub>].

### 5.4.3 C-F Activation 2-(2,4-difluorophenyl)pyridine



To a solution of **56** (0.28 g, 0.5 mmol) in toluene (5 mL), 2-(2,4-difluorophenyl)pyridine (0.1 g, 0.5 mmol) was added. The yellow solution was stirred for 24 hours at room temperature. The solvent was removed and 5 mL of hexane were added obtaining a white solid precipitate **57**, which was isolated and placed in a glovebox. The solvent from the filtrate was removed and placed into the glovebox. C<sub>6</sub>D<sub>6</sub> was then added as well as ferrocene (9.5 mg, 0.05 mmol). The <sup>1</sup>H NMR spectrum suggests the presence of a 92% of compound **58** from the integration versus ferrocene. <sup>1</sup>H, <sup>13</sup>C and <sup>19</sup>F NMR experiments are in agreement with the literature.<sup>[381,383]</sup>

- **Synthesis of [<sup>Dipp</sup>NacnacMg(F)] (57)**<sup>[383]</sup>

<sup>1</sup>H NMR (400.13 MHz, C<sub>6</sub>D<sub>6</sub>, 298K) δ 7.11-7.00 [br. m, 12H, Ar\* of <sup>Dipp</sup>Nacnac], 4.84 [s, 2H, CH of <sup>Dipp</sup>Nacnac], 3.01 [m, 8H, CH, <sup>i</sup>Pr, Ar\* of <sup>Dipp</sup>Nacnac], 1.49 [s, 12H, CH<sub>3</sub> of <sup>Dipp</sup>Nacnac], 1.11-1.09 [d, 24H, , J = 6.8 Hz, CH<sub>3</sub>, <sup>i</sup>Pr, Ar\* of <sup>Dipp</sup>Nacnac], 0.97-0.95 [d, 24H, , J = 7.6 Hz, CH<sub>3</sub>, <sup>i</sup>Pr, Ar\* of <sup>Dipp</sup>Nacnac].

<sup>19</sup>F {<sup>1</sup>H} NMR (376.40 MHz, C<sub>6</sub>D<sub>6</sub>, 298K) δ -188.1 [s, 2F].

- **Synthesis of 2-(2-butyl-4-fluorophenyl)pyridine (58)**<sup>[381]</sup>

<sup>1</sup>H NMR (400.13 MHz, CDCl<sub>3</sub>, 298K) δ 8.67-8.66 [d, J = 5.1 Hz, 1H], 7.74-7.69 [td, J = 1.9 Hz, J = 7.6 Hz, 1H], 7.37-7.26 [m, 2H], 7.26-7.20 [m, 1H], 7.04-6.97 [m, 1H], 6.97-6.92 [m, 1H], 2.72-2.64 [m, 2H, CH<sub>2</sub> of Bu], 1.49-1.37 [m, 2H, CH<sub>2</sub> of Bu], 1.24-1.18 [m, 2H, CH<sub>2</sub> of Bu], 0.78 (t, J = 7.5 Hz, 3H, CH<sub>3</sub> of Bu).

<sup>19</sup>F {<sup>1</sup>H} NMR (376.40 MHz, C<sub>6</sub>D<sub>6</sub>, 298K) δ -114.4 [s, 1F].

#### 5.4.4 General Experimental Procedure for Metallation Reactions at NMR Tube Scale

Metallation reactions were performed in a J. Young's NMR tube at NMR scale following the following procedure. In a glovebox, the NMR tube was filled with 0.2 mmol of base **36**, 10 mol% of ferrocene (0.0035 g, 0.02 mmol) as internal standard and 0.409 g of *d*<sub>8</sub>-THF. The initial ratio of base calculated by integration in <sup>1</sup>H NMR relative to the ferrocene. 0.2 mmol of fluoroaromatic derivative, was introduced and the reactions times were measured from this point in regular intervals of time until full conversion by <sup>1</sup>H NMR spectrum. All the yields were calculated by integration of the products relative to the ferrocene in the <sup>1</sup>H NMR spectrum. The NMR spectrums of the compounds correspond to the isolated species obtained for compounds **48** to **51**.

### 5.4.5 DOSY NMR Studies

- **Reaction of [(<sup>Dipp</sup>Nacnac)MgTMP] with 1,3,5-trifluorobenzene**

In a J. Young's NMR tube, 1,3,5-trifluorobenzene (2.13  $\mu$ L, 0.02 mmol) was added to a solution of [(<sup>Dipp</sup>Nacnac)MgTMP] (0.0112 g, 0.02 mmol) in *d*<sub>8</sub>-THF (0.5 mL). 2.75  $\mu$ L of TMS (tetramethylsilane) were added in order to use as internal standard in the DOSY experiment.<sup>[7]</sup>

## Chapter 6 Conclusions and Outlook

Advancing the understanding of cooperative effects in bimetallic complexes is one of the main topics of research in our group. On the other hand, cooperative effects of single metal systems due to special metal-ligand and ligand-ligand partnerships have hardly been explored. This thesis fills this gap in the knowledge, by advancing the applications of s-block organometallics in catalysis, as well as deprotonative metallation and C-F bond activation processes. However, the priority of this thesis has been the reactivity of s-block monometallic systems by cooperative effects in different organic transformations.

Alkali-metal organometallics have been widely used in many stoichiometric applications in synthetic chemistry, especially in deprotonation reactions; however, they have hardly been explored in catalytic processes. This thesis assesses their potential as valuable precatalysts for challenging intermolecular hydroamination reaction. The precatalysts used  $[MCH_2SiMe_3]$  combine an alkali-metal cation ( $Li^+$ ,  $Na^+$  or  $K^+$ ) with the trimethylsilylmethyl anionic ligand ( $CH_2SiMe_3^-$ ), which appeared to be excellent candidates to overcome the high kinetic barrier of this type of reaction. These alkyl reagents have been able to achieve good yields and selectivity using a wide range of amines with substituted vinylarenes and alkynes under excellent reaction conditions (room temperature and short timescales). Additionally, a dramatic alkali-metal effect has been observed. Gaining some more information about these catalytic transformations, the stoichiometric reactions



between the precatalysts and piperidine have been performed. Solid and solution state characterisation of these species have been achieved isolating the potential active catalysts in the catalytic cycle.

Moving to group 2 in the periodic table, the analogous magnesium complex  $[\text{Mg}(\text{CH}_2\text{SiMe}_3)_2]$  was unable to catalyse the same hydroamination processes, even when forcing the reaction conditions. However, the lower reactivity of magnesium can be overcome due to the synergic behaviour, where the alkali-metal can coordinate and activate the unsaturated organic molecule, facilitating the addition of the amide group (Figure 6.1).

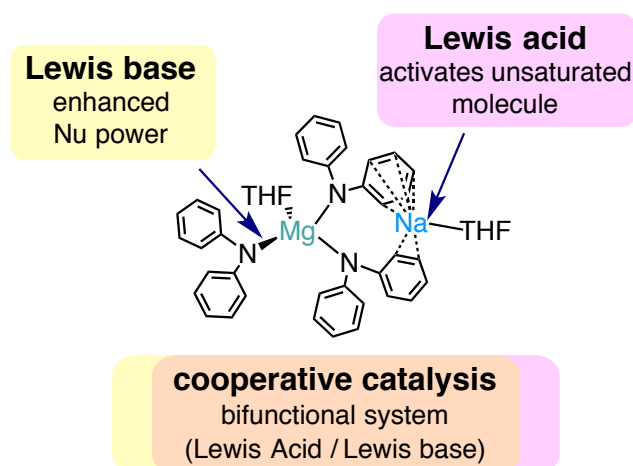


Figure 6.1: Example of a bifunctional catalyst.

Higher temperatures (80 °C) and longer reaction times were required in some cases compared to the monometallic alkali-metal catalysts and an alkali-metal effect has also been observed, where the  $[(\text{PMDETA})_2\text{KMg}(\text{CH}_2\text{SiMe}_3)_4]$  acts as the best catalyst for these reactions. Solid-state and solution studies have also been performed using lower and higher order amido magnesiate.

Moving into other synthetic applications, the investigation of new synthetic processes using monometallic magnesium compounds has also been achieved. Finding new applications of  $\beta$ -diketiminate magnesium complexes, the regioselective magnesiation of a range of different heterocyclic and aromatic complexes has been accomplished. A bifunctional  $\beta$ -diketiminate magnesium base has been specifically designed, combining a basic (kinetically activated) TMP group with the sterically demanding  $\beta$ -diketiminate anionic ligand, which acting as a clamp can retain the sensitive anions formed (Figure 6.2).

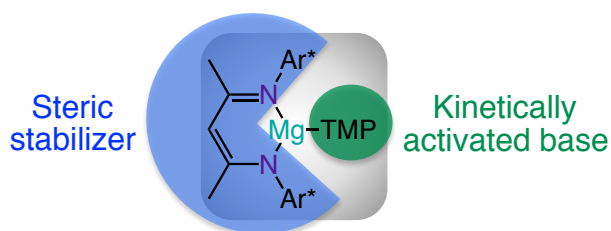


Figure 6.2: Bifunctional  $\beta$ -diketiminate magnesium base.

Additionally, these magnesiated anions have been used as synthetic platforms for further C-C bond formation via Negishi cross-coupling reactions.

Comparative studies by changing the TMP group to a butyl have been investigated. Thus, in the case of fluoroaromatic molecules a dramatic change of reactivity has been observed, where  $[\text{D}^{\text{Dipp}}\text{NacnacMg}(\text{THF})\text{Bu}]$  facilitates nucleophilic aromatic substitution in contrast to the deprotonative metallation achieved by  $[\text{D}^{\text{Dipp}}\text{NacnacMg}(\text{TMP})]$ .

These investigations open a new door to expand the synthetic potential of s-block organometallic reagents in catalytic and stoichiometric processes. Catalytic applications of group 1 and 2 organometallic complexes, such as hydrogenation or hydrosilation reactions, have emerged in the recent years, suggesting an

environmentally benign and potential alternative to transition metal catalysts. Additionally, the synergic parentship between alkali-metal and magnesium complexes break new ground towards new catalytic applications of these ate compounds in catalysis.

Furthermore, the synthetic potential of the  $\beta$ -diketimate magnesium manifolds can be expanded into new routes such as transition-metal free oxidative homocoupling reactions. The enhanced stability of the magnesium intermediates, generated by the protective shell of the sterically demanding  $\{\text{Dipp}^{\text{Nacnac}}\}$  ligand, brings in close proximity the carbanions in the dimeric complexes making them good candidates for oxidative homocoupling reactions through TEMPO, for example. Initial results for nucleophilic aromatic substitutions have been obtained using  $[\text{Dipp}^{\text{Nacnac}}\text{Mg}(\text{THF})\text{Bu}]$  with 2-(2,4-difluorophenyl)pyridine, which could be expanded to other fluoroaromatic derivatives.

## Chapter 7 Experimental

### 7.1 General Experimental Techniques

#### 7.1.1 Schlenk Techniques

All the experiments were performed under protective argon inert atmosphere and using standard Schlenk techniques. The Schlenk equipment provided a dry and inert atmosphere, which was needed as most of the reactants and products formed were air and moisture sensitive. This special equipment consists of a Schlenk line and Schlenk tubes, where the reactions are carried out, and a filter is occasionally used (Figure 7.1).

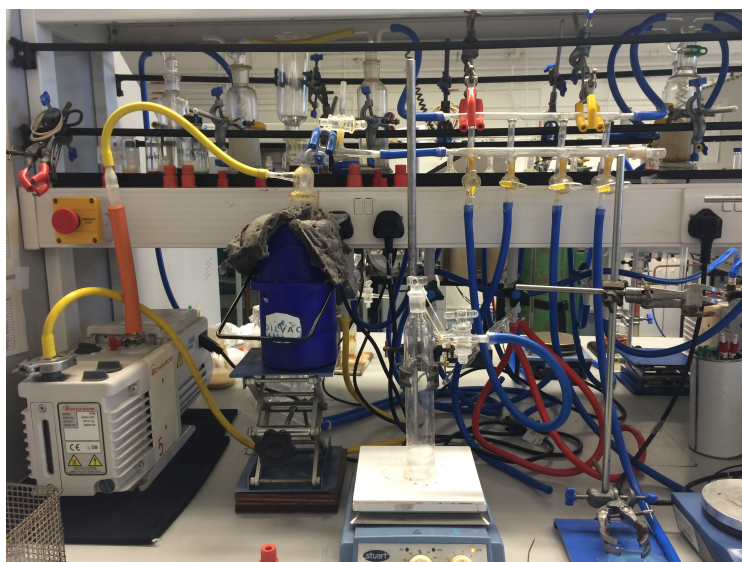


Figure 7.1: Schlenk line used in order to perform the experiments.

The line contained an inert gas/vacuum manifold, which had two separate compartments; one connected to a vacuum pump and the other connected to a supply of dry argon. All Schlenk glassware contained ground-glass joints, which were lightly greased before being connected together. This was to seal the joints securely and also prevent the glass from getting stuck together. To condense any volatile substances from being detrimental to the reaction taking place and to protect the vacuum pump, a liquid nitrogen cooled trap was attached to the end of the Schlenk line. A pressure release bubbler is incorporated into the line to ensure there is no buildup of pressure.

The Schlenk line used had four connectors, which could be attached to the piece of apparatus needed. Each connector had a two-way tap so that either vacuum or argon could be applied where appropriate. Air was removed from the Schlenk by applying a vacuum for fifteen minutes; the tap was then turned to allow argon in. This process was repeated a further three times to ensure a dry and inert atmosphere in the Schlenk tube. When solvents or reagents were to be added to the Schlenk tube a positive argon flow would be applied to ensure no air entered. Solvents are transferred using a syringe and needle, which has been flushed with argon twelve times.

### **7.1.2 Glovebox**

The use of a glovebox has also been required. A standard glovebox was used when products, which were air and moisture sensitive had to be weighed, stored and also prepared for NMR experiments (Figure 7.2).



Figure 7.2: Glovebox.

The glovebox is made of two main chambers. The larger chamber contains the large glass window and gloves and is the area where the work is carried out. The chamber is filled with dry argon. The smaller chamber is called the port; it contains an inner and outer door. The purpose of the two doors is to allow items to be placed in the large chamber without air entering. Items are placed in the port and a vacuum supplied, the port is then filled with argon. This process is carried out a further two times. The gas in the glovebox is constantly circulated over a scrubber, which removes any air or moisture, which may be present in the system.

### 7.1.3 Solvent Purification

As most of the reagents and products are air and moisture sensitive all solvents were dried and degassed before use. All of the solvents used during this project were distilled over nitrogen, in the presence of sodium and benzophenone. When sodium is reacted with benzophenone gives a ketyl radical which is blue in colour. This is very reactive

with oxygen and water to give a colourless or yellow solution. Thus these substances act as self-indicators for ensuring the removal of oxygen and water from the solvent.

#### 7.1.4 Analytical Procedures

All NMR spectra were recorded on a Bruker AV3 or AV 400 MHz, or on a AV 600 MHz spectrometers, operating at 400.13 MHz for  $^1\text{H}$ , 100.61 MHz for  $^{13}\text{C}$  and 376.40 MHz for  $^{19}\text{F}$ . All  $^{13}\text{C}$  NMR spectra were proton decoupled. The NMR assignments were performed, in some cases, with the help  $^1\text{H}$ ,  $^{13}\text{C}$ -HSQC, COSY, DOSY and HMBC experiments.  $^1\text{H}$  and  $^{13}\text{C}\{^1\text{H}\}$  chemical shifts are expressed in parts per million ( $\delta$ , ppm) and referenced to residual solvent peaks. Elemental analyses were performed using a Perkin Elmer 2400 elemental analyser.

X-ray crystallography data were collected on Oxford Diffraction Gemini S or Xcalibur E instruments with graphite-monochromated Mo  $K\alpha$  ( $\lambda = 0.71073 \text{ \AA}$ ) or Cu  $K\alpha$  ( $\lambda = 1.54180 \text{ \AA}$ ) radiation.<sup>[394]</sup> Data for compounds **43**, **44** and **47** were measured at Station I19 of the DIAMOND synchrotron radiation source using  $0.6889 \text{ \AA}$  radiation and a Crystal Logics diffractometers with Rigaku Saturn 724+ CCD detector; data collection and processing used Rigaku and Bruker software.<sup>[394,395]</sup> All structures were solved and refined to convergence on  $F^2$  for all independent reflections by the full-matrix least squares method using SHELXL-2014/7<sup>[394,395]</sup> or by the GaussNewton algorithm using OLEX2.<sup>[396]</sup>

## 7.2 Synthesis of Starting Materials

- **Synthesis of [Mg(CH<sub>2</sub>SiMe<sub>3</sub>)<sub>2</sub>]**

To a 500 mL three-neck round bottom flask were added Mg turnings (4.00 g, 165 mmol) and Et<sub>2</sub>O (100 mL). ClCH<sub>2</sub>SiMe<sub>3</sub> (19 mL, 165 mmol) was suspended in Et<sub>2</sub>O (50 mL) and added drop wise. The resulting grey solution was refluxed for 1 hour. To the cooled suspension was added 1,4-dioxane (10 mL, 88.11 mmol) and the pale grey mixture stirred for 3 days. The suspension was then filtered through celite and glass wool and washed with Et<sub>2</sub>O (3 x 20 mL) giving a pale straw filtrate. Removal of the solvent in vacuo afforded a white solid which was purified by sublimation at 175 °C to obtain pure Mg(CH<sub>2</sub>SiMe<sub>3</sub>)<sub>2</sub> (typical yield 8.5-9.5 g, 63-70%).

<sup>1</sup>H NMR (400.13 MHz, d<sub>8</sub>-THF, 298 K) δ -1.77 [s, 2H, CH<sub>2</sub>], -0.11 [s, 9H, CH<sub>3</sub>].

- **Synthesis of [NaCH<sub>2</sub>SiMe<sub>3</sub>]**

To a suspension of NaOtBu (2.88 g, 30 mmol) in hexane (15 mL) was added drop wise LiCH<sub>2</sub>SiMe<sub>3</sub> (30 mL of a 1 M solution of LiCH<sub>2</sub>SiMe<sub>3</sub> in pentane). The reaction was stirred overnight. The resultant peach suspension was filtered, washed with hexane (3 x 20 mL) and dried under vacuum to afford a white solid (typical yield 2.53 g, 76%).

<sup>1</sup>H NMR (400.13 MHz, C<sub>6</sub>D<sub>6</sub>, 298 K) δ -2.45 [s, 2H, CH<sub>2</sub>], 0.14 [s, 9H, CH<sub>3</sub>].

- **Synthesis of [KCH<sub>2</sub>SiMe<sub>3</sub>]**

To a suspension of KOtBu (3.37 g, 30 mmol) in hexane (15 mL) was added drop wise LiCH<sub>2</sub>SiMe<sub>3</sub> (30 mL of a 1 M solution of LiCH<sub>2</sub>SiMe<sub>3</sub> in pentane). The reaction was stirred overnight. The resultant suspension was filtered, washed with hexane (3 x 20 mL) and dried under vacuum to afford a white solid (typical yield 2.99 g, 79%).



**$^1\text{H}$  NMR (400.13 MHz,  $\text{C}_6\text{D}_6$ , 298 K)**  $\delta$  -2.20 [s, 2H,  $\text{CH}_2$ ], -0.20 [s, 9H,  $\text{CH}_3$ ].

- **Synthesis of  $[\text{LiMg}(\text{CH}_2\text{SiMe}_3)_3]$  (26)**<sup>[191]</sup>

To a solution of  $[\text{Li}(\text{CH}_2\text{SiCH}_3)]$  (1 mL of a 1 M solution in hexane, 1 mmol) in hexane (10 mL)  $[\text{Mg}(\text{CH}_2\text{SiCH}_3)_2]$  (0.22 g, 1 mmol) was added and the resulting suspension was stirred for 1 hour affording a clear solution. THF (0.08 mL, 1 mmol) was then added and the clear solution was transferred to the freezer (-28 °C). Clear, colourless crystals formed after 1 day, which were isolated and placed into the glovebox. (0.04 g, 11%).

**$^1\text{H}$  NMR (400.13 MHz,  $\text{C}_6\text{D}_6$ , 298 K)**  $\delta$  -1.36 [s, 6H,  $\text{SiCH}_2$ ], 0.25 [s, 27H,  $\text{Si}(\text{CH}_3)_3$ ].

**$^7\text{Li}$  NMR (155.5 MHz,  $\text{C}_6\text{D}_6$ , 298 K)**  $\delta$  0.38.

- **Synthesis of  $[\text{NaMg}(\text{CH}_2\text{SiMe}_3)_3]$  (27)**<sup>[128]</sup>

$[\text{Na}(\text{CH}_2\text{SiCH}_3)]$  (0.11 g, 1 mmol),  $[\text{Mg}(\text{CH}_2\text{SiCH}_3)_2]$  (0.22 g, 1 mmol) and hexane (10 mL) were added and stirred at room temperature during one hour. After this time the solvent was removed. A mixture of hexane (5 mL) and toluene (5 mL) were then introduced and it was heated until solution. The resulting colourless solution was placed in the fridge. After 24 hours the white solid was filtered and placed in a glovebox. (0.19 g, 61%).

**$^1\text{H}$  NMR (400.13 MHz,  $\text{C}_6\text{D}_6$ , 298 K)**  $\delta$  -1.71 [s, 6H,  $\text{SiCH}_2$ ], 0.28 [s, 27H,  $\text{Si}(\text{CH}_3)_3$ ].

- **Synthesis of  $[\text{KMg}(\text{CH}_2\text{SiMe}_3)_3]$  (28)**<sup>[126]</sup>

In a Schlenk, a suspension of  $[\text{K}(\text{CH}_2\text{SiCH}_3)]$  (0.13 g, 1 mmol) and  $[\text{Mg}(\text{CH}_2\text{SiCH}_3)_2]$  (0.22 g, 1 mmol) in hexane (10 mL) was stirred for 1 hour at room temperature. 2 mL of toluene were then introduced and the mixture was gently heated. The

resulting colourless solution was allowed to cool slowly to room temperature affording a crop of colourless crystals of was isolated (0.16 g, 49%).

**$^1\text{H}$  NMR (400.13 MHz,  $\text{C}_6\text{D}_6$ , 298 K)  $\delta$  -1.68 [s, 6H,  $\text{SiCH}_2$ ], 0.35 [s, 27H, s,  $\text{Si}(\text{CH}_3)_3$ ].**

- **Synthesis of [(TMEDA) $_2$ Li $_2$ Mg(CH $_2$ SiMe $_3$ ) $_4$ ] (29)<sup>[191]</sup>**

To a solution of [Li(CH $_2$ SiCH $_3$ )] (2 mL of a 1 M solution in hexane, 2 mmol) in hexane (10 mL), [Mg(CH $_2$ SiCH $_3$ ) $_2$ ] (0.22 g, 1 mmol) was added and the resulting suspension was stirred for 1 hour affording an almost clear solution. TMEDA (0.3 mL, 2 mmol) was then added giving a clear solution which was transferred to the freezer (-28 °C). After 1 day colourless crystals were formed, which were isolated and placed to the glovebox (0.28 g, 46%).

**$^1\text{H}$  NMR (400.13 MHz,  $\text{C}_6\text{D}_6$ , 298 K)  $\delta$  -1.99 [s, 2H,  $\text{SiCH}_2$ ], 0.46 [s, 9H,  $\text{Si}(\text{CH}_3)_3$ ], 1.65 [s, 2H, NCH $_2$ , TMEDA], 2.02 [s, 6H, N(CH $_3$ ) $_2$ , TMEDA].**

**$^7\text{Li}$  NMR (155.5 MHz,  $\text{C}_6\text{D}_6$ , 298 K)  $\delta$  0.82.**

- **Synthesis of [(TMEDA) $_2$ Na $_2$ Mg(CH $_2$ SiMe $_3$ ) $_4$ ] (30)**

To a suspension of [Na(CH $_2$ SiCH $_3$ )] (0.22 g, 2 mmol) in hexane (10 mL) [Mg(CH $_2$ SiCH $_3$ ) $_2$ ] (0.22 g, 1 mmol) was added and the suspension stirred for 1 hour. TMEDA (0.30 mL, 2 mmol) was then added and the almost clear solution transferred to the freezer (-28 °C). After 1 day a crop of clear, colourless crystals was isolated (0.35 g, 54%).

**$^1\text{H}$  NMR (400.13 MHz,  $\text{C}_6\text{D}_6$ , 298 K)  $\delta$  -1.78 [s, 2H,  $\text{SiCH}_2$ ], 0.47 [s, 9H,  $\text{Si}(\text{CH}_3)_3$ ], 1.67 [s, 2H, NCH $_2$ , TMEDA], 1.92 [s, 6H, N(CH $_3$ ) $_2$ , TMEDA].**

- **Synthesis of [(PMDETA)<sub>2</sub>K<sub>2</sub>Mg(CH<sub>2</sub>SiMe<sub>3</sub>)<sub>4</sub>] (31)**<sup>[126]</sup>

To a suspension of [K(CH<sub>2</sub>SiCH<sub>3</sub>)] (0.12 g, 1 mmol) in hexane (10 mL) [Mg(CH<sub>2</sub>SiCH<sub>3</sub>)<sub>2</sub>] (0.22 g, 1 mmol) was added and the suspension stirred for 1 hour. PMDETA (0.10 mL, 0.5 mmol) was then added giving a clear solution with a yellow oil deposited at the bottom of the Schlenk. The Schlenk was transferred to the freezer (-28 °C) overnight. A crop of clear, colourless crystals was isolated (0.20 g, 50%).

<sup>1</sup>H NMR (400.13 MHz, C<sub>6</sub>D<sub>6</sub>, 298 K) δ -1.56 [s, 8H, SiCH<sub>2</sub>], 0.47 [s, 36H, Si(CH<sub>3</sub>)<sub>3</sub>], 1.72 - 1.76 [m, 16H, NCH<sub>2</sub>, PMDETA], 1.83 [s, 6H, NCH<sub>3</sub>, PMDETA], 1.91 [s, 24H, N(CH<sub>3</sub>)<sub>2</sub>, PMDETA].

- **Synthesis of [Dipp<sup>Na</sup>NacnacH]**<sup>[397]</sup>

To a solution of 2,4-pentanedione (4.52 mL, 44.4 mmol) and 2,6-diisopropylaniline (19.57 mL, 107 mmol) in ethanol (200 mL), 12 M of HCl (5 mL) was added. The mixture was refluxed for 3 days. The solvent was removed to leave a pink solid residue, which was refluxed with hexane (300 mL) for 1 hour. The solid was filtered and placed in a 1 L flask where it was treated with 200 mL of a saturated aqueous Na<sub>2</sub>CO<sub>3</sub> solution and 300 mL of CH<sub>2</sub>Cl<sub>2</sub>. The slurry was stirred until the solid dissolved. The organic layer was separated, dried with MgSO<sub>4</sub> and filtered. The solvent was removed and the product was washed with cold (0 °C) methanol obtaining a white solid (14.5 g, 78%).

<sup>1</sup>H (400.13 MHz, CDCl<sub>3</sub>, 298 K): δ 12.12 [s, 1H, NH of Dipp<sup>Na</sup>NacnacH], 7.14 [s, 6H, Ar\* 3.325 of Dipp<sup>Na</sup>Nacnac], 4.89 [s, 1H, CH of Dipp<sup>Na</sup>Nacnac], 3.19-3.08 [sept, 4H, J = 7.2 Hz, CH, <sup>i</sup>Pr, Ar\* of Dipp<sup>Na</sup>Nacnac], 1.73 [s, 6H, CH<sub>3</sub> of Dipp<sup>Na</sup>Nacnac], 1.24-1.22 [d, 12H, J = 6.9 Hz, CH<sub>3</sub>, <sup>i</sup>Pr, Ar\* of Dipp<sup>Na</sup>Nacnac], 1.15-1.13 [d, 12H, J = 6.9 Hz, CH<sub>3</sub>, <sup>i</sup>Pr, Ar\* of Dipp<sup>Na</sup>Nacnac].

- **Synthesis of [<sup>Dipp</sup>NacnacMg(TMP)] (36)**<sup>[106]</sup>

Mg(TMP)<sub>2</sub> was prepared *in situ* by refluxing over 1 hour a mixture of *n*Bu<sub>2</sub>Mg (4 mL of 1M solution in hexane, 4 mmol) and TMP(H) (1.36 mL, 8 mmol) in hexane (10 mL). <sup>Dipp</sup>NacnacH (1.66 g, 4 mmol) was then added and the resulting yellow solution was heated to reflux for 1 hour. Overnight storage of the solution in the freezer (-30 °C) provided a batch of colourless crystals of (<sup>Dipp</sup>Nacnac)Mg(TMP) (1.35 g, 58 %).

**<sup>1</sup>H NMR (400.13 MHz, C<sub>6</sub>D<sub>6</sub>, 298K )** δ 7.13 [s, 6H, Ar\* of <sup>Dipp</sup>Nacnac], 4.86 [s, 1H, CH of <sup>Dipp</sup>Nacnac], 3.28-3.18 [sept, 4H, *J* = 7.8 Hz, CH, <sup>i</sup>Pr, Ar\* of <sup>Dipp</sup>Nacnac], 1.69 [s, 6H, CH<sub>3</sub> of <sup>Dipp</sup>Nacnac], 1.66 [m, 2H, CH<sub>2</sub>, γ-TMP], 1.40-1.38 [d, 12H, *J* = 6.8 Hz CH<sub>3</sub>, <sup>i</sup>Pr, Ar\* of <sup>Dipp</sup>Nacnac], 1.20 [m, 2H, CH<sub>2</sub>, β-TMP], 1.18-1.17 [d, 12H, *J* = 6.7 Hz, CH<sub>3</sub>, <sup>i</sup>Pr, Ar\* of <sup>Dipp</sup>Nacnac], 0.95 [s, 12H, CH<sub>3</sub>, TMP].

- **Synthesis of [<sup>Dipp</sup>NacnacMg(THF)Bu] (56)**<sup>[106]</sup>

A Schlenk tube was charged with THF (10 mL) and *n*Bu<sub>2</sub>Mg (4 mL of a 1M solution of Bu<sub>2</sub>Mg in hexane, 4 mmol) followed by the addition of 1.66 g of <sup>Dipp</sup>NacnacH (4 mmol) and the resulting pale yellow solution was stirred for 1 hour at room temperature. The solution was concentrated *in vacuo* and left to stand at -30 °C in the freezer. After 24 hours, a crop of colorless crystals was obtained (1.23 g, 54%).

**<sup>1</sup>H NMR (400.13 MHz, C<sub>6</sub>D<sub>6</sub>, 298K )** δ 7.17 [s, 6H, Ar\* of <sup>Dipp</sup>Nacnac], 4.80 [s, 1H, CH of <sup>Dipp</sup>Nacnac], 3.57 [m, 4H, OCH<sub>2</sub>, THF], 3.30 [m, 4H, CH, <sup>i</sup>Pr, Ar\* of <sup>Dipp</sup>Nacnac], 1.66 [s, 6H, CH<sub>3</sub> of <sup>Dipp</sup>Nacnac], 1.47 [m, 2H, CH<sub>2</sub>, Bu], 1.36 [m, 2H, CH<sub>2</sub>, Bu], 1.30 [m, 4H, CH<sub>2</sub>, THF], 1.30 [d, 12H, CH<sub>3</sub>, <sup>i</sup>Pr, Ar\* of <sup>Dipp</sup>Nacnac], 1.23 [d, 12H, CH<sub>3</sub>, <sup>i</sup>Pr, Ar\* of <sup>Dipp</sup>Nacnac], 0.92 [t, 3H, CH<sub>3</sub>, Bu], -0.35 [m, 2H, Mg-CH<sub>2</sub>, Bu].

### 7.3 Crystallographic Data

	24	25
Empirical formula	C <sub>36</sub> H <sub>72</sub> Li <sub>4</sub> N <sub>4</sub> O <sub>4</sub>	C <sub>14</sub> H <sub>28</sub> N <sub>2</sub> Na <sub>2</sub> O
Mol. Mass	652.73	286.36
Crystal system	Monoclinic	Hexagonal
Space group	P 2 <sub>1</sub> /n	P 6 <sub>1</sub>
a/ Å	17.4465(11)	10.2293(2)
b/ Å	11.9724(5)	10.2293(2)
c/ Å	20.7681(13)	26.6996(6)
α	90	90
β	111.632(7)	90
γ	90	120
V/ Å <sup>3</sup>	4032.4(4)	2419.51(11)
Z	4	6
λ / Å	0.71073	0.71073
μ mm <sup>-1</sup>	1.075	1.179
2θmax °	51.988	60.346
Measured reflections	15231	24738
Unique reflections	7907	4466
R <sub>int</sub>	0.0444	0.0358
Observed rflns [ I >2s(I)]	4941	3972
Goof	1.024	1.034
R [on F, obs rflns only]	0.0743	0.0349
wR [on F <sup>2</sup> , all data]	0.2345	0.0802
Largest diff. Peak/hole. e/Å <sup>-3</sup>	0.423/-0.239	0.226/-0.192

	<b>32</b>	<b>33</b>
Empirical formula	$C_{54}H_{108}Mg_2N_6Na_2O_6$	$C_{54}H_{108}Mg_2N_6K_2O_6$
Mol. Mass	1032.06	1064.30
Crystal system	Triclinic	Monoclinic
Space group	P -1	P 2 <sub>1</sub> /n
a/ Å	11.6474(5)	9.6967(15)
b/ Å	11.7398(7)	16.663(3)
c/ Å	23.4025(8)	19.296(3)
$\alpha$	100.805(4)	90
$\beta$	94.008(3)	93.162(14)
$\gamma$	106.319(4)	90
V/ Å <sup>3</sup>	2991.0(2)	3113.1(8)
Z	2	12
$\lambda$ / Å	1.5418	0.71073
$\mu$ mm <sup>-1</sup>	1.146	0.930
2 $\theta$ max °	146.58	57.888
Measured reflections	43397	13216
Unique reflections	11830	7038
$R_{int}$	0.0316	0.0761
Observed rflns [ $I > 2s(I)$ ]	9231	2362
Goof	1.02	0.965
R [on F, obs rflns only]	0.1576	0.1037
wR [on F <sup>2</sup> , all data]	0.1752	0.3118
Largest diff. Peak/hole. e/Å <sup>-3</sup>	0.486/-0.363	0.9639/-0.3915

	34	35
Empirical formula	C <sub>32</sub> H <sub>72</sub> Mg <sub>1</sub> N <sub>8</sub> Na <sub>2</sub>	C <sub>38</sub> H <sub>86</sub> K <sub>2</sub> Mg <sub>1</sub> N <sub>10</sub>
Mol. Mass	639.26	785.67
Crystal system	Monoclinic	Orthorhombic
Space group	P 2 <sub>1</sub> /n	28.5536(5)
a/ Å	10.4760(14)	16.6156(3)
b/ Å	19.224(2)	20.3352(3)
c/ Å	19.864(2)	19.296(3)
α	90	90
β	93.733(10)	90
γ	90	90
V/ Å <sup>3</sup>	3991.9(8)	9647.7(3)
Z	4	8
λ / Å	0.71073	1.5418
μ mm <sup>-1</sup>	1.064	1.082
2θmax °	52	146
Measured reflections	19600	42734
Unique reflections	7810	9557
R <sub>int</sub>	0.0781	0.0344
Observed rflns [ <i>I</i> >2σ( <i>I</i> )]	4183	7899
GooF	1.012	1.023
R [on <i>F</i> , obs rflns only]	0.0711	0.0652
wR [on <i>F</i> <sup>2</sup> , all data]	0.2205	0.1851
Largest diff. Peak/hole. e/Å <sup>-3</sup>	0.613/-0.381	0.864/-0.624

	39	40
Empirical formula	C <sub>32</sub> H <sub>45</sub> Mg <sub>1</sub> N <sub>5</sub>	C <sub>93</sub> H <sub>110</sub> Mg <sub>2</sub> N <sub>10</sub>
Mol. Mass	524.04	1416.52
Crystal system	Monoclinic	Monoclinic
Space group	P2 <sub>1</sub> /n	P2 <sub>1</sub> /n
a/ Å	11.5906(4)	15.3537(5)
b/ Å	15.2013(6)	14.2772(5)
c/ Å	17.8446(7)	19.1707(8)
α	90.00	90.00
β	98.976(4)	104.615(4)
γ	90.00	90.00
V/ Å <sup>3</sup>	3105.6(2)	4066.4(3)
Z	4	2
λ / Å	1.54180	0.71073
μ mm <sup>-1</sup>	0.693	0.082
2θmax °	145.86	58.7
Measured reflections	21057	25760
Unique reflections	6086	10388
R <sub>int</sub>	0.0226	0.0280
Observed rflns [I>2s(I)]	5378	7675
Goof	1.040	1.026
R [on F, obs rflns only]	0.0419	0.0453
wR [on F <sup>2</sup> , all data]	0.1150	0.1183
Largest diff. Peak/hole. e/Å <sup>-3</sup>	0.269/-0.204	0.276/-0.238



	41	43
Empirical formula	$C_{70}H_{90}Mg_2N_{10}O_1$	$C_{74}H_{102}Mg_2N_6O_1$
Mol. Mass	1212.27	1140.23
Crystal system	Monoclinic	Triclinic
Space group	$P2_1/n$	P-1
a/ Å	13.0738(4)	12.3525(7)
b/ Å	14.2398(5)	12.4080(8)
c/ Å	19.0456(6)	22.7369(14)
$\alpha$	90	101.488(3)
$\beta$	92.872(3)	92.550(3)
$\gamma$	90	93.804(3)
$V/ \text{Å}^3$	3541.2(2)	3401.6(4)
Z	2	2
$\lambda / \text{Å}$	0.71073	0.6889
$\mu \text{ mm}^{-1}$	1.137	0.079
$2\theta_{\text{max}}^\circ$	57.998	51.0
Measured reflections	18999	42336
Unique reflections	9058	13767
$R_{\text{int}}$	0.0249	0.0635
Observed rflns [ $I > 2s(I)$ ]	6862	9222
Goof	1.019	1.066
$R$ [on $F$ , obs rflns only]	0.0497	0.0561
wR [on $F^2$ , all data]	0.1297	0.1595
Largest diff. Peak/hole. $e/\text{Å}^{-3}$	0.617/-0.371	0.432/-0.388

	44	47
Empirical formula	C <sub>44</sub> H <sub>55</sub> F <sub>2</sub> Mg <sub>1</sub> N <sub>3</sub> O <sub>1</sub>	C <sub>41</sub> H <sub>54</sub> Mg <sub>1</sub> N <sub>4</sub> O <sub>2</sub>
Mol. Mass	704.22	705.26
Crystal system	Triclinic	Triclinic
Space group	P-1	P-1
a/ Å	9.2553(9)	8.5700(6)
b/ Å	12.7671(13)	11.6230(8)
c/ Å	16.8484(16)	21.8670(15)
α	84.318(2)	104.360(3)
β	82.946(2)	92.391(3)
γ	86.524(2)	99.597(3)
V/ Å <sup>3</sup>	1963.7(3)	2072.7(3)
Z	2	2
λ / Å	0.6889	0.6889
μ mm <sup>-1</sup>	0.086	1.130
2θmax °	51.2	50.916
Measured reflections	16112	39658
Unique reflections	8089	39658
R <sub>int</sub>	0.0442	0.0655
Observed rflns [I>2s(I)]	6867	28963
GooF	1.119	1.077
R [on F, obs rflns only]	0.0477	0.0608
wR [on F <sup>2</sup> , all data]	0.1275	0.1770
Largest diff. Peak/hole. e/Å <sup>-3</sup>	0.370/0.390	0.409/-0.340

<b>50</b>	
Empirical formula	C <sub>39</sub> H <sub>50</sub> F <sub>4</sub> MgN <sub>2</sub> O
Mol. Mass	663.14
Crystal system	Monoclinic
Space group	P 2 <sub>1</sub> /n
a/ Å	12.4430(4)
b/ Å	16.6363(6)
c/ Å	18.2241(6)
α	90
β	97.499(3)
γ	90
V/ Å <sup>3</sup>	3740.2(2)
Z	4
λ / Å	1.54184
μ mm <sup>-1</sup>	1.1776
2θmax °	146.34
Measured reflections	15184
Unique reflections	7339
R <sub>int</sub>	0.0246
Observed rflns [I>2σ(I)]	6085
Goof	1.0423
R [on F, obs rflns only]	0.0539
wR [on F <sup>2</sup> , all data]	0.1603
Largest diff. Peak/hole. e/Å <sup>3</sup>	0.4161/-0.2267

---

## References

- [1] J. Clayden, *Organolithiums: Selectivity for Synthesis*, Elsevier, Oxford, **2002**.
- [2] M. Schlosser, in *Organometallics Synth. Third Man.* (Ed.: M. Schlosser), John Wiley & Sons Ltd., Chichester, **2013**, pp. 1–222.
- [3] E. Carl, D. Stalke, in *Lithium Compd. Org. Synth.* (Eds.: R. Luisi, V. Capriati), Wiley-VCH Verlag GmbH & Co. KGaA, Weinheim, Germany, **2014**, pp. 1–32.
- [4] E. Weiss, *Angew. Chem. Int. Ed.* **1993**, *32*, 1501–1670.
- [5] D. R. Armstrong, P. García-Álvarez, A. R. Kennedy, R. E. Mulvey, S. D. Robertson, *Chem. Eur. J.* **2011**, *17*, 6725–6730.
- [6] T. Niklas, D. Stalke, M. John, *Chem. Commun.* **2015**, *51*, 1275–1277.
- [7] S. Bachmann, B. Gernert, D. Stalke, *Chem. Commun.* **2016**, *52*, 12861–12864.
- [8] C. Schade, P. von Ragué Schleyer, *Adv. Organomet. Chem.* **1987**, *27*, 169–278.
- [9] V. H. Gessner, C. Däschlein, C. Strohmam, *Chem. Eur. J.* **2009**, *15*, 3320–3334.
- [10] M. G. Davidson, D. Garcia-Vivo, A. R. Kennedy, R. E. Mulvey, S. D. Robertson, *Chem. Eur. J.* **2011**, *17*, 3364–3369.
- [11] D. R. Armstrong, M. G. Davidson, D. Garcia-Vivo, A. R. Kennedy, R. E. Mulvey, S. D. Robertson, *Inorg. Chem.* **2013**, *52*, 12023–12032.

- 
- [12] M. B. Smith, J. March, *March's Advanced Organic Chemistry*, Wiley, New York, **2013**.
- [13] T. Kottke, D. Stalke, *Angew. Chem. Int. Ed.* **1993**, *32*, 580–582.
- [14] M. Schlosser, *Angew. Chem. Int. Ed.* **1964**, *3*, 287–306.
- [15] L. Orzechowski, G. Jansen, S. Harder, *Angew. Chem. Int. Ed.* **2009**, *48*, 3825–3829.
- [16] J. Barluenga, F. J. Fañanás, M. Yus, *J. Org. Chem.* **1981**, *46*, 1281–1283.
- [17] M. A. Nichols, P. G. Williard, *J. Am. Chem. Soc.* **1993**, *115*, 1568–1572.
- [18] J. A. Garden, D. R. Armstrong, W. Clegg, J. García-Alvarez, E. Hevia, A. R. Kennedy, R. E. Mulvey, S. D. Robertson, L. Russo, *Organometallics* **2013**, *32*, 5481–5490.
- [19] M. Lappert, A. Protchenko, A. Seeber, *Metal Amide Chemistry*, Wiley, Chichester, **2009**.
- [20] R. E. Mulvey, S. D. Robertson, *Angew. Chem. Int. Ed.* **2013**, *52*, 11470–11487.
- [21] T. “Li” Rathman, J. A. Schwindeman, *Org. Process Res. Dev.* **2014**, *18*, 1192–1210.
- [22] D. B. Collum, A. J. McNeil, A. Ramirez, *Angew. Chem. Int. Ed.* **2007**, *46*, 3002–3017.
- [23] J. C. Riggs, K. J. Singh, M. Yun, D. B. Collum, *J. Am. Chem. Soc.* **2008**, 13709–13717.
- [24] P. Zhao, A. Condo, I. Keresztes, D. B. Collum, *J. Am. Chem. Soc.* **2004**, *126*, 3113–3118.

- 
- [25] D. R. Armstrong, D. Barr, W. Clegg, R. E. Mulvey, D. Reed, R. Snaith, K. Wade, *J. Chem. Soc., Chem. Commun.* **1986**, *11*, 869–870.
- [26] R. E. Mulvey, *Chem. Soc. Rev.* **1991**, *20*, 167–209.
- [27] W. Clegg, K. W. Henderson, L. Horsburgh, F. M. Mackenzie, R. E. Mulvey, *Chem. Eur. J.* **1998**, *4*, 53–56.
- [28] C. Su, R. Hopson, P. G. Williard, *J. Am. Chem. Soc.* **2013**, *135*, 12400–12406.
- [29] E. Hevia, A. R. Kennedy, R. E. Mulvey, D. L. Ramsay, S. D. Robertson, *Chem. Eur. J.* **2013**, *19*, 14069–14075.
- [30] N. D. R. Barnett, R. E. Mulvey, W. Clegg, P. a. O’Neil, *J. Am. Chem. Soc.* **1991**, *113*, 8187–8188.
- [31] R. Neufeld, M. John, D. Stalke, *Angew. Chem. Int. Ed.* **2015**, *54*, 6994–6998.
- [32] J. Knizek, I. Krossing, H. Nöth, H. Schwenk, T. Seifert, *Chem. Ber.* **1997**, *130*, 1053–1062.
- [33] M. Driess, H. Pritzkow, M. Skipinski, U. Winkler, *Organometallics* **1997**, *16*, 5108–5112.
- [34] J. L. Atwood, R. Grüning, *J. Organomet. Chem.* **1977**, *137*, 101–111.
- [35] K. F. Tesh, T. P. Hanusa, J. C. Huffman, *Inorg. Chem.* **1990**, *29*, 1584–1586.
- [36] A. R. Kennedy, J. Klett, C. T. O’Hara, R. E. Mulvey, G. M. Robertson, *Eur. J. Inorg. Chem.* **2009**, 5029–5035.
- [37] D. R. Armstrong, A. R. Kennedy, R. E. Mulvey, S. D. Robertson, *Chem. Eur. J.* **2011**, *17*, 8820–8831.

- 
- [38] G. Wu, M. Huang, *Chem. Rev.* **2006**, *106*, 2596–2616.
- [39] R. E. Mulvey, *Acc. Chem. Res.* **2009**, *42*, 743–755.
- [40] P. Schorigin, *Berichte der Dtsch. Chem. Gesellschaft* **1908**, *41*, 2723–2728.
- [41] G. Wittig, G. Fuhrmann, *Chem. Ber.* **1940**, *73B*, 1197–1218.
- [42] H. Gilman, R. L. Bebb, *J. Am. Chem. Soc.* **1939**, *61*, 109–112.
- [43] V. Snieckus, *Chem. Rev.* **1990**, *90*, 879–933.
- [44] M. C. Whisler, S. MacNeil, V. Snieckus, P. Beak, *Angew. Chem. Int. Ed.* **2004**, *43*, 2206–2225.
- [45] J. M. Saá, *Helv. Chim. Acta* **2002**, *85*, 814–840.
- [46] S. T. Chadwick, R. A. Rennels, J. L. Rutherford, D. B. Collum, *J. Am. Chem. Soc.* **2000**, *122*, 8640–8647.
- [47] M. Schlosser, *Angew. Chem. Int. Ed.* **2005**, *44*, 376–393.
- [48] R. E. Mulvey, F. Mongin, M. Uchiyama, Y. Kondo, *Angew. Chem. Int. Ed.* **2007**, *46*, 3802–3824.
- [49] R. A. Finnegan, *Tetrahedron Lett.* **1963**, *4*, 429–433.
- [50] A. J. Chalk, T. J. Hoogeboom, *J. Organomet. Chem.* **1968**, *11*, 615–618.
- [51] D. W. Slocum, R. Moon, J. Thompson, D. S. Coffey, J. D. Li, M. G. Slocum, A. Siegel, R. Gayton-Garcia, *Tetrahedron Lett.* **1994**, *35*, 385–388.
- [52] L. Lochmann, J. Trekoval, *J. Organomet. Chem.* **1987**, *326*, 1–7.
- [53] M. Schlosser, *Pure Appl. Chem.* **1988**, *60*, 1627–1634.

- 
- [54] L. Lochmann, *Eur. J. Inorg. Chem.* **2000**, 1115–1126.
- [55] P. Benrath, M. Kaiser, T. Limbach, M. Mondeshki, J. Klett, *Angew. Chem. Int. Ed.* **2016**, *55*, 10886–10889.
- [56] J. D. Roberts, D. Y. Curtin, *J. Am. Chem. Soc.* **1946**, *68*, 1658–1660.
- [57] M. Schlosser, G. Katsoulos, S. Takagishi, *Synlett* **1990**, 747–748.
- [58] F. Yves, C. Comoy, *Lithium Compounds in Organic Synthesis*, Wiley-VCH Verlag GmbH & Co. KGaA, Weinheim, Germany, **2014**.
- [59] P. Fleming, D. F. Oshea, *J. Am. Chem. Soc.* **2011**, *133*, 1698–1701.
- [60] G. W. Gribble, T. C. Barden, D. A. Johnson, *Tetrahedron* **1988**, *44*, 3195–3202.
- [61] R. J. Mattson, C. P. Sloan, *J. Org. Chem.* **1990**, *55*, 3410–3412.
- [62] R. Chinchilla, C. Nájera, M. Yus, *Chem. Rev.* **2004**, *104*, 2667–2722.
- [63] S. Harder, *Chem. Rev.* **2010**, *110*, 3852–3876.
- [64] J. Seayad, A. Tillack, C. G. Hartung, M. Beller, *Adv. Synth. Catal.* **2002**, *344*, 795–813.
- [65] P. Horrillo-Martínez, K. C. Hultzsich, A. Gil, V. Branchadell, *European J. Org. Chem.* **2007**, 3311–3325.
- [66] P. Bellham, M. S. Hill, G. Kociok-Köhn, *Dalton Trans.* **2015**, *44*, 12078–12081.
- [67] R. McLellan, A. R. Kennedy, S. A. Orr, S. D. Robertson, R. E. Mulvey, *Angew. Chem. Int. Ed.* **2017**, *56*, 1036–1041.
- [68] L. S. Levitt, *Science* **1954**, *120*, 33–35.
- [69] L. Perera, W. A. Beard, L. G. Pedersen, S. H. Wilson, *Inorg. Chem.* **2017**, *56*,



- 313–320.
- [70] B. Haag, M. Mosrin, H. Ila, V. Malakhov, P. Knochel, *Angew. Chem. Int. Ed.* **2011**, *50*, 9794–9824.
- [71] P. Knochel, W. Dohle, N. Gommermann, F. F. Kneisel, F. Kopp, T. Korn, I. Sapountzis, V. A. Vu, *Angew. Chem. Int. Ed.* **2003**, *42*, 4302–4320.
- [72] S. Harder, Ed. , *Alkaline-Earth Metal Compounds*, Springer Heidelberg, Berlin, Heidelberg, **2013**.
- [73] D. Seyferth, *Organometallics* **2009**, *28*, 1598–1605.
- [74] W. Schlenk, W. Schlenk, *Ber. Dtsch. Chem. Ges.* **1929**, *62*, 920–924.
- [75] A. C. Cope, *J. Am. Chem. Soc.* **1935**, *57*, 2238–2240.
- [76] F. W. Walker, E. C. Ashby, *J. Am. Chem. Soc.* **1969**, *91*, 3845–3850.
- [77] R. Neufeld, T. L. Teuteberg, R. Herbst-Irmer, R. A. Mata, D. Stalke, *J. Am. Chem. Soc.* **2016**, *138*, 4796–4806.
- [78] A. Krasovskiy, P. Knochel, *Angew. Chem. Int. Ed.* **2004**, *43*, 3333–3336.
- [79] C. Schnegelsberg, S. Bachmann, M. Kolter, T. Auth, M. John, D. Stalke, K. Koszinowski, *Chem. Eur. J.* **2016**, *22*, 7752–7762.
- [80] L. Meunier, *C. R. Hebd. Seances Acad. Sci.* **1903**, *136*, 758–159.
- [81] C. R. Hauser, H. G. Walker, *J. Am. Chem. Soc.* **1947**, *69*, 295–297.
- [82] P. E. Eaton, C.-H. Lee, Y. Xiong, *J. Am. Chem. Soc.* **1989**, *111*, 8016–8018.
- [83] P. E. Eaton, Y. S. Xiong, R. Gilardi, *J. Am. Chem. Soc.* **1993**, *115*, 10195–10202.
- [84] M. X. Zhang, P. E. Eaton, *Angew. Chem. Int. Ed.* **2002**, *41*, 2169–2171.

- 
- [85] M. Shilai, Y. Kondo, T. Sakamoto, *J. Chem. Soc. Perkin Trans. 1* **2001**, 442–444.
- [86] Y. Kondo, A. Yoshida, T. Sakamoto, *J. Chem. Soc. Perkin Trans. 1* **1996**, 2331–2332.
- [87] A. Krasovskiy, V. Krasovskaya, P. Knochel, *Angew. Chem. Int. Ed.* **2006**, *45*, 2958–2961.
- [88] P. García-Álvarez, D. V. Graham, E. Hevia, A. R. Kennedy, J. Klett, R. E. Mulvey, C. T. O'Hara, S. Weatherstone, *Angew. Chem. Int. Ed.* **2008**, *47*, 8079–8081.
- [89] D. R. Armstrong, P. García-Álvarez, A. R. Kennedy, R. E. Mulvey, J. A. Parkinson, *Angew. Chem. Int. Ed.* **2010**, *49*, 3185–3188.
- [90] R. Neufeld, D. Stalke, *Chem. Eur. J.* **2016**, *22*, 12624–12628.
- [91] C. Jones, *Coord. Chem. Rev.* **2010**, *254*, 1273–1289.
- [92] Y. Tsai, *Coord. Chem. Rev.* **2012**, *256*, 722–758.
- [93] L. Bourget-Merle, M. F. Lappert, J. R. Severn, *Chem. Rev.* **2002**, *102*, 3031–3065.
- [94] C. Camp, J. Arnold, *Dalton Trans.* **2016**, *45*, 14462–14498.
- [95] C. Chen, S. M. Bellows, P. L. Holland, *Dalton Trans.* **2015**, *44*, 16654–16670.
- [96] M. Arrowsmith, B. Maitland, G. Kociok-Köhn, A. Stasch, C. Jones, M. S. Hill, *Inorg. Chem.* **2014**, *53*, 10543–10552.
- [97] S. J. Bonyhady, C. Jones, S. Nembenna, A. Stasch, A. J. Edwards, G. J. McIntyre, *Chem. Eur. J.* **2010**, *16*, 938–955.
- [98] S. S. Sankaranarayana Pillai Nembenna, S. Nagendran, H. W. Roesky, *Acc.*

- Chem. Res.* **2011**, *44*, 157–170.
- [99] S. Harder, *Organometallics* **2002**, *21*, 3782–3787.
- [100] A. Stasch, C. Jones, *Dalton Trans.* **2011**, *40*, 5659–5672.
- [101] S. P. Green, C. Jones, A. Stasch, *Science* **2007**, *318*, 1754–1757.
- [102] S. P. Green, C. Jones, A. Stasch, *Angew. Chem. Int. Ed.* **2008**, *47*, 9079–9083.
- [103] S. J. Bonyhady, S. P. Green, C. Jones, S. Nembenna, A. Stasch, *Angew. Chem. Int. Ed.* **2009**, *48*, 2973–2977.
- [104] R. Lalrempuia, C. E. Kefalidis, S. J. Bonyhady, B. Schwarze, L. Maron, A. Stasch, C. Jones, *J. Am. Chem. Soc.* **2015**, *137*, 8944–8947.
- [105] S. Harder, J. Spielmann, J. Intemann, H. Bandmann, *Angew. Chem. Int. Ed.* **2011**, *50*, 4156–4160.
- [106] S. E. Baillie, V. L. Blair, T. D. Bradley, W. Clegg, J. Cowan, R. W. Harrington, A. Hernán-Gómez, A. R. Kennedy, Z. Livingstone, E. Hevia, *Chem. Sci.* **2013**, *4*, 1895–1905.
- [107] T. E. Stennett, S. Harder, *Chem. Soc. Rev.* **2016**, *45*, 1112–1128.
- [108] S. Harder, J. Brettar, *Angew. Chem. Int. Ed.* **2006**, *45*, 3474–3478.
- [109] R. L. Webster, *Dalton Trans.* **2017**, *46*, 4483–4498.
- [110] M. H. Chisholm, J. C. Huffman, K. Phomphrai, *J. Chem. Soc. Dalt. Trans.* **2001**, 222–224.
- [111] B. M. Chamberlain, M. Cheng, D. R. Moore, T. M. Ovitt, E. B. Lobkovsky, G. W. Coates, *J. Am. Chem. Soc.* **2001**, *123*, 3229–3238.

- [112] F. Drouin, T. J. J. Whitehorne, F. Schaper, *Dalton Trans.* **2011**, *40*, 1396–1400.
- [113] M. Arrowsmith, M. S. Hill, T. Hadlington, G. Kociok-Köhn, C. Weetman, *Organometallics* **2011**, *30*, 5556–5559.
- [114] C. Weetman, M. S. Hill, M. F. Mahon, *Polyhedron* **2016**, *103*, 115–120.
- [115] C. Weetman, M. S. Hill, M. F. Mahon, *Chem. Eur. J.* **2016**, *22*, 7158–7162.
- [116] A. G. M. Barrett, C. Brinkmann, M. R. Crimmin, M. S. Hill, P. Hunt, P. A. Procopiou, *J. Am. Chem. Soc.* **2009**, *131*, 12906–12907.
- [117] M. R. Crimmin, M. Arrowsmith, A. G. M. Barrett, I. J. Casely, M. S. Hill, P. A. Procopiou, *J. Am. Chem. Soc.* **2009**, *131*, 9670–9685.
- [118] M. R. Crimmin, I. J. Casely, M. S. Hill, *J. Am. Chem. Soc.* **2005**, *127*, 2042–2043.
- [119] M. D. Anker, M. Arrowsmith, P. Bellham, M. S. Hill, G. Kociok-Köhn, D. J. Liptrot, M. F. Mahon, C. Weetman, *Chem. Sci.* **2014**, *5*, 2826.
- [120] R. E. Mulvey, S. D. Robertson, in *Top. Organomet. Chem.* (Ed.: Z. Xi), Springer, Heidelberg, **2014**, pp. 129–158.
- [121] J. Wanklyn, *Proc. R. Soc. London* **1858**, *9*, 341–345.
- [122] G. Wittig, F. J. Meyer, G. Lange, *Justus Liebigs Ann. Chem* **1951**, *571*, 167–201.
- [123] R. E. Mulvey, S. D. Robertson, in *Top. Organomet. Chem.* (Ed.: S. Harder), Springer, Heidelberg, **2013**, pp. 103–140.
- [124] A. J. Martínez-Martínez, A. R. Kennedy, R. E. Mulvey, C. T. O’Hara, *Science* **2014**, *346*, 834–837.
- [125] M. Hatano, T. Matsumura, K. Ishihara, *Org. Lett.* **2005**, *7*, 573–6.

- [126] S. E. Baillie, T. D. Bluemke, W. Clegg, A. R. Kennedy, J. Klett, L. Russo, M. de Tullio, E. Hevia, *Chem. Commun.* **2014**, 50, 12859–12862.
- [127] W. Clegg, B. Conway, A. R. Kennedy, J. Klett, R. E. Mulvey, L. Russo, *Eur. J. Inorg. Chem.* **2011**, 721–726.
- [128] S. E. Baillie, W. Clegg, P. García-Álvarez, E. Hevia, A. R. Kennedy, J. Klett, L. Russo, *Chem. Commun.* **2011**, 47, 388–390.
- [129] A. Hernán-Gómez, T. D. Bradley, A. R. Kennedy, Z. Livingstone, S. D. Robertson, E. Hevia, *Chem. Commun.* **2013**, 49, 8659–8661.
- [130] M. De Tullio, A. Hernán-Gómez, Z. Livingstone, W. Clegg, A. R. Kennedy, R. W. Harrington, A. Antiñolo, A. Martínez, F. Carrillo-Hermosilla, E. Hevia, *Chem. Eur. J.* **2016**, 22, 17646–17656.
- [131] C. Glock, H. Görls, M. Westerhausen, *Chem. Commun.* **2012**, 48, 7094–7096.
- [132] C. Glock, F. M. Younis, S. Ziemann, H. Görls, W. Imhof, S. Krieck, M. Westerhausen, *Organometallics* **2013**, 32, 2649–2660.
- [133] F. M. Younis, S. Krieck, H. Görls, M. Westerhausen, *Organometallics* **2015**, 34, 3577–3585.
- [134] F. M. Younis, S. Krieck, H. Görls, M. Westerhausen, *Dalton Trans.* **2016**, 45, 6241–6250.
- [135] A. L. Reznichenko, K. C. Hultsch, in *Top Organomet Chem* (Eds.: V.P. Ananikov, M. Tanaka), Springer Berlin Heidelberg, **2013**, pp. 51–114.
- [136] T. E. Müller, K. C. Hultsch, M. Yus, F. Foubelo, M. Tada, *Chem. Rev.* **2008**, 108, 3795–3892.

- 
- [137] J. Hannedouche, E. Schulz, *Chem. Eur. J.* **2013**, *19*, 4972–4985.
- [138] T. E. Müller, M. Beller, *Chem. Rev.* **1998**, *98*, 675–703.
- [139] R. Severin, S. Doye, *Chem. Soc. Rev.* **2007**, *36*, 1407–1420.
- [140] M. Beller, C. Breindl, T. H. Riermeier, M. Eichberger, H. Trauthwein, *Angew. Chem. Int. Ed.* **1998**, *37*, 3389–3391.
- [141] S. M. Coman, V. I. Parvulescu, *Org. Process Res. Dev.* **2015**, *19*, 1327–1355.
- [142] R. Hili, A. K. Yudin, *Nat. Chem. Biol.* **2006**, *2*, 284–287.
- [143] S.-L. Shi, S. L. Buchwald, *Nat. Chem.* **2015**, *7*, 38–44.
- [144] J. Penafiel, L. Maron, S. Harder, *Angew. Chem. Int. Ed.* **2014**, *53*, 201–206.
- [145] M. Beller, J. Seayad, A. Tillack, H. Jiao, *Angew. Chem. Int. Ed.* **2004**, *43*, 3368–3398.
- [146] L. Huang, M. Arndt, K. Gooßen, H. Heydt, L. J. Gooßen, *Chem. Rev.* **2015**, *115*, 2596–2697.
- [147] F. Alonso, I. P. Beletskaya, M. Yus, *Chem. Rev.* **2004**, *104*, 3079–3159.
- [148] M. S. Hill, D. J. Liptrot, C. Weetman, *Chem. Soc. Rev.* **2016**, *45*, 972–988.
- [149] C. Brinkmann, A. G. M. Barrett, M. S. Hill, P. A. Procopiou, *J. Am. Chem. Soc.* **2012**, *134*, 2193–2207.
- [150] B. Liu, T. Roisnel, J.-F. Carpentier, Y. Sarazin, *Angew. Chem. Int. Ed.* **2012**, *51*, 4943–4946.
- [151] S. Hong, T. J. Marks, *Acc. Chem. Res.* **2004**, *37*, 673–686.
- [152] J.-S. Ryu, G. Y. Li, T. J. Marks, *J. Am. Chem. Soc.* **2003**, *125*, 12584–12605.

- [153] R. Wegler, G. Pieper, *Chem. Ber.* **1950**, *83*, 1–6.
- [154] R. J. Schlott, J. C. Falk, K. W. Narducy, *J. Org. Chem.* **1972**, *37*, 4243–4245.
- [155] D. Tzalis, C. Koradin, P. Knochel, *Tetrahedron Lett.* **1999**, *40*, 6193–6195.
- [156] G. P. Pez, J. E. Galle, *Pure Appl. Chem.* **1985**, *57*, 1917–1926.
- [157] B. W. Howk, E. L. Little, S. L. Scott, G. M. Whitman, *J. Am. Chem. Soc.* **1954**, *76*, 1899–1902.
- [158] J. Pretula, K. Kaluzynski, B. Wisniewski, R. Szymanski, T. Loontjens, S. Penczek, *J. Polym. Sci. Part a-Polymer Chem.* **2008**, *46*, 830–843.
- [159] S. Tobisch, *Chem. Eur. J.* **2014**, *20*, 8988–9001.
- [160] C. G. Hartung, C. Breindl, A. Tillack, M. Beller, *Tetrahedron* **2000**, *56*, 5157–5162.
- [161] D. R. Armstrong, E. Brammer, T. Cadenbach, E. Hevia, A. R. Kennedy, *Organometallics* **2013**, *32*, 480–489.
- [162] D. R. Armstrong, H. S. Emerson, A. Hernán-Gómez, A. R. Kennedy, E. Hevia, *Dalton Trans.* **2014**, *43*, 14229–14238.
- [163] P. J. Davidson, M. F. Lappert, R. Pearce, *Acc. Chem. Res.* **1974**, *7*, 209–217.
- [164] P. J. Davidson, M. F. Lappert, R. Pearce, *Chem Rev* **1976**, *76*, 219–242.
- [165] W. Clegg, A. R. Kennedy, J. Klett, R. E. Mulvey, L. Russo, *Eur. J. Inorg. Chem.* **2012**, 2989–2994.
- [166] A. G. M. Barrett, M. R. Crimmin, M. S. Hill, G. Kociok-Köhn, J. R. Lachs, P. A. Procopiou, *Dalton Trans.* **2008**, 1292–1294.

- [167] K. D. Hesp, M. Stradiotto, *J. Am. Chem. Soc.* **2010**, *132*, 18026–18029.
- [168] A. Reyes-Sánchez, I. García-Ventura, J. J. García, *Dalton Trans.* **2014**, *43*, 1762–1768.
- [169] M. Otsuka, H. Yokoyama, K. Endo, T. Shibata, *Org. Biomol. Chem.* **2012**, *10*, 3815.
- [170] A. G. M. Barrett, M. R. Crimmin, M. S. Hill, P. B. Hitchcock, P. A. Procopiou, *Angew. Chem. Int. Ed.* **2007**, *46*, 6339–6342.
- [171] M. Otsuka, H. Yokoyama, K. Endo, T. Shibata, *Org. Biomol. Chem.* **2012**, *10*, 3815–3818.
- [172] K. Takabe, T. Katagiri, J. Tanaka, *Bull. Chem. Soc. Jpn.* **1973**, *46*, 222–225.
- [173] D. H. Kim, S. S. Park, S. H. Park, J. Y. Jeon, H. B. Kim, B. Y. Lee, *RSC Adv.* **2017**, *7*, 5948–5956.
- [174] D. F. Lawson, D. R. Brumbaugh, M. L. Stayer, J. R. Schreffler, T. A. Antkowiak, D. Saffles, K. Morita, Y. Ozawa, S. Nakayama, in *Appl. Anionic Polym. Res.* (Ed.: R.P. Quirk), **1998**, pp. 77–87.
- [175] J. F. Dunne, D. B. Fulton, A. Ellern, A. D. Sadow, *J. Am. Chem. Soc.* **2010**, *132*, 17680–17683.
- [176] P. C. Andrews, W. Clegg, R. E. Mulvey, P. A. O’Neil, H. M. M. Wilson, *Chem. Commun.* **1993**, *14*, 1142–1144.
- [177] D. R. Armstrong, D. Barr, W. Clegg, S. M. Hodgson, R. E. Muhey, D. Reed, R. Snaith, D. S. Wright, *J. Am. Chem. Soc.* **1989**, *111*, 4719–4727.
- [178] A. R. Kennedy, R. E. Mulvey, A. Robertson, *Chem. Commun.* **1998**, 89–90.



- [179] D. Li, I. Keresztes, R. Hopson, P. G. Williard, *Acc. Chem. Res.* **2009**, *42*, 270–280.
- [180] P. S. Pregosin, *Acta Crystallogr. Sect. C* **2013**, *69*, 1433–1436.
- [181] Y. Cohen, L. Avram, L. Frish, *Angew. Chem. Int. Ed.* **2005**, *44*, 520–554.
- [182] R. Neufled, D. Stalke, *Chem. Sci.* **2015**, *6*, 3354–3364.
- [183] S. Bachmann, R. Neufeld, M. Dzemski, D. Stalke, *Chem. Eur. J.* **2016**, *22*, 8462–8465.
- [184] J. Liang, A. C. Hoepker, R. F. Algera, Y. Ma, D. B. Collum, *J. Am. Chem. Soc.* **2015**, *137*, 6292–6303.
- [185] J. a Seijas, M. P. Vázquez-Tato, C. Entenza, M. M. Martínez, M. G. Ónega, S. Veiga, *Tetrahedron Lett.* **1998**, *39*, 5073–5076.
- [186] C. Unkelbach, H. S. Rosenbaum, C. Strohmam, *Chem. Commun.* **2012**, *48*, 10612–10614.
- [187] T. Mizuta, S. Sakaguchi, Y. Ishii, *J. Org. Chem.* **2005**, *70*, 2195–2199.
- [188] N. P. Mankad, *Chem. Eur. J.* **2016**, *22*, 5822–5829.
- [189] J. Park, S. Hong, *Chem. Soc. Rev.* **2012**, *41*, 6931–6943.
- [190] X. Zhou, M. Zhu, *J. Organometallic Chem.* **2002**, *647*, 28–49.
- [191] S. E. Baillie, W. Clegg, P. García-Álvarez, E. Hevia, A. R. Kennedy, J. Klett, L. Russo, *Organometallics* **2012**, *31*, 5131–5142.
- [192] V. M. Arredondo, S. Tian, F. E. McDonald, T. J. Marks, *J. Am. Chem. Soc.* **1999**, *121*, 3633–3639.

- [193] D. R. Armstrong, C. Dougan, D. V. Graham, E. Hevia, A. R. Kennedy, *Organometallics* **2008**, *27*, 6063–6070.
- [194] E. Weiss, D. Kristallstruktur, *Chem. Ber.* **1968**, 35–40.
- [195] E. Weiss, G. Hencken, *J. Organomet. Chem.* **1970**, *21*, 265–268.
- [196] R. E. Mulvey, *Chem. Commun.* **2001**, 1049–1056.
- [197] T. Han, J. Utko, L. B. Jerzykiewicz, P. Sobota, *Dalton Trans.* **2011**, *40*, 12660–12662.
- [198] Y.-C. Liu, C.-H. Lin, B.-T. Ko, R.-M. Ho, *J. Polym. Sci. Part A Polym. Chem.* **2010**, *48*, 5339–5347.
- [199] E. Hevia, D. J. Gallagher, A. R. Kennedy, R. E. Mulvey, C. T. O'Hara, C. Talmard, *Chem. Commun.* **2004**, 791, 2422–2423.
- [200] R. Neufeld, D. Stalke, *Chem. Sci.* **2015**, *6*, 3354–3364.
- [201] R. A. Lewis, G. Wu, T. W. Hayton, *Inorg. Chem.* **2011**, *50*, 4660–4668.
- [202] W. Clegg, K. W. Henderson, R. E. Mulvey, P. A. O'Neil, *Chem. Commun.* **1993**, 969–970.
- [203] W. Clegg, K. W. Henderson, R. E. Mulvey, P. A. O'Neil, *J. Chem. Soc., Chem. Commun.* **1994**, 769–770.
- [204] J. Clayden, in *Chem. Organolithium Compd.* (Eds.: Z. Rappoport, I. Marek), John Wiley & Sons Ltd., Chichester, **2004**, p. 495.
- [205] N. Plé, A. Turck, K. Couture, G. Quéguiner, *J. Org. Chem.* **1995**, *60*, 3781–3786.

- [206] K. W. Henderson, W. J. Kerr, *Chem. Eur. J.* **2001**, *7*, 3430–3437.
- [207] A. Kawachi, S. Nagae, Y. Onoue, O. Harada, Y. Yamamoto, *Chem. Eur. J.* **2011**, *17*, 8005–8008.
- [208] P. E. Eaton, K. A. Lukin, *J. Am. Chem. Soc.* **1993**, *115*, 11370–11375.
- [209] W. Schlecker, A. Huth, E. Ottow, *J. Org. Chem.* **1995**, *60*, 8414–8416.
- [210] N. Momiyama, H. Okamoto, M. Shimizu, M. Terada, *Chirality* **2015**, *27*, 464–475.
- [211] T. Ooi, Y. Uematsu, K. Maruoka, *J. Org. Chem.* **2003**, *68*, 4576–4578.
- [212] T. Klatt, J. T. Markiewicz, C. Sämann, P. Knochel, *J. Org. Chem.* **2014**, *79*, 4253–4269.
- [213] J. A. Joule, K. Mills, in *Heterocycl. Chem.* (Ed.: Backwell), Wiley, Chichester, **2010**, pp. 369–372.
- [214] A. R. Katritzky, C. A. Ramsden, J. A. Joule, V. V. Zhdankin, *Handbook of Heterocyclic Chemistry*, Elsevier, Oxford, **2010**.
- [215] N. Edraki, A. R. Mehdipour, M. Khoshneviszadeh, R. Miri, *Drug Discov. Today* **2009**, *14*, 1058–1066.
- [216] A. R. Katritzky, S. Rachwal, B. Rachwal, *Tetrahedron* **1996**, *52*, 15031–15070.
- [217] S. P. Roche, J. A. Porco Jr, *Angew. Chem. Int. Ed.* **2011**, *50*, 4068–4093.
- [218] D. M. Stout, *Chem. Rev.* **1982**, *82*, 223–243.
- [219] F. Mongin, G. Quéguiner, *Tetrahedron* **2001**, *57*, 4059–4090.
- [220] S. E. Baillie, V. L. Blair, D. C. Blakemore, D. Hay, A. R. Kennedy, D. C. Pryde, E.

- Hevia, *Chem. Commun.* **2012**, 48, 1985–1987.
- [221] A. Seggio, F. Chevallier, M. Vaultier, F. Mongin, *J. Org. Chem.* **2007**, 72, 6602–6605.
- [222] F. Chevallier, F. Mongin, *Chem. Soc. Rev.* **2008**, 37, 595–609.
- [223] G. Quéguiner, F. Marsais, V. Snieckus, J. Epsztajn, *Adv. Heterocycl. Chem.* **1991**, 52, 187–304.
- [224] A. Turck, N. Plé, F. Mongin, G. Quéguiner, *Tetrahedron* **2001**, 57, 4489–4505.
- [225] Z. Dong, G. C. Clososki, S. H. Wunderlich, A. Unsinn, J. Li, P. Knochel, *Chem. Eur. J.* **2009**, 15, 457–468.
- [226] M. H. Chisholm, K. Choojun, J. C. Gallucci, P. M. Wambua, *Chem. Sci.* **2012**, 3, 3445.
- [227] B. D. Kenney, M. Breslav, R. Chang, R. Glaser, B. D. Harris, C. A. Maryanoff, J. Mills, A. Roessler, B. Segmuller, F. J. J. Villani, *J. Org. Chem.* **2007**, 72, 9798–9801.
- [228] K. Shen, Y. Fu, J.-N. Li, L. Liu, Q.-X. Guo, *Tetrahedron* **2007**, 63, 1568–1576.
- [229] M. Navamal, C. McGrath, J. Stewart, P. Blans, F. Villamena, J. Zweier, J. C. Fishbein, *J. Org. Chem.* **2002**, 67, 9406–9413.
- [230] K.-S. Yeung, in *Top. Heterocycl. Chem.* (Ed.: G.W. Gribble), Springer Berlin Heidelberg, **2012**, pp. 47–76.
- [231] R. J. Nevagi, S. N. Dighe, S. N. Dighe, *Eur. J. Med. Chem.* **2015**, 97, 561–581.
- [232] M. Mosrin, P. Knochel, *Org. Lett.* **2009**, 11, 1837–1840.

- 
- [233] M. Uzelac, A. R. Kennedy, E. Hevia, R. E. Mulvey, *Angew. Chem. Int. Ed.* **2016**, *55*, 13147–13150.
- [234] M. S. Hill, D. J. MacDougall, M. F. Mahon, *Dalton Trans.* **2010**, *39*, 11129–11131.
- [235] M. S. Hill, G. Kociok-Köhn, D. J. MacDougall, M. F. Mahon, C. Weetman, *Dalton Trans.* **2011**, *40*, 12500–12509.
- [236] D. Kratzert, D. Leusser, D. Stern, J. Meyer, F. Breher, D. Stalke, *Chem. Commun.* **2011**, *47*, 2931–2933.
- [237] P. J. Wheatley, *Acta Crystallogr.* **1957**, *10*, 182–187.
- [238] C. Hilf, F. Bosold, K. Harms, J. C. W. Lohrenz, M. Marsch, M. Schmieczek, G. Boche, *Chem. Ber.* **1997**, *130*, 1201–1212.
- [239] A. R. Kennedy, R. E. Mulvey, S. D. Robertson, *Dalton Trans.* **2010**, *39*, 9091–9099.
- [240] A. J. Arduengo III, H. V. R. Dias, F. Davidson, R. L. Harlow, *J. Organomet. Chem.* **1993**, *462*, 13–18.
- [241] D. Zhang, H. Kawaguchi, *Organometallics* **2006**, *25*, 5506–5509.
- [242] P. L. Arnold, I. J. Casely, Z. R. Turner, R. Bellabarba, R. B. Tooze, *Dalton Trans.* **2009**, 7236–7247.
- [243] M. Arrowsmith, M. S. Hill, D. J. MacDougall, M. F. Mahon, *Angew. Chem. Int. Ed.* **2009**, *48*, 4013–4016.
- [244] A. R. Kennedy, J. Klett, R. E. Mulvey, S. D. Robertson, *Eur. J. Inorg. Chem.* **2011**, 4675–4679.

- [245] S. He, P. Li, X. Dai, C. C. McComas, C. Du, P. Wang, Z. Lai, H. Liu, J. Yin, P. G. Bulger, et al., *Tetrahedron Lett.* **2014**, *55*, 2212–2216.
- [246] H. Naka, M. Uchiyama, Y. Matsumoto, A. E. H. Wheatley, M. McPartlin, J. V. Morey, Y. Kondo, *J. Am. Chem. Soc.* **2007**, *129*, 1921–1930.
- [247] S. Usui, Y. Hashimoto, J. V. Morey, A. E. H. Wheatley, M. Uchiyama, *J. Am. Chem. Soc.* **2007**, *129*, 15102–15103.
- [248] J.-M. L'Helgoual'ch, A. Seggio, F. Chevallier, M. Yonehara, E. Jeanneau, M. Uchiyama, F. Mongin, *J. Org. Chem.* **2008**, *73*, 177–183.
- [249] F. Mongin, A. Bucher, J. P. Bazureau, O. Bayh, H. Awad, F. Trécourt, *Tetrahedron Lett.* **2005**, *46*, 7989–7992.
- [250] Y. Ohki, T. Hatanaka, K. Tatsumi, *J. Am. Chem. Soc.* **2008**, *130*, 17174–17186.
- [251] S. Harder, J. Boersma, L. Brandsma, J. A. Kanters, W. Bauer, R. Pi, P. von R. Schleyer, H. Schöllhorn, U. Thewalt, *Organometallics* **1989**, *8*, 1688–1696.
- [252] A. P. Dove, V. C. Gibson, P. Hormnirun, E. L. Marshall, J. A. Segal, A. J. P. White, D. J. Williams, *Dalton Trans.* **2003**, 3088.
- [253] D. V. Graham, E. Hevia, A. R. Kennedy, R. E. Mulvey, C. T. O'Hara, C. Talmard, *Chem. Commun.* **2006**, 417–419.
- [254] V. L. Blair, A. R. Kennedy, J. Klett, R. E. Mulvey, *Chem. Commun.* **2008**, 5426–5428.
- [255] V. E. Matulis, Y. S. Halauko, O. A. Ivashkevich, P. N. Gaponik, *J. Mol. Struct. THEOCHEM* **2009**, *909*, 19–24.
- [256] A. Krasinski, V. V. Fokin, K. B. Sharpless, *Org. Lett.* **2004**, *6*, 1237–1240.

- [257] G. Aromí, L. A. Barrios, O. Roubeau, P. Gamez, *Coord. Chem. Rev.* **2011**, *255*, 485–546.
- [258] W.-Q. Fan, A. R. Katritzky, in *Compr. Heterocycl. Chem. II* (Eds.: A.R. Katritzky, C.W. Rees, E.F. V. Scriven), Elsevier Science Ltd, Oxford, **1996**, pp. 1–126.
- [259] T. Eicher, S. Hauptmann, A. Speicher, in *Chem. Heterocycles*, Wiley-VCH Verlag GmbH & Co. KGaA, Weinheim, FRG, **2003**, pp. 52–121.
- [260] E. Nagaradja, F. Chevallier, T. Roisnel, V. Dorcet, Y. S. Halauko, O. A. Ivashkevich, V. E. Matulis, F. Mongin, *Org. Biomol. Chem. Chem.* **2014**, *12*, 1475–1487.
- [261] J. M. Divse, S. B. Mhaske, C. R. Charolkar, D. G. Sant, S. G. Tupe, M. V. Deshpande, V. M. Khedkar, L. U. Nawale, D. Sarkar, V. S. Pore, *New J. Chem.* **2017**, *41*, 470–479.
- [262] A. Ayati, S. Emami, A. Foroumadi, *Eur. J. Med. Chem.* **2016**, *109*, 380–392.
- [263] J. M. Lopchuk, in *Top. Heterocycl. Chem.* (Ed.: G.W. Gribble), Springer Berlin Heidelberg, **2012**, pp. 415–440.
- [264] S. Ohta, I. Kawasaki, T. Uemura, M. Yamashita, T. Yoshioka, S. Yamaguchi, *Chem. Pharm. Bull.* **1997**, *45*, 1140–1145.
- [265] T. L. Gilchrist, G. E. Gymer, *Adv. Heterocycl. Chem.* **1974**, *16*, 33–85.
- [266] R. Raap, *Can. J. Chem.* **1971**, *49*, 1792–1798.
- [267] S. Ghose, T. L. Gilchrist, *J. Chem. Soc. Perkin Trans. 1* **1991**, 775–779.
- [268] D. Liu, W. Gao, Q. Dai, X. Zhang, *Org. Lett.* **2005**, *7*, 4907–4910.
- [269] Q. Dai, W. Gao, D. Liu, L. M. Kapes, X. Zhang, *J. Org. Chem.* **2006**, *71*, 3928–

- 3934.
- [270] V. L. Blair, D. C. Blakemore, D. Hay, E. Hevia, D. C. Pryde, *Tetrahedron Lett.* **2011**, *52*, 4590–4594.
- [271] D. V. Partyka, J. B. Updegraff, M. Zeller, A. D. Hunter, T. G. Gray, *Organometallics* **2007**, *26*, 183–186.
- [272] E. C. Keske, O. V. Zenkina, R. Wang, C. M. Crudden, *Organometallics* **2012**, *31*, 6215–6221.
- [273] D. V. Partyka, L. Gao, T. S. Teets, J. B. Updegraff, N. Deligonul, T. G. Gray, *Organometallics* **2009**, *28*, 6171–6182.
- [274] T. J. Robilotto, N. Deligonul, J. B. Updegraff, T. G. Gray, *Inorg. Chem.* **2013**, *52*, 9659–9668.
- [275] S. Hohloch, W. Frey, C.-Y. Su, B. Sarkar, *Dalton Trans.* **2013**, *42*, 11355–11358.
- [276] B. Sureshbabu, V. Ramkumar, S. Sankararaman, *Dalton Trans.* **2014**, *43*, 10710–10712.
- [277] A. R. Katritzky, X. Lan, J. Z. Yang, O. V. Denisko, *Chem. Rev.* **1998**, *98*, 409–548.
- [278] E. Nawrot, A. Jonczyk, *J. Fluor. Chem.* **2009**, *130*, 466–469.
- [279] A. R. Katritzky, J. Wu, W. Kuzmierkiewicz, S. Rachwal, *Liebigs Ann. der Chemie* **1994**, 1–5.
- [280] P. E. Goss, *Breast Cancer Res. Treat.* **1998**, *49*, S59–S65.
- [281] Y. X. Yuan, P.-J. Wei, W. Qin, Y. Zhang, J. L. Yao, R.-A. Gu, *Eur. J. Inorg. Chem.* **2007**, 4980–4987.



- [282] H. Duan, S. Sengupta, J. L. Petersen, N. G. Akhmedov, X. Shi, *J. Am. Chem. Soc.* **2009**, *131*, 12100–12102.
- [283] V. Tangoulis, T. F. Zafiroopoulos, *J. Chem Soc., Chem. Commun.* **1995**, 1347–1348.
- [284] R. A. Layfield, J. J. W. McDouall, S. A. Sulway, F. Tuna, D. Collison, R. E. P. Winpenny, *Chem. Eur. J.* **2010**, *16*, 4442–4446.
- [285] X. Xue, G.-T. Li, Y.-H. Peng, L. Wu, B.-L. Wu, *J. Coord. Chem.* **2011**, *64*, 1953–1962.
- [286] Y.-C. Shen, Z.-J. Li, J.-K. Cheng, Y.-Y. Qin, Y.-G. Yao, *Inorg. Chem. Commun.* **2007**, *10*, 888–890.
- [287] S. Krawczyk, M. Gdaniec, *Acta Crystallogr. Sect. E* **2005**, *61*, o2967–o2969.
- [288] J. Zhao, S. Zhang, W.-X. Zhang, Z. Xi, *Organometallics* **2011**, *30*, 3464–3467.
- [289] A. Sadhukhan, M. C. Hobbs, A. J. H. M. Meijer, I. Coldham, *Chem. Sci.* **2017**, *8*, 1436–1441.
- [290] D. M. Tellers, J. C. M. Ritter, R. G. Bergman, *Inorg. Chem.* **1999**, *38*, 4810–4818.
- [291] L. Becker, V. V. Burlakov, P. Arndt, A. Spannenberg, W. Baumann, H. Jiao, U. Rosenthal, *Chem. Eur. J.* **2013**, *19*, 4230–4237.
- [292] C. Wang, X. Zhang, M. Xue, Y. Zhang, Q. Shen, *Organometallics* **2013**, *32*, 3618–3624.
- [293] J. Zhao, S. Zhang, W. X. Zhang, Z. Xi, *Organometallics* **2012**, *31*, 8370–8374.
- [294] E. Iravani, B. Neumüller, *Organometallics* **2003**, *22*, 4129–4135.

- 
- [295] I. L. Fedushkin, A. G. Morozov, V. A. Chudakova, G. K. Fukin, V. K. Cherkasov, *Eur. J. Inorg. Chem.* **2009**, *3*, 4995–5003.
- [296] C. Weetman, M. D. Anker, M. Arrowsmith, M. S. Hill, G. Kociok-Köhn, D. J. Liptrot, M. F. Mahon, *Chem. Sci.* **2016**, *7*, 628–641.
- [297] I. L. Fedushkin, A. G. Morozov, O. V. Rassadin, G. K. Fukin, *Chem. Eur. J.* **2005**, *11*, 5749–5757.
- [298] M. Purzycki, W. Liu, G. Hilmersson, F. F. Fleming, *Chem. Commun.* **2013**, *49*, 4700–4002.
- [299] R. Sott, J. Granander, G. Hilmersson, *J. Am. Chem. Soc.* **2004**, *126*, 6798–6805.
- [300] E. Vitaku, D. T. Smith, J. T. Njardarson, *J. Med. Chem.* **2014**, *57*, 10257–10274.
- [301] A.-Y. Guan, C.-L. Liu, X.-F. Sun, Y. Xie, M.-A. Wang, *Bioorganic Med. Chem.* **2016**, *24*, 342–353.
- [302] H.-W. Lin, C.-W. Lu, L.-Y. Lin, Y.-H. Chen, W.-C. Lin, K.-T. Wong, F. Lin, *J. Mater. Chem. A* **2013**, *1*, 1770–1777.
- [303] M. Hedidi, G. Bentabed-Ababsa, A. Derdour, Y. S. Halauko, O. A. Ivashkevich, V. E. Matulis, F. Chevallier, T. Roisnel, V. Dorcet, F. Mongin, *Tetrahedron* **2016**, *72*, 2196–2205.
- [304] V. N. Kozhevnikov, Y. Zheng, M. Clough, H. A. Al-Attar, G. C. Griffiths, K. Abdullah, S. Raisys, V. Jankus, M. R. Bryce, A. P. Monkman, *Chem. Mater.* **2013**, *25*, 2352–2358.
- [305] M. Schlosser, F. Mongin, *Chem. Soc. Rev.* **2007**, *36*, 1161–1172.
- [306] K. Nakatsu, K. Kafuku, H. Yamaoka, *Inorganica Chim. Acta* **1981**, *54*, L69–L70.

- [307] A. R. Kennedy, R. E. Mulvey, R. I. Urquhart, S. D. Robertson, *Dalton Trans.* **2014**, *43*, 14265–14274.
- [308] H. Ott, U. Pieper, D. Leusser, U. Flierler, J. Henn, D. Stalke, *Angew. Chem. Int. Ed.* **2009**, *48*, 2978–2982.
- [309] P. C. Andrews, D. R. Armstrong, C. L. Raston, B. A. Roberts, B. W. Skelton, A. H. White, *J. Chem. Soc., Dalt. Trans.* **2001**, 996–1006.
- [310] W.-P. Leung, L.-H. Weng, R.-J. Wang, T. C. W. Mak, *Organometallics* **1995**, *14*, 4832–4836.
- [311] C. Jones, C. H. L. Kennard, C. L. Raston, G. Smithe, *J. Organomet. Chem.* **1990**, *396*, C39–C42.
- [312] A. Kimyonok, B. Domercq, A. Haldi, J.-Y. Cho, J. R. Carlise, X.-Y. Wang, L. E. Hayden, S. C. Jones, S. Barlow, S. R. Marder, et al., *Chem. Mater.* **2007**, *19*, 5602–5608.
- [313] S. Takizawa, H. Echizen, J. Nishida, T. Tsuzuki, S. Tokito, Y. Yamashita, *Chem. Lett.* **2006**, *35*, 748–749.
- [314] H. J. Park, J. N. Kim, H.-J. Yoo, K.-R. Wee, S. O. Kang, D. W. Cho, U. C. Yoon, *J. Org. Chem.* **2013**, *78*, 8054–8064.
- [315] Y. Feng, X. Zhuang, D. Zhu, Y. Liu, Y. Wang, M. R. Bryce, *J. Mater. Chem. C* **2016**, *4*, 10246–10252.
- [316] D. L. Comins, D. H. LaMunyon, *Tetrahedron Lett.* **1988**, *29*, 773–776.
- [317] T. Kawashima, T. Takao, H. Suzuki, *J. Am. Chem. Soc.* **2007**, *129*, 11006–11007.

- [318] C. T. Carver, P. L. Diaconescu, *J. Am. Chem. Soc.* **2008**, *130*, 7558–7559.
- [319] K. L. Miller, B. N. Williams, D. Benitez, C. T. Carver, K. R. Ogilby, E. Tkatchouk, W. A. Goddard, P. L. Diaconescu, *J. Am. Chem. Soc.* **2009**, *132*, 342–355.
- [320] P. L. Diaconescu, *Curr. Org. Chem.* **2008**, *12*, 1388–1405.
- [321] U. Eisner, J. Kuthan, *Chem. Rev.* **1972**, *72*, 1–42.
- [322] E. Silva, P. Varandas, A. Silva, *Synthesis* **2013**, *45*, 3053–3089.
- [323] J. Kuthan, A. Kurfürst, *Ind. Eng. Chem. Prod Res. Dev.* **1982**, *21*, 191–261.
- [324] Y. Kohari, Y. Okuyama, E. Kwon, T. Furuyama, N. Kobayashi, T. Otuki, J. Kumagai, C. Seki, K. Uwai, G. Dai, et al., *J. Org. Chem.* **2014**, *79*, 9500–9511.
- [325] R. M. Martin, R. G. Bergman, J. A. Ellman, *Org. Lett.* **2013**, *15*, 444–447.
- [326] W. Zhang, X. Yang, W. Chen, X. Xu, L. Li, H. Zhai, Z. Li, *J. Agric. Food Chem.* **2010**, *58*, 2741–2745.
- [327] W. Clegg, L. Dunbar, L. Horsburgh, R. E. Mulvey, *Angew. Chem. Int. Ed.* **1996**, *35*, 753–755.
- [328] S. D. Robertson, A. R. Kennedy, J. J. Liggat, R. E. Mulvey, *Chem. Commun.* **2015**, *51*, 5452–5455.
- [329] T. Wiklund, S. Olsson, A. Lennartson, *Monatshefte für Chemie* **2011**, *142*, 813–819.
- [330] D. R. Armstrong, C. M. M. Harris, A. R. Kennedy, J. J. Liggat, R. McLellan, R. E. Mulvey, M. D. T. Urquhart, S. D. Robertson, *Chem. Eur. J.* **2015**, *21*, 14410–14420.

- [331] S. A. Orr, A. R. Kennedy, J. J. Liggat, R. McLellan, R. E. Mulvey, S. D. Robertson, *Dalton Trans.* **2016**, 45, 6234–6240.
- [332] J. Intemann, M. Lutz, S. Harder, *Organometallics* **2014**, 33, 5722–5729.
- [333] H. Xie, X. Hua, B. Liu, C. Wu, D. Cui, *J. Organomet. Chem.* **2015**, 798, 335–340.
- [334] P. Jochmann, T. S. Dols, T. P. Spaniol, L. Perrin, L. Maron, J. Okuda, *Angew. Chem. Int. Ed.* **2010**, 49, 7795–7798.
- [335] J. Intemann, H. Bauer, J. Pahl, L. Maron, S. Harder, *Chem. Eur. J.* **2015**, 21, 11452–11461.
- [336] D. Barr, R. Snaith, R. E. Mulvey, D. Reed, *Polyhedron* **1988**, 7, 665–668.
- [337] D. O’Hagan, *Chem. Soc. Rev.* **2008**, 37, 308–319.
- [338] S. Purser, P. R. Moore, S. Swallow, V. Gouverneur, *Chem. Soc. Rev.* **2008**, 37, 320–330.
- [339] K. Müller, C. Faeh, F. Diederich, *Science* **2007**, 317, 1881–1886.
- [340] D. O’Hagan, H. S. Rzepa, *Chem. Commun.* **1997**, 645–652.
- [341] D. M. Lemal, *J. Org. Chem.* **2004**, 69, 1–11.
- [342] J.-P. Bégué, D. Bonnet-Delpon, *Bioorganic and Medicinal Chemistry of Fluorine*, Wiley-VCH: Hoboken, NJ, USA, **2008**.
- [343] P. Kirsch, *Modern Fluoroorganic Chemistry*, Wiley-VCH Verlag GmbH & Co. KGaA, Weinheim, Germany, **2004**.
- [344] T. Hiyama, *Organofluorine Compounds*, Springer Berlin Heidelberg, Berlin, Heidelberg, **2000**.

- [345] J. B. Doyon, A. Jain, *Org. Lett.* **1999**, *1*, 183–185.
- [346] X. Jia, J. Wang, X. Ding, J. Yang, N. Li, N. Zhao, Z. Huang, *J. Org. Chem.* **2015**, *80*, 10874–10882.
- [347] X. Xu, J. Jia, H. Sun, Y. Liu, W. Xu, Y. Shi, D. Zhang, X. Li, *Dalton Trans.* **2013**, *42*, 3417–3428.
- [348] S. I. Källäne, M. Teltewskoi, T. Braun, B. Braun, *Organometallics* **2015**, *34*, 1156–1169.
- [349] E. Clot, O. Eisenstein, N. Jasim, S. A. Macgregor, J. E. McGrady, R. N. Perutz, *Acc. Chem. Res.* **2011**, *44*, 333–348.
- [350] S. D. Pike, M. R. Crimmin, A. B. Chaplin, *Chem. Commun.* **2017**, *53*, 3615–3633.
- [351] H. H. Büker, N. M. M. Nibbering, D. Espinosa, F. Mongin, M. Schlosser, *Tetrahedron Lett.* **1997**, *38*, 8519–8522.
- [352] T. Klis, S. Lulinski, J. Serwatowski, *Curr. Org. Chem.* **2008**, *12*, 1479–1501.
- [353] M. Schlosser, E. Marzi, *Chem. Eur. J.* **2005**, *11*, 3449–3454.
- [354] D. Balcells, E. Clot, O. Eisenstein, *Chem. Rev.* **2010**, *110*, 749–823.
- [355] S. A. Hauser, I. Prokes, A. B. Chaplin, *Chem. Commun.* **2015**, *51*, 4425–4428.
- [356] T. Furukawa, M. Tobisu, N. Chatani, *J. Am. Chem. Soc.* **2015**, *137*, 12211–12214.
- [357] P. L. Coe, A. J. Waring, T. D. Yarwood, *J. Chem. Soc. Perkin Trans. 1* **1995**, *21*, 2729–2737.

- [358] K. C. Caster, C. G. Keck, R. D. Walls, *J. Org. Chem.* **2001**, *66*, 2932–2936.
- [359] R. J. Harper, E. J. Soloski, C. Tamborski, *J. Org. Chem.* **1964**, *29*, 2385–2389.
- [360] S. H. Wunderlich, P. Knochel, *Angew. Chem. Int. Ed.* **2009**, *48*, 9717–9720.
- [361] S. Preshlock, M. Tredwell, V. Gouverneur, *Chem. Rev.* **2016**, *116*, 719–766.
- [362] H. Amii, K. Uneyama, *Chem. Rev.* **2009**, *109*, 2119–2183.
- [363] L. Wang, H. Sun, X. Li, O. Fuhr, D. Fenske, *Dalton Trans.* **2016**, *45*, 18133–18141.
- [364] A. D. Sun, K. Leung, A. D. Restivo, N. A. LaBerge, H. Takasaki, J. A. Love, *Chem. Eur. J.* **2014**, *20*, 3162–3168.
- [365] H. Luo, G. Wu, S. Xu, K. Wang, C. Wu, Y. Zhang, J. Wang, *Chem. Commun.* **2015**, *51*, 13321–13323.
- [366] X. Xu, H. Sun, Y. Shi, J. Jia, X. Li, *Dalton Trans.* **2011**, *40*, 7866–7872.
- [367] S. Sahu, M. G. Quesne, C. G. Davies, M. Dürr, I. Ivanović-Burmazovic, M. A. Siegler, G. N. L. Jameson, S. P. De Visser, D. P. Goldberg, *J. Am. Chem. Soc.* **2014**, *136*, 13542–13545.
- [368] F. Lu, H. Sun, A. Du, L. Feng, X. Li, *Org. Lett.* **2014**, *16*, 772–775.
- [369] T. Ahrens, J. Kohlmann, M. Ahrens, T. Braun, *Chem. Rev.* **2015**, *115*, 931–972.
- [370] W. Chen, C. Bakewell, M. R. Crimmin, *Synthesis* **2016**, *48*, A-L.
- [371] M. Teltewskoi, J. A. Panetier, S. A. Macgregor, T. Braun, *Angew. Chem. Int. Ed.* **2010**, *49*, 3947–3951.
- [372] R. J. Lindup, T. B. Marder, R. N. Perutz, A. C. Whitwood, *Chem. Commun.*

- 2007**, *35*, 3664–3666.
- [373] W.-H. Guo, Q.-Q. Min, J.-W. Gu, X. Zhang, *Angew. Chem. Int. Ed.* **2015**, *54*, 9075–9078.
- [374] M. R. Crimmin, M. J. Butler, A. J. P. White, *Chem. Commun.* **2015**, *51*, 15994–15996.
- [375] T. Chu, Y. Boyko, I. Korobkov, G. I. Nikonov, *Organometallics* **2015**, *34*, 5363–5365.
- [376] R. Azhakar, H. W. Roesky, H. Wolf, D. Stalke, *Chem. Commun.* **2013**, *49*, 1841–1843.
- [377] A. Jana, P. P. Samuel, G. Tavčar, H. W. Roesky, C. Schulzke, *J. Am. Chem. Soc.* **2010**, *132*, 10164–10170.
- [378] P. P. Samuel, A. P. Singh, S. P. Sarish, J. Matussek, I. Objartel, H. W. Roesky, D. Stalke, *Inorg. Chem.* **2013**, *52*, 1544–1549.
- [379] K. Matsubara, T. Ishibashi, Y. Koga, *Org. Lett.* **2009**, *11*, 1765–1768.
- [380] T. Hatakeyama, S. Ito, M. Nakamura, E. Nakamura, *J. Am. Chem. Soc.* **2005**, *127*, 14192–14193.
- [381] Y. Xiong, J. Wu, S. Xiao, J. Xiao, S. Cao, *J. Org. Chem.* **2013**, *78*, 4599–4603.
- [382] Y. Sun, H. Sun, J. Jia, A. Du, X. Li, *Organometallics* **2014**, *33*, 1079–1081.
- [383] C. Bakewell, A. J. P. White, M. R. Crimmin, *J. Am. Chem. Soc.* **2016**, *138*, 12763–12766.
- [384] C. Heiss, E. Marzi, F. Mongin, M. Schlosser, *European J. Org. Chem.* **2007**, 669–675.



- [385] M. Simonetti, G. J. P. Perry, X. C. Cambeiro, F. Juliá-Hernández, J. N. Arokianathar, I. Larrosa, *J. Am. Chem. Soc.* **2016**, *138*, 3596–3606.
- [386] T. Tanabe, W. W. Brennessel, E. Clot, O. Eisenstein, W. D. Jones, *Dalton Trans.* **2010**, *39*, 10495–10509.
- [387] A. S. Romanov, M. Bochmann, *Organometallics* **2015**, *34*, 2439–2454.
- [388] J. A. Hatnean, R. Beck, J. D. Borrelli, S. A. Johnson, *Organometallics* **2010**, *29*, 6077–6091.
- [389] O. Rivada-Wheelaghan, M. A. Ortuño, J. Díez, A. Lledós, S. Conejero, *Angew. Chem. Int. Ed.* **2012**, *51*, 3936–3939.
- [390] J. Chu, X. Han, C. E. Kefalidis, J. Zhou, L. Maron, X. Leng, Y. Chen, *J. Am. Chem. Soc.* **2014**, *136*, 10894–10897.
- [391] H. Li, J. Liu, C. L. Sun, B. J. Li, Z. J. Shi, *Org. Lett.* **2011**, *13*, 276–279.
- [392] H. Hao, H. W. Roesky, Y. Ding, C. Cui, M. Schormann, H.-G. Schmidt, M. Noltemeyer, B. Žemva, *J. Fluor. Chem.* **2002**, *115*, 143–147.
- [393] D. J. Liptrot, M. S. Hill, M. F. Mahon, *Angew. Chem. Int. Ed.* **2014**, *53*, 6224–6227.
- [394] G. M. Sheldrick, *Acta Crystallogr.* **2008**, *A64*, 112–122.
- [395] G. M. Sheldrick, *Acta Crystallogr.* **2015**, *C71*, 3–8.
- [396] O. V. Dolomanov, L. J. Bourhis, R. J. Gildea, J. A. K. Howard, H. Puschmann, *J. Appl. Crystallogr.* **2009**, *42*, 339–341.
- [397] M. Stender, R. J. Wright, B. E. Eichler, J. Prust, M. M. Olmstead, H. W. Roesky, P. P. Power, *J. Chem. Soc. Dalt. Trans.* **2001**, 3465–3469.